PHASE SHIFT ANALYSIS IN NUCLEAR ASTROPHYSICS

Sergey Dubovichenko

Phase Shift Analysis in Nuclear Astrophysics

Reviewers
Academician of the European Academy of Natural Sciences, corresponding member of the Russian Academy of Natural Sciences, Doctor of phys. and math. Sciences, Republic of Kazakhstan (RK), professor **Burtebayev N. T.** (INP, Almaty, RK)

Academician of the European Academy of Natural Sciences, Doctor of phys. and math. sciences RK and RF, professor **Burkova N. A.** (al-Farabi KazNU, Almaty, RK)

Scientific Editor of English edition
PhD **Albert V. Dzhazairov-Kakhramanov** (APFI, Almaty, RK)

Translated into English
Julia S. Dubovichenko (APFI, Almaty, RK)

Phase Shift Analysis in Nuclear Astrophysics

By

Sergey Dubovichenko

Cambridge
Scholars
Publishing

Phase Shift Analysis in Nuclear Astrophysics

By Sergey Dubovichenko

This book first published 2022

Cambridge Scholars Publishing

Lady Stephenson Library, Newcastle upon Tyne, NE6 2PA, UK

British Library Cataloguing in Publication Data
A catalogue record for this book is available from the British Library

ISBN (10): 1-5275-8283-3
ISBN (13): 978-1-5275-8283-5

CONTENTS

INTRODUCTION

In many problems of nuclear physics at low energies and nuclear astrophysics, knowledge of the scattering elastic phase shifts, which can be determined from the differential cross sections of the scattering of various nuclear particles, is necessary [1]. Such phase shifts are used, in particular, for the construction of intercluster interaction potentials, for example, in the potential cluster model (PCM) of light nuclei [2]. The procedure of phase shift analysis consists of the decomposition of the total scattering amplitude in a row by partial waves or amplitudes and the analysis of the parameters that appear at the same time, which are termed scattering phase shifts. Such phase shifts allow us to obtain data about the nature of strong interactions, the structure of resonance states, and the general structure of an atomic nucleus [1].

Two-body processes with the formation of resonances in nuclear physics at low energies can also be investigated by means of phase shift analysis. To solve this problem, it is necessary to consider in detail the energetic behavior of the resonance partial scattering amplitude [1,3]. As a result, phase shift analysis plays a large role in the investigation of nuclear resonances in scattering processes and the determination of their quantum numbers. Research into scattering processes by means of phase shift analysis can help clarify many important aspects of the interactions of nuclear particles, because such analysis is based only on the most general laws of conservation and displays close connections to the experimental data [1,3].

The problem of determining or extracting the nuclear phase shifts from cross sections of elastic scattering in the mathematical plane is reduced to a multiple parameter variation problem. In other words, using the experimental scattering cross sections of nuclear particles and the mathematical expressions obtained in the quantum mechanics, which describe these cross sections according to some δ_L parameters, the nuclear scattering phase shifts can be known. Consequently, a multiple parameter variation problem arises in finding these parameters for the set interval of values while taking into account the generalized Levinson theorem [4]. In different nuclear systems, depending on the energy of the colliding particles, the number of elastic scattering phase shifts can change from 1–3 to 10–20 [5].

This book is directly based on the results of about twenty scientific articles published over the last five to seven years in Russia, Europe, the USA, and the CIS countries. It consists of three chapters. The first chapter

is devoted to a description of the general mathematical methods for calculating some nuclear characteristics. The general criteria and methods of creation of the intercluster potentials in a continuous and discrete spectrum, which are used further for the consideration of some nuclei in the three-body model (described in the third chapter), are defined.

The second chapter presents methods and results of the phase shift analysis of elastic scattering of the following nuclear particles at low and astrophysical energies: $^{4}He^{4}He$, $n^{3}He$, $p^{6}Li$, $p^{12}C$, $n^{12}C$, $p^{13}C$, $p^{14}C$, $n^{16}O$, $p^{16}O$, and $^{4}He^{12}C$. These results have been used to construct the potential cluster model (PCM) of pair intercluster interaction potentials in a continuous spectrum. Here, the various experimental measurements, methods of calculating differential cross sections, computer programs, and results of the phase shift analysis of elastic scattering of the stated particles, are all considered. For the first system, $^{4}He^{4}He$, only the main expressions for the phase shift analysis, the computer program, and versions of the control account are given at 25–29 MeV. For other systems, the approximate energy range 1–2.5 MeV is considered. In an elastic $^{4}He^{12}C$ scattering, a phase shift analysis was undertaken in the range 1.5–6.5 MeV. The areas of phase shift analysis given here are defined by the existence of experimental data on differential cross sections for angular distributions or excitation functions.

The results obtained for the three-body single-channel models of some light nuclear nuclei, namely, ^{7}Li, ^{9}Be, and ^{11}B, are given in Chapter Three. They allow one to check the adequacy of the construction of pair intercluster potentials on the basis of the elastic scattering phase shifts and characteristics of the bound states of light atomic nuclei. These results allow us to determine the applicability of the obtained potentials to three-body problems. The checked potentials are thus used for the calculation of some primary characteristics of thermonuclear processes in the preliminary nucleosynthesis of the universe and some solar cycles [2].

We note that the second and, particularly, the third chapters of this book almost completely coincide with the results given in the corresponding chapters of other books by the author, including *Preliminary Nucleosynthesis of the Universe* (2014, Lambert Academy Publ. GmbH & Co. KG: Saarbrucken, Germany, 668 pages) [2]. This material is found in this book (*Phase Shift Analysis in Nuclear Astrophysics*) primarily in order to reduce the size of book [2] and allow the future possibility of its enlargement and the addition of new material on thermonuclear reactions in the next edition. At the same time, the present book can also be extended by the inclusion of new results on phase shift analysis and the three-body model.

I

METHODS OF SOLVING THE SCHRÖDINGER EQUATION

Introduction

The set of problems of theoretical nuclear physics, especially in the field of light atomic nuclei and low energies, requires the ability to solve the Schrödinger equation or the coupled system of equations of this type. A wave function, which describes a quantum state of some system of nuclear particles and, in principle, contains all the information about such state is a result of the solution.

There are many varied mathematical methods for the solution of differential equations or their second-order systems, of which one is the Schrödinger equation. Quite abstract methods of solving such equations, which are rather difficult to apply in the solution of a concrete equation, like the Schrödinger equation type, are usually given in the mathematical literature. The problem usually arises in the choice of the optimum mathematical and numerical method applicable to the consideration of certain problems based on the solutions of the Schrödinger equation.

This chapter is devoted to the solution of these problems and describes some mathematical methods that are directly applicable to locating the wave functions from the Schrödinger equation of scattering problems of nuclear particles and their bound states. The numerical methods applicable to the problems of a continuous and discrete spectrum of states, which allow us to obtain end results with almost complete accuracy, are considered. On the basis of these methods, the possibility of writing computer programs in the BASIC computer language using the Borland Turbo Basic Compiler and the Fortran-90 language is considered, which can assist in solving all problems of nuclear physics considered here.

Many problems of nuclear physics can be considered using only the central part of the nuclear forces [6,7]. In this case, we are dealing with only one Schrödinger equation or system of unrelated equations (taking into account the spin-orbital interaction) and the mathematical problem is solved

rather simply. The account of tensor components of nuclear forces leads us to the system of bound Schrödinger equations [8,9], the solution of which is slightly more difficult, but quite feasible by many methods, including those described in [10].

We provide the mathematical and numerical methods used for the solution of Schrödinger equations for the central potentials at positive and negative eigenvalues in this chapter. We also consider their application to the analysis of the scattering quantum problem and bound-state energies of nuclear particles. In other words, the methods of investigating nuclear scattering phase shifts and the calculation of bound-state energies of light nuclei within the modified potential two-cluster model (MPCM) [2] are given.

1.1 The general methods of solving the Schrödinger equation

Here the general formulation of the problem for the solution of the Schrödinger equation with positive continuous and negative discrete eigenvalues is considered. Entry and boundary conditions for solving this problem are determined in relation to a description of the physical processes and states in nuclear physics and nuclear astrophysics.

1.1.1 The central real potentials

The Schrödinger equation for the central forces of interaction between two nuclear particles without spin-orbital and tensor potentials has the following form [1,6,7,11]

$$u''(r)+\left[k^2-V_{\rm c}(r)-V_{\rm coul}(r)-\frac{L(L+1)}{r^2}\right]u(r)=0\ , \qquad (1.1.1)$$

where r is the scalar relative distance between particles in fm (1 fermi = 10^{-15} m); u is the solution of the equation, i.e. wave function (WF); u'' is its second derivative; $V_{\rm coul}(r) = 2\mu/\hbar^2\ Z_1Z_2/r$ is the Coulomb potential reduced to the dimension of fm^{-2}; $\hbar$ is the Plank constant = 1.055 10^{-34} J s (Joule-second); Z_1 and Z_2 are the charges of particles in terms of their elementary charge (1 e.c. – elementary charge = 1.60 10^{-19} C – Coulomb); the constant $\hbar^2/m_0$ = 41.4686 MeV fm^2 (1 MeV – megaelectronvolt = 1.60 10^{-13} Joule); m_0 is the atomic mass unit (1 amu – atomic mass unit = 1.66 10^{-27} kg.); $V_{\rm cf} = L(L+1)/r^2$ is the centrifugal potential, which depends on the value of the

orbital moment of the relative movement of the L particles; $k^2 = 2\mu E/\hbar^2$ is the wave number of the relative motion in fm^2; E is the energy of particles in MeV; $\mu = \frac{m_1 m_2}{m_1 + m_2}$ is the reduced mass of two particles in amu; $V_c(r)$ is the central part of the nuclear potential, equal to $2\mu/\hbar^2\ V_n(r)$; $V_n(r)$ is the radial dependence of the potential, which is often accepted in the form $V_0 \exp(-\alpha r^2)$ or $V_0 \exp(-\alpha r)$; V_0 is the potential depth in MeV; $\eta = \frac{\mu Z_1 Z_2}{\hbar^2 k} = 0.0344476 Z_1 Z_2/k$ is the Coulomb parameter; the Coulomb potential can be presented in the form

$$V_{coul}(r) = 2\eta k/r = A_c/r.$$

If the spin-orbital interaction is taken into account, then the central potential has the form [1,6,7]

$$V_c(r) = 2\mu/\hbar^2\ [V_n(r) + V_{sl}(r)],$$

$$V_{sl}(r) = (\boldsymbol{SL})\ V_{0sl}\ F(r),$$

where $F(r)$ is the functional dependence of the potential on the relative distance between particles, which can also be accepted in the form of the Gaussian function $\exp(-\alpha r^2)$ or exponent $\exp(-\alpha r)$.

The ***(SL)*** value is called the spin-orbital operator and its values can be found from the well-known expression [6,7]

$$(\boldsymbol{SL})\ u(r) = 1/2\ [J(J+1) - L(L+1) - S(S+1)]\ u(r),$$

where J is the total moment of the system; L is the orbital moment; and S is the spin of the system of particles. Taking into account the spin-orbital interaction, the Schrödinger equation is split into a system of uncoupled equations, each of which allows the finding of the WF for the concrete total moment.

Sometimes, the Coulomb R_c radius is entered into the potential of interaction; then the Coulomb part of the potential takes a slightly different form

$$V_{coul}(r) = \frac{2\mu}{\hbar^2} \begin{cases} \dfrac{Z_1 Z_2}{r} & r > R_c \\ Z_1 Z_2 \left(3 - \dfrac{r^2}{R_c^2}\right) \Big/ 2R_c & r < R_c \end{cases}. \quad (1.1.2)$$

Equation (1.1.1) forms the Cauchy problem with initial conditions that lie outside physical reasoning The first initial condition demands equality to zero of the WF at $u(0) = 0$. As the WF reflects the probability of some processes or states of the quantum particles, this condition means that two particles cannot completely merge and occupy the same volume. The second statement of the Cauchy problem involves the determination of the value of the first derivative of this function. However, for reasons of physical limitation, it is impossible to determine the value of this derivative; therefore it is taken to equal some constant, which determines the amplitude of the wave function. In numerical calculation, $u'(0) = 0.1–1$ is usually accepted. The real amplitude of the function, which is used for numerous physical calculations, is defined from the asymptotic conditions imposed on this function at long distances of $r \to R$, when the nuclear potential is almost equal to zero.

The asymptotics of the wave function at long distances, when $V_c(r \to R) \to 0$, offer the solution of equation (1.1.1) without nuclear potential, and can be presented as follows

$$u_L(r \to R) \to F_L(kr) + \mathrm{tg}(\delta_L) G_L(kr), \quad (1.1.3)$$

or

$$u_L(r \to R) \to \cos(\delta_L) F_L(kr) + \sin(\delta_L) G_L(kr),$$

where F_L and G_L are the scattering Coulomb functions [12,13]. These are partial solutions of equation (1.1.1) without the nuclear part of the potential, i.e. when $V_c = 0$.

Interlacing the numerical solution $u(r)$ of equation (1.1.1) at long distances (R at about 10–20 fm) with these asymptotics, it is possible to find the real amplitude of the function and the scattering phase shift δ_L for each L at the given energy of the interacting particles. The scattering phase shifts in the concrete system of the nuclear particles can be determined from phase shift analysis of the experimental data in terms of their elastic scattering (Chapter 2). Furthermore, variation of the parameters of nuclear potential in the previously determined form in equation (1.1.1) is carried out and those

parameters that allow us to describe the results of the phase shift analysis are determined. Thus, the problem of the description of scattering processes of nuclear particles consists of the search for the parameters of the nuclear potential that can describe the results of phase shift analysis and the experimental data for the scattering cross sections.

We consider the procedure of interlacing the wave functions with asymptotics in more detail. At $r = R$, it is possible to write down two equalities for the WF along with their derivatives [14]

$$Nu_L(R) = F_L(kR) + \mathrm{tg}(\delta_L)G_L(kR),$$

$$Nu'_L(R) = F'_L(kR) + \mathrm{tg}(\delta_L)G'_L(kR),$$

where N is a normalizing multiplier. It is possible to consider similar expressions, not for the function and derivative, but only for the function in two different points

$$\begin{aligned} Nu_L(R_1) &= F_L(kR_1) + \mathrm{tg}(\delta_L)G_L(kR_1), \\ Nu_L(R_2) &= F_L(kR_2) + \mathrm{tg}(\delta_L)G_L(kR_2). \end{aligned} \tag{1.1.4}$$

We enter the notations

$$\begin{aligned} F_1 &= F_L(kR_1), & F_2 &= F_L(kR_2), \\ G_1 &= G_L(kR_1), & G_2 &= G_L(kR_2), \\ u_1 &= u_L(R_1), & u_2 &= u_L(R_2), \end{aligned}$$

and find the value N, for example, from the first equation

$$N = [F_1 + \mathrm{tg}(\delta_L)G_1]/u_1.$$

Substituting this expression into the second equation, we obtain

$$\mathrm{tg}(\delta_L) = (u_1F_2 - u_2F_1)/(u_2G_1 - u_1G_2) = A_L. \tag{1.1.5}$$

then

$$\delta_L = \mathrm{arctg}(A_L).$$

Normalization of the function, for the purposes of investigating phase shifts, is of no importance. However, if we need the normalized WF, i.e. the

total scattering function is also required, then it is better to consider the second equation from (1.1.3), written down in the form of (1.1.4) and having performed similar operations to those given above. If the scattering phase shift results in the same expression, then we write the normalization in the form

$$N = [\cos(\delta_L)F_1+\sin(\delta_L)G_1]/u_1,$$

or

$$N = [\cos(\delta_L)F_2+\sin(\delta_L)G_2]/u_2.$$

In so doing, we can completely define the behavior of the wave function, its amplitude and phase shift, in all ranges of solutions for equation (1.1.1), from zero to some large value of R, which define the WF asymptotics.

1.1.2 The central complex potentials

If the inelastic channel of scattering or reactions is open in nuclear processes, then it is necessary to use the complex potential of interaction, taking into account the decrease in the stream of particles from the elastic channel [6]. Now, the potential takes a form

$$V_c = V_r(r) + iV_m(r), \tag{1.1.6}$$

where $V_r(r)$ is the real part of the potential and $V_m(r)$ is its imaginary part. The wave function also becomes complex and can be written in the form

$$u(r) = x(r) + iy(r). \tag{1.1.7}$$

Then, the Schrödinger equation (1.1.1) can be rewritten in the form of a coupled equation system as

$$\begin{aligned} x''(r) + [k^2 - V_r(r) - V_{coul}(r) - L(L+1)/r^2]x(r) &= -V_m y(r), \\ y''(r) + [k^2 - V_r(r) - V_{coul}(r) - L(L+1)/r^2]y(r) &= V_m x(r), \end{aligned} \tag{1.1.8}$$

with initial conditions in the form

$$x(r=0) = 0, \qquad x'(r=0) = \text{const},$$
$$y(r=0) = 0, \qquad y'(r=0) = \text{const}.$$

In the numerical calculations, the value of the constant (const.) for the derivatives of the wave functions is set at the level 0.1–1. The asymptotics of wave functions are represented as follows [6]

$$u(r) = H^{+}(r) + SH^{-}(r) = [F(r) + iG(r)] + S[F(r) - iG(r)], \quad (1.1.9)$$

where H^{+} is the Hankel function; F and G are the Coulomb functions; and S is the scattering matrix, which has the form

$$S = e^{2i\delta} = S_1 + iS_2 = \cos(2\delta) + i\sin(2\delta).$$

In taking into account the inelastic processes, the phase shifts of the elastic scattering become complex and are represented as follows

$$\delta = \sigma + i\Delta,$$

where σ and Δ are the real and imaginary parts of the phase shift. Then, the scattering matrix can be rewritten in the form

$$S = e^{2i\delta} = e^{-2\Delta}e^{2i\sigma} = \eta e^{2i\sigma} = \eta(S_1 + iS_2) = \eta[\cos(2\sigma) + i\sin(2\sigma)], \quad (1.1.10)$$

where $\eta = e^{-2\Delta}$ is the inelasticity parameter. For the determination of the scattering phase shifts and the parameter of inelasticity, we can write out the boundary conditions for the functions in two points in the form of a logarithmic derivative

$$\frac{u_1}{u_2} = \frac{H_1^{+} + SH_1^{-}}{H_2^{+} + SH_2^{-}}, \quad (1.1.11)$$

from which it is easy to find

$$S = \frac{u_2 H_1^{+} - u_1 H_2^{+}}{u_1 H_2^{-} - u_2 H_1^{-}}.$$

Substituting the expressions for the Hankel functions given above (1.1.9), and splitting the real and imaginary parts, we obtain

$$S = \frac{C + i\mathrm{D}}{A + iB} = K + iM, \quad (1.1.12)$$

where

$$K = \frac{AC + BD}{A^2 + B^2}, \qquad M = \frac{AD - BC}{A^2 + B^2}, \tag{1.1.13}$$

and

$A = b - a,$ $B = - c - d,$

$C = a + b,$ $D = c - d,$

$a = x_2F_1 - x_1F_2,$ $b = y_1G_2 - y_2G_1,$

$c = y_2F_1 - y_1F_2,$ $d = x_1G_2 - x_2G_1.$

Thus, all elements of the S matrix are expressed through the Coulomb functions and the solutions of the initial Schrödinger equation (1.1.8) with the given nuclear potential.

Comparing the real and imaginary parts of expressions (1.1.10) and (1.1.12), we obtain

$$\begin{aligned} S_1 &= \cos(2\sigma) = K/\eta, \\ S_2 &= \sin(2\sigma) = M/\eta, \end{aligned} \tag{1.1.14}$$

and

$$\begin{aligned} S^2 &= \eta^2(S_1 + S_2)^2 = \eta^2, \\ S^2 &= K^2 + M^2, \end{aligned} \tag{1.1.15}$$

from which we find

$\eta^2 = K^2 + M^2,$

giving the inelasticity parameter. Knowing these values, we can obtain

$$A = \mathrm{tg}(\sigma) = \frac{S_2}{1 + S_1}, \tag{1.1.16}$$

then

$$\sigma = \text{arctg}(A). \qquad (1.1.17)$$

It is easy enough to check that when $V_m = 0$ and equation (1.1.8) become independent, then $\eta = 1$ and the results for the phase shifts (1.1.5) and (1.1.16) coincide.

For the determination of the normalization of the WF, we use expressions (1.1.9) and (1.1.7)

$$N(x+iy) = H^{+}(r) + SH^{-}(r) = [F(r) + iG(r)] + (S_1 + iS_2)\,[F(r) - iG(r)],$$

from which we find

$$N = \frac{Ax + By}{x^2 + y^2} + i\frac{Bx - Ay}{x^2 + y^2},$$

where

$$A = (1 + S_1)F(r) + S_2G(r),\ B = (1 - S_1)G(r) + S_2F(r).$$

Generally, normalization of a complex WF can be written down in the form of a complex value as follows

$$Nu(r) = (N_1 + iN_2)(x + iy) = N_1x - N_2y + i[N_1y + N_2x] = v + iw.$$

Here, v and w are already normalized total wave functions of the scattering. Equating the real and imaginary parts, we have

$$N_1 = \frac{Ax + By}{x^2 + y^2}, \qquad N_2 = \frac{Bx - Ay}{x^2 + y^2},$$

which are general expressions for determining the normalization of WF scattering in the case of complex potentials [15].

1.2 The numerical methods of solving the Schrödinger equation

For the numerical solution of the Schrödinger equation, it is possible to use the finite-difference method (FDM) [7], presenting the function and its

derivative in the form of the central differences and using the Runge-Kutta method (RKM) [16] or the Numerov method (NM) [17], which allows us to obtain a higher accuracy solution for the initial equation.

1.2.1 The central real potentials

We can write the Schrödinger equation for the central nuclear forces (1.1.1) in the form of [6]

$$u''(r) + [k^2 - V(r)]u(r) = 0. \quad (1.2.1)$$

To solve it, we can use the finite-difference method, for which the second derivative can be presented as follows [7]

$$u''(r) = [u(r + h) - 2u(r) + u(r - h)]/h^2 = [u(r_{i+1}) - 2u(r_i) + u(r_{i-1})]/h^2, \quad (1.2.2)$$

where h is a step of the finite-difference grid, for the determination of which the whole interval of h values, from zero to some value of R, are divided into N parts

$$h = R/N.$$

Here, R is the top limit at which the interlacing of the numerical solution of equation (1.2.1) with asymptotics is carried out. Then

$$r_i = hi, \quad u_i = u(r_i),$$

where i changes from 0 to N ($r_0 = 0$ and $r_N = R$). Now, expression (1.2.2) can be rewritten in the form

$$u'' = [u_{i+1} - 2u_i + u_{i-1}]/h^2,$$

and the whole equation is rewritten as

$$[u_{i+1} - 2u_i + u_{i-1}]/h^2 + [k^2 - V(r_i)]u_i = 0,$$

which we find with an order of accuracy $O(h^2)$ equal to h^2, i.e. the method is in proportion to a square of a step [7]

$$u_{i+1} = \left[2 + h^2 V(r_i) - h^2 k^2\right] u_i - u_{i-1} + O(h^2). \quad (1.2.3)$$

Here, $i = 1, 2 \ldots N - 1$. The function at $r = 0$ has to be equal to zero and in the first step it can be accepted as equal to some constant, which defines only a function of normalization without affecting its behavior at various values of r. From here, the WF on the following step of u_2 can be found and this process repeats until i does not become equal to $N - 1$. Such a procedure allows us to find the whole array of WF values at all points from zero to R. Furthermore, we carry out its interlacing in two points, for example, at $r_N = R$ and $r_{N-5} = R - 5h$, as described in paragraph 1.1.1. The second point is defined experimentally in each case and depends on the energy of the particles, but at small energies it usually recedes by 3–5 steps [18].

Below, we give an example of the program written in Fortran-90 to realize the method described. The following designations are set.

U – the array of the WF with a dimension of N,
H – the look-up of the WF,
N – the number of steps,
A0 – the V_0 depth of the central part of the potential in fm^{-2},
R0 – the α width of the central part of the potential in fm^{-2},
L – the orbital moment,
RC – the Coulomb radius R_c in fm,
AK – the Coulomb coefficient A_c in the description of equation (1.1.1),
SK – the wave number of k^2 in fm^{-2}.

```
SUBROUTINE FUN(U,H,N,A0,R0,L,RC,AK,SK)
IMPLICIT REAL(8) (A-Z)
INTEGER N,L,K
DIMENSION U(0:N)
! INITIAL VALUES
U(0)=0.0D0; U(1)=0.1D0; RR=1.0D0/RC
LL=L*(L+1); BB=AK/(2.0D0*RCU); HK=H*H; SHS=SK*HK-2.0D0
! CALCULATION THE VALUES OF THE Vc(R) POTENTIAL
DO K=1,N-1
X=K*H; XX=X*X
V=A0*DEXP(-R0*XX)+LL/XX
IF (X>RC) THEN
V=V+AK/X
ELSE
V=V+(3.0D0-(X*RR)**2)*BB
ENDIF
! CALCULATION THE VALUES OF THE WAVE FUNCTION
Q=V*HK-SHS
```

```
U(K+1)=Q*U(K)-U(K-1)
ENDDO
END
```

The WF $u(r)$ is the calculation result at the given L for the Schrödinger equation (1.2.1) in the range of values from 0 to R.

1.2.2 The central complex potentials

If there is a system of equations (1.1.8) for the complex potential [18]

$$\begin{aligned} x''(r) + [\, k^2 - V_r(r) - V_{coul}(r) - L(L+1)/r^2 \,]x(r) &= - V_m y(r), \\ y''(r) + [\, k^2 - V_r(r) - V_{coul}(r) - L(L+1)/r^2 \,]y(r) &= V_m x(r), \end{aligned} \tag{1.2.4}$$

then, using the same representation of a derivative in the finite-difference form

$$u'' = [u_{i+1} - 2u_i + u_{i-1}]/h^2,$$

for functions x and y we obtain

$$\begin{aligned} x_{i+1} &= [\, 2 - A_i h^2 \,]x_i - x_{i-1} - h^2 V_m(r_i) y_i, \\ y_{i+1} &= [2 - A_i h^2 \,]y_i - y_{i-1} + h^2 V_m(r_i) x_i, \end{aligned} \tag{1.2.5}$$

where

$$A_i = k^2 - V_r(r_i) - V_{coul}(r_i) - L(L+1)/r_i^2.$$

In addition, setting the values of functions in the two first points

$$x_0 = 0, \quad x_1 = \text{const.}, \qquad y_0 = 0, \quad y_1 = \text{const.},$$

it is possible to find the values of functions in all other points [18], as well as for expression (1.2.3). The interlacing procedure of the numerical function with its own asymptotics in the case of complex potentials is described in paragraph 1.1.2.

1.2.3 The Runge-Kutta method for central real potentials

Here, we consider the other method of solving such equations. This is the fourth-order Runge-Kutta method per step h [16,19,20,21,22]. The standard method of the solution of one differential equation of the first order is

$$y' = f(x,y), \tag{1.2.6}$$

with the initial condition

$$y(x_0) = y_0,$$

which consists of the presentation of the solution on an interval from 0 to some value of R in the form

$$y_{n+1} = y_n + \Delta y_n, \tag{1.2.7}$$

where n can change from 0 to N ($R = x_N = hN$); h is a step in the solution; and Δy_n is obtained from the expression

$$\Delta y_n = 1/6(k_1 + 2k_2 + 2k_3 + k_4), \tag{1.2.8}$$

where

$$k_1 = hf(x_n,y_n), \qquad k_2 = hf(x_n+h/2, y_n+k_1/2),$$
$$k_3 = hf(x_n+h/2, y_n+k_2/2), \qquad k_4 = hf(x_n+h, y_n+k_3).$$

In the case of a system of two differential equations of the first order [16-22], we have

$$y' = f(x,y,z),$$
$$z' = g(x,y,z), \tag{1.2.9}$$

with initial conditions

$$y(x_0) = y_0, \qquad z(x_0) = z_0.$$

The solutions are found from the expressions

$$y_{n+1} = y_n + \Delta y_n, \qquad (1.2.10)$$
$$z_{n+1} = z_n + \Delta z_n,$$

where

$$\Delta y_n = 1/6(k_1 + 2k_2 + 2k_3 + k_4), \qquad (1.2.11)$$
$$\Delta z_n = 1/6(m_1 + 2m_2 + 2m_3 + m_4),$$

and

$$k_1 = hf(x_n,y_n,z_n), \qquad m_1 = hg(x_n,y_n,z_n),$$
$$k_2 = hf(x_n+h/2, y_n+k_1/2, z_n+m_1/2), \qquad m_2 = hg(x_n+h/2, y_n+k_1/2, z_n+m_1/2),$$
$$k_3 = hf(x_n+h/2, y_n+k_2/2, z_n+m_2/2), \qquad m_3 = hg(x_n+h/2, y_n+k_2/2, z_n+m_2/2),$$
$$k_4 = hf(x_n+h, y_n+k_3, z_n+m_3), \qquad m_4 = hg(x_n+h, y_n+k_3, z_n+m_3).$$

In the case of one differential equation of the second order of the form (1.2.1)

$$y'' = g(x,y,y'), \qquad (1.2.12)$$

with initial conditions

$$y(0) = y_0, \qquad y'(0) = y'_0,$$

we substitute

$$z = y',$$

then we obtain a system of the form

$$y' = z, \qquad (1.2.13)$$
$$z' = g(x,y,z),$$

with initial conditions

$$y(0) = y_0, \qquad z(0) = z_0.$$

The solution of which $f(x,y,z) = z$ can be presented as follows

$$\Delta y_n = hz_n + 1/6h(m_1 + m_2 + m_3), \qquad (1.2.14)$$

$\Delta z_n = 1/6(m_1 + 2m_2 + 2m_3 + m_4)$,

and

$k_1 = hz_n$, $m_1 = hg(x_n,y_n,z_n)$,
$k_2 = h(z_n+m_1/2)$, $m_2 = hg(x_n+h/2, y_n+k_1/2, z_n+m_1/2)$,
$k_3 = h(z_n+m_2/2)$, $m_3 = hg(x_n+h/2, y_n+k_2/2, z_n+m_2/2)$,
$k_4 = h(z_n+m_3)$, $m_4 = hg(x_n+h, y_n+k_3, z_n+m_3)$.

The error of the Runge-Kutta method is in the order of $O(h^4)$, which is higher than for the previous case of the FDM.

Below we present an example of the program in Fortran-90 to realize the method described. The following designations are set.

U – the array of the WF with a dimension of N,
H – the look-up of the WF,
N – the number of steps,
A0 – the V_0 depth of the central part of the potential in fm^{-2},
R0 – the α width of the central part of potential in fm^{-2},
L – the orbital moment,
RC – the Coulomb radius R_c in fm,
AK – the Coulomb coefficient A_c in the description of equation (1.1.1),
SK – the wave number k^2 in fm^{-2}.

```
SUBROUTINE FUNRK(U,H,N,A0,R0,L,RC,AK,SK)
IMPLICIT REAL(8) (A-Z)
INTEGER I,N,L
DIMENSION U(0:N)
! THE SOLUTION OF THE SCHRÖDINGER EQUATION BY RUNGE-
KUTT METHOD IN ALL AREA OF VARIABLES
VA1=0.0D0;! VA1 - the value of function in zero
PA1=1.0D-1;! PA1 - Value of a derivative in zero
DO I=0,N-1
X=H*I+1.0D-15
CALL RRUN(VB1,PB1,VA1,PA1,H,X,L,SK,A0,R0)
VA1=VB1; PA1=PB1; U(I+1)=VA1
ENDDO
END
SUBROUTINE RRUN(VB1,PB1,VA1,PA1,H,X,L,SK,A0,R0)
IMPLICIT REAL(8) (A-Z)
INTEGER L
```

```
! THE SOLUTION OF THE SCHRÖDINGER EQUATION BY THE
RUNGE-KUTT METHOD BY ONE STEP
X0=X; Y1=VA1
CALL FA(X0,Y1,FK1,L,SK,A0,R0)
FK1=FK1*H; FM1=H*PA1
X0=X+H/2.0D0; Y2=VA1+FM1/2.0D0
CALL FA(X0,Y2,FK2,L,SK,A0,R0,A1,R1)
FK2=FK2*H; FM2=H*(PA1+FK1/2.0D0); Y3=VA1+FM2/2.0D0
CALL FA(X0,Y3,FK3,L,SK,A0,R0,A1,R1)
FK3=FK3*H; FM3=H*(PA1+FK2/2.0D0); X0=X+H; Y4=VA1+FM3
CALL FA(X0,Y4,FK4,L,SK,A0,R0,A1,R1)
FK4=FK4*H; FM4=H*(PA1+FK3)
PB1=PA1+(FK1+2.0D0*FK2+2.0D0*FK3+FK4)/6.0D0
VB1=VA1+(FM1+2.0D0*FM2+2.0D0*FM3+FM4)/6.0D0
END

SUBROUTINE FA(X,Y,FF,L,SK,A0,R0)
IMPLICIT REAL(8) (A-Z)
INTEGER L,L1
! CALCULATION F (X,Y) FUNCTION IN THE RUNGE–KUTT METHOD
VC=A0*DEXP(-R0*X*X)+A1*DEXP(-R1*X*X)
IF (X>RC) GOTO 1
VK=(3.0D0-(X/RC)**2)*AK/(2.0D0*RCU)
GOTO 2
1 VK=AK/X
2 FF=-(SK-VK-VC-L*(L+1)/(X*X))*Y
END
```

The result of the calculation is the wave function $u(r)$ at a given L, which is the solution of the Schrödinger equation (1.2.1) in the range of values from 0 to R.

1.2.4 The calculation of wave functions by Numerov's method

We still have the Schrödinger equation in the general form

$$u''(r) + a(r)u(r) = 0,$$

where

$$a(r) = \left[k^2 - V_c(r) \right],$$

$$V_c(r) = 2\mu / \hbar^2 V_n(r) + 2\mu / \hbar^2 \frac{Z_1 Z_2}{r} + \frac{L(L+1)}{r^2},$$

$$V_n(r) = -V_0 \exp(-\alpha r^2)$$

where V_0 is the potential depth parameter in MeV and α is the parameter of its width in fm^{-2}.

In Numerov's method [17], the WF at a given energy can be found from the expression

$$u_{n+1} = \frac{\left(2 - \frac{5}{6} h^2 a_n\right) u_n - \left(1 + \frac{1}{12} h^2 a_{n-1}\right) u_{n-1}}{1 + \frac{1}{12} h^2 a_{n+1}} + O(h^6).$$

Using this method, we can find the WF with a convergence rate of $O(h^4)$ [17] more easily than with the Runge-Kutta method having a convergence of $O(h^4)$. Here,

$u_{n-1} = u(r_{n-1}),$ $r_{n-1} = (n-1)h,$ $h = R/N,$

where R is the upper limit of integration of the equation; N is the number of steps of integration; and h is the value of a step, n = 1, … N - 1 and

$u(0) = 0, u(1) = \text{const}.$

We present an example of the program written in Fortran-90 to realize the method described. The following designations are set.

U – the array of the WF with a dimension of N,
H – the look-up of the WF,
N – the number of steps,
A0 – the V_0 depth of the central part of the potential in fm^{-2},
R0 – the α width of the central part of potential in fm^{-2},
L – the orbital moment,
RC – the Coulomb radius R_c in fm,
AK – the Coulomb coefficient A_c in the description of equation (1.1.1),

SK – the wave number of k^2 in fm^{-2}.

```
SUBROUTINE FUN(U,H,N,A0,R0,L,RC,AK,SK)
IMPLICIT REAL(8) (A-Z)
INTEGER N,L,I
DIMENSION U(0:N),V(0:N)
! INITIAL VALUES
U(0)=0.0D0; U(1)=0.1D0; Q0=0.0D0; RR=1/RC; HK=H*H; SHS=SK*HK
LL=L*(L+1);          BB=AK/(2.0D0*RC);          AA=1.0D0/12.0D0;
DD=5.0D0/6.0D0
! CALCULATION OF VALUES FOR THE Vc(r) POTENTIAL
DO I=1,N-1,2
X=I*H; XX=X*X; XP=(I+1)*H; XXP=XP*XP
V(I)=A0*DEXP(-R0*XX) +LL/XX
V(I+1)=A0*DEXP(-R0*XXP)+LL/XXP
IF (X>RC) THEN
V(I)=V(I)+AK/X
V(I+1)=V(I+1)+AK/XP
ELSE
V(I)=V(I)+(3.0D0-(X*RR)**2)*BB
V(I+1)=V(I+1)+(3.0D0-(XP*RR)**2)*BB
ENDIF
ENDDO
! CALCULATION OF VALUES FOR THE WAVE FUNCTION
DO I=1,N-1,1
Q1=SHS-V(I)*HK; Q2=SHS-V(I+1)*HK; B=(1.0D0+AA*Q2)
U(I+1)=((2.0D0-DD*Q1)*U(I)-(1.0D0+AA*Q0)*U(I-1))/B; Q0=Q1
ENDDO
END
```

The result is the WF $u(r)$ at a given L, which is the solution of the Schrödinger equation (1.2.1) in the range of values from 0 to R.

1.2.5 Methods of calculating the binding energy of a two-body system

Phase shifts can be used for the construction not only of scattering potentials, but also of bound states (BS): ground (GS) or excited (ES) states. We give two methods for the calculation of the binding energy of a two-body nuclear system. Such a situation arises, for example, in the S wave of the $^4He^2H$ system of ^6Li, where the BS potential is constructed by the corresponding

phase shift and its parameters are then specified according to the values of the binding energy, mean square radius, and asymptotic constant (AC) [23].

1.2.5.1 The finite-difference method

The first approach is based on the finite-difference method, which is described in detail in [7,10]. Here, we briefly present some methods of investigating the binding energy and the WF for the bound states and scattering processes. The Schrödinger equation [7] for the central potential is

$$u'' + [k^2 - V(r)]\, u = 0,$$

with this or that boundary condition at $k^2 < 0$ to form the boundary value problem of the Sturm-Liouville type with the boundary conditions

$$u(r = 0) = u_0 = 0,$$

$$u'(r = R)/u(r = R) = u'_N/\, u_N = f(\eta, L, Z_N),$$

where f is the logarithmic derivative; η is the Coulomb parameter; $Z_N = 2kr_N$; $n = 1,2,\ldots$; N is the number of steps; and $r_N = R$ is the upper bound of the interval of integration of the equation. At the transition to the second derivative to the final difference [24,25,26]

$$u'' = [u_{n+1} - 2u_n + u_{n-1}]/h^2,$$

which turns into a determined system of linear algebraic equations

$$u_{n+1} + [h^2k^2 - h^2V(r) - 2]u_n + u_{n-1} = 0.$$

The condition of equality to zero of its determinant D_N is

$$D_N = \begin{pmatrix} \theta_1 & 1 & 0 & . & . & . & 0 \\ \alpha_2 & \theta_2 & 1 & 0 & . & . & 0 \\ 0 & \alpha_3 & \theta_3 & 1 & 0 & . & 0 \\ . & . & . & . & . & . & . \\ . & . & . & . & . & . & . \\ 0 & . & 0 & 0 & \alpha_{N-1} & \theta_{N-1} & 1 \\ 0 & . & 0 & 0 & 0 & \alpha_N & \theta_N \end{pmatrix} = 0,$$

allowing one to define the eigen binding energy of the system of two particles of k_0. Here, N is the number of equations; $h = R/N$ is the step of the finite-difference grid; R is an interval of the solution of the equation, for example, from zero to 30 fm, and

$\alpha_n = 1, \quad \alpha_N = 2, \quad \theta_n = k^2h^2 - V_nh^2 - 2,$

$\theta_N = k^2h^2 - V_Nh^2 - 2 + 2hf(\eta,L,Z_N), \quad Z_N = 2kr_N,$

$r_n = nh, \quad n = 1,2 \ldots..N, \qquad k = \sqrt{|k^2|},$

$$f(\eta, L, Z_n) = -k - \frac{2k\eta}{Z_n} - \frac{2k(L-\eta)}{Z_n^2},$$

where $V_n = V(r_n)$ is the potential of the interaction clusters for point r_n. Recording of the boundary conditions in the form of a logarithmic derivative $f(\eta,L,Z_n)$ allows us to consider the Coulomb interaction, i.e. the effects, and an asymptotic of the WF of the Whittaker function for the BS.

This type of logarithmic derivative of the wave function of the bound state in the external area can be obtained from the integrated representation of the Whittaker function [27]

$$f(\eta, L, Z) = -k - \frac{2k\eta}{Z} - \frac{2k(L-\eta)}{Z^2} S,$$

where

$$S = \frac{\int_0^\infty t^{L+\eta+1}(1+t/z)^{L-\eta-1} e^{-t} dt}{\int_0^\infty t^{L+\eta}(1+t/z)^{L-\eta} e^{-t} dt}.$$

The calculations show that the S value does not exceed 1.05 and its influence on the binding energy of the two-body system is negligible.

The calculation of a determinant of D_N is carried out on recurrent formulas of the form

$D_{-1} = 0, D_0 = 1,$ (1.2.15)

$D_n = \theta_n D_{n-1} - \alpha_n D_{n-2}$,
$n = 1 \ldots N$.

To find the wave functions of bound states, another recurrent process is used

$$u_0 = 0, \quad u_1 = \text{const.}, \qquad (1.2.16)$$
$$u_n = -\theta_{n-1} u_{n-1} - u_{n-2},$$
$$n = 2 \ldots N,$$

where const. is any number—this is usually set in the range 0.01–0.1.

As such, at the given energy of the system it is possible to find the determinant and wave function of the bound state. With the energy leading to zero determinants of

$$D_N(k_0) = 0,$$

it considers the eigen energy of system and the wave function at this energy presents the eigenfunctions of the problem.

The last recurrence relation is used also to search for the WF in the case of a continuous spectrum of eigenvalues, i.e. at the previously given energy ($k^2 > 0$) of particle scattering [10]. The text of the computer program written in Fortran-90 is given in [28].

1.2.5.2 The variation method

The second method for discovering the binding energy is based on variation of the decomposition of the wave function on a non-orthogonal Gaussian basis (VM). We briefly give a description of this method and the computer program written in Fortran-90 is provided in [28]. More detailed statements can be found in [10]. Wave functions in the matrix elements for the ground and resonance states are presented through decomposition on a non-orthogonal Gaussian basis of the form

$$\Phi_L(r) = \frac{\chi_L(r)}{r} = r^L \sum_i C_i \exp(-\beta_i r^2),$$

found by the variation method for the bound states or by the approximation of Gaussian functions of the numerical wave functions of resonance levels [29].

For the determination of the spectrum of eigen energies and wave functions in the standard variation method of decomposition of the WF on an orthogonal basis, the matrix problem is solved on the eigenvalues [30]

$$\sum_i (H_{ij} - EI_{ij})C_i = 0 ,$$

where H is a symmetric Hamiltonian matrix; I is a unity matrix; E stands for the eigenvalues; and C stands for the eigenvectors of the problem.

In this case, on the non-orthogonal basis of the Gaussian functions, we come to a generalized matrix problem of the form [31]

$$\sum_i (H_{ij} - EL_{ij})C_i = 0 ,$$

where L is the matrix of overlapping integrals, which, on an orthogonal basis, is turned into a unity matrix I.

By using the WF in the form given above, we can easily find the expressions for all two-body matrix elements [31]

$$H_{ij} = T_{ij} + V_{ij} + \left\langle j \left| \frac{Z_1 Z_2}{r} \right| i \right\rangle + \left\langle j \left| \frac{\hbar^2 L(L+1)}{2\mu r^2} \right| i \right\rangle ,$$

$$N_0 = \left[\sum C_i C_j L_{ij} \right]^{-1/2} ,$$

$$T_{ij} = -\frac{\hbar^2}{2\mu} \frac{\sqrt{\pi}(2L-1)!!}{2^{L+1}\beta_{ij}^{L+1/2}} \left\{ L(2L+1) - L^2 - \frac{\beta_i \beta_j (2L+1)(2L+3)}{\beta_{ij}^2} \right\} ,$$

$$V_{ij} = \int V(r) r^{2L+2} \exp(-\beta_{ij} r^2) ,$$

$$L_{ij} = \frac{\sqrt{\pi}(2L+1)!!}{2^{L+2}\beta_{ij}^{L+3/2}} ,$$

$$\left\langle j \left| \frac{Z_1 Z_2}{r} \right| i \right\rangle = \frac{Z_1 Z_2 \, L!}{2\beta_{ij}^{L+1}} ,$$

$$\left\langle j \left| \frac{\hbar^2 L(L+1)}{2\mu r^2} \right| i \right\rangle = \frac{\sqrt{\pi}(2L-1)!!}{2^{L+1}\beta_{ij}^{L+1/2}} \frac{L(L+1)\hbar^2}{2\mu} , \qquad \beta_{ij} = \beta_i + \beta_j .$$

In the case of the Gaussian potential of intercluster interaction, the matrix element of the V_{ij} potential is defined in the analytical form

$$V_{ij} = V_0 \frac{\sqrt{\pi}(2L+1)!!}{2^{L+2}(\beta_{ij}+\alpha)^{L+3/2}},$$

where V_0 and α are parameters of the depth and width of the potential.

1.2.5.3 Methods of solving the generalized matrix problem

Here, we briefly present the methods of solving the generalized matrix problem [2]. By considering the eigenvalues and eigenfunctions of the generalized matrix problem, after the decomposition of the WF on a non-orthogonal Gaussian basis, we proceed from the standard Schrödinger equation in the general form [32]

$$H\chi = E\chi,$$

where H is a Hamiltonian; E is the energy of the system; and χ is the wave function.

Expanded in a series of WFs on a non-orthogonal variation basis

$$\chi = \sum_i C_i \varphi_i,$$

and set in the initial system, we multiply from the left using a complex interfaced basic function φ_i^* and integrating by all variables. As a result, we obtain the known matrix system of the form [33]

$$(H - EL)C = 0.$$

This gives the generalized matrix problem for finding eigenvalues and eigenfunctions [34,35]. If the decomposition of the WF is carried out on an orthogonal basis, the matrix of overlapping integrals L turns into a unity matrix I, and we have a standard problem on eigenvalues, for the solution of which there is a set of methods [36].

For solutions of the generalized matrix problem, there are also a number of known methods, given, for example, in [16]. Here at the beginning, we will stop using a standard method for the solution of the generalized matrix problem for the Schrödinger equation, which arises in the use of the non-

orthogonal variation basis in nuclear physics/nuclear astrophysics. Then, we consider its modification or an alternative method, which can be more conveniently applied to the solution of this problem in numerical calculations by modern computers [34].

Therefore, to determine the spectrum of eigenvalues of energy and wave functions in the variation method, using the decomposition of the WF on a non-orthogonal Gaussian basis, the generalized matrix problem on eigenvalues [16] is solved by

$$\sum_i (H_{ij} - EL_{ij})C_i = 0 \ , \qquad (1.2.17)$$

where H is a symmetric Hamiltonian matrix; L is the matrix of overlapping integrals; E stands for eigenvalues of the energy; and C stands for the eigenvectors of the problem.

Presenting matrix L in the form of multiplication of the lower N and the upper V triangular matrices [35], after simple transformations, we move on to the usual eigenvalue problem

$$H'C' = EIC',$$

or

$$(H' - EI)C' = 0,$$

where

$$H' = N^{-1}\mathrm{H}V^{-1}, \qquad C' = VC,$$

and V^{-1} and N^{-1} are the inverse matrices in relation to the V and N matrices.

Furthermore, we find the matrices of N and V, carrying out a triangularization of the symmetric L matrix [36], for example, by the Khaletsky method [35]. Then, we determine the inverse matrices N^{-1} and V^{-1}, for example, by the Gauss method and calculate the matrix elements $H' = N^{-1}\mathrm{H}V^{-1}$. Furthermore, we find the total diagonal of the E matrix $(H' - EI)$ and calculate its determinant $\det(H' - EI)$ at energy E.

Energy E leads us to the zero determinant of the eigen energy of the problem and the eigenvectors of the orthogonal equation correspond to its C' vectors. Once we know C', it is not difficult to find the eigenvectors of the initial problem C (1.2.17), because the matrix V^{-1} is already known. The method described for the generalized matrix problem, applied to the usual matrix problem on eigenvalues and functions, is called Schmidt

orthogonalization [27]. However, in some problems, at some values of the variation parameters, the procedure for finding the inverse matrix is unstable and the working of the computer program results in an overflow.

As such, we consider an alternative method for the numerical solution of the generalized matrix problem on eigenvalues, free of such difficulties and having a higher processing speed on the computer. The initial matrix equation (1.2.17) is the homogeneous system of linear equations and has nontrivial solutions only if its determinant, det(*H* - *EL*), is equal to zero. For numerical methods realized using a computer, it is not obligatory to decompose the matrix *L* to the triangular matrices and find a new *H′* matrix and new *C′* vector, defining the inverse matrices as described above in the use of the standard method.

It is possible to decompose at the non-diagonal, the symmetric matrix *(H - EL)* to the triangular matrix and, by numerical methods in the set area of values, to look for the energies that give us the zero of its determinant, i.e. that are eigen energies. In a real physical problem, it is usually not required to look for all eigenvalues and eigenfunctions; rather, it is necessary to find only 1 or 2 eigenvalues for a certain system energy and, as a rule, the lowest values and eigen wave functions correspond to them.

As such, using the Khaletsky method for example, the initial *(H - EL)* matrix decomposes in to two triangular matrices and, in the main diagonal of the top triangular *V* matrix, we have the units

$$A = H - EL = NV.$$

Its determinant at the condition of det(*V*) = 1 [35] is calculated

$$D(E) = \det(A) = \det(N)\cdot\det(V) = \det(N) = \prod_{i=1}^{m} n_{ii}$$

for zero, by which we find the necessary eigenvalue *E*, i.e. the value of energy looked for. Here, *m* is the dimension of the matrices and a determinant of the triangular *N* matrix is equal to the product of its diagonal elements [35].

Thus, the result is quite a simple problem to search for the zero functionality of one variable

$$D(E) = 0,$$

the numerical solution of which does not display significant complexity and can be executed with the desired accuracy, for example, by the bisection

method [37].

As a result, we remove the need to look for two inverse matrices, V and N, and to carry out several matrix multiplications to obtain a new H' matrix and then a final eigenvector matrix C. The lack of such operations, especially the search for the inverse matrix, considerably increases the speed of finding the solution using a computer, irrespective of the programming language.

It is possible to use the concept of residuals [16] for accurate estimation of the solution, i.e. the accuracy of the decomposition of an initial matrix to two triangular matrices. After the decomposition of matrix A to the triangular, the matrix of residuals [16] is calculated as the difference between the initial matrix A and the matrix

$$S = NV,$$

where N and V are the found numerical triangular matrices. The difference of all elements with an initial A matrix is calculated by

$$A_N = S - A.$$

The A_N matrix of residuals gives a deviation of the approximate NV value found by the numerical methods from true values of each element of an initial A matrix. It is possible to carry out the summation of all elements of the A_N matrix to obtain the numerical value of the residual. In all variational calculations given here, the method described above was used and the maximum value of any element of the A_N matrix did usually not exceed the 10^{-10} value.

The stated method, which is appears quite obvious in its numerical execution, allows us to obtain good stability for the algorithm of the solution of any considered physical problem and does not lead to the overflow problem during the working of the computer program [38]. Thus, the described alternative method for finding the eigenvalues of the generalized matrix problem [10], considered on the basis of variation methods for the solution of the Schrödinger equation, and with the use of a non-orthogonal variation basis, removes the instability arising in the application of the usual methods of the solution of such mathematical problems, i.e. the usual method of Schmidt orthogonalization.

1.2.6 Methods of calculating the Coulomb phase shifts

For the practical calculation of the characteristics of nuclear reactions and scattering processes, in many cases, it is necessary to know, as a rule with high precision, the numerical values of the Coulomb functions for the given point R and Coulomb phase shifts in the wide range of values of the Coulomb parameter η. There are a number of numerical methods that can be applied to find these values; however, the known ways of calculating Coulomb phase shifts have a number of shortcomings and in using them it is necessary to observe a certain caution.

The Coulomb phase shifts are defined through the G-function as follows [6,39]

$\sigma_L = \arg\{\Gamma(L+1+i\eta)\}$ and to satisfy the recurrent process

$$\sigma_L = \sigma_{L-1} + \operatorname{arctg}\left(\frac{\eta}{L}\right),$$

where $\eta = \dfrac{\mu Z_1 Z_2}{\hbar^2 k}$ is the Coulomb parameter; μ is the reduced mass of two particles; k is the wave number of the relative movement and $k^2 = 2\mu E/\hbar^2$; and E is the energy of the colliding particles in the center of mass. From this it is possible to obtain the following obvious expression

$$\alpha_L = \sigma_L - \sigma_0 = \sum_{n=1}^{L} \operatorname{arctg}\left(\frac{\eta}{n}\right), \qquad \alpha_0 = 0. \tag{1.2.18}$$

The most natural impression of the Coulomb phase shifts is gained on the basis of an integrated formula for the Γ-function [39,52]

$\sigma_L = \operatorname{arctg}(y/x)$,

where

$$y = \int_0^\infty \exp(-t)t^L sin(\eta \ln t)dt$$
$$x = \int_0^\infty \exp(-t)t^L cos(\eta \ln t)dt \tag{1.2.19}$$

However, the direct calculation of these integrals appears rather a complex problem because the subintegral functions are quickly oscillating at $t \to 0$. Therefore, different approximations and asymptotic decomposition, for example, such as the representation of the phase shift at $L = 0$, are often used in the form of [41]

$$\sigma_0 = -\eta + \frac{\eta}{2}\ln(\eta^2+16) + \frac{7}{2}\mathrm{arctg}(\eta/4) - [\mathrm{arctg}\eta + \mathrm{arctg}(\eta/2) + \mathrm{arctg}(\eta/3)] -$$

$$-\frac{\eta}{12(\eta^2+16)}\left[1+\frac{1}{30}\frac{\eta^2-48}{(\eta^2+16)^2}+\frac{1}{105}\frac{\eta^4-160\eta^2+1280}{(\eta^2+16)^4}+....\right]$$

or for $L >> 1$ [6]

$$\sigma_L = \alpha(L+1/2) + \eta(\ln\beta - 1) + \frac{1}{\beta}\left(-\frac{\sin\alpha}{12}+\frac{\sin 3\alpha}{360\beta^2}-\frac{\sin 5\alpha}{1260\beta^4}+\frac{\sin 7\alpha}{1680\eta^6}-...\right)$$

where

$$\alpha = \mathrm{arctg}\left(\frac{\eta}{L+1}\right) \quad , \quad \beta = \sqrt{\eta^2+(L+1)^2} \quad .$$

Using these formulae, all other phase shifts are defined from the recurrent relations (1.2.18). Though both representations can be processed at high speed on a computer, the phase shifts come out with some error, which can only be estimated by comparing the obtained result with the tabular data or calculations of the exact formulae. In addition, the last formula is right only at $L \approx 100$ and the recurrent process gives an additional error in the value of the phase shifts.

Other representations of the Coulomb phase shifts also are known, in particular, at $\eta >> 1$ [42]

$$\sigma_0 = \frac{\pi}{4} + \eta(\log\eta - 1) - \sum_{s=1}^{\infty}\frac{B_s}{2s(2s-1)\eta^{2s-1}} \quad , \qquad (1.2.20)$$

where B_s stands for the Bernoulli numbers [39]; however, the application of a similar decomposition works well only at $\eta \approx 100$. In [41,42], it has been shown that it is possible to obtain eight true signs taking into account only

the first member of the sum (1.2.20) at $\eta = 85$. At small η, a row converges badly and requires the setting or calculation of the Bernoulli numbers.

In [41], we find another way to determine the Coulomb phase shifts

$$\sigma_L = \eta\Psi(L+1) + \sum_{n=1}^{\infty}\left[\frac{\eta}{L+n} - \text{arctg}\left(\frac{\eta}{L+n}\right)\right] , \qquad (1.2.21)$$

which can be obtained from the known form of the recorded Γ-function [39]

$$\Gamma(z) = \Gamma(x+iy) = r\exp(i\phi) = r(\cos\phi + i\sin\phi),$$

where

$$\varphi = y\Psi(x) + \sum_{n=0}^{\infty}(\text{tg}\omega_n - \omega_n) \quad , \qquad \omega_n = \text{arctg}\left(\frac{y}{x+n}\right) \quad ,$$

and $\Psi(x)$ is a logarithmic derivative of the Γ-function [39], which, for the whole argument has the form

$$\Psi(L+1) = -C+1+1/2+.....+1/L.$$

Here, $C = 0.5772156649.....$ is Euler's constant [39]. Such a series will congregate quicker when η is less and L is more. This formula covers the area opposite to that represented in (1.2.20) and at $1 < \eta < 50$ both decompositions show poor convergence.

To estimate the remainder term of series (1.2.21), we decompose an arctangent in series at $\eta/n << 1$, which is always possible at big n or small η. Then we obtain

$$\sigma_0 = -C\eta + \sum_{n=1}^{\infty}\left(\frac{\eta^3}{3n^3} - \frac{\eta^5}{5n^5} + \frac{\eta^7}{7n^7} - ...\right) \quad . \qquad (1.2.22)$$

From this, it is clear that the remainder of series will have an order of the value η^3/n^2 [16]. A series (1.2.22) at $\eta > 1$ converges rather poorly and as for obtaining, for example, a relative accuracy of 10^{-8}, it is necessary to take into account the tens of thousands of terms in this series.

However, such a row allows for the significant improvement of convergence at $\eta \approx 1$ [50] after transformation to the form

$$\sigma_0 = -\eta C + \frac{1}{3}\eta^3 S + \sum_{n=1}^{\infty}\left[\frac{\eta}{n} - \operatorname{arctg}\left(\frac{\eta}{n}\right) - \frac{1}{3}\frac{\eta^3}{n^3}\right] , \qquad (1.2.23)$$

where $S = \sum_{k=1}^{\infty}\frac{1}{k^3}$ = 1.202056903... . It is simple to discover that the residual term of such a series is equal to η^5/n^4 and for obtaining eight true signs it is necessary to consider only a few hundred members of the series at $\eta \approx 1$.

Series (1.2.23), given above, allows additional improvement of convergence, after its transformation to the form [50]

$$\sigma_0 = -\eta C + \frac{1}{3}\eta^3 S - \frac{1}{5}\eta^5 D + \sum_{n=1}^{\infty}\left[\frac{\eta}{n} - \operatorname{arctg}\left(\frac{\eta}{n}\right) - \frac{1}{3}\frac{\eta^3}{n^3} + \frac{1}{5}\frac{\eta^5}{n^5}\right] , \qquad (1.2.24)$$

where $D = \sum_{k=1}^{\infty}\frac{1}{k^5}$ = 1.036927751... . Such a series converges very quickly and has a residual member of an order of η^7/n^6. To satisfy the accuracy stated above, it is necessary to consider only a few tens of terms.

A program in BASIC for the calculation of Coulomb phase shifts is given below, using the decomposition method described above in a row and on the basis of integrated representations (1.2.19) and series (1.2.24). The description of some parameters is given in the program.

REM PROGRAM OF THE CALCULATION OF THE COULOMB PHASE SHIFTS

```
DEFDBL A-Z
DEFINT I,J,K,L,N,M
M=4000
DIM V(M): CLS
EPS=1.0E-15: REM CALCULATION ACCURACY
H=1: REM COULOMB PARAMETER
REM CALCULATION OF PHASE SHIFTS ON THE BASIS OF RANKS
C=0.577215665: A1=1.202056903/3: A2=1.036927755/5: F=0: S1=0
3 F=F+1
B=H/F-ATN(H/F)
S1=S1+B
IF B<EPS GOTO 2
GOTO 3
2 D=0: S=0
4 D=D+1
A=H/D-ATN(H/D)-(H/D)^3/3+(H/D)^5/5
```

```
S=S+A
IF A<EPS GOTO 1
GOTO 4
1 FAZ=-C*H+A1*H^3-A2*H^5+S
FAZ1=-C*H+S1
PRINT "FAZ = ";FAZ; "    N = ";D
PRINT "FAZ1 = ";FAZ1;"  N = ";F
REM *** CALCULATION OF THE PHASE SHIFTS ON THE BASIS OF
INTEGRATED REPRESENTATION ***
NN=4000: E=1E-300: N=500: R1=0.1: R2=1: R3=40: HH=R1/N
H1=HH/NN: H2=(R2-R1)/NN: H3=(R3-R2)/NN: YY=0
FOR K=1 TO N
AA=(K-1)*HH
FOR I=0 TO NN
X=H1*I+AA+E
V(I)=EXP(-X)*SIN(H*LOG(X))
NEXT I
CALL SIM(NN,H1,V(),Y1)
YY=YY+Y1
NEXT K
FOR I=0 TO NN
X=H2*I+R1
V(I)=EXP(-X)*SIN(H*LOG(X))
NEXT
CALL SIM(NN,H2,V(),Y1)
YY=YY+Y1
FOR I=0 TO NN
X=H3*I+R2
V(I)=EXP(-X)*SIN(H*LOG(X))
NEXT
CALL SIM(NN,H3,V(),Y1)
YY=YY+Y1
XX=0
FOR K=1 TO N
AA=(K-1)*HH
FOR I=0 TO NN
X=H1*I+AA+E
V(I)=EXP(-X)*COS(H*LOG(X))
NEXT I
CALL SIM(NN,H1,V(),X1)
XX=XX+X1
```

```
NEXT K
FOR I=0 TO NN
X=H2*I+R1
V(I)=EXP(-X)*COS(H*LOG(X))
NEXT
CALL SIM(NN,H2,V(),X1)
XX=XX+X1
FOR I=0 TO NN
X=H3*I+R2
V(I)=EXP(-X)*COS(H*LOG(X))
NEXT
CALL SIM(NN,H3,V(),X1)
XX=XX+X1
AA=ATN(YY/XX)
PRINT "FAZA = ";AA
END

SUB SIM(N,H,V(5000),S)
A=0: B=0
FOR I=1 TO N-1 STEP 2
B=B+V(I)
NEXT
FOR J=2 TO N-2 STEP 2
A=A+V(J)
NEXT
S=H*(V(0)+V(N)+2*A+4*B)/3
END SUB
```

The phase shifts given in Table 1.2.1 have been calculated using this program on the basis of formula (1.2.24) [50]. The error makes about half of the last sign.

Table 1.2.1. Calculation of the Coulomb phase shifts.

η	σ_0	η	σ_0
0.1	-0.05732294	0.6	-0.27274381
0.2	-0.11230222	0.8	-0.30422560
0.3	-0.16282067	1.0	-0.30164032
0.4	-0.20715583	1.3	-0.23921678
0.5	-0.24405830	1.5	-0.16293977

We note that, for obtaining identical accuracy when calculating by formulae (1.2.24) and (1.2.22), in the last case designated as σ_1, it is necessary to consider approximately seven hundred times more members of the term (with an accuracy of 10^{-15}), as is clear from the given results of the calculation at $\eta = 1$

$\sigma_0 = -0.30164032059$ for $N = 106$,
$\sigma_1 = -0.30164032060$ for $N = 69337$.

The calculation of the Coulomb phase shifts on the basis of integrated representation can be executed to divide all intervals of integration into several parts. The most strongly subintegral function changes at small t, therefore we divide the integration interval into the following parts 0–0.1, 0.1–1, and 1–40 (at $t = 40$ the subintegral function has a value of the order 10^{-17}), and we divide the first part (0–0.1) into $N = 500$ parts. The calculation of the integrals by all parts gives us the phase shift value -0.30164031, which differs from the result obtained above on the basis of rank only on the unit of the eighth sign. We note that the calculation of such integrals (1.2.19) on an Intel Pentium 200 MMX computer takes several minutes, while the calculation of a row (1.2.24) takes a fraction of a second.

1.2.7 Methods of calculating the Coulomb functions

Here we move on to consideration of the Coulomb scattering functions, the regular $F_L(\eta,\rho)$ and irregular $G_L(\eta,\rho)$ parts of which are linearly independent solutions of the radial Schrödinger equation (1.2.1), only with a Coulomb potential, which has the form [6,9]

$$\chi_L''(\rho) + \left(1 - \frac{2\eta}{\rho} - \frac{L(L+1)}{\rho^2}\right)\chi_L(\rho) = 0 \quad , \tag{1.2.25}$$

where $\chi_L = F_L(\eta,\rho)$ or $G_L(\eta,\rho)$; $\rho = kr$; and $\eta = \frac{\mu Z_1 Z_2}{\hbar^2 k}$ is the Coulomb parameter.

The Wronskian of these functions and their derivatives have the following appearance [6]

$$W_1 = F_L' G_L - F_L G_L' = 1,$$
$$W_2 = F_{L-1} G_L - F_L G_{L-1} = \frac{L}{\sqrt{\eta^2 + L^2}}. \qquad (1.2.26)$$

The recurrence relations are written in the form

$$L[(L+1)^2 + \eta^2]^{1/2} u_{L+1} = (2L+1)\left[\eta + \frac{L(L+1)}{\rho}\right] u_L - (L+1)[L^2 + \eta^2]^{1/2} u_{L-1},$$

$$(L+1)u_L' = \left[\frac{(L+1)^2}{\rho} + \eta\right] u_L - [(L+1)^2 + \eta^2]^{1/2} u_{L+1}, \qquad (1.2.27)$$

$$Lu_L' = [L^2 + \eta^2]^{1/2} u_{L-1} - \left[\frac{L^2}{\rho} + \eta\right] u,$$

where $u_L = F_L(\eta,\rho)$ or $G_L(\eta,\rho)$. The asymptotics at $\rho \to \infty$ can be presented in the form [40]

$$F_L = \sin(\rho - \eta \ln 2\rho - \pi L/2 + \sigma_L), \qquad (1.2.28)$$
$$G_L = \cos(\rho - \eta \ln 2\rho - \pi L/2 + \sigma_L).$$

There are many methods and approximations for the calculation of the Coulomb functions [6,41,42,43,44,45,46,47]. However, a quickly converging representation allowing one to obtain the values with fine precision and for a wide range of values of the variables with only a small cost of computer time [48] has been described rather recently. The Coulomb functions in such a method are presented in the form of continued fractions [49]

$$f_L = F_L' / F_L = b_0 + \cfrac{a_1}{b_1 + \cfrac{a_2}{b_2 + \cfrac{a_3}{b_3 + \ldots.}}}, \qquad (1.2.29)$$

where

$b_0 = (L + 1)/\rho + \eta/(L + 1)$,

$b_n = [2(L + n) + 1][(L + n)(L + n + 1) + \eta\rho]$,

$a_1 = - \rho[(L + 1)^2 + \eta^2](L + 2)/(L + 1)$,

$a_n = - \rho^2[(L + n)^2 + \eta^2][(L + n)^2 - 1]$,

and

$$P_L + iQ_L = \frac{G_L' + iF_L'}{G_L + iF_L} = \frac{i}{\rho}\left(b_0 + \frac{a_1}{b_1 + \dfrac{a_2}{b_2 + \dfrac{a_3}{b_3 + \ldots.}}} \right), \tag{1.2.30}$$

where

$$b_0 = \rho - \eta, \qquad b_n = 2(b_0 + in), \tag{1.2.31}$$
$$a_n = - \eta^2 + n(n - 1) - L(L + 1) + i\eta(2n - 1).$$

Such a method of calculation is applicable in the range $\rho \geq \eta + \sqrt{\eta^2 + L(L+1)}$ and easily allows one to obtain high precision thanks to the fast convergence of the continued fractions. As the Coulomb η parameter usually has the value unit order and L, as a rule, a value of no more than 3–5, the method already yields good results at $\rho > 5$ fm. In this area, it is necessary to know the Coulomb functions by numerical calculation of the nuclear functions of scattering and reactions.

Using (1.2.29–1.2.31) it is possible to obtain good communication between the Coulomb functions and their derivatives [50,51]

$$F_L' = f_L F_L , \tag{1.2.32}$$
$$G_L = (F_L' - P_L F_L)/Q_L = (f_L - P_L)F_L/Q_L ,$$
$$G_L' = P_L G_L - Q_L F_L = [P_L(f_L - P_L)/Q_L - Q_L]F_L .$$

As such, setting some F_L values in point ρ, we find all other functions and their derivatives within the accuracy of a constant multiplier, defined

using the Wronskian (1.2.26). Calculation of the Coulomb functions for the given formulae and their comparison with the tabular material [52] show that it is possible to easily obtain eight to nine correct signs if ρ meets the above condition.

The text of a computer program for the calculation of the Coulomb scattering wave functions is given below. Here, the following designations hold.

G – Coulomb parameter,
L – orbital moment of this partial wave,
X – distance from the center, on which the Coulomb functions are calculated,
FF and GG – Coulomb functions,
FP and GP – their derivatives,
W – the Wronskian, determining the accuracy of calculation of the Coulomb functions (the first formula in expression (1.2.26)).

```
SUB CULFUN(G,X,L,FF,GG,FP,GP,W)
REM SUBPROGRAMME OF CALCULATION OF THE COULOMB
FUNCTIONS *****
Q=G:R=X: GK=Q*Q: GR=Q*R:RK=R*R: K=1: F0=1
B01=(L+1)/R+Q/(L+1):BK=(2*L+3)*((L+1)*(L+2)+GR)
AK= - R*((L+1)^2+GK)/(L+1)*(L+2):DK=1/BK: DEHK=AK*DK
S=B01+DEHK
1 K=K+1
AK= - RK*((L+K)^2 - 1)*((L+K)^2+GK)
BK=(2*L+2*K+1)*((L+K)*(L+K+1)+GR)
DK=1/(DK*AK+BK)
IF DK>0 GOTO 3
2 F0= - F0
3 DEHK=(BK*DK - 1)*DEHK
S=S+DEHK
IF (ABS(DEHK) - 1E - 10)>0 GOTO 1
FL=S: K=1:RMG=R - Q
LL=L*(L+1): CK= - GK - LL:DK=Q: GKK=2*RMG
HK=2: AA1=GKK*GKK+HK*HK: PBK=GKK/AA1
RBK= - HK/AA1: OMEK=CK*PBK-DK*RBK
EPSK=CK*RBK+DK*PBK: PB=RMG+OMEK: QB=EPSK
4 K=K+1: CK= - GK - LL+K*(K - 1): DK=Q*(2*K - 1)
HK=2*K: FI=CK*PBK - DK*RBK+GKK:
PSI=PBK*DK+RBK*CK+HK
```

```
AA2=FI*FI+PSI*PSI: PBK=FI/AA2: RBK= - PSI/AA2
VK=GKK*PBK - HK*RBK: WK=GKK*RBK+HK*PBK
OM=OMEK: EPK=EPSK
OMEK=VK*OM - WK*EPK - OM
EPSK=VK*EPK+WK*OM - EPK:
PB=PB+OMEK
QB=QB+EPSK
IF (ABS(OMEK)+ABS(EPSK) - 1E - 10)>0 GOTO 4
PL= - QB/R: QL=PB/R
G0=(FL - PL)*F0/QL
G0P=(PL*(FL - PL)/QL - QL)*F0
F0P=FL*F0
ALFA=1/(SQR(ABS(F0P*G0 - F0*G0P)))
GG=ALFA*G0
GP=ALFA*G0P
FF=ALFA*F0
FP=ALFA*F0P
W=1 - FP*GG+FF*GP
END SUB
```

The results of the control account of the Coulomb functions for $\eta = 1$ [53,54] and their comparison with the tabular data [52] are given in Table 1.2.2. It is clear that at $\eta = 1$ and $L = 0$, the correct results are given for $\rho = kr = 1$. The value of the Wronskian (1.2.26) presented in the form $(W_1 - 1)$ at any ρ does not exceed 10^{-15}-10^{-16}.

Table 1.2.2. Coulomb functions.

ρ	F_0 (Our calculation)	F_0 *[52]*	F_0' (Our calculation)	F_0' *[52]*
1	0.22752621	0.22753	0.34873442	0.34873
5	0.68493741	0.68494	-0.72364239	-0.72364
10	0.47756082	0.47756	0.84114311	0.84114
15	-0.97878958	-0.97879	0.31950815	0.31951
20	-0.32922554	-0.32923	-0.92214689	-0.92215

ρ	G_0	G_0 *[52]*	G_0'	G_0' *[52]*
1	2.0430972	2.0431	-1.2635981	-1.2636
5	-0.89841436	-0.89841	-0.51080476	-0.51080
10	0.94287424	0.94287	-0.43325965	-0.43326

15	0.34046374	0.34046	0.91053182	0.91053
20	-0.97242840	-0.97243	0.31370038	0.31370

ρ	F_2	G_2	F'_2	G'_2
1	1.47867E-02	1.26407E 01	4.70896E-02	-2.73727E 01
5	1.18637E 00	3.82961E-01	1.54145E-01	-7.93149E-01
10	-9.63615E-01	4.81305E-01	4.24848E-01	8.25557E-01
15	-2.27973E-01	-1.01918E 00	-9.33599E-01	2.12743E-01
20	-1.01801E 00	-1.62845E-01	-1.55072E-01	-9.57506E-01

The correctness of the function's calculation at $L = 2$ is easy to check using the recurrent formulae (1.2.27). Knowing the functions and their derivatives at $L = 0$, in the second formula (1.2.27) we find the functions at $L = 1$. Then, using the third formula, we find their derivatives for $L = 1$. Continuing this process it is easy to find all functions and their derivatives at any L [50].

Below, we provide the text of the same computer program for the calculation of the Coulomb scattering wave functions in the algorithmic language Fortran-90. The designated parameters practically coincide with the previous program. Here, on the basis of (1.2.29) and (1.2.30), the functions are defined at $L = 0$; for finding functions at all other L, the recurrence relations are used. To ensure the greatest possible accuracy of the results, as in the previous case, double accuracy is used. Here, the following designations are set.

Q – Coulomb parameter η,
LM – orbital moment of this partial wave,
R – distance from the center on which the Coulomb functions are calculated,
F and G – Coulomb functions,
W – the Wronskian, determining the accuracy of the calculation of the Coulomb functions (the first formula in expression (1.2.26)).

```
SUBROUTINE CULFUN(LM,R,Q,F,G,W)
! SUBPROGRAMME OF CALCULATION OF THE COULOMB
! FUNCTIONS
IMPLICIT REAL(8) (A-Z)
INTEGER L,K,LL,LM
EP=1.0D-015; L=0; F0=1.0D0
GK=Q*Q; GR=Q*R; RK=R*R
B01=(L+1)/R+Q/(L+1)
K=1; BK=(2*L+3)*((L+1)*(L+2)+GR)
```

```
AK=-R*((L+1)**2+GK)/(L+1)*(L+2)
DK=1.0D0/BK
DEHK=AK*DK
S=B01+DEHK
15 K=K+1
AK=-RK*((L+K)**2-1)*((L+K)**2+GK)
BK=(2*L+2*K+1)*((L+K)*(L+K+1)+GR)
DK=1.D0/(DK*AK+BK)
IF (DK>0.0D0) GOTO 35
25 F0=-F0
35 DEHK=(BK*DK-1.0D0)*DEHK
S=S+DEHK
IF (ABS(DEHK)>EP) GOTO 15
FL=S; K=1; RMG=R-Q; LL=L*(L+1)
CK=-GK-LL; DK=Q; GKK=2.0D0*RMG
HK=2.0D0; AA1=GKK*GKK+HK*HK
PBK=GKK/AA1; RBK=-HK/AA1
AOMEK=CK*PBK-DK*RBK
EPSK=CK*RBK+DK*PBK
PB=RMG+AOMEK; QB=EPSK
52 K=K+1
CK=-GK-LL+K*(K-1); DK=Q*(2*K-1)
HK=2.0D0*K; FI=CK*PBK-DK*RBK+GKK
PSI=PBK*DK+RBK*CK+HK
AA2=FI*FI+PSI*PSI; PBK=FI/AA2
RBK=-PSI/AA2; VK=GKK*PBK-HK*RBK
WK=GKK*RBK+HK*PBK; OM=AOMEK
EPK=EPSK; AOMEK=VK*OM-WK*EPK-OM
EPSK=VK*EPK+WK*OM-EPK; PB=PB+AOMEK
QB=QB+EPSK
IF ((ABS(AOMEK)+ABS(EPSK))>EP) GOTO 52
PL=-QB/R; QL=PB/R
G0=(FL-PL)*F0/QL; G0P=(PL*(FL-PL)/QL-QL)*F0; F0P=FL*F0
ALFA=1.0D0/DSQRT(ABS(F0P*G0-F0*G0P))
G=ALFA*G0; GP=ALFA*G0P
F=ALFA*F0; FP=ALFA*F0P
W=1.0D0-FP*G+F*GP
IF (LM==0) GOTO 123
AA=DSQRT(1.0D0+Q**2)
BB=1.0D0/R+Q
F1=(BB*F-FP)/AA
```

```
G1=(BB*G-GP)/AA
WW1=F*G1-F1*G-1.0D0/DSQRT(Q**2+1.0D0)
IF (LM==1) GOTO 234
DO L=1,LM-1
AA=DSQRT((L+1)**2+Q**2)
BB=(L+1)**2/R+Q
CC=(2*L+1)*(Q+L*(L+1)/R)
DD=(L+1)*DSQRT(L**2+Q**2)
F2=(CC*F1-DD*F)/L/AA
G2=(CC*G1-DD*G)/L/AA
WW2=F1*G2-F2*G1-(L+1)/DSQRT(Q**2+(L+1)**2)
F=F1; G=G1; F1=F2; G1=G2
ENDDO
234 F=F1; G=G1
123 END
```

This program yields the same results in terms of the control account as previously shown in BASIC.

1.3 Program for the calculation of phase shifts for the central real potentials

Below we present a computer program for the calculation of the real phase shifts of elastic scattering by the finite-difference method and the Runge-Kutta method in BASIC, showing good coincidence of the results obtained in both ways. Here the following designations are accepted.

NN – lowest value of the energy cycle,
NV – top value of the energy cycle,
NH – step of the energy cycle,
EH – energy step,
EN – the lowest value of energy,
AM1 – the mass of the first particle in amu,
AM2 – the mass of the second particle in amu,
PM – the reduced mass of μ,
Z1 – charge of the first particle in terms of charge “e”,
Z2 – charge of the second particle in terms of charge “e”,
A1 – $\hbar^2/M_N = 41.4686$ constant, where M_N is the mass of a nucleon in amu, equal to 1,
AK1 – constant at Coulomb potential $1.439975\, Z_1 Z_2\, 2\mu/\hbar^2$,
N – number of steps at the integration of the Schrödinger equation,

H – step value for the integration of the Schrödinger equation,
R00 – distance at which the interlacing of the numerical functions with asymptotics is carried out,
V0 – depth of the nuclear potential,
R0 – radius of the nuclear potential,
RCU – Coulomb radius,
L – orbital moment,
EL – energy of particles in the laboratory system,
ECM – energy of particles in the system of the center of masses,
SK – square of the k^2 wave number,
SS – wave number k,
G – Coulomb parameter = $3.44476\ 10^{-2} Z_1 Z_2\ \mu/k$,
F1(I) – the phase shift at the set energy obtained by the finite-difference method,
F2(I) – the phase shift shifts at the set energy obtained by the Runge-Kutta method,
ABS(F1(I) - F2(I)) – difference of phase shifts in the degree obtained by the different methods,

ABS(F1(I) - F2(I))/ABS(F1(I))*100 – relative difference of the phase shifts in percentages.

REM PROGRAM OF CALCULATION OF THE REAL PHASE SHIFTS

```
REM *** DETERMINATION OF VARIABLES ****
DEFDBL A - Z: DEFINT I,J,K,L,N,M: CLS
NN=4000: DIM EL(100), F1(100), ECM(100), F2(100)
DIM V1(NN), U(NN), V(NN), U1(NN)
PRINT "  EL    ECM    FKR    FRK   ERR - DEG   ERR - %"
REM ***** DETERMINATION OF THE INITIAL VALUES ******
PI=3.14159265359: NN=1: NV=20: NH=1: EH=1: EN=0
AM1=2: AM2=4: Z1=1: Z2=2: A1=41.4686
 PM=AM1*AM2/(AM1+AM2)
B1=2*PM/A1: AK1=1.439975*Z1*Z2*B1: N=1000: R00=20: H=R00/N
V0=76.12: R0=.2: A2= - V0*B1: RCU=0: L=0
REM *********** BEGINNING OF THE CYCLE ON ENERGY ******
FOR I=NN TO NV STEP NH: EL(I)=EN+EH*I: ECM(I)=EL(I)*PM/AM1
SK=ECM(I)*B1: SS=SQR(SK): G=3.44476E - 02*Z1*Z2*PM/SS
REM ***** CALCULATION OF THE COULOMB FUNCTIONS *****
X1=H*SS*(N - 4): X2=H*SS*(N): CALL CUL(G,X1,L0,F1,G1,W1)
CALL CUL(G,X2,L0,F2,G2,W2)
```

```
REM *** CALCULATION OF THE PHASE SHIFTS OF BY THE
FINITE-DIFFERENCE METHOD ***
CALL FUN(N,H,U1(),L,A2,AK1,SK,R0,RCU)
D1=U1(N - 4): D2=U1(N): AF= - (F1 - F2*D1/D2)/(G1 - G2*D1/D2)
FF=ATN(AF): IF FF>0 GOTO 90: FF=FF+PI
90 XN1=(COS(FF)*F2+SIN(FF)*G2)/D2: F1(I)=FF*180/PI
REM *** CALCULATION OF THE PHASE SHIFTS BY THE RUNGE-
KUTT METHOD***
CALL FUNRK(V(),N,H): D1=V(N - 4): D2=V(N)
AF= - (F1 - F2*D1/D2)/(G1 - G2*D1/D2): F33=ATN(AF)
IF F33>0 GOTO 91: F33=F33+PI
91 XN2=(COS(F33)*F2+SIN(F33)*G2)/D2: F2(I)=F33*180/PI
REM ********* PHASE SHIFT PRINTING **************
PRINT USING "+#.####^^^^ "; EL(I); ECM(I); F1(I); F2(I); ABS(F1(I) -
F2(I)); ABS(F1(I) - F2(I))/ABS(F1(I))*100: NEXT I
STOP

SUB CUL(G,X,L,F0,G0,W)
REM CALCULATION OF COULOMB SCATTERING FUNCTIONS
Q=G: R=X: F0=1: K=1: GK=Q*Q: GR=Q*R: RK=R*R
B01=(L+1)/R+Q/(L+1): BK=(2*L+3)*((L+1)*(L+2)+GR)
AK= - R*((L+1)^2+GK)/(L+1)*(L+2): DK=1/BK: DEHK=AK*DK
S=B01+DEHK
1 K=K+1: AK= - RK*((L+K)^2 - 1)*((L+K)^2+GK)
BK=(2*L+2*K+1)*((L+K)*(L+K+1)+GR): DK=1/(DK*AK+BK)
IF DK>0 GOTO 3
2 F0= - F0
3 DEHK=(BK*DK - 1)*DEHK: S=S+DEHK
IF (ABS(DEHK) - 1E - 06)>0 GOTO 1: FL=S: K=1: RMG=R - Q
LL=L*(L+1): CK= - GK - LL: DK=Q: GKK=2*RMG: HK=2
AA1=GKK*GKK+HK*HK: PBK=GKK/AA1: RBK= - HK/AA1
OMEK=CK*PBK - DK*RBK: EPSK=CK*RBK+DK*PBK
PB=RMG+OMEK: QB=EPSK
5 K=K+1: CK= - GK - LL+K*(K - 1): DK=Q*(2*K - 1): HK=2*K
FI=CK*PBK - DK*RBK+GKK: PSI=PBK*DK+RBK*CK+HK
AA2=FI*FI+PSI*PSI: PBK=FI/AA2: RBK= - PSI/AA2
VK=GKK*PBK - HK*RBK: WK=GKK*RBK+HK*PBK
OM=OMEK: EPK=EPSK: OMEK=VK*OM - WK*EPK - OM
EPSK=VK*EPK+WK*OM - EPK: PB=PB+OMEK: QB=QB+EPSK
IF (ABS(OMEK)+ABS(EPSK) - 1E - 06)>0 GOTO 5: PL= - QB/R
QL=PB/R: G0=(FL - PL)*F0/QL: G0P=(PL*(FL - PL)/QL - QL)*F0
```

```
F0P=FL*F0: ALFA=1/(SQR(ABS(F0P*G0 - F0*G0P))): G0=ALFA*G0
GP=ALFA*G0P: F0=ALFA*F0: FP=ALFA*F0P: W=1 - FP*G0+F0*GP
END SUB

SUB FUN(N,H,U(5000),L,AV,AK,SK,R0,RCU)
REM ***** THE SOLUTION OF THE SCHRÖDINGER EQUATION BY
THE FINITE-DIFFERENCE METHOD *****
U(0)=0:  U(1)=0.001: HK=H*H: FOR K=1 TO N - 1: X=K*H
Q1=AV*EXP( - R0*X*X)+L*(L+1)/(X*X): IF X>RCU GOTO 11
Q1=Q1+(3 - (X/RCU)^2)*AK/(2*RCU): GOTO 22
11 Q1=Q1+AK/X
22 Q2= - Q1*HK - 2+SK*HK: U(K+1)= - Q2*U(K) - U(K - 1): NEXT K
END SUB

SUB FUNRK(V(5000),N,H)
REM ****** THE SOLUTION OF THE SCHRÖDINGER EQUATION
BY THE RUNGE-KUTT METHOD IN ALL AREA OF VARIABLES **
VA1=0: REM VA1 – The value of the function in zero
PA1=1.0E - 05: REM PA1 - The value of function on the first step
FOR I=0 TO N - 1: X=H*I+1.0E - 05
CALL RRUN(VB1,PB1,VA1,PA1,H,X)
VA1=VB1:  PA1=PB1:  V(I+1)=VA1: NEXT
END SUB

SUB RRUN(VB1,PB1,VA1,PA1,H,X)
REM ***** THE SOLUTION OF THE SCHRÖDINGER EQUATION BY
THE RUNGE-KUTT METHOD BY THE ONE STEP *****
X0=X: Y1=VA1: CALL F(X0,Y1,FK1): FK1=FK1*H: FM1=H*PA1
X0=X+H/2: Y2=VA1+FM1/2: CALL F(X0,Y2,FK2): FK2=FK2*H
FM2=H*(PA1+FK1/2): Y3=VA1+FM2/2: CALL F(X0,Y3,FK3)
FK3=FK3*H: FM3=H*(PA1+FK2/2): X0=X+H: Y4=VA1+FM3
CALL F(X0,Y4,FK4): FK4=FK4*H: FM4=H*(PA1+FK3)
PB1=PA1+(FK1+2*FK2+2*FK3+FK4)/6
VB1=VA1+(FM1+2*FM2+2*FM3+FM4)/6
END SUB

SUB F(X,Y,F)
REM * FUNCTION EVALUATION OF F (X, Y) IN THE RUNGE-KUTT
METHOD *
SHARED SK,A2,R0,AK1,L,RCU
VC=A2*EXP(-R0*X^2): IF X>RCU GOTO 121
```

```
VK=(3-(X/RCU)^2)*AK1/(2*RCU): GOTO 222
121 VK=AK1/X
222 F=-(SK-VK-VC-L*(L+1)/(X^2))*Y
END SUB
```

To carry out the control, we used the finite-difference method with the classical nucleon-nucleon Reid potential [55]. The form of $^1P_1$ potential and calculation of scattering phase shifts are given. Our calculations for phase shifts with such potentials are given in Table 1.3.1 in comparison with the Reid results.

Table 1.3.1. Comparison of results for the Reid potential.

E, MeV	δ, radian, [55]	δ, radian, (Our calculation)
48	-0.071	-0.072
144	-0.312	-0.314
208	-0.456	-0.458
352	-0.708	-0.710

It is clear from these results that the coincidence of both calculations, at an accuracy of about several thousands of radian, presents a good example of the efficiency of the numerical methods used and the accuracy of the working of the computer program described.

We thus compare the accuracy with which it is possible to obtain the phase shifts by two methods: the Runge-Kutta method and the finite-difference method. We give the calculation results of phase shifts for these two methods (FDM, finite-difference method and RKM, Runge-Kutta method) for the S scattering phase shift in the $^2H^4He$ system (parameters of the potential were obtained by us in [56] $V_0 = 76.12$ MeV, $\alpha = 0.2$ fm^{-2}, $R_c = 0$ fm, $L = 0$ and represent the alternative variant of similar potentials offered for the first time in [57,58,59,60]) and the extent of their coincidence in degrees (ERR - DEG) and percent (ERR - %) [61]. Here EL and ECM refer to the energy in the laboratory system and the system of the center of mass of the colliding particles, respectively.

EL	ECM	FKR	FRK	ERR - DEG	ERR - %
+1.0000E+00	+6.6667E-01	+1.5053E+02	+1.5052E+02	+8.4828E-03	+5.6353E-03
+2.0000E+00	+1.3333E+00	+1.2598E+02	+1.2597E+02	+1.2241E-02	+9.7170E-03
+3.0000E+00	+2.0000E+00	+1.0892E+02	+1.0890E+02	+1.4219E-02	+1.3055E-02
+4.0000E+00	+2.6667E+00	+9.5886E+01	+9.5871E+01	+1.5547E-02	+1.6214E-02
+5.0000E+00	+3.3333E+00	+8.5335E+01	+8.5319E+01	+1.6536E-02	+1.9378E-02
+6.0000E+00	+4.0000E+00	+7.6457E+01	+7.6440E+01	+1.7629E-02	+2.3057E-02
+7.0000E+00	+4.6667E+00	+6.8801E+01	+6.8782E+01	+1.8828E-02	+2.7365E-02
+8.0000E+00	+5.3333E+00	+6.2083E+01	+6.2063E+01	+1.9867E-02	+3.2000E-02
+9.0000E+00	+6.0000E+00	+5.6102E+01	+5.6081E+01	+2.0743E-02	+3.6974E-02
+1.0000E+01	+6.6667E+00	+5.0715E+01	+5.0693E+01	+2.1731E-02	+4.2848E-02
+1.1000E+01	+7.3333E+00	+4.5818E+01	+4.5795E+01	+2.2996E-02	+5.0189E-02
+1.2000E+01	+8.0000E+00	+4.1334E+01	+4.1310E+01	+2.4399E-02	+5.9028E-02
+1.3000E+01	+8.6667E+00	+3.7206E+01	+3.7180E+01	+2.5677E-02	+6.9014E-02
+1.4000E+01	+9.3333E+00	+3.3383E+01	+3.3356E+01	+2.6730E-02	+8.0071E-02
+1.5000E+01	+1.0000E+01	+2.9825E+01	+2.9798E+01	+2.7712E-02	+9.2913E-02
+1.6000E+01	+1.0667E+01	+2.6500E+01	+2.6471E+01	+2.8870E-02	+1.0894E-01
+1.7000E+01	+1.1333E+01	+2.3379E+01	+2.3349E+01	+3.0323E-02	+1.2970E-01

The worst result is shown in the last line with 0.13 % at an energy of 17 MeV. Following on, we give the results of calculations of the $S_{1/2}$ phase shift for elastic $^3H^4He$ scattering at low energies by two methods [61]. For the parameters of the potential, the following values were used: V_0 = -67.5 MeV; α = 0.15747 fm^{-2}; R_c = 3.095 fm; and L = 0 [56,61].

EL	ECM	FKR	FRK	ERR - DEG	ERR - %
+1.0000E-01	+4.2857E-02	+1.8000E+02	+1.8000E+02	+3.0506E-07	+1.6948E-07
+1.1000E+00	+4.7143E-01	+1.7204E+02	+1.7204E+02	+1.2686E-03	+7.3739E-04
+2.1000E+00	+9.0000E-01	+1.6139E+02	+1.6138E+02	+2.8364E-03	+1.7575E-03
+3.1000E+00	+1.3286E+00	+1.5211E+02	+1.5211E+02	+4.0288E-03	+2.6486E-03
+4.1000E+00	+1.7571E+00	+1.4419E+02	+1.4419E+02	+4.9487E-03	+3.4320E-03
+5.1000E+00	+2.1857E+00	+1.3729E+02	+1.3729E+02	+5.6562E-03	+4.1198E-03
+6.1000E+00	+2.6143E+00	+1.3113E+02	+1.3113E+02	+6.2638E-03	+4.7767E-03
+7.1000E+00	+3.0429E+00	+1.2555E+02	+1.2555E+02	+6.8101E-03	+5.4240E-03
+8.1000E+00	+3.4714E+00	+1.2045E+02	+1.2044E+02	+7.2653E-03	+6.0317E-03
+9.1000E+00	+3.9000E+00	+1.1574E+02	+1.1573E+02	+7.6262E-03	+6.5892E-03
+1.0100E+01	+4.3286E+00	+1.1134E+02	+1.1133E+02	+7.9425E-03	+7.1336E-03
+1.1100E+01	+4.7571E+00	+1.0721E+02	+1.0720E+02	+8.2671E-03	+7.7111E-03
+1.2100E+01	+5.1857E+00	+1.0331E+02	+1.0330E+02	+8.6088E-03	+8.3328E-03
+1.3100E+01	+5.6143E+00	+9.9620E+01	+9.9611E+01	+8.9358E-03	+8.9699E-03
+1.4100E+01	+6.0429E+00	+9.6112E+01	+9.6103E+01	+9.2141E-03	+9.5868E-03
+1.5100E+01	+6.4714E+00	+9.2768E+01	+9.2759E+01	+9.4404E-03	+1.0176E-02
+1.6100E+01	+6.9000E+00	+8.9572E+01	+8.9563E+01	+9.6453E-03	+1.0768E-02
+1.7100E+01	+7.3286E+00	+8.6509E+01	+8.6499E+01	+9.8700E-03	+1.1409E-02
+1.8100E+01	+7.7571E+00	+8.3566E+01	+8.3556E+01	+1.0139E-02	+1.2133E-02

The deviation of these results for the last line does not exceed 0.012 %.

All these results show that the accuracy of the phase shifts of nuclear scattering obtained from these calculations, by both methods, is at the level

of tenth-hundredths of a percent and thus either of these ways can be applied to the real calculation of nuclear phase shifts of elastic scattering in any cluster system with central forces.

We present the text of a computer program in Fortran-90 for calculating elastic scattering phase shifts, in this case, of protons on ^{7}Li. The program carries out the calculation of the elastic scattering phase shifts of two particles using a scattering wave function by the methods described in detail above with a given accuracy. In this case, the absolute accuracy is 10^{-3} radians. Moving on to the computer program, note that the descriptions of the parameters of variables in the calculation and the interaction potential blocks of the program and subprograms are listed along with the program.

PROGRAM FAZ_p7Li

```
! THE PROGRAM OF CALCULATION OF PHASE SHIFTS OF SCATTERING FOR THE SET ACCURACY
IMPLICIT REAL(8) (A-Z)
INTEGER(4) I,L,N
REAL(8) FA1(0:1000),ECM(0:1000),EL(0:1000)
DIMENSION U1(0:1024000)
! ***************** The nuclear data ******************
AM1=1.00727646577D0; ! The P mass
AM2=7.01600455D0 ! The 7Li mass
Z1=1.0D0 ! The P charge
Z2=3.0D0          ! The 7Li charge
PI=4.0D0*DATAN(1.0D0) ! The Pi number
PM=AM1*AM2/(AM1+AM2) ! The reduced mass
! ***************** The constants ************************
A1=41.4686D+00
B1=2.0D0*PM/A1
AK1=1.439975D+00*Z1*Z2*B1
GK=3.44476D-02*Z1*Z2*PM
! ***************** The initial values ****************
NN=0 ! The initial value of a step
NV=30 ! The number of steps at calculation of the phase shifts
NH=1 ! The step value
EH=0.01D0 ! The step in MeV for the calculation of the phase shifts
EN=0.3D0  ! The lower value of energy of the calculation of the phase shifts
EPF=1.0D-003 ! The accuracy of the calculation of the phase shifts
! *************** The potentials ************************
V0=1685.783D0 ! The potential depth in MeV of the attracting part
R0=1.D0 ! The potential radius of the attracting part in Fm
```

```
V1=0.0D0 ! The potential depth in MeV of the repulsive part
R1=1.0D0 ! The potential radius of the repulsive part in Fm
A0=-V0*B1; A1=V1*B1 ! The recalculation of depth of potentials in Fm-2
RCU=0.0D0 ! The coulomb radius in Fm
L=1 ! The orbital moment
! ************ The parameters for finding of the phase shifts ********
DO I=NN,NV,NH
N=1000 ! The initial number of steps of calculation of the WF
RR=10.0D0 ! The initial distance for calculation of the WF
H=RR/N ! The initial distance for calculation of the WF
EL(I)=EN+I*EH ! The energy in a lab system
ECM(I)=EL(I)*PM/AM1 ! The recalculation of energy in the system of the
center of masses
SK=ECM(I)*B1 ! The square of the number
SS1=DSQRT(SK) ! The wave number
G=GK/SS1 ! Coulomb parameter
! ******* The subprogramme of calculation of the phase shifts *****
CALL
FAZ(G,SS1,I,RR,EPF,N,PI,H,L,U1,FA1,A0,A1,R0,R1,RCU,AK1,SK)
PRINT *,EL(I)*1000,FA1(I)
ENDDO
! ******************** The record of results in the file *********
OPEN (1,FILE='FAZ-P-7Li.DAT')
DO I=NN,NV,NH
WRITE(1,*) EL(I)*1000,FA1(I)
ENDDO
CLOSE(1)
END

SUBROUTINE FUN(N,H,A0,A1,R0,R1,L,RCU,AK,SK,U)
! *** The subprogramme of calculation of the wave function ***********
IMPLICIT REAL(8) (A-Z)
INTEGER(4) K,L,N
DIMENSION U(0:1024000)
U(0)=0.0D0
U(1)=0.010D0
HK=H*H
DO K=1,N-1
X=K*H
Q1=A0*DEXP(-R0*X*X)+L*(L+1)/(X*X)+A1*DEXP(-R1*X*X)
IF (X>RCU) GOTO 1157
```

```
Q1=Q1+(3.0D0-(X/RCU)**2)*AK/(2.0D0*RCU)
GOTO 1158
1157 Q1=Q1+AK/X
1158 Q2=-Q1*HK-2.0D0+SK*HK
U(K+1)=-Q2*U(K)-U(K-1)
ENDDO
END

SUBROUTINE FAZ(G,SS,I,RR,EPF,N,PI,H,L,U,FA,A0,A1,
R0,R1,RCU,AK,SK)
! ********** The subprogramme of calculation of the phase shifts ****
IMPLICIT REAL(8) (A-Z)
INTEGER(4) N,L,I
DIMENSION U(0:1024000),FA(0:1000)
FN=1000.0; FR=1000.0
125 X1=H*SS*(N-4)
X2=H*SS*N
CALL CULFUN(L,X1,G,F1,G1,W0,EP)
CALL CULFUN(L,X2,G,F2,G2,W0,EP)
CALL FUN(N,H,A0,A1,R0,R1,L,RCU,AK,SK,U)
U10=U(N-4); U20=U(N)
AF=-(F1-F2*U10/U20)/(G1-G2*U10/U20)
F=DATAN(AF)
IF(F<0.0D0) THEN
F=F+PI
ENDIF
IF(ABS(F)<1.0D-10) THEN
F=0.0D0
ENDIF
IF (ABS(FN-F)>EPF) THEN
FN=F
N=N+100
H=RR/N
GOTO 125
ENDIF
IF (ABS(FR-F)>EPF) THEN
FR=F
RR=RR+1
N=N+0.2*N
H=RR/N
GOTO 125
```

```
ENDIF
FA(I)=F*180.0D0/PI
END

SUBROUTINE CULFUN(LM,R,Q,F,G,W,EP)
! **** Subprogramme of the calculation of the Coulomb functions *****
IMPLICIT REAL(8) (A-Z)
INTEGER L,K,LL,LM
EP=1.0D-015
L=0
F0=1.0D0
GK=Q*Q
GR=Q*R
RK=R*R
B01=(L+1)/R+Q/(L+1)
K=1
BK=(2*L+3)*((L+1)*(L+2)+GR)
AK=-R*((L+1)**2+GK)/(L+1)*(L+2)
DK=1.0D0/BK
DEHK=AK*DK
S=B01+DEHK
15 K=K+1
AK=-RK*((L+K)**2-1.D0)*((L+K)**2+GK)
BK=(2*L+2*K+1)*((L+K)*(L+K+1)+GR)
DK=1.D0/(DK*AK+BK)
IF (DK>0.0D0) GOTO 35
25 F0=-F0
35 DEHK=(BK*DK-1.0D0)*DEHK
S=S+DEHK
IF (ABS(DEHK)>EP) GOTO 15
FL=S
K=1
RMG=R-Q
LL=L*(L+1)
CK=-GK-LL
DK=Q
GKK=2.0D0*RMG
HK=2.0D0
AA1=GKK*GKK+HK*HK
PBK=GKK/AA1
RBK=-HK/AA1
```

```
AOMEK=CK*PBK-DK*RBK
EPSK=CK*RBK+DK*PBK
PB=RMG+AOMEK
QB=EPSK
52 K=K+1
CK=-GK-LL+K*(K-1.)
DK=Q*(2.*K-1.)
HK=2.*K
FI=CK*PBK-DK*RBK+GKK
PSI=PBK*DK+RBK*CK+HK
AA2=FI*FI+PSI*PSI
PBK=FI/AA2
RBK=-PSI/AA2
VK=GKK*PBK-HK*RBK
WK=GKK*RBK+HK*PBK
OM=AOMEK
EPK=EPSK
AOMEK=VK*OM-WK*EPK-OM
EPSK=VK*EPK+WK*OM-EPK
PB=PB+AOMEK
QB=QB+EPSK
IF (( ABS(AOMEK)+ABS(EPSK) )>EP) GOTO 52
PL=-QB/R
QL=PB/R
G0=(FL-PL)*F0/QL
G0P=(PL*(FL-PL)/QL-QL)*F0
F0P=FL*F0
ALFA=1.0D0/( (ABS(F0P*G0-F0*G0P))**0.5 )
G=ALFA*G0
GP=ALFA*G0P
F=ALFA*F0
FP=ALFA*F0P
W=1.0D0-FP*G+F*GP
IF (LM==0) GOTO 123
AA=(1.0D0+Q**2)**0.5
BB=1.0D0/R+Q
F1=(BB*F-FP)/AA
G1=(BB*G-GP)/AA
WW1=F*G1-F1*G-1.0D0/(Q**2+1.0D0)**0.5
IF (LM==1) GOTO 234
DO L=1,LM-1
```

```
AA=((L+1)**2+Q**2)**0.5
BB=(L+1)**2/R+Q
CC=(2*L+1)*(Q+L*(L+1)/R)
DD=(L+1)*(L**2+Q**2)**0.5
F2=(CC*F1-DD*F)/L/AA
G2=(CC*G1-DD*G)/L/AA
WW2=F1*G2-F2*G1-(L+1)/(Q**2+(L+1)**2)**0.5
F=F1; G=G1; F1=F2; G1=G2
ENDDO
234 F=F1; G=G1
123 CONTINUE
END
```

Below, we give the results of the control account using this program for the elastic scattering of protons on ^{7}Li in the *P* wave, i.e. at $L = 1$ with the potential specified in the program. Here, *E* is the energy of particles in keV and δ is a phase shift in degrees. Inscriptions for these values (*E* and δ) are not provided in the program.

E, keV	δ, degree
300.000000000000000	1.463012825309583
310.000000000000000	1.741580427189647
320.000000000000000	2.045211169193295
329.999999999999900	2.453917192921778
339.999999999999900	2.942034339443802
350.000000000000000	3.523983257335034
360.000000000000000	4.304066622497790
370.000000000000000	5.290031443719053
380.000000000000000	6.616684565601776
390.000000000000000	8.497854783693313
400.000000000000000	11.283887289718910
410.000000000000000	15.871292305763380
420.000000000000000	24.460811168704080
430.000000000000000	44.290494570708410
440.000000000000000	90.056769406018120
449.999999999999900	131.858294233151700
459.999999999999900	149.289857654389200
470.000000000000000	157.183982976260500
480.000000000000000	161.471562673128100
490.000000000000000	164.171993502029300
500.000000000000000	165.996407865298600

510.000000000000000	167.276268596475400
520.000000000000000	168.211429040413200
530.000000000000000	168.940799322204100
540.000000000000000	169.548066545885000
550.000000000000000	170.004755252677600
560.000000000000000	170.371698377092600
570.000000000000100	170.660104736125200
580.000000000000100	170.910851757862900
590.000000000000000	171.148334224319700
600.000000000000000	171.325330286482400

It is clear from these results that at 440 keV the P_1 phase shift reaches resonance value at 90°, which is really at an energy of 441 keV [28].

1.4 Program for calculating scattering phase shifts for the central complex potentials

We present the program for calculating complex phase shifts of elastic scattering by the finite-difference method in BASIC. The following designations are accepted.

NN – the lower value of the energy cycle,
NV – the upper value of the energy cycle,
LN – the lower value of the orbital moment,
LV – the upper value of the orbital moment,
LH – a step value of the orbital moment,
AM1 – the mass of the first particle in amu,
AM2 – the mass of the second particle in amu,
PM – the reduced mass of μ,
Z1 – charge of the first particle in terms of charge “e”,
Z2 – charge of the second particle in terms of charge “e”,
A1 – constant $\hbar^2/M_N = 41.4686$, where M_N is the mass of a nucleon in amu, equal to 1,
AK – constant at the Coulomb potential $1.439975\ Z_1Z_2\ 2\mu/\hbar^2$,
N – number of steps at the integration of the Schrödinger equation,
HH – step value at integration of the Schrödinger equation,
R00 – distance at which the interlacing of numerical functions with asymptotics is carried out,
VR1 – the depth of the real potential,
RRR – the radius of the real potential,
AR – the diffusivity of the real potential of the Woods-Saxon potential,

VC1 – the depth of the imaginary part of the potential,
RRC – the radius of the imaginary part of the potential,
AC – the diffusivity of the imaginary part of the Woods-Saxon potential,
RCU – the Coulomb radius,
L – the orbital moment,
E1 () – the energy of particles in the laboratory system,
E () – the energy of particles in the system of the center of masses,
SK – the square of the wave number of k^2,
SS – the k wave number,
GG – the Coulomb parameter = $3.44476\ 10^{-2} Z_1 Z_2\ \mu/k$.

REM ** THE CALCULATION OF THE COMPLEX SCATTERING PHASE SHIFTS

```
CLS: DEFDBL A-Z: DEFINT I,J,K,L,N,M: NN=4000: N=100
DIM E(N), DE(N), DEE(N), FAZA(N,15), E1(N), X(NN), Y(NN), ETA(N,15), SIG(N,15), SEC(N), FAZ(N,15)
DIM V(NN),W(NN),FM(20),FR(20),FR1(20),FM1(20),ET(N)
REM  ****************************************
A$ =" THE COMPLEX PHASE SHIFTS"
B$=" E(CM) FAZR(EXP) FAZR(TEOR) FAZC(EXP) FAZC(TEOR)  ETA(TEOR) "
SAVE=0: G$="C:\BASICA\FAZCOM\FAZALAL1.DAT"
PRINT  "----------------------------------------------------------------": PRINT B$
REM ************ THE TYPE OF THE POTENTIALS ************
PI=4*ATN(1): NN=1: NV=1: LN=0: LV=10: LH=2: AM1=4: AM2=4
Z1=2: Z2=2: A1=41.4686: PM=AM1*AM2/(AM1+AM2): B1=2*PM/A1
AK=1.439975*Z1*Z2*B1: N=2000: R00=20: HH=R00/N
REM *************** AL - AL 51.1 ******************
E1(1)=51.1
REM ********** THE PHASE SHIFTS AL - AL 51.1 ***************
FR(0)=291: FR(2)=245: FR(4)=163: FR(6)=28: FR(8)=4.2: FR(10)=0.5
FM(0)=0.51: FM(2)=0.51: FM(4)=0.53: FM(6)=0.855: FM(8)=0.985
FM(10)=0.998: FOR I=NN TO NV: E(I)=E1(I)*PM/AM1: NEXT I
FOR I=LN TO LV STEP LH: FR1(I)=FR(I)*PI/180
REM FM1(I)=FM(I)*PI/180
NEXT I: REM ********* THE  INITIAL PARAMETERS  ********
V22=122: A22=0.74: R22=1.81: V33=11: A33=0.74: R33=1.81
RCU=1.81: VN2=-V22*B1: VN3=-V33*B1
REM  ** CALCULATION OF THE SCATTERING  PHASE SHIFTS **
FOR JJ=NN TO NV: SK=E(JJ)*B1: SS=SQR(SK)
```

```
GG=3.44476E-02*Z1*Z2*PM/SS: SIGMRR=0: SIGMAS=0
FOR L=LN TO LV STEP LH
CALL FUN (X(), Y(),  R22, VN2, A22, R33, VN3, A33, RCU, L, SK, AK)
RR1=HH*SS*(N-5): RR2=HH*SS*N: X1=X(N-5): X2=X(N)
Y1=Y(N-5): Y2=Y(N)
REM *********   THE COULOMB FUNCTIONS ********
CALL CUL(GG,RR1,L,F1,G1,FP1,GP1)
CALL CUL(GG,RR2,L,F2,G2,FP2,GP2)
REM ********** THE SEARCH OF PHASE SHIFTS *********
AA1=X2*F1-X1*F2: BB1=Y1*G2-Y2*G1: DD1=X1*G2-X2*G1
CC1=Y2*F1-Y1*F2: AA=BB1-AA1: BB=-CC1-DD1: CC=AA1+BB1
DD=CC1-DD1: DD0=AA^2+BB^2: SS1=(AA*CC+BB*DD)/DD0
SS2=(AA*DD-BB*CC)/DD0: ETA(JJ,L)=SQR(SS1^2+SS2^2)
SS22=SS2/ETA(JJ,L): SS11=SS1/ETA(JJ,L)
SIG(JJ,L)=-LOG((ETA(JJ,L)))/2
FAZ=SS22/(1+SS11): FAZ(JJ,L)=ATN(FAZ): IF FAZ(JJ,L)>0 GOTO 901
FAZ(JJ,L)=FAZ(JJ,L)+PI
901 FAZA(JJ,L)=FAZ(JJ,L)*180/PI: IF SIG(JJ,L)>0 GOTO 911
SIG(JJ,L)=SIG(JJ,L)+PI
911 SIG(JJ,L)=SIG(JJ,L)*180/PI: A=FAZ(JJ,L)
SIGMAR = SIGMAR + (2*L+1)*(1 - (ETA(JJ,L))^2)
SIGMAS = SIGMAS + (2*L+1)*(ETA(JJ,L))^2*(SIN(A))^2
PRINT USING " +#.###^^^^ "; L; FR(L); FAZA(JJ,L); FM(L); SIG(JJ,L)
ETA(JJ,L): NEXT L: SIGMAR=10*4*PI*SIGMAR/SK
SIGMAS=10*4*PI*SIGMAS/SK
PRINT "       SIGR - THEOR = ";SIGMAR;
PRINT "       SIGS - THEOR = ";SIGMAS: NEXT JJ
REM ******* THE CALCULATION OF DIF. CROSS SECTIONS *****
FOR J=NN TO NV: SK=E(J)*B1: SS=SQR(SK)
GG=3.44476E-02*Z1*Z2*PM/SS: SIGMAR=0: SIGMAS=0
FOR L=LN TO LV STEP LH: A=FR1(L): ET(L)=FM(L)
SIGMAR = SIGMAR + (2*L+1)*(1 - (ET(JJ,L))^2)
SIGMAS = SIGMAS + (2*L+1)*(ET(JJ,L))^2*(SIN(A))^2: NEXT L
SIGMAR=10*4*PI*SIGMAR/SK: SIGMAS=10*4*PI*SIGMAS/SK
PRINT "       SIGR - EXP = ";SIGMAR;
PRINT "       SIGS - EXP = ";SIGMAS
NEXT J: TMI=10: TMA=90: TH=1
CALL SEC (FR1(), GG, SS, TMI, TMA, TH, SEC(), ET(), LN, LV, LH, 1)
FOR T=TMI TO TMA/3 STEP TH
PRINT USING " ####.##   "; T; SEC(T); T+20; SEC(T+20); T+40;
SEC(T+40); T+60; SEC(T+60): NEXT
```

```
REM **************   FILE RECORDING ************
IF SAVE=0 THEN STOP: OPEN "O",1,G$
PRINT#1, "ALPHA-ALPHA FOR LAB E=";: PRINT#1, E1(NN)
FOR T=TMI TO TMA STEP TH: PRINT#1, USING " #.###^^^^
";T;SEC(T)
NEXT
END

SUB CUL(GG,RR2,L,F2,G2,FP2,GP2)
Q=GG: R=RR2: F0=1: GK=Q*Q: GR=Q*R: RK=R*R
B01=(L+1)/R+Q/(L+1): K=1: BK=(2*L+3)*((L+1)*(L+2)+GR)
AK=-R*((L+1)^2+GK)/(L+1)*(L+2)
DK=1/BK: DEHK=AK*DK: S=B01+DEHK
112 K=K+1: AK=-RK*((L+K)^2-1)*((L+K)^2+GK)
BK=(2*L+2*K+1)*((L+K)*(L+K+1)+GR): DK=1/(DK*AK+BK)
IF DK>0 GOTO 132: F0=-F0
132 DEHK=(BK*DK-1)*DEHK: S=S+DEHK
IF (ABS(DEHK)-1E-10)>0 GOTO 112: FL=S: K=1: RMG=R-Q
LL=L*(L+1): CK=-GK-LL: DK=Q: GKK=2*RMG: HK=2
AA1=GKK*GKK+HK*HK: PBK=GKK/AA1: RBK=-HK/AA1
OMEK=CK*PBK-DK*RBK: EPSK=CK*RBK+DK*PBK
PB=RMG+OMEK: QB=EPSK
152 K=K+1: CK=-GK-LL+K*(K-1): DK=Q*(2*K-1): HK=2*K
FI=CK*PBK-DK*RBK+GKK: PSI=PBK*DK+RBK*CK+HK
AA2=FI*FI+PSI*PSI: PBK=FI/AA2: RBK=-PSI/AA2
VK=GKK*PBK-HK*RBK: WK=GKK*RBK+HK*PBK: OM=OMEK
EPK=EPSK: OMEK=VK*OM-WK*EPK-OM
EPSK=VK*EPK+WK*OM-EPK
PB=PB+OMEK: QB=QB+EPSK
IF (ABS(OMEK)+ABS(EPSK)-1E-10)>0 GOTO 152: PL=-QB/R
QL=PB/R: G0=(FL-PL)*F0/QL: G0P=(PL*(FL-PL)/QL-QL)*F0
F0P=FL*F0: ALFA=1/(SQR(ABS(F0P*G0-F0*G0P))): G2=ALFA*G0
GP2=ALFA*G0P: F2=ALFA*F0: FP2=ALFA*F0P
W=1-FP2*G2+F2*GP2
END SUB

SUB FUN(X(5000), Y(5000), R2, V2, A2, R3, V3, A3, RCU, L, SK, AK)
SHARED HH,N:  HK=HH*HH: X(0)=0: X(1)=1E-3: Y(0)=0: Y(1)=1E-3
FOR K=1 TO N-1: R=K*HH: FR1=V2/(1+EXP((R-R2)/A2))
FC1=V3/(1+EXP((R-R3)/A3)): FR=SK-FR1-L*(L+1)/R^2
IF R>RCU GOTO 177: FR=FR-AK/(2*RCU)*(3-(R/RCU)^2): GOTO 188
```

```
177 FR=FR-AK/R
188 FC=FC1: F=2-FR*HK: G=FC*HK: X(K+1)=F*X(K)-X(K-1)-G*Y(K)
Y(K+1)=F*Y(K)-Y(K-1)+G*X(K): NEXT
END SUB

SUB SEC (F(100), GG, SS, TMI, TMA, TH, S(100), E(100), LMI, LMA,
LH, NYS)
SHARED PI: DIM S0(20),P(20)
RECUL1=0: AIMCUL1=0: CALL CULFAZ(GG,S0())
FOR TT=TMI TO TMA STEP TH: T=TT*PI/180: XP=COS(T)
A=2/(1-XP): BB=-GG*A: ALO=GG*LOG(A)+2*S0(0)
RECUL=BB*COS(ALO): AIMCUL=BB*SIN(ALO)
IF NYS=0 GOTO 555
PT=PI-T: X1P=COS(PT): A1=2/(1-X1P): BB1=-GG*A1
ALO1=GG*LOG(A)+2*S0(0): RECUL1=BB1*COS(ALO1)
AIMCUL1=BB1*SIN(ALO1)
555 RENUC=0: AIMNUC=0: RENUC1=0: AIMNUC1=0
FOR L=LMI TO LMA STEP LH: AL=E(L)*COS(2*F(L))-1
BE=E(L)*SIN(2*F(L)): LL=2*L+1: SL=2*S0(L)
CALL POLLEG(XP,L,P())
RENUC=RENUC+LL*(BE*COS(SL)+AL*SIN(SL))*P(L)
AIMNUC=AIMNUC+LL*(BE*SIN(SL)-AL*COS(SL))*P(L)
IF NYS=0 GOTO 556: CALL POLLEG(X1P,L,P())
RENUC1=RENUC+LL*(BE*COS(SL)+AL*SIN(SL))*P(L)
AIMNUC1=AIMNUC+LL*(BE*SIN(SL)-AL*COS(SL))*P(L)
556 NEXT L: RE=RECUL+RECUL1+RENUC+RENUC1
AIM=AIMCUL+AIMCUL1+AIMNUC+AIMNUC1
S(TT)=10*(RE^2+AIM^2)/4/SS^2: NEXT TT: END SUB
SUB POLLEG(X,L,P(20))
P(0)=1: P(1)=X: FOR I=2 TO L: P(I)=(2*I-1)*X/I*P(I-1)-(I-1)/I*P(I-2)
NEXT
END SUB

SUB CULFAZ(G,F(20))
C=0.577215665: S=0: N=50: A1=1.202056903/3: A2=1.036927755/5
FOR I=1 TO N: A=G/I-ATN(G/I)-(G/I)^3/3+(G/I)^5/5
S=S+A: NEXT: FAZ=-C*G+A1*G^3-A2*G^5+S: F(0)=FAZ
FOR I=1 TO 20: F(I)=F(I-1)+ATN(G/(I)): NEXT
END SUB
```

We provide the results of the control account in this program. The real physical scattering process in the $^4He^4He$ system of nuclear particles was considered at an energy of 51.1 MeV with a complex potential. Experimental data on differential cross sections are given in [62]. An analysis of these data in the optical model was carried out in the same paper. Consequently, the parameters of the Woods-Saxon potential were found

$$V(r) = \frac{V + iW}{\left[\exp\left(\frac{r-R}{a}\right)+1\right]} + V_c(r), \qquad (1.4.1)$$

where $V_c(r)$ is the Coulomb potential and

$V = -122 \pm 3$ MeV, $W = -11 \pm 2$ MeV,

$R = 1.81$ fm, $a = 0.74 \pm 0.03$ fm, $R_c = R$.

Such a potential leads to scattering phase shifts and parameters of inelasticity, which are given in Table 1.4.1. Moreover the total experimental cross section of the reaction $\sigma_r = 770 \pm 100$ mb is given in [62] for this energy.

Using these parameters of the potential, calculation of the scattering phase shifts is given in Table 1.4.1 and the total cross section of the reactions of $\sigma_r = 766.1$ mb was discovered using the program given above. It is clear that, practically speaking, all the calculated values (apart from the last real phase shift for $L = 10$), within the error margin, coincide with the results presented in [62]. If we use the phase shift in [62], then the cross section of reactions gives a value $\sigma_r = 764.7$ mb, which, as previously, is in good agreement with the experimental data.

Table 1.4.1. Results of phase shift analysis.

L	δ, degree, [62]	δ, degree, (Our calculation)	η [62]	η (Our calculation)
0	111±4	1.123E+02	0.51±0.07	5.102E-01
2	65±4	6.655E+01	0.51±0.07	5.177E-01
4	163±4	1.649E+02	0.53±0.07	5.414E-01
6	28±3	2.935E+01	0.855±0.03	8.501E-01
8	4.2±0.6	4.422E+00	0.985±0.004	9.841E-01
10	0.5±0.1	7.464E -01	0.998±0.001	9.972E-01

As such, in the case of the real central potentials, the general and numerical methods of the solution of the Schrödinger equation are considered. The accuracy of the physical calculations that allow one to obtain such methods and their full applicability to the finding of the nuclear scattering phase shifts is shown. The control calculations of the nuclear scattering phase shifts of various nuclear particles by the finite-difference method and by the Runge-Kutta method with the real interaction potentials are executed and a mutual comparison is carried out, showing the coincidence of the results with an accuracy of the order of several-hundredths of a percent.

The case when the central potential contains both real and imaginary parts is considered. Then, the Schrödinger equation moves into the coupled equation system. The general and numerical methods of the solution of such a system with rather simple initial and asymptotic conditions are stated. For this case, the control calculations of the nuclear scattering phase shifts and their comparison with some results obtained in other works are also given.

1.5 Creation of the intercluster potentials

Here, we describe in more detail the procedure for the construction of the intercluster partial potentials at the given orbital moment L, having defined the criteria and the sequence of finding the parameters, and having specified their errors and ambiguities. First of all, there are the parameters of the BS potentials, which, at the given number of the states allowed and forbidden in this partial wave, are fixed quite unambiguously on the binding energy, the radius of the nucleus, and an asymptotic constant in the considered channel.

The accuracy on which these parameters of the BS potential are determined is connected, first of all, to the AC accuracy, which is usually around 10–20 %. The accuracy of the experimental determination of the charge radius is usually much higher than 3–5 %. Such a potential does not contain other ambiguities as the classification of states according to Young tableaux allows one to unambiguously fix the number of BS, forbidden or allowed states in this partial wave; the complete determination of its depth and potential width entirely depends on the AC value. The principles of determining the number of the FS and AS are given in the partial wave described, for example, in [2].

It is important to note that the calculations of the charge radius in any model contain errors, i.e. errors that are a result of the model's accuracy. In any model, the values of such a radius depend on the integral of the model WF, i.e. the model errors of such functions are summarized. The values of

the AC are determined by an asymptotic of the model of the WF at one point of the asymptotic and appear to contain significantly smaller errors. As such, generally BS potentials have to be constructed and, first of all, coordinated as much as possible with the values of the AC obtained on the basis of independent methods, which allow one to take the AC from the experimental data [63].

The intercluster potential of the non-resonance scattering process on the phase shifts at the given number of the BS, allowed and forbidden states in the considered partial wave, is also constructed quite unambiguously. The accuracy of the determination of the parameters of such a potential is connected, first of all, to the accuracy of extraction of the phase shifts from the experimental data and can reach 20–30 %. Here, such a potential does not contain ambiguities, as the classification of states according to Young tableaux allows one to unambiguously fix the number of BS; the complete determination of its depth and the potential width with the given depth is defined by a form of this phase shift.

At the creation of the non-resonance scattering potential according to the data on the spectra of the nucleus in a certain channel, it is difficult to estimate the accuracy of finding its parameters, even at the given number of BS; however, it appears that it does not exceed the error in the previous case by much. Such a potential is usually supposed for the area of energy up to 1 MeV, leading to the phase shift closing to zero, or giving a smoothly falling phase shift shape, as there are no resonance levels in the spectra of the nucleus.

In the analysis of resonance scattering, when at the considered partial wave with an energy of up to 1 MeV there is a rather narrow resonance with a width of about 10–50 keV at the given number of BS, the potential is also constructed completely unambiguously. At the given number of BS, its depth is unambiguously fixed by the resonance energy of the level and the width is completely defined by the width of the resonance. The error of its parameters usually does not exceed the error of the determination of the width of such a level at about 3–5 %. The same applies to the construction of the partial potential by phase shifts and the determination of its parameters by resonance in the spectra of the nucleus.

As a result, none of the potentials contain ambiguities, allowing one to correctly describe the total cross sections of the processes of radiative capture [2,28], without the obvious involvement of such concepts as the spectroscopic S_f factor, i.e. its value is accepted as being equal to the unit, as used in [64]. In other words, by consideration of the capture reaction in the modified PCM [2] for the potentials of the processes correlated in a continuous spectrum, with the characteristics of the scattering processes and

a discrete spectrum describing the main properties of the BS of the nucleus, coordinated in a continuous spectrum, it is not necessary to enter an additional multiplier S_f [64] any more. It appears that all the effects present in the reaction, including the probability of cluster configuration, are considered at the creation of the interaction potentials.

This is possible because the potentials are constructed while taking into account the structure of the FS and on the basis of the description of the observed, i.e. the experimental characteristics, of the interacting clusters in the initial channel, along with some nuclei formed in the final state in the case of the description of its cluster design consisting of the initial particles. As such, the presence of S_f, taking into account the wave functions of the BS clusters, is defined on the basis of such potentials in the solution of the Schrödinger equation (1.1.1).

In conclusion, we note that in the case of the creation of partial interaction potentials, they are considered to not only depend on the L orbital moment, but also on the S total spin and the J total moment of the cluster system. In other words, for the different moments, L, S, J, we have different values for the parameters. Usually the *E1* or *M1* transitions between different states $^{(2S+1)}L_J$ in continuous and discrete spectra are considered and thus the potentials of these states will vary.

1.6 Potentials and wave functions

The intercluster interaction potentials for each partial wave, i.e. for the given orbital moment L, and the pointlike Coulomb member can be chosen in the form

$$V(r) = V_0\exp(-\gamma r^2) + V_1\exp(-\delta r^2), \tag{1.6.1}$$

or

$$V(r) = V_0\exp(-\gamma r^2). \tag{1.6.2}$$

Here the parameters V_0 and V_1, γ, and δ are the potential parameters. They are usually derived from best description of the phase shifts of elastic scattering taken during the phase shift analysis from the experimental data of the differential cross sections, i.e. angular distributions or excitation functions.

The Coulomb potential at the zero Coulomb radius of $R_{coul} = 0$ is written in the form

$$V_{\text{coul}}(\text{МэВ}) = 1.439975 \cdot \frac{Z_1 Z_2}{r},$$

where r is the relative distance between the particles of the initial channel in fm and Z stands for the charges of the particles in terms of an elementary charge "e".

The behavior of the wave function of the bound states, including the ground states of the nucleus in the cluster channels at long distances, is characterized by the asymptotic constant C_w, which is defined by Whittaker's function [65]

$$\chi_L(r) = \sqrt{2k_0} C_w W_{-\eta L+1/2}(2k_0 r), \tag{1.6.3}$$

where $\chi_L(R)$ is the numerical wave function of the bound state obtained from the solution of the radial Schrödinger equation and normalized to the unit; $W_{-\eta L+1/2}$ is Whittaker's function of the bound state defining the asymptotic behavior of the WF and being the solution of the same equation without nuclear potential, i.e. at long distances R; k_0 is the wave number caused by the channel binding energy; η is the Coulomb parameter after being determined further; and L is the orbital moment of the bound state.

The asymptotic constant is the important nuclear characteristic defining the behavior of the "tail", i.e. the asymptotics of the wave function at long distances. In many cases, the knowledge of A nucleus in the cluster channel $b+c$ defines the value of an astrophysical S-factor for the process of radiative capture of $b(c,\gamma)A$ [63]. The asymptotic constant is proportional to the nuclear vertex constant for the virtual process of $A \rightarrow b+c$, which is a matrix element of this process on the mass surface [66].

1.7 Methods of phase shift analysis

Knowing the experimental differential cross sections of the elastic scattering, it is possible to find the set of parameters called the phase shifts $\delta^J_{S,L}$, allowing us to describe the behavior of these cross sections with a certain accuracy. The quality of the description of the experimental data, on the basis of some theoretical function (a functionality of several variables), can be estimated using the χ^2 method, which is presented in the form [6]

$$\chi^2 = \frac{1}{N}\sum_{i=1}^{N}\left[\frac{\sigma_i^t(\theta) - \sigma_i^e(\theta)}{\Delta\sigma_i^e(\theta)}\right]^2 = \frac{1}{N}\sum_{i=1}^{N}\chi_i^2, \tag{1.7.1}$$

where σ^e and σ^t are the experimental and theoretical values, i.e. calculated at some given values of the phase shift $\delta^J_{S,L}$ cross sections of the elastic scattering of the nuclear particles for the scattering angle *i*; $\Delta\sigma^e$ is an error of the experimental cross sections for this angle; and *N* is the number of experimental measurements.

The expressions describing the differential cross sections present the decomposition of some functionality $d\sigma(\theta)/d\Omega$ in the numerical series [6]; it is necessary to find such variation parameters of the decomposition $\delta^J_{S,L}$, which best describe its behavior. As the expressions for the differential cross sections are usually exact [6], with an indefinite increase in members of the decomposition of *L*, the value χ^2 has to aspire to zero. This criterion was used to choose a certain set of phase shifts leading to a minimum χ^2, which could be applied as a global minimum in this multiple parameter variation problem [5]. The methods and criteria of the phase shift analysis used in these calculations are given in more detail in [5,10].

As such, to discover the scattering phase shifts according to the experimental cross sections, the procedure for the minimization of χ^2 functionality (1.7.1), as functions of a certain number of variables, was executed, with each one being a $\delta^J_{S,L}$ phase shift of some partial wave. For the solution of this problem, a minimum χ^2 in some limited area of values of these variables is looked for; however, it is also possible to find a set of local χ^2 minima with the unit order value in this area. The choice of the smallest of them may correspond to a global minimum, which is the solution of such a variation problem.

We used the stated criteria and methods to carry out phase shift analysis at low energies, which is important for the majority of the astrophysical problems. All expressions for the calculation of the differential cross sections of the elastic scattering of particles with different spins, which are required for carrying out the phase shift analysis in the systems described above, are given in the corresponding paragraphs of Chapter 2.

1.8 General principles of the three-body model

We consider the radial Schrödinger equation with central nuclear forces for the wave function of the system of three particles [67,68]

$$(H - E)\Phi_{l,\lambda}(r,R) = 0, \qquad (1.8.1)$$

where

$$H = T + V,$$

$$T = T_1 + T_2 = -\frac{\hbar^2}{2\mu}\Delta_r - \frac{\hbar^2}{2\mu_0}\Delta_R\,, \qquad (1.8.2)$$
$$V = V_{12} + V_{23} + V_{13},$$

$$\mu = \frac{m_2 m_3}{m_{23}}\,, \quad \mu_0 = \frac{m_1 m_{23}}{m}\,,$$

$$m_{23} = m_2 + m_3\,, \quad m = m_1 + m_2 + m_3\,.$$

Here, m and μ are the masses and the reduced mass of three particles; Δ is the Laplace operator with the two coordinates of r and R; T and V are operators of kinetic and potential energy; H is the complete Hamiltonian of the system; and E is the energy of the system, i.e. the eigenvalues of energy in this system for the given Hamiltonian.

The r value in such a record defines the distance between particles 2 and 3, which are in a triangular formulation of three bodies with the orbital moment λ, while R is the distance between the first particle, which is located at the top of the triangle, and the center of mass of the first two particles with the orbital moment l.

The total three-body wave function of such a system has the form [67]

$$\Psi(r,R) = \sum_{l,\lambda} \Phi_{l,\lambda}(r,R)\mathrm{Y}_{\mathrm{LS}}^{\mathrm{JM}}(\hat{r},\hat{R})\,,$$

and its angular part $\mathrm{Y}_{\mathrm{LS}}^{\mathrm{JM}}(\hat{r},\hat{R})$ is written in the usual form [69,70,71]

$$\mathrm{Y}_{\mathrm{LS}}^{\mathrm{JM}}(\hat{r},\hat{R}) = \sum_{\mathrm{M_S M_L}} \left\langle LM_{\mathrm{L}} SM_{\mathrm{S}} \middle| JM \right\rangle \mathrm{Y}_{\mathrm{LM_L}}(\hat{r},\hat{R})\chi_{\mathrm{SM_S}}(\sigma)\,.$$

Here, $L = l + \lambda$ is the total orbital moment; S is the total spin of the system; J is the total moment of the considered system of particles; M represents the projections of these moments; $\mathrm{Y}_{\mathrm{LS}}^{\mathrm{JM}}(\hat{r},\hat{R})$ is the spin-angular function [69-71]; and $\Phi_{l,\lambda}$ is the radial wave function, which is usually

written in the form

$$\Phi_{l,\lambda}(r,R) = Nr^{\lambda}R^{l}\sum_{i} C_i \exp(-\alpha_i r^2 - \beta_i R^2) = N\sum_{i} C_i \Phi_i \,, \tag{1.8.3}$$

where r and R are the scalar distances between particles; $\hat{r}$ and $\hat{R}$ are the angles between the directions of the vectors of r and R and the axis z; Y_{LM} is the spherical function [72]; and χ_{SM} is the spin function of the system depending on the σ spin of the particles, with angular brackets designating the Clebsch-Gordan coefficients [72].

In the actual calculations, for certain values of the variational parameters α_i and β_i (1.8.3), we find the energy of the system, which gives the zero determinant of the system (1.8.1); then, by varying these parameters, we search for the minimum energy. In the following step, we increase the dimension of the N basis and repeat all calculations until the size of the eigenvalue, i.e. the binding energy E_N, on the next step of N does not begin and differs from the previous E_{N-1} value at size ε, which is usually set at the level 0.1–1.0 %. According to the general variation principle [9], this minimum energy will also be the real three-body binding energy of the system, i.e. the binding energy of an atomic nucleus in the cluster model considered here.

1.9 Variation methods of the three-body model

The matrix elements of the Hamiltonian system (1.8.2) and the overload integrals calculated on the basis of Φ_i (1.8.3) functions have the form [73]

$$T_{ij} = \frac{\pi}{16} N^2 \frac{\hbar^2}{m_N} \frac{(2l+1)!!(2\lambda+1)!!}{2^{l+\lambda}} \alpha_{ij}^{-\lambda-1/2} \beta_{ij}^{-l-1/2} G_{ij} \,,$$

$$G_{ij} = \frac{B_{ij}(\alpha,\lambda)}{\mu\beta_{ij}} + \frac{B_{ij}(\beta,l)}{\mu_0\alpha_{ij}} \,, \qquad B_{ij}(\delta,\nu) = \frac{\nu^2}{2\nu+1} + \frac{\delta_i\delta_j}{\delta_{ij}^2}(2\nu+3) - \nu \,,$$

$$L_{ij} = \frac{\pi}{16} N^2 \frac{(2l+1)!!(2\lambda+1)!!}{2^{l+\lambda}} \alpha_{ij}^{-\lambda-3/2} \beta_{ij}^{-l-3/2} \,, \qquad N = \left(\sum_{ij} C_i C_j L_{ij} \right)^{-1/2} \,,$$

with the potentials (the designations used here are: cb, centrifugal, coul, and Coulomb)

$$[(V_{cb})_R]_{ij} = \frac{\pi}{16} N^2 \frac{\hbar^2}{\mu_0} l(l+1) \frac{(2l-1)!!(2\lambda+1)!!}{2^{l+\lambda}} \alpha_{ij}^{-\lambda-3/2} \beta_{ij}^{-l-1/2},$$

$$[(V_{cb})_r]_{ij} = \frac{\pi}{16} N^2 \frac{\hbar^2}{\mu} \lambda(\lambda+1) \frac{(2\lambda-1)!!(2l+1)!!}{2^{l+\lambda}} \alpha_{ij}^{-\lambda-1/2} \beta_{ij}^{-l-3/2},$$

$$[\{V_{coul}(23)\}_r]_{ij} = Z_2 Z_3 \frac{\pi}{16} N^2 \frac{2}{\sqrt{\pi}} \frac{(2l+1)!!}{2^l} \frac{\lambda!}{\alpha_{ij}^{\lambda+1} \beta_{ij}^{l+3/2}},$$

$$[\{V_{coul}(12)\}_R]_{ij} = Z_1 Z_2 \frac{\pi}{16} N^2 \frac{2}{\sqrt{\pi}} \frac{(2\lambda+1)!!}{2^\lambda} \frac{l!}{\beta_{ij}^{l+1} \alpha_{ij}^{\lambda+3/2}},$$

$$[\{V_{coul}(13)\}_R]_{ij} = Z_1 Z_3 \frac{\pi}{16} N^2 \frac{2}{\sqrt{\pi}} \frac{(2\lambda+1)!!}{2^\lambda} \frac{l!}{\beta_{ij}^{l+1} \alpha_{ij}^{\lambda+3/2}},$$

$$(V_{23})_{ij} = \frac{\pi}{16} N^2 V_{23} \frac{(2l+1)!!(2\lambda+1)!!}{2^{l+\lambda}} (\alpha_{ij} + \gamma_{23})^{-\lambda-3/2} \beta_{ij}^{-l-3/2},$$

$$\alpha_{ij} = \alpha_i + \alpha_j, \qquad \beta_{ij} = \beta_i + \beta_j.$$

Furthermore, for example, at values of $l = 1$ and $\lambda = 0$, we have the following expressions for the matrix elements from the nuclear potentials of the form (1.6.2)

$$(V_{12})_{ij} = \frac{\pi}{16} N^2 \frac{3V_{12}}{2A_{ij}^{3/2}(\beta_{ij} + \gamma_{12})} \left[\frac{a^2 \gamma_{12}^2}{A_{ij}} + 1 \right],$$

where

$$A_{ij} = \alpha_{ij}\beta_{ij} + \gamma_{12}(\alpha_{ij} + a^2 \beta_{ij}) \quad , \quad a = m_3 / m_{23} \quad .$$

In the case of $l = 0$ and $\lambda = 0$ for this part of the potential, we find the expression

$$(V_{12})_{ij} = \frac{\pi}{16} N^2 \frac{V_{12}}{A_{ij}^{3/2}} .$$

Here, the value γ_{12} is the parameter of the width of the Gaussian potential and V_{12} is its depth between the corresponding couple of particles, which, in this case, is 12 or 13.

For a case of any l when $\lambda = 0$, it is possible to obtain the expression

$$(V_{12})_{ij} = \frac{\pi}{16} N^2 V_{12} \frac{(2l+1)!!}{2^l} \frac{d_{ij}^l}{A_{ij}^{l+3/2}},$$

where

$$d = \alpha_{ij} + \gamma_{12} a^2 .$$

The mean square mass radius of a nucleus in such a model is presented in the form [74]

$$< r^2 >_m = m_1 / m < r^2 >_{m1} + m_2 / m < r^2 >_{m2} + m_3 / m < r^2 >_{m3} + A / m ,$$

$$A = \frac{\pi}{16} N^2 \frac{(2l+1)!!(2\lambda+1)!!}{2^{l+\lambda+1}} \sum_{ij} C_i C_j \alpha_{ij}^{-\lambda-3/2} \beta_{ij}^{-l-3/2} \left(\frac{2\lambda+3}{\alpha_{ij}} \mu + \frac{2l+3}{\beta_{ij}} \mu_0 \right),$$

$$\mu = \frac{m_2 m_3}{m_{23}}, \quad \mu_0 = \frac{m_1 m_{23}}{m}, \quad m_{23} = m_2 + m_3, \quad m = m_1 + m_2 + m_3 \quad .$$

The mean square charge radius of a nucleus in the three-body model has the form

$$< r^2 >_z = Z_1 / Z < r^2 >_{z1} + Z_2 / Z < r^2 >_{z2} + Z_3 / Z < r^2 >_{z3} + B / Z .$$

Here, the value B is expressed through the moments of particles, variation parameters, and coefficients of decomposition of the WF as follows.

$$B = \frac{\pi}{16} N^2 \frac{(2l+1)!!(2\lambda+1)!!}{2^{l+\lambda+1}} \sum_{ij} C_i C_j \alpha_{ij}^{-\lambda-3/2} \beta_{ij}^{-l-3/2} \left(\frac{2l+3}{\beta_{ij}} C + \frac{2\lambda+3}{\alpha_{ij}} D \right) +$$

$$+ N^2 E (\lambda+1)!(l+1)! \sum_{ij} \frac{C_i C_j}{2\alpha_{ij}^{\lambda+2} \beta_{ij}^{l+2}} ,$$

$$C = \frac{Z_1 m_{23}^2 + Z_{23} m_1^2}{m^2} , \qquad Z_{23} = Z_2 + Z_3 ,$$

$$D = \frac{Z_2 m_3^2 + Z_3 m_2^2}{m_{23}^2} ,$$

$$E = \frac{m_1}{m m_{23}} (Z_3 m_2 - Z_2 m_3) .$$

As the charge and mass radiuses of the clusters—a proton, a deuteron, a triton, helium-3, and α particles—the following values were accepted: $\langle r \rangle_{zn} = 0$ fm, $\langle r \rangle_{mn} = \langle r \rangle_{mp} = \langle r \rangle_{zp} = 0.877$ fm, $\langle r \rangle_{md} = \langle r \rangle_{zd} = 1.96$ fm, $\langle r \rangle_{mt} = \langle r \rangle_{zt} = 1.72$ fm, $\langle r \rangle_{m3He} = \langle r \rangle_{z3He} = 1.88$ fm, $\langle r \rangle_{m\alpha} = \langle r \rangle_{z\alpha} = 1.67$ fm [75,76,77,78].

To find the binding energy of a nucleus in the three-body model, the initial values of the variation α_i and β_i parameters were found from a linear grid of the form

$$\alpha_i = i/30, \qquad \beta_i = 2\alpha_i.$$

The independent variation of each of these parameters at the given number of iterations was carried out to minimize the energy of the system with a given accuracy ε. This variation method differs a little from the similar variant of the VM for the usual two-body problem [28,79,80].

To check the variation three-body method of calculation and the computer program considered above, the model problem for three particles interacting in the Afnan-Tang potential [81] with averaging of the triplet and singlet states was used. For the binding energy of a system such as that described in [81], the value of -7.74 MeV was obtained, while the value -7.76 MeV was found in [82]; the non-orthogonal variation method, with a change in the α and β parameters of the wave function on the basis of a

tangential grid, was used. On the basis of the methods stated above, using the independent variation of all parameters and the dimension basis $N = 5$, we obtained the value -7.83 MeV. As such, the binding energy of the model system considered here, obtained using the methods described above, was approximately 1 % different to the results in [81,82]; we consider this to be a reasonably good result.

Conclusion

All the major mathematical expressions and some programs for investigating the elastic scattering phase shifts and calculations of nuclear characteristics are given in relation to the three-body model. The alternative methods of finding the eigenvalues for the two or three-body generalized variation problems have been described. Such methods lead to a steadier numerical scheme of the variation solution of the Schrödinger equation in comparison to the usual methods of Schmidt orthogonalization.

The criteria for the creation of two partial potentials on the basis of the scattering phase shifts and the general principles of searching for such phase shifts to undertake their analysis have been defined. Several ways of calculating the values of the wave function applicable to both a scattering problem and a discrete spectrum have been described. The finite-difference and variation methods of investigating the binding energy of a nuclear system, based on two and three partial models, have also been given.

II

PHASE SHIFT ANALYSIS

In many problems of low energy nuclear physics and nuclear astrophysics, knowledge of elastic scattering phase shifts, which can be determined from the differential cross sections of elastic scattering of various nuclear particles, is necessary [1]. The procedure for phase shift analysis consists of the decomposition of the total scattering amplitude in terms of partial waves or amplitudes and analyses the parameters that appear, which are called phase shifts. Such phase shifts allow us to obtain data on the nature of strong interactions, the structure of resonance states, and the general structure of atomic nuclei [1]. Phase shifts are used, in particular, for the creation of intercluster interaction potentials in the three-body potential cluster model or in relation to some astrophysical problems [2].

Introduction

The problem of determining or extracting the nuclear phase shifts from the cross sections of elastic scattering in the mathematical plan is reduced to a multiple parameter variation problem. In other words, when the experimental scattering cross sections of nuclear particles and mathematical expressions obtained in the quantum mechanics, which describe these cross sections depending on certain parameters with δ_L as the nuclear phase shifts, the polyvalent variation problem is used to find the required parameters at a given interval of values. This interval is usually in the area of phase shift values of 0 and 180°, if we take into account the conclusions of the generalized Levinson theorem [4].

Since there are no general methods for solving the multi-parameter variational problem to find the global minimum, we can expect to find mostly only some local minima at each energy and, on the basis of physical considerations, we choose those that could be solutions to the original problem. One of the criteria of this selection process is the requirement of smoothness in the behavior of each partial nuclear phase shift as a function of energy in the non-resonance area and the transition of its value through 90° at resonance energy [1], while also finding a phase shift in the given

area of angles.

In different nuclear systems, depending on the energy of the colliding particles, the number of elastic scattering phase shifts can change from 1–3 to 10–20 [5]. For example, in ^{4}He^{4}He scattering, we used up to 20 partial waves and, for example, in the p^{12}C system at low energies, as will be shown further, only one partial ^2S phase shift was used. In this chapter, the various experimental measurements, methods of calculation of differential cross sections, including computer programs, and results of the phase shift analysis of elastic ^{4}He^{4}He, n^{3}He, p^{6}Li, p^{12}C, n^{12}C, p^{13}C, p^{14}C, n^{16}O, p^{16}O, and ^{4}He^{12}C scattering, are all examined.

For the first system given above, only the control account at energies of 22 and 30 MeV, used for the verification of the computer program, is considered. This system is considered in more detail in [2]. For other scattering processes, the area of 1–2.5 MeV was analysed, apart from the last system in ^{4}He^{12}C scattering, where a phase shift analysis was made in the range 1.5–6.5 MeV.

2.1 Phase shift analysis of elastic ^{4}He^{4}He scattering

Here we consider measurements of the elastic scattering differential cross sections and the results of the phase shift analysis obtained from these cross sections for ^{4}He^{4}He systems at different energies. The basic data of these studies, concerning energies up to 120 MeV, but not in all of this area, were developed through the serial phase shift analysis of experimentally-measured differential cross sections of elastic scattering [83].

2.1.1 Overview of the experiment on ^{4}He^{4}He elastic scattering

We provide a short review of the experimental data and results of the phase shift analysis of ^{4}He^{4}He elastic scattering in a number of different works:

1. Measurement of the elastic scattering differential cross sections and phase shift analysis in the energy range 0.6–3.0 MeV (l.s.) were undertaken in [84]. The cross sections and phase shifts are specified in the form of a table, which is very convenient and assists in finding the phase shifts for any time.
2. The energy range 3.0–5.0 MeV was considered in [85], but the phase shifts and cross sections of scattering are given only in the figures.
3. The energy range 3.8–11.9 MeV was analysed in [86]. The results of the phase shift analysis are given in a table while the scattering

differential cross sections are shown only in the figures.

4. Very accurate measurements of elastic scattering differential cross sections and phase shift analysis are found in [87,88], where experimental cross sections and scattering phase shifts for the energy range 13–22.9 MeV are given in tables.
5. The area 12.9–21.6 MeV was also considered in [89], but the cross sections and phase shifts are given only in the figures.
6. Very good data for energies in the range 18.0–29.5 MeV are provided in [90]; the elastic scattering cross sections and results of the phase shift analysis are presented in detailed tables.
7. Experimental measurements of cross sections and phase shift analysis were carried out at energies in the range 23.1–38.4 MeV in [91]; however, only the scattering cross section is specified in a table.
8. Measurements of cross sections and phase shift analysis in the range 53–120 MeV are presented in [92], but only tabular phase shifts are given while the scattering cross sections are given in the figures.
9. Experimental study of the elastic scattering cross sections for energies in the range 36.8–47.3 MeV was carried out in [93]; detailed tables present the measurement results of differential cross sections, but phase shift analysis on these data was not carried out. Theoretical research into some energies in this area is available only in [94], where a search for parameters of the optical potential was undertaken and then phase shifts of $^{4}He^{4}He$ elastic scattering were obtained. The quality of the optical adjustment made in this area of energies leaves much to be desired, as shown in the figures in [94]. In addition, during extraction of the phase shifts of the optical potential, only the real part was calculated and an imaginary part was considered that is too small, located at 1–2°, which does not seem justified for energies in the region of 40 MeV or higher.
10. The energies of 38.5, 49.9, and 51.1 MeV were considered in [95,96,97], respectively, and the differential cross sections were measured; however, a phase shift analysis was not carried out for these data. Instead, in [95,97] the parameters of the optical potentials and, on that basis, those obtained in [97], the elastic scattering phase shifts were calculated.

From the review provided, it is clear that a standard phase shift analysis of the experimental data, i.e. elastic scattering differential cross sections in the $^{4}He^{4}He$ system at energies of 36.85–51.1 MeV, has not been undertaken. The adjustment of the parameters of the optical potentials for the energy range 23–47 MeV [94] can hardly be considered satisfactory, which is not

surprising, as all these results were obtained in the 1960s when the computing facilities and methods of advanced numerical calculation were only just beginning to develop.

Therefore, it is interesting to carry out an accurate and comprehensive analysis of the experimental phase shift of elastic scattering differential cross sections in the energy range 37–51 MeV. The tabular representation of the experimental cross sections of ^{4}He^{4}He elastic scattering in this area of energies, provided in [93,95,96], allows us to carry out such an analysis. However, we will be limited only by the operational capacity of the computer program; the results of such analysis are given in [5,83] and book [2].

2.1.2 The phase shift analysis method of ^{4}He^{4}He elastic scattering

We consider here the problem of phase shift analysis and the method of determining phase shifts from the experimental data, i.e. we will define the ways and approaches used in our phase shift analysis. The elastic scattering differential cross section of identical particles with spin 0 + 0 is defined by the scattering phase shifts of the identical particles, as follows [6]:

$$\frac{d\sigma(\theta)}{d\Omega} = \left| f(\theta) + f(\pi - \theta) \right|^2, \tag{2.1.1}$$

where the scattering amplitude is presented in the form of the sum of Coulomb and nuclear amplitudes

$$f(\theta) = f_c(\theta) + f_N(\theta), \tag{2.1.2}$$

and also expressed through the nuclear δ_l and Coulomb σ_l phase shifts [6]:

$$f_c(\theta) = -\left(\frac{\eta}{2k \sin^2(\theta/2)} \right) \exp\{i\eta \ln[\sin^{-2}(\theta/2)] + 2i\sigma_0\}, \tag{2.1.3}$$

$$f_N(\theta) = \frac{1}{2ik} \sum_l (2l+1) \exp(2i\sigma_l)[S_l - 1] P_l(\cos\theta),$$

where k is the wave number of the relative movement of $k^2 = 2\mu E/\hbar^2$ particles; E is the energy of the colliding particles in the center of mass; μ is the reduced mass; η is the Coulomb parameter; θ is the scattering angle;

and $P_L(\cos\theta)$ stands for the Legendre polynomials.

Usually, the nuclear phase shifts of elastic scattering are presented in the form

$$\delta_L = \mathrm{Re}\delta_L + i\mathrm{Im}\delta_L,$$

then, for a scattering matrix and parameters of inelasticity we obtain

$$S_L(k) = \eta_L(k)\exp[2i\mathrm{Re}\delta_L(k)],$$

$$\eta_L(k) = \exp[-2\mathrm{Im}\delta_L(k)].$$

The summation in expression (2.1.3) is carried out only by even-numbered L, as odd partial waves do not contribute to the total cross section, and carried out for some L, the values of which depend on the energy.

For the Coulomb scattering amplitude (2.1.3), using the expression

$$D = \sin^{-2}(\theta/2) = 2/[1 - \cos(\theta)],$$

it is possible to write the form

$$f_c = -\eta D/2k\,[\cos(C) + i\sin(C)],$$

where

$$C = 2\sigma_0 + \eta\ln D.$$

The nuclear amplitude can be provided in the following form

$$f_N = \frac{1}{2k}\sum_L \hat{L}\left\{\begin{array}{l}\left[B\cos(2\sigma_L) + A\sin(2\sigma_L)\right] + \\ +i\left[B\sin(2\sigma_L) - A\cos(2\sigma_L)\right]\end{array}\right\}P_L(x)\,, \qquad (2.1.4)$$

where $x = \cos(\theta)$; $\hat{L} = 2L + 1$; $A = \eta_L\cos(2\delta_L) - 1$; and $B = \eta_L\sin(2\delta_L)$ depending only on the nuclear phase shifts, the parameter of inelasticity, and the orbital moment.

The Coulomb scattering phase shifts are expressed through the gamma-function [6]

$$\sigma_L = \arg\{\Gamma(L+1+i\eta)\}\,,$$

and satisfy the recurrent process

$$\sigma_L = \sigma_{L+1} - \mathrm{arctg}\left(\frac{\eta}{L+1}\right),$$

by which it is possible to obtain the following expression for the Coulomb phase shifts

$$\alpha_L = \sigma_L - \sigma_0 = \sum_{n=1}^{L} \mathrm{arctg}\left(\frac{\eta}{n}\right), \qquad \alpha_0 = 0.$$

The value α_l is used in the transformed expression (2.1.3). If we take out the general multiplier $\exp(2i\sigma_0)$, then, $\sigma_l \to \alpha_l$ with $\alpha_0 = 0$, which relieves us of the need to calculate the Coulomb phase shifts in an explicit form; the Coulomb amplitude thus takes the following form

$$f_c(\theta) = -\left(\frac{\eta}{2k\sin^2(\theta/2)}\right)\exp\{i\eta\ln[\sin^{-2}(\theta/2)]\} \quad . \qquad (2.1.5)$$

In the ^{4}He^{4}He problem with zero spin, the set of phase shifts depends on the total moment J and spin S passes into δ_l. As $S = 0$, the total moment is equal to the orbital moment $J = L$.

2.1.3 Verification of the computer program

To carry out this phase shift analysis, a computer program written in BASIC using the Turbo Basic Compiler from Borland International Inc. was written [98] using the mode of double accuracy; it was then transferred into the Fortran-90 language [2]. The program was tested according to the earlier phase shift analysis presented in various works at different energies [10]. Here we provide only some of these tests.

For example, at an energy of 6.47 MeV (l.s.), the following phase shifts are given in [86]: $\delta_0 = 79.5° \pm 2°$; $\delta_2 = 80.8° \pm 2°$. In our phase shift analysis, the values $\delta_0 = 80.43°$ and $\delta_2 = 80.73°$ occur at $\chi^2 = 0.18$. The error in determining the cross sections from the figures in [86] was accepted as being equal to 10 %, explaining such a small value for χ^2.

At an energy of 13 MeV in [88], the following values were obtained: $\delta_0 = 29° \pm 4°$, $\delta_2 = 103° \pm 8°$, $\delta_4 = 3° \pm 1.5°$; our analysis gives $\delta_0 = 28.37°$, $\delta_2 = 105.03°$, $\delta_4 = 2.62°$ at $\chi^2 = 3.43$.

$\delta_0 = 7° \pm 2°$, $\delta_2 = 104° \pm 4°$, $\delta_4 = 16.2° \pm 2°$ was found in the same work for 17.8 MeV; in our calculations we found the values $\delta_0 = 7.25°$, $\delta_2 = 103.93°$, $\delta_4 = 17.0°$ at $\chi^2 = 0.46$.

In [88], the following phase shifts were obtained for an energy of 22.9 MeV: $\delta_0 = 169.7° \pm 2°$, $\delta_2 = 94.0° \pm 2°$, $\delta_4 = 59.2° \pm 2°$, $\delta_6 = 1.09°$. Our phase shift analysis using these data gives: $\delta_0 = 169.30°$, $\delta_2 = 94.49°$, $\delta_4 = 59.55°$, $\delta_6 = 1.0°$ at $\chi^2 = 1.46$.

At the energies of 13, 17.8, and 22.9 MeV, the differential cross sections, their errors, scattering phase shifts, and the value χ^2 are specified in the tables in [88], but it is possible to compare only the scattering phase shifts. It is rather difficult to compare χ^2 because in [86,88] the value of χ^2 determined above is not considered (1.7.1), however, its derivative depends on some constants connected to the experimental technique.

We present the control account executed for ^{4}He^{4}He elastic scattering at an energy of 29.5 MeV in more detail. In [90], which presents the experimental cross sections and results of the phase shift analysis (see Table 2.1.1), 0.68 was obtained for the average χ^2 value; however, the methods of its calculation differ a little from those stated above and thus this value cannot be compared directly to our results. The result obtained from our calculations with the phase shifts from [90] for the average χ^2 on all points was 1.086. If we consider the weighting multipliers from [90], it is possible to obtain a value of 0.6, which aligns quite well with the results of this work.

Furthermore, we carried out detailed calculations for the minimization of χ^2 using our program (presented further on) and compared the results with the experimental data [90]. For the average χ^2, a value of 0.600 was obtained (instead of 1.086), i.e. an almost twofold improvement in the quality of the description of the observed experiment with very little change in the values of the phase shifts, as shown in Table 2.1.1.

Table 2.1.1. Comparison of the results of phase shift analysis from [90] and our results at energies of 25.5 MeV and 29.5 MeV.

δ_L, deg	29.5 MeV		25.5 MeV	
	Results [90]	Our results	Results [90]]	Our results
δ_0	150.88±0.17	150.76	160.36±1.01	160.49
δ_2	86.90±0.13	86.61	89.37±1.54	89.00
δ_4	121.19±0.17	121.00	88.64±1.77	88.60
δ_6	2.20±0.11	2.16	1.61±0.39	1.41
δ_8	0.11±0.08	0.09	0.36±0.19	0.18

In [90], the data were obtained for an energy of 25.5 MeV, the phase shifts of which are also shown in Table 2.1.1. Our calculation with these phase shifts gives us a value of $\chi^2 = 2.127$. Carrying out an additional variation of the scattering phase shifts, we obtain a noticeable improvement in the description of the available data with $\chi^2 = 0.886$. For the phase shift values given in the last column of Table 2.1.1, which coincide with the results in the limits given in [90], the scattering phase shifts errors were obtained.

Small differences in scattering phase shifts can be caused by the various values for constants or masses of particles, which are used in such calculations. For example, it is possible to use exact values for the mass of particles or their entire quantities, and the constant $\hbar^2/m_0$ can be different to the value 41.4686 MeV fm^2 used here. Therefore, in general, we may consider that, in all the cases presented above, which can be used as control cases for our results, and in the error limits given in various works for phase shifts, a reasonable level of coincidence with data obtained previously by a number of authors is achieved.

2.1.4 The program for ^{4}He^{4}He and ^{4}He^{12}C phase shift analysis

Below we present the computer program written in Fortran for ^{4}He^{4}He and ^{4}He^{12}C phase shift analysis. The analysis made depends on the values of the NYS and LH parameters. In the case of ^{4}He^{4}He, they have to be equal to 1 and 2, respectively, to carry out ^{4}He^{12}C phase shift analysis with values equal to 0 and 1. Additionally, for large energies of about 30–40 MeV, the NP parameter has to be equal

NP = 2*LMA+LH,

but not the LMA, which allows us to takie into account the complex part of the scattering phase shifts.

The designations of some initial parameters of the program are given below.

Z1=2.0D0; Z2=2.0D0 – charges of particles,
AM1=4.0D0; AM2=4.0D0 – mass of the alpha particles,
LMI=0 – the initial orbital moment,
LH=1 – the step of the moment,
LMA=2 – the maximum orbital moment,
EP=1.0D-10 – accuracy of the search for a minimum,
NI=10 – the number of iterations,

NT=22 – the number of experimental points,
EL=13.0D0 – the laboratory energy of the elastic scattering of particles,
A1=41.4686D0 – constant value $\hbar^2/m_0$,
PM=AM1*AM2/(AM1+AM2) – the reduced mass of the particles,
FH=0.010D0 – the initial step in searching for a minimum,
NYS=1 – call word – if = 1 then ^{4}He^{4}He, and if = 0 then ^{4}He^{12}C for the search of phase shifts for two different systems of particles.

Below we present the text of the computer program written in Fortran-90.

```
PROGRAM FAZ_AL_AL
! THE PROGRAM OF THE PHASE SHIFT ANALYSIS FOR AL-AL
! AND AL-12C
IMPLICIT REAL(8) (A - Z)
INTEGER L,I,NT,LMI,LMA,LH,NYS,NP,NTT,NV,NI,LMI1,LH1,NPP
DIMENSION ST(0:50),FR(0:50),FM(0:50),ET(0:50),
XP(0:50),ETA(0:50)
COMMON /A/ PI,NT,TT(0:50),GG,SS,LMI,LMA,LH,NYS,NP
COMMON /B/ SE(0:50),DS(0:50),DE(0:50),NTT
COMMON /C/ LH1,LMI1,P1,NPP
! ************* INITIAL VALUES **************
PI=4.0D0*DATAN(1.0D0)
P1=PI
Z1=2.0D0; Z2=2.0D0
AM1=4.0D0; AM2=4.0D0
AM=AM1+AM2
A1=41.46860D0
PM=AM1*AM2/(AM1+AM2)
B1=2.0D0*PM/A1
LMI=0; LMI1=LMI; LH=2; LH1=LH
LMA=4; LMA1=LMA
NYS=1; ! IF =1 THEN 4HE4HE, IF = 0 THEN 4HE12C
EP=1.0D-010
NV=1
FH=0.010D0
NI=10
!NP=2*LMA+LH
NP=LMA
NPP=NP
! ***************** CROSS SECTIONS ****************
```

```
SE(1)=1357.0D0; SE(2)=1203.0D0; SE(3)=1074.0D0;
SE(4)=870.0D0; SE(5)=759.0D0
SE(6)=688.0D0; SE(7)=467.0D0; SE(8)=271.0D0;
SE(9)=196.0D0; SE(10)=130.0D0
SE(11)=93.90D0;SE(12)=57.0D0; SE(13)=350D0;
SE(14)=130D0; SE(15)=280D0
SE(16)=24.7; SE(17)=86.5; SE(18)=157; SE(19)=270
SE(20)=337.0D0; SE(21)=408.0D0; SE(22)=418.0D0
DE(1)=39.0D0; DE(2)=40.0D0; DE(3)=24.0D0;
DE(4)=20.0D0; DE(5)=16.0D0;
DE(6)=17.0D0
DE(7)=12.0D0; DE(8)=7.0D0; DE(9)=4.10D0;
DE(10)=3.60D0; DE(11)=20D0;
DE(12)=1.50D0
DE(13)=1.1; DE(14)=1.0; DE(15)=0.4; DE(16)=0.7;
DE(17)=2.0; DE(18)=3.6
DE(19)=6.50D0; DE(20)=7.40D0; DE(21)=8.20D0;
DE(22)=8.30D0
TT(1)=22.0D0;  TT(2)=24.0D0;  TT(3)=26.0D0;
TT(4)=28.0D0; TT(5)=30.0D0
TT(6)=32.0D0;  TT(7)=35.0D0;  TT(8)=40.0D0;
TT(9)=42.0D0
TT(10)=45.0D0; TT(11)=46.0D0; TT(12)=48.0D0;
TT(13)=50.0D0
TT(14)=52.0D0; TT(15)=55.0D0; TT(16)=60.0D0;
TT(17)=65.0D0
TT(18)=70.0D0; TT(19)=75.0D0; TT(20)=80.0D0;
TT(21)=85.0D0; TT(22)=90.0D0
! *************** FOR AL-AL ON E=13 ***************
NT=22;  NTT=NT; EL=13.0D0
FR(0)=29.0D0;  FR(2)=103.0D0;  FR(4)=3.0D0
FM(0)= 0.0D0;  FM(2)=  0.0D0;  FM(4)=0.0D0
OPEN (4,FILE='FAZ.DAT')
DO L=LMI,LMA,LH
READ(4,*) L,FR(L),FM(L)
ENDDO
CLOSE(4)
! ************* ENERGY IN LAB. SYSTEM *************
DO L=LMI,LMA,LH
FM(L)=FM(L)*PI/180.0D0
FR(L)=FR(L)*PI/180.0D0
```

```
ET(L)=DEXP(-2.0D0*FM(L))
ENDDO
FH=FH*PI/180.0D0
DO I=LMI,LMA,LH
XP(I)=FR(I)
XP(I+LMA+LH)=FM(I)
ENDDO
! ********** TRANSFORM TO C.M. ******************
EC=EL*PM/AM1
SK=EC*B1
SS=DSQRT(SK)
GG=3.44476D-002*Z1*Z2*PM/SS
! ******* DIFFERENTIAL CROSS SECTION ************
CALL VAR(ST,FH,NI,XP,EP,XI,NV)
PRINT*, "XI-KV=; NI=; EL=",XI,NI,EL
! ********** TOTAL CROSS SECTION ****************
SIGMAR=0.0D0; SIGMAS=0.0D0
DO L=LMI,LMA,LH
FR(L)=XP(L)
FM(L)=XP(L+LMA+LH)
A=FR(L)
ETA(L)=1
!ETA(L)=DEXP(-2.0D0*FM(L))
SIGMAR=SIGMAR+(2*L+1)*(1-(ETA(L))**2)
SIGMAS=SIGMAS+(2*L+1)*(ETA(L))**2*(DSIN(A))**2
ENDDO
SIGMAR=10.0D0*4.0D0*PI*SIGMAR/SK
SIGMAS=10.0D0*4.0D0*PI*SIGMAS/SK
PRINT*, "SIGMR-TOT=",SIGMAR
PRINT*, "SIGMS-TOT=",SIGMAS
PRINT*, "    T         SE         ST         XI"
! ***************** RESULTS ***********************
DO I=1,NT
WRITE(*,2) TT(I),SE(I),ST(I),DS(I)
ENDDO
PRINT*
PRINT*, "   L    FR(L)     FM(L)"
DO L=LMI,LMA,LH
FM(L)=FM(L)*180.0D0/PI
FR(L)=FR(L)*180.0D0/PI
WRITE(*,1) L,FR(L),FM(L)
```

```
ENDDO
OPEN (4,FILE='SEC-AL-AL.DAT')
WRITE(4,*)  "            AL-AL LAB E=; XI=",EL,XI
WRITE(4,*) "      T            SE            ST            XI"
DO I=1,NT
WRITE(4,2) TT(I),SE(I),ST(I),DS(I)
ENDDO
WRITE(4,*)
WRITE(4,*) "    L     FR(L)      FM(L)"
DO L=LMI,LMA,LH
WRITE(4,1) L,FR(L),FM(L)
ENDDO
CLOSE(4)
OPEN (4,FILE='FAZ.DAT')
DO L=LMI,LMA,LH
WRITE(4,1) L,FR(L),FM(L)
ENDDO
CLOSE(4)
1 FORMAT(1X,I5,E15.6,2X,E15.6)
2 FORMAT(1X,4(E10.3,2X))
3 FORMAT(1X,E15.5,2X,I5)
END

SUBROUTINE VAR(ST,PHN,NI,XP,EP,AMIN,NV)
IMPLICIT REAL(8) (A - Z)
INTEGER I,NP,LMI,LH,NT,NV,NI,IIN,NN,IN
DIMENSION XPN(0:50),XP(0:50),ST(0:50)
COMMON /C/ LH,LMI,PI,NP
COMMON /B/ SE(0:50),DS(0:50),DE(0:50),NT
!SHARED LH,LMI,NT,PI,DS(),NP
! ************** SEARCH OF THE MINIMUM ****************
DO I=LMI,NP,LH
XPN(I)=XP(I)
ENDDO
NN=LMI
PH=PHN
CALL DET(XPN,ST,ALA)
B=ALA
IF (NV==0) GOTO 3012
DO IIN=1,NI
NN=-LH
```

```
GOTO 1119
1159 XPN(NN)=XPN(NN)-PH*XP(NN)
1119 NN=NN+LH
IF (NN>NP) GOTO 3012
IN=0
2229 A=B
XPN(NN)=XPN(NN)+PH*XP(NN)
IF (XPN(NN)<0.0D0) GOTO 1159
IN=IN+1
CALL DET(XPN,ST,ALA)
B=ALA
IF (B<A) GOTO 2229
C=A
XPN(NN)=XPN(NN)-PH*XP(NN)
IF (IN>1) GOTO 3339
PH=-PH
GOTO 5559
3339 IF (ABS((C-B)/(B))<EP) GOTO 4449
 PH=PH/2.0D0
5559 B=C
GOTO 2229
4449 PH=PHN
B=C
IF (NN<NP) GOTO 1119
AMIN=B
PH=PH/NI
ENDDO
3012  AMIN=B
DO I=LMI,NP,LH
XP(I)=XPN(I)
ENDDO
END

SUBROUTINE DET(XP,ST,XI)
IMPLICIT REAL(8) (A - Z)
INTEGER I,N
DIMENSION XP(0:50),ST(0:50)
COMMON /B/ SE(0:50),DS(0:50),DE(0:50),N
! ********** DETERMINANT **********
S=0.0D0
CALL SEC(XP,ST)
```

```
DO I=1,N
S=S+((ST(I)-SE(I))/DE(I))**2
DS(I)=((ST(I)-SE(I))/DE(I))**2
ENDDO
XI=S/N
END

SUBROUTINE SEC(XP,S)
IMPLICIT REAL(8) (A - Z)
INTEGER I,NP,LH,LMI,LMA,NT,NYS,L
DIMENSION S0(0:50),P(0:50),FR(0:50),ET(0:50), S(0:50),XP(0:50)
COMMON /A/ PI,NT,TT(0:50),GG,SS,LMI,LMA,LH,NYS,NP
! ********** CALCULATION OF THE CROSS SECTIONS ********
DO I=LMI,LMA,LH
FR(I)=XP(I)
ET(I)=1.0D0
! IF NP=LMA GOTO 1234
! ET(I)=EXP(-2*XP(I+LMA+LH))
ENDDO
RECUL1=0.0D0; AIMCUL1=0.0D0
CALL CULFAZ(GG,S0)
DO I=1,NT
T=TT(I)*PI/180.0D0
X=DCOS(T)
A=2.0D0/(1-X)
S00=2.0D0*S0(0)
BB=-GG*A
ALO=GG*DLOG(A)+S00
RECUL=BB*DCOS(ALO)
AIMCUL=BB*DSIN(ALO)
IF (NYS==0) GOTO 555
X1=DCOS(T)
A1=2.0D0/(1.0D0+X1)
BB1=-GG*A1
ALO1=GG*DLOG(A1)+S00
RECUL1=BB1*COS(ALO1)
AIMCUL1=BB1*SIN(ALO1)
555 RENUC=0.0D0; AIMNUC=0.0D0
DO L=LMI,LMA,LH
AL=ET(L)*DCOS(2.0D0*FR(L))-1.0D0
BE=ET(L)*DSIN(2.0D0*FR(L))
```

```
LL=2.0D0*L+1.0D0
SL=2.0D0*S0(L)
CALL POLLEG(X,L,P)
RENUC=RENUC+LL*(BE*DCOS(SL)+AL*DSIN(SL))*P(L)
AIMNUC=AIMNUC+LL*(BE*DSIN(SL)-AL*DCOS(SL))*P(L)
ENDDO
IF (NYS==0) GOTO 556
AIMNUC=2.0D0*AIMNUC
RENUC=2.0D0*RENUC
556 RE=RECUL+RECUL1+RENUC
AIM=AIMCUL+AIMCUL1+AIMNUC
S(I)=10.0D0*(RE**2+AIM**2)/4.0D0/SS**2
ENDDO
END

SUBROUTINE POLLEG(X,L,P)
IMPLICIT REAL(8) (A - Z)
INTEGER I,L
DIMENSION P(0:50)
! ************** THE LEGENDRE POLINOMIALS *************
P(0)=1.0D0
P(1)=X
DO I=2,L
A=I*1.0D0
P(I)=(2.0D0*A-1)*X/A*P(I-1)-(A-1.0D0)/A*P(I-2)
ENDDO
END

SUBROUTINE CULFAZ(G,F)
! ************** THE COULOMB PHASE SHIFTS **************
IMPLICIT REAL(8) (A - Z)
INTEGER I
DIMENSION F(0:50)
C=0.577215665D0
S=0.0D0; N=50
A1=1.202056903D0/3.0D0
A2=1.0369277550D0/5.0D0
DO I=1,N
AA=I*1.0D0
A=G/AA-DATAN(G/AA)-(G/AA)**3/3.0D0+(G/AA)**5/5.0D0
S=S+A
```

```
ENDDO
FAZ=-C*G+A1*G**3-A2*G**5+S
F(0)=FAZ
DO I=1,20
A=I*1.0D0
F(I)=F(I-1)+DATAN(G/A)
ENDDO
END
```

Furthermore, the control account for finding $^4He^4He$ elastic scattering phase shifts at an energy of 13 MeV is provided. The phase shifts $\delta_0 = 29° \pm 4°$, $\delta_2 = 103° \pm 8°$, and $\delta_4 = 3° \pm 1.5°$ are presented in [88]. These phase shifts are accepted as initial and present further variations in 10 iterations using the previous program in the Turbo Basic Compiler [10] and on the basis of the program given above. From this, we find values of $\delta_0 = 28.37°$, $\delta_2 = 105.03°$, and $\delta_4 = 2.62°$ at $\chi^2 = 3.43$; this is clarified in the following with the results of the program written in Fortran-90.

χ^2	NI
3.943880354539536	1
3.437578175376997	2
3.432394633290976	3
3.432107724455588	4
3.432044190539325	5
3.432020692528544	6
3.432007556422437	7
3.432005733725609	8
3.432004938728721	9
3.432004743298262	10

$\chi^2 =$; NI = 10; EL = 3.43200 10 1300

θ	σ_e	σ_t	χ^2_i
.22000E+02	.13570E+04	.12796E+04	.39401E+01
.24000E+02	.12030E+04	.11346E+04	.29238E+01
.26000E+02	.10740E+04	.10008E+04	.93096E+01
.28000E+02	.87000E+03	.87464E+03	.53776E-01
.30000E+02	.75900E+03	.75523E+03	.55540E-01
.32000E+02	.68800E+03	.64266E+03	.71117E+01
.35000E+02	.46700E+03	.48793E+03	.30429E+01
.40000E+02	.27100E+03	.27340E+03	.11779E+00
.42000E+02	.19600E+03	.20443E+03	.42244E+01

.45000E+02	.13000E+03	.12007E+03	.76028E+01
.46000E+02	.93900E+02	.97112E+02	.21321E+01
.48000E+02	.57000E+02	.58891E+02	.15896E+01
.50000E+02	.32500E+02	.30767E+02	.24826E+01
.52000E+02	.12300E+02	.12398E+02	.95282E-02
.55000E+02	.22800E+01	.20301E+01	.39027E+00
.60000E+02	.24700E+02	.24774E+02	.11250E-01
.65000E+02	.86500E+02	.85514E+02	.24313E+00
.70000E+02	.15700E+03	.16800E+03	.93323E+01
.75000E+02	.27000E+03	.25509E+03	.52640E+01
.80000E+02	.33700E+03	.33073E+03	.71799E+00
.85000E+02	.40800E+03	.38184E+03	.10177E+02
.90000E+02	.41800E+03	.39987E+03	.47720E+01

L	δ_r	δ_m
0	.283717E+02	.000000E+00
2	.105030E+03	.000000E+00
4	.261561E+01	.000000E+00

For the list of results above, the following designations are accepted: θ is the scattering angle; σ_e is the experimental cross section; σ_t is the calculated cross sections; χ^2_i is partial χ^2 for the angle *i*-th; δ_r is the real part of the phase shift; δ_m is the imaginary part of the phase shift; χ^2 is the average value for all points; and EL is the energy in the laboratory system.

The orbital moment of the phase shifts is specified as follows: in the first line, $L = 0$; in the second, $L = 2$; and in the third, $L = 4$. In the search for a minimum, as in [10], 10 iterations NI were used. However, in this case the accuracy of the EP was set to be equal to 10^{-10}, while in the previous version it was set as 10^{-5} [10]. The first χ^2 and NI columns of the list show the convergence of χ^2 with the number of iterations NI.

The control account is provided for an energy of 29.5 MeV; as described in [10], using the program in BASIC we obtained the following phase shifts $\delta_0 = 150.76$, $\delta_2 = 86.61$, $\delta_4 = 121.00$, $\delta_6 = 2.16$, and $\delta_8 = 0.09$ with $\chi^2 = 0.602$ (Table 2.1.1). Looking at the phase shifts given by the program, $\chi^2 = 0.600$ is the result for the number of iterations NI = 0.

$\chi^2 =$; NI = 0; EL = 0.600328 0 29.50

θ	σ_e	σ_t	χ^2_i
.22040E+02	.15230E+04	.15134E+04	.64891E+00
.24050E+02	.11640E+04	.11664E+04	.55570E-01
.26050E+02	.88590E+03	.86843E+03	.38892E+01

.28050E+02	.61610E+03	.61957E+03	.23236E+00
.30060E+02	.42260E+03	.41922E+03	.35643E+00
.32060E+02	.27000E+03	.26762E+03	.34211E+00
.34060E+02	.16020E+03	.16006E+03	.24306E-02
.36070E+02	.91500E+02	.91163E+02	.44395E-01
.38070E+02	.55530E+02	.55230E+02	.16734E+00
.40070E+02	.44680E+02	.44765E+02	.12421E+00
.42080E+02	.52960E+02	.52530E+02	.76193E+00
.44080E+02	.71740E+02	.71346E+02	.28489E+00
.46080E+02	.95440E+02	.94808E+02	.57926E+00
.48080E+02	.11846E+03	.11754E+03	.12657E+01
.50090E+02	.13558E+03	.13552E+03	.72584E-02
.52090E+02	.14562E+03	.14590E+03	.26152E+00
.54090E+02	.14760E+03	.14758E+03	.53350E-03
.56090E+02	.13986E+03	.14072E+03	.14564E+01
.58100E+02	.12710E+03	.12655E+03	.43671E+00
.60100E+02	.10783E+03	.10745E+03	.23062E+00
.62100E+02	.86660E+02	.86114E+02	.46841E+00
.64100E+02	.66120E+02	.65522E+02	.75651E+00
.66100E+02	.48430E+02	.48481E+02	.10080E-01
.68110E+02	.37430E+02	.37301E+02	.17753E+00
.70110E+02	.33770E+02	.33732E+02	.43056E-01
.72110E+02	.38340E+02	.38461E+02	.13210E+00
.74110E+02	.50740E+02	.51308E+02	.10928E+01
.76110E+02	.70820E+02	.71187E+02	.24362E+00
.78110E+02	.95550E+02	.96239E+02	.60125E+00
.80110E+02	.12420E+03	.12403E+03	.27579E-01
.82110E+02	.15340E+03	.15182E+03	.22344E+01
.84110E+02	.17750E+03	.17683E+03	.42129E+00
.86110E+02	.19700E+03	.19657E+03	.17685E+00
.88110E+02	.20974E+03	.20905E+03	.51222E+00
.90110E+02	.21120E+03	.21302E+03	.29660E+01

L	δ_r	δ_m
0	.150760E+03	.000000E+00
2	.866100E+02	.000000E+00
4	.121000E+03	.000000E+00
6	.216000E+01	.000000E+00
8	.900000E-01	.000000E+00

The difference in value χ^2 at 0.02 is the result of rounding errors of the phase shifts when registering their values in the file from the program in BASIC and their subsequent processing in Fortran-90. Hereafter, the imaginary part of the phase shift δ_m is equal to zero for all values of the orbital moment in this paragraph.

Using these phase shifts as initial values, with an additional variation according to the new program in Fortran-90 given above with 10 iterations and with the greatest possible accuracy of 10^{-15}, we obtained the result with the smallest χ^2 value.

χ^2 = ; NI = ; EL = 0.571434 10 29.500

θ	σ_e	σ_t	χ^2_i
.22040E+02	.15230E+04	.15144E+04	.52763E+00
.24050E+02	.11640E+04	.11671E+04	.90939E-01
.26050E+02	.88590E+03	.86891E+03	.36792E+01
.28050E+02	.61610E+03	.61990E+03	.27763E+00
.30060E+02	.42260E+03	.41943E+03	.31337E+00
.32060E+02	.27000E+03	.26775E+03	.30469E+00
.34060E+02	.16020E+03	.16015E+03	.33034E-03
.36070E+02	.91500E+02	.91219E+02	.30734E-01
.38070E+02	.55530E+02	.55273E+02	.12333E+00
.40070E+02	.44680E+02	.44803E+02	.25848E+00
.42080E+02	.52960E+02	.52569E+02	.62951E+00
.44080E+02	.71740E+02	.71391E+02	.22342E+00
.46080E+02	.95440E+02	.94863E+02	.48325E+00
.48080E+02	.11846E+03	.11761E+03	.10869E+01
.50090E+02	.13558E+03	.13560E+03	.13302E-02
.52090E+02	.14562E+03	.14600E+03	.47518E+00
.54090E+02	.14760E+03	.14770E+03	.17885E-01
.56090E+02	.13986E+03	.14085E+03	.19094E+01
.58100E+02	.12710E+03	.12668E+03	.25354E+00
.60100E+02	.10783E+03	.10757E+03	.10341E+00
.62100E+02	.86660E+02	.86228E+02	.29377E+00
.64100E+02	.66120E+02	.65613E+02	.54400E+00
.66100E+02	.48430E+02	.48542E+02	.48101E-01
.68110E+02	.37430E+02	.37326E+02	.11519E+00
.70110E+02	.33770E+02	.33722E+02	.70632E-01
.72110E+02	.38340E+02	.38419E+02	.55430E-01
.74110E+02	.50740E+02	.51240E+02	.84900E+00
.76110E+02	.70820E+02	.71105E+02	.14712E+00
.78110E+02	.95550E+02	.96154E+02	.46141E+00

.80110E+02	.12420E+03	.12395E+03	.59440E-01
.82110E+02	.15340E+03	.15175E+03	.24240E+01
.84110E+02	.17750E+03	.17678E+03	.48540E+00
.86110E+02	.19700E+03	.19654E+03	.20525E+00
.88110E+02	.20974E+03	.20903E+03	.54586E+00
.90110E+02	.21120E+03	.21300E+03	.29054E+01

L	δ_r	δ_m
0	.150729E+03	.000000E+00
2	.865625E+02	.000000E+00
4	.120914E+03	.000000E+00
6	.211725E+01	.000000E+00
8	.662343E-01	.000000E+00

It appears that it is possible to reduce χ^2 to 0.571 thanks to the increased accuracy in finding a minimum for such a multiparameter variation problem, in comparison to the programs in BASIC presented in [10].

2.2 Phase shift analysis of $^4He^{12}C$ elastic scattering

We consider here the methods of phase shift analysis for non-identical particles with spins 0 + 0 and the results of the phase shift analysis for elastic scattering in the $^4He^{12}C$ system at astrophysical energies. To obtain these results, the same computer program as that used for $^4He^4He$ elastic scattering was used, but with other program parameters (see paragraph 2.1.4) [99].

2.2.1 Differential cross sections

In the case of elastic scattering of non-identical particles with zero spin the expression for the cross section takes the simplest form [6]

$$\frac{d\sigma(\theta)}{d\Omega} = \left| f(\theta) \right|^2 ,$$

where the total scattering amplitude $f(\theta)$ is presented in the form of the sum of the Coulomb $f_c(\theta)$ and nuclear $f_N(\theta)$ amplitudes

$$f(\theta) = f_c(\theta) + f_N(\theta),$$

which are expressed through the nuclear $\delta_L \to \delta_L + i\Delta_L$ and Coulomb σ_L scattering phase shifts; the form of the amplitudes is given at the beginning of this chapter (see paragraph 2.1.2).

For the cross section of the elastic scattering at $f_c = 0$, the expression is known

$$\sigma_s = \frac{\pi}{k^2}\sum_L\left[(2L+1)\left(\left|1-S_L\right|^2\right)\right] = \frac{4\pi}{k^2}\sum_L(2L+1)\eta_L^2\sin^2\delta_L \ . \qquad (2.2.1)$$

The summation in this expression, unlike for ^{4}He^{4}He scattering, is carried out for all possible L.

2.2.2 Phase shift analysis

We present the results of the phase shift analysis obtained for ^{4}He^{12}C elastic scattering in the energy range 1.5–6.5 MeV. Previously, the phase shift analysis of the differential cross sections at energies of 2.5–5.0 MeV was carried out [100]. A possible description of such scattering phase shifts on the basis of potentials with forbidden states was undertaken by us in [101]. Here, using the experimental data on the excitation functions at seven angles from [100], we have repeated the phase shift analysis [100] in the energy range 2.5–4.5 MeV. These results can be considered a control test for our new computer program in Fortran-90 and the calculation methods used. We note that the measurement of excitation functions at such a small number of points on the scattering angles is not enough to reproduce the shape of angular distributions of ^{4}He^{12}C elastic scattering, even at low energies and with good accuracy. Therefore, it is possible that the phase shift analysis does not allow one to obtain completely unambiguous values, especially for the S waves, in spite of the fact that the known results of phase shift analysis were used [100].

Further results of our analysis are presented by points in figs. 2.2.1–2.2.5. In Fig. 2.2.1, the S phase shift values of average χ^2, obtained for various scattering energies, are shown. As can be seen in these figures, the S phase shift differs from the data presented in [100]; this is shown by the solid curve; the phase shifts in all other partial waves will show relatively good agreement with the results in [100]. However, with the data on excitation functions undertaken from the figures in [100], the possible error in the present phase shift analysis depends on the accuracy of the data on cross sections at about 2–3°, which in general allows us to explain the divergence in the results of these analyses for the S elastic scattering phase shifts.

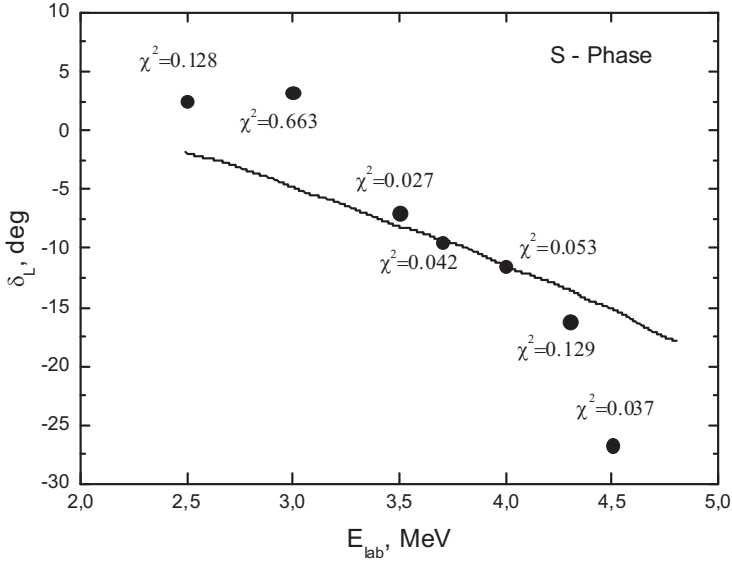

Fig. 2.2.1. *S* phase shift of $^{4}He^{12}C$ elastic scattering. The curve gives data from [100]. The points represent the results obtained by us on the basis of data in [100].

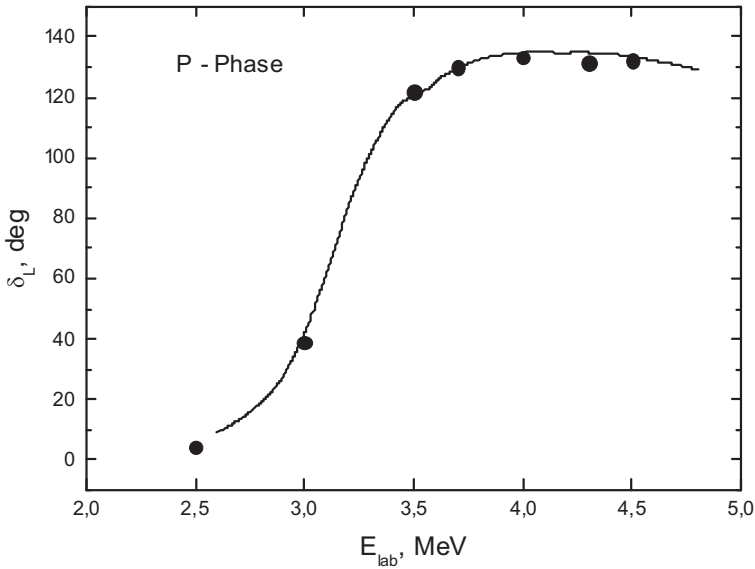

Fig. 2.2.2. *P* phase shift of $^{4}He^{12}C$ elastic scattering; the designations are the same as Fig. 2.2.1.

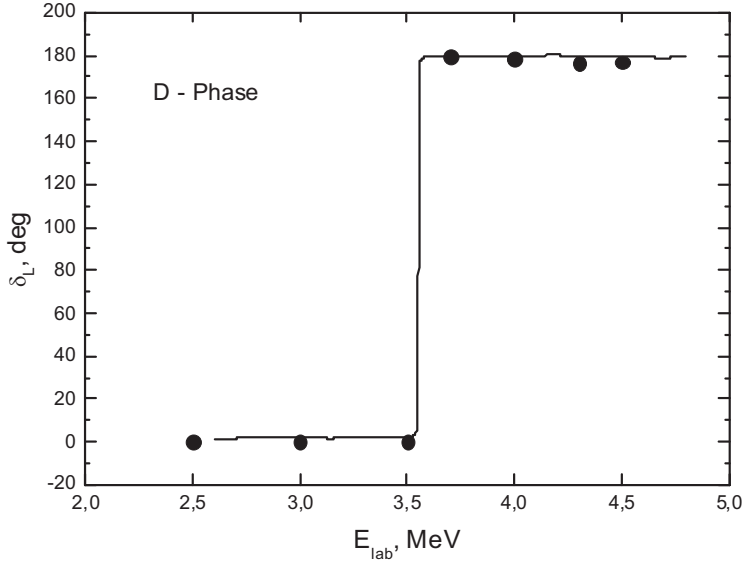

Fig. 2.2.3. *D* phase shift of $^{4}He^{12}C$ elastic scattering; the designations are the same as Fig. 2.2.1.

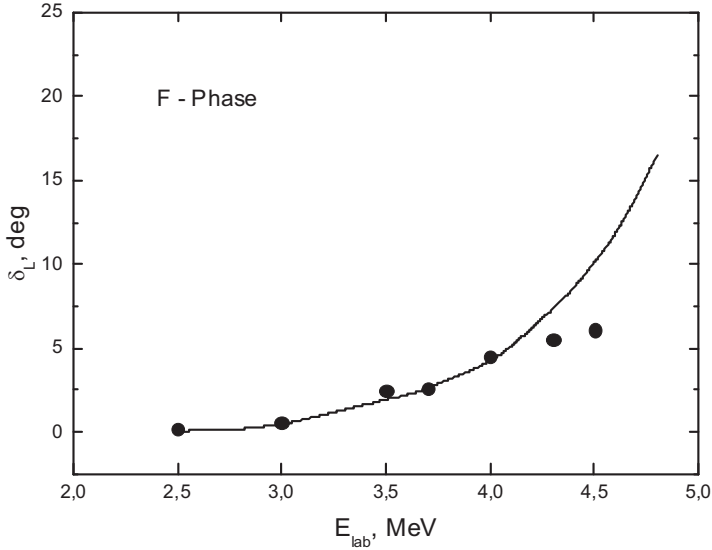

Fig. 2.2.4. *F* phase shift of $^{4}He^{12}C$ elastic scattering. The designations are the same as Fig. 2.2.1.

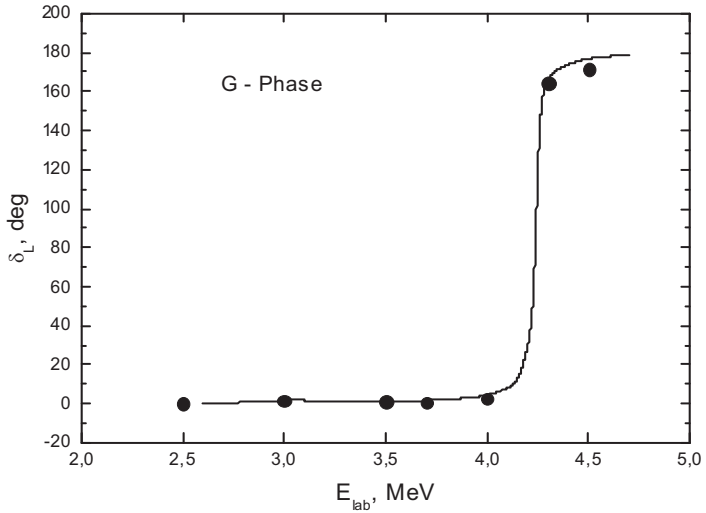

Fig. 2.2.5. *G* phase shift of $^4He^{12}C$ elastic scattering. The designations are the same as Fig. 2.2.1.

In [102], a very accurate phase shift analysis of the experimental data at 49 energies in the range 1.5–6.5 MeV was made. Using these data, we carried out phase shift analyses at energies of 1.466, 1.973, 2.073, 2.870, 3.371, 4.851, 5.799, and 6.458 MeV.

The results obtained in our analysis are presented in tables 2.2.1–2.2.8 together with the average χ^2 values compared to the tabular data presented in [102]. The spectrum of resonance levels and their widths observed in $^4He^{12}C$ elastic scattering and given in the review are shown in Table 2.2.9 [103].

Table 2.2.1. The results of phase shift analysis of $^4He^{12}C$ elastic scattering and their comparison to data presented in [102] at an energy of 1.466 MeV.

E_{lab} = 1.466 MeV (χ^2 = 0.055)		
L	δ° (Our)	δ° [102]
0	-0.2	0.5±1.0
1	-0.4	-0.1±1.0
2	-1.1	-0.8±1.0

Table 2.2.2. The results of phase shift analysis of $^4He^{12}C$ elastic scattering and their comparison to data presented in [102] at an energy of 1.973 MeV.

E_{lab} = 1.973 MeV (χ^2 = 0.077)		
L	δ° (Our)	δ° [102]
0	-2.6	-0.5±1.0
1	0.0	0.9±1.7
2	1.2	-0.1±1.3

Table 2.2.3. The results of phase shift analysis of $^4He^{12}C$ elastic scattering and their comparison to data presented in [102] at an energy of 2.073 MeV.

E_{lab} = 2.073 MeV (χ^2 = 0.029)		
L	δ° (Our)	δ° [102]
0	-1.2	0±0.8
	-0.1	0.1±1.2
2	-1.1	-0.6±0.9

Table 2.2.4. The results of phase shift analysis of $^4He^{12}C$ elastic scattering and their comparison to data presented in [102] at an energy of 2.870 MeV.

E_{lab} = 2.870 MeV (χ^2 = 0.038)		
L	δ° (Our)	δ° [102]
0	-3.1	-1±1.1
1	21.3	22.0±1
2	0.0	0.4±0.9
3	0.5	1.0±0.5

Table 2.2.5. The results of phase shift analysis of $^4He^{12}C$ elastic scattering and their comparison to data presented in [102] at an energy of 3.371 MeV.

E_{lab} = 3.371 MeV (χ^2 = 0.1)		
L	δ° (Our)	δ° [102]
0	169.4	-
1	103.4	103.7±1.7
2	-1.7	0.0±0.7
3	0.2	0.8±0.6

Table 2.2.6. The results of phase shift analysis of $^4He^{12}C$ elastic scattering and their comparison to data presented in [102] at an energy of 4.851 MeV.

E_{lab} = 4.851 MeV (χ^2 = 0.26)		
L	δ° (Our)	δ° [102]
0	164.2	164±1.1
1	128.4	129.5±0.9
2	177.1	178.8±0.9
3	15.5	16.4±0.8
4	176.9	177.2±0.8
5	-0.3	0.5±0.5

Table 2.2.7. The results of phase shift analysis of $^4He^{12}C$ elastic scattering and their comparison to data presented in [102] at an energy of 5.799 MeV.

E_{lab} = 5.799 MeV (χ^2 = 0.37)		
L	Reδ° (Our)	Reδ°
0	162	-
1	128.2	-

Table 2.2.8. The results of phase shift analysis of $^4He^{12}C$ elastic scattering and their comparison to data presented in [102] at an energy of 6.458 MeV.

E_{lab} = 6.458 MeV (χ^2 = 0.41)		
L	δ° (Our)	δ°
0	151.2	153±5
1	119.8	119.4±1

2	83.2	83±0.6
3	86.0	-
4	173.8	175.3±0.7
5	-1.0	0.2±0.4

2	172	172±1.9
3	120.8	122.0±4
4	176.4	179.1±1.2
5	0.8	2±0.8
6	0.1	0.4±0.4

Looking at these tables, it is clear that the $^4He^{12}C$ scattering energy of 3.371 MeV falls on the energy level of 3.324 MeV with a width of 480±20 keV, as specified in Table 2.2.9 and the review in [103]. However, in the tables in [102] the phase shift for the *S* waves is not given (dashes in Table 2.2.5) at this energy; our phase shift analysis, based on the real phase shifts of scattering, allows us to define all scattering phase shifts.

Table 2.2.9. Spectrum of levels of ^{16}O in $^4He^{12}C$ elastic scattering with T = 0 isospin [103]. Here, J^π is the total moment and parity; E_{lab} is the energy of the projectile particle in the laboratory system; and Γ_{cm} is the level width in the system of the center of mass. In the table, levels with a width of less than 1 keV are italicized and the states are shown in bold (discussed in the text).

E_{lab}, MeV	J^π	Γ_{cm}, keV
3.324	**1^-**	**480±20**
3.5770±0.5	*2^+*	*0.625±0.1*
4.259	4^+	27±3
5.245±8	*4^+*	*0.28±0.05*
5.47	0^+	2500
5.809±18	**2^+**	**73±5**
5.92±20	3^-	800±100
6.518±10	0^+	1.5±0.5
7.043±4	1^-	99±7

The energy of 5.799 MeV falls on the level of 5.809±18 MeV with a width of 73(3) keV [103] (see Table 2.2.9); in the tables presented in [102], the values of scattering phase shifts for some partial waves are not given (dashes in Table 2.2.7). In the phase shift analysis carried out here, it is

possible to describe the differential elastic scattering cross sections with an average value of $\chi^2 = 0.37$ and find all partial phase shifts (Table 2.2.7). The non-resonance energies at 2.870, 4.851, and 6.458 MeV (see tables 2.2.4, 2.2.6, and 2.2.8) are described by phase shifts, which, within the error limits given in [102] and taking into account a possible 10 % error due to the extraction of experimental data from the figures [102], coincide with the results in [102]. The last three energies of 1.466, 1.973, and 2.073 MeV (see tables 2.2.1, 2.2.2, and 2.2.3) are compatible with the zero values of nuclear phase shifts, i.e. they have ±1° values and correspond purely to the Coulomb interaction—Rutherford scattering.

In figs. 2.2.6–2.2.13, a description of the experimental differential cross sections of ^{4}He^{12}C elastic scattering are shown [102] with the scattering phase shifts at all considered energies given in tables 2.2.8–2.2.1. In the process of our phase shift analysis, it was necessary to transfer the differential cross sections and angles given in [102] in the laboratory to the system of the center of masses, making the calculations more convenient. The small differences in the scattering phase shifts can be caused by various values of constants or particle masses that are used in such an analysis. For example, it is possible to use exact values for the mass of particles [75] or their entire quantities, and the constant $\hbar^2/m_0$ can differ from 41.4686 MeV fm^2. In addition, the accuracy of the definition of scattering phase shifts on the basis of the data in [102] has been estimated by us at the level of 1–2°.

A comparison of results of the last phase shift analysis [104], obtained on the basis of the experimental data in [102] (points) and phase shift analysis in [100] (squares), is given in figs. 2.2.14–2.2.18. As can be seen from the results given in tables 2.2.1–2.2.8 and figs. 2.2.14–2.2.18, the phase shifts practically coincide with the conclusions in [102], but differ a little from the data in [100], especially for the *S* scattering wave. The analysis in [100] was made in the early 1960s when advanced computing facilities did not practically exist and modern programming and computing had only just started to develop. The analysis in [102] was performed in the late 1980s using far more developed computers and programming systems.

Thus, as a result of the phase shift analysis described here, it is possible to draw the following conclusions:

1. The energy of 3.371 MeV falls on the level of 3.324 MeV with quite a big width of 0.48 MeV; in the *P* wave, the smooth resonance is well represented.

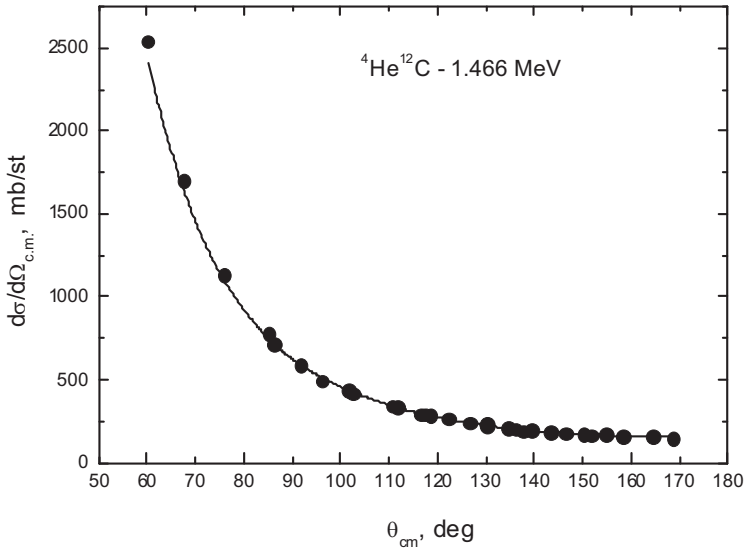

Fig. 2.2.6. Cross section of ^{4}He^{12}C elastic scattering at 1.466 MeV. The points represent the experimental data of [102], while the curve describes the results of phase shift analysis.

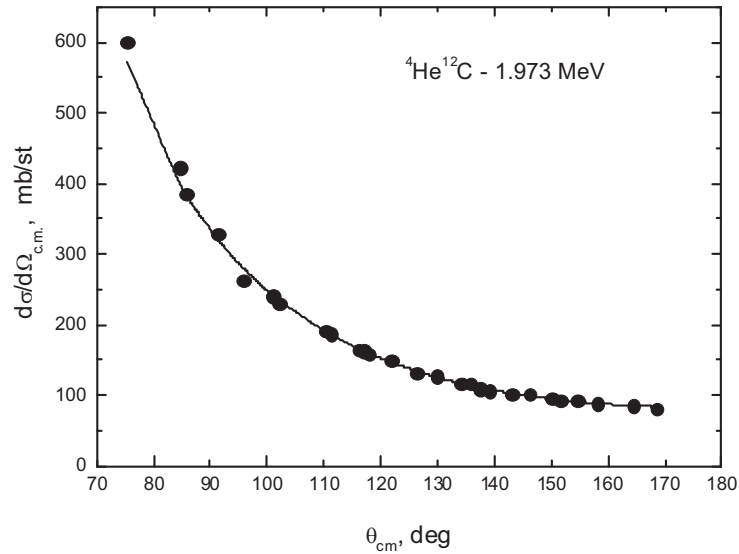

Fig. 2.2.7. The same as in Fig. 2.2.6, but at an energy of 1.973 MeV.

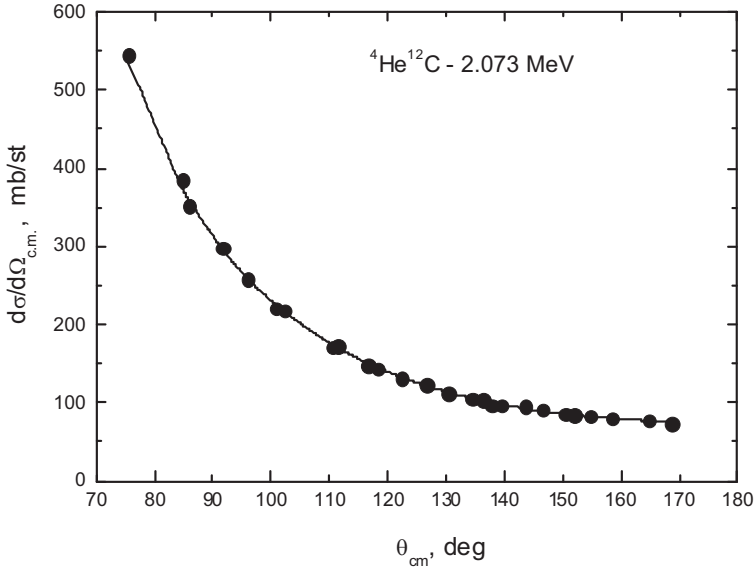

Fig. 2.2.8. The same as in Fig. 2.2.6, but at an energy of 2.073 MeV.

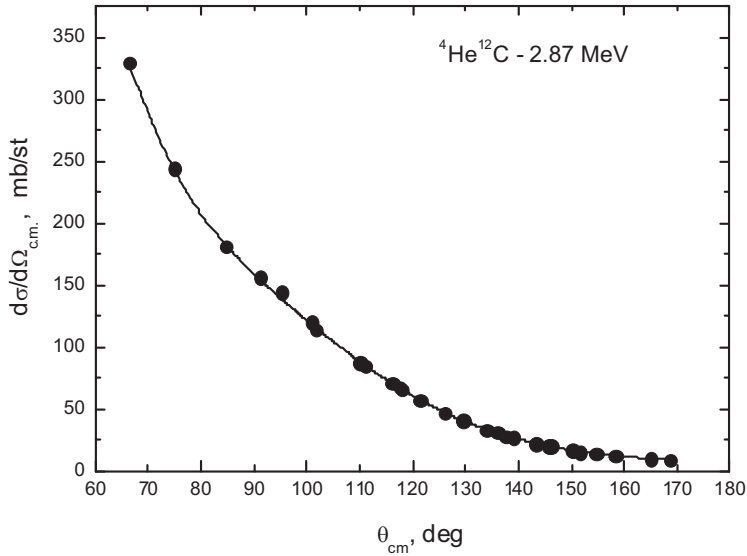

Fig. 2.2.9. The same as in Fig. 2.2.6, but at an energy of 2.87 MeV.

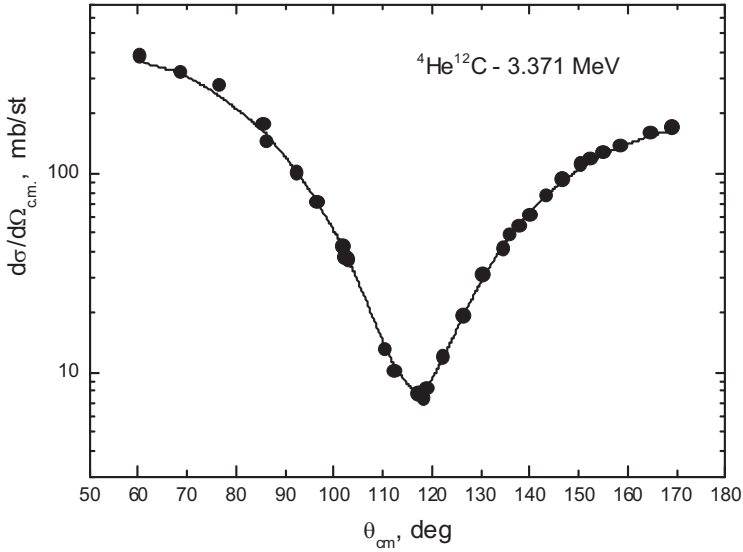

Fig. 2.2.10. The same as in Fig. 2.2.6, but at an energy of 3.371 MeV.

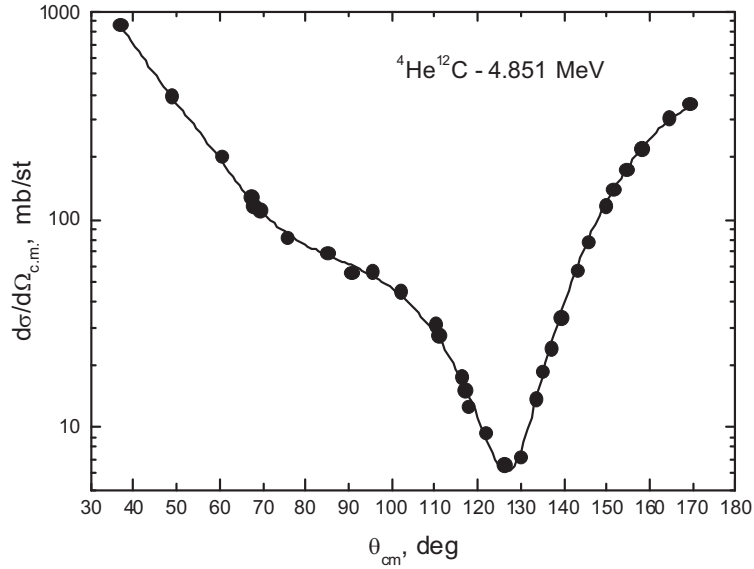

Fig. 2.2.11. The same as in Fig. 2.2.6, but at an energy of 4.851 MeV.

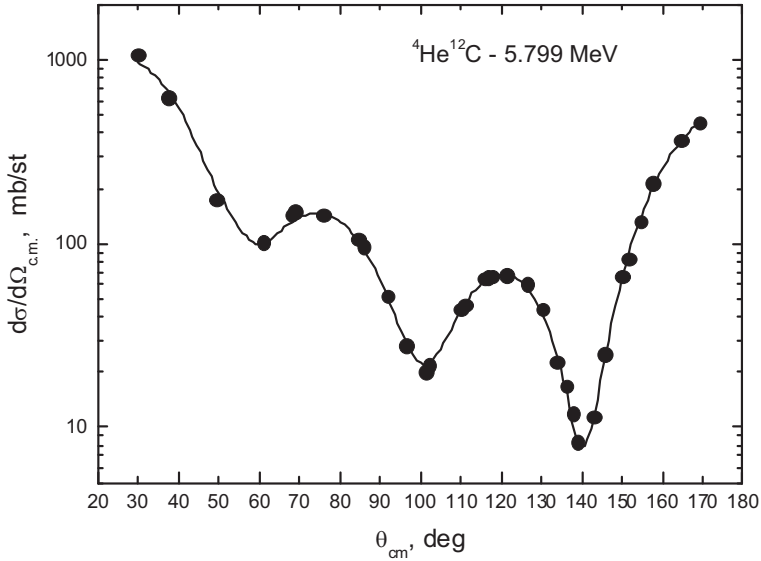

Fig. 2.2.12. The same as in Fig. 2.2.6, but at an energy of 5.799 MeV.

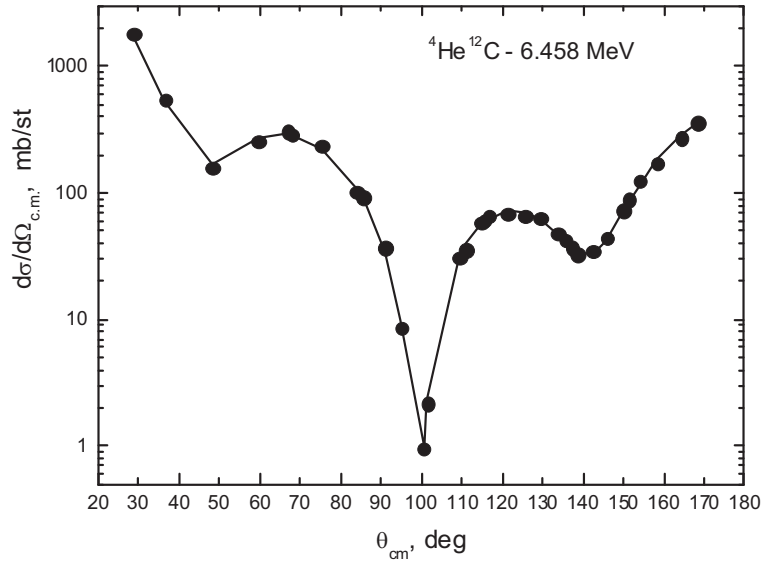

Fig. 2.2.13. The same as in Fig. 2.2.6, but at an energy of 6.458 MeV.

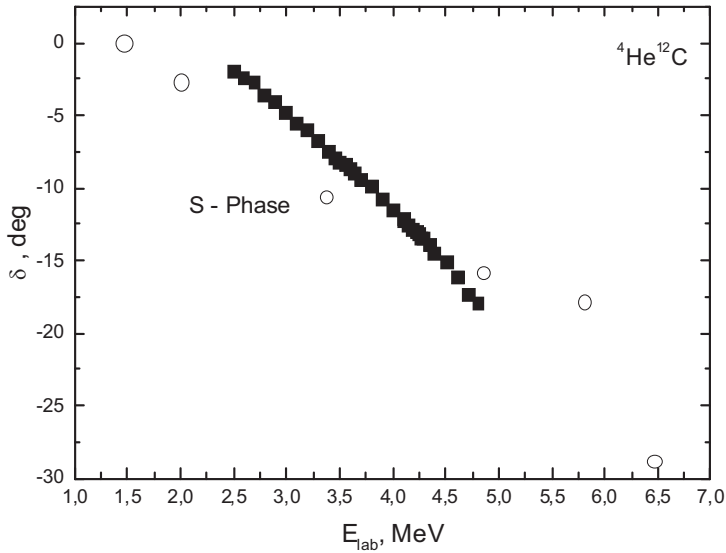

Fig. 2.2.14. The *S* phase shift of $^4He^{12}C$ elastic scattering. The squares represent data from [100], while the circles represent our results [104], obtained on the basis of data in [102].

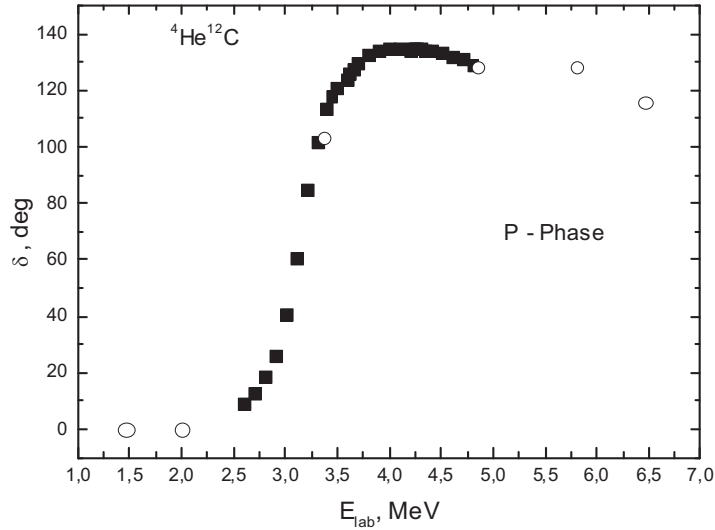

Fig. 2.2.15. *P* phase shift of $^4He^{12}C$ elastic scattering. The designations are the same as Fig. 2.2.14.

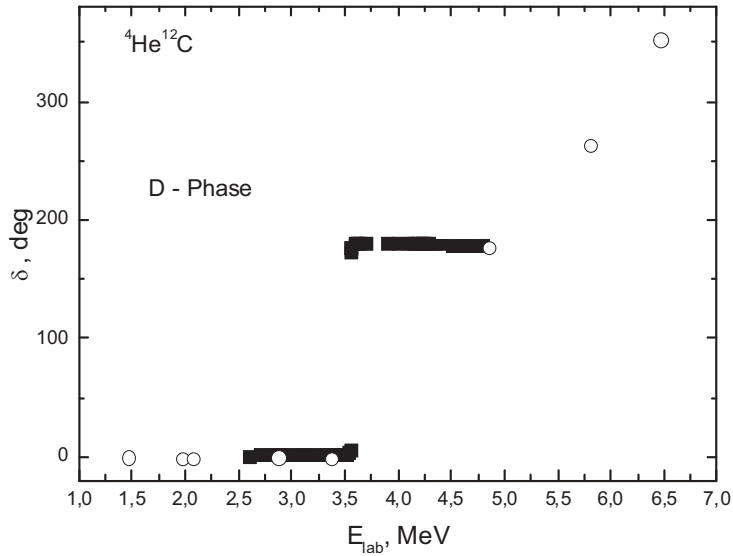

Fig. 2.2.16. *D* phase shift of $^4He^{12}C$ elastic scattering. The designations are the same as Fig. 2.2.14.

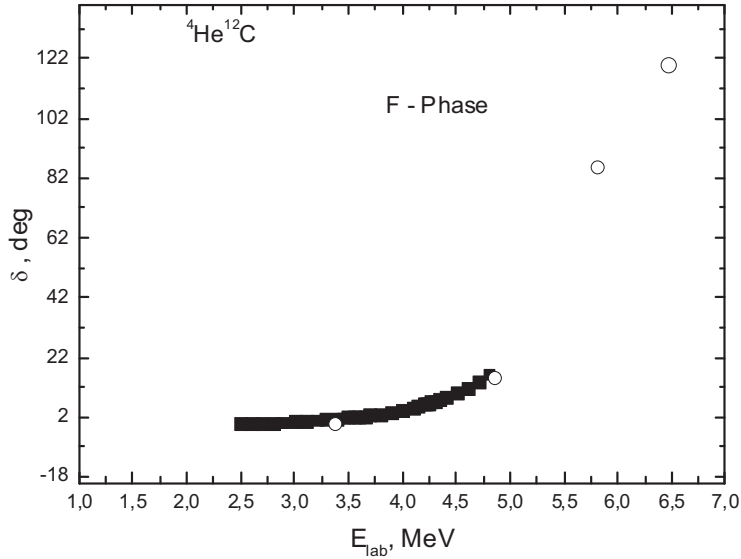

Fig. 2.2.17. *F* phase shift of $^4He^{12}C$ elastic scattering. The designations are the same as Fig. 2.2.14.

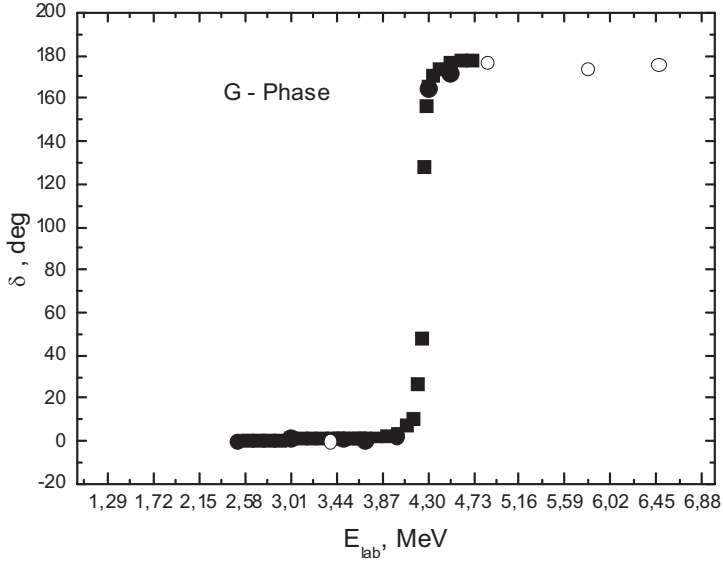

Fig. 2.2.18. *G* phase shift of $^{4}He^{12}C$ elastic scattering. The designations are the same as Fig. 2.2.14.

2. According to [100,102], in the *D* wave, a resonance corresponding to the level at 3.577 MeV with a very small width of 0.625 keV is observed. At this energy, as shown in Fig. 2.2.16, the transition of the phase shift through 90°, presented also in tables 2.2.5 and 2.2.6, is observed. In addition, in the results of analysis [102] another resonance appears at 5.799 MeV; at this energy in the *D* wave, we find the level of 5.809 MeV with a relatively large width of 73 keV. For this energy, the value of the phase shift (see Table 2.2.7) is almost equal to 90°. As a result, the *D* phase shift given in Fig. 2.2.16 passes through 90° twice, i.e. it corresponds to two resonances, which are present with this partial wave.
3. At an energy of 4.259 MeV with a width of 27 keV in the *G* wave there is a resonance level; in the results of [100] and [102] there is a visible disturbance of the phase shift, as shown in Fig. 2.2.18.
4. The energy of 5.799 MeV is about a resonance at 5.47 MeV with a very large width of 5 MeV and the moment 0^{+}; the *S* phase shift sees a greater increase.
5. There is a resonance with a width of 0.8 MeV and $J^{\pi} = 3^{-}$ for the *F* wave at the energy of 5.92 MeV and the *F* phase shift shown in Fig. 2.2.17, at this energy, has a value of about 90º (see also the results

given in tables 2.2.7 and 2.2.8 for the *F* elastic scattering phase shifts).

6. At three energies in the range 1.47–2.07 MeV, we can observe that pure Rutherford scattering and all nuclear phase shifts are almost equal to zero.

Furthermore, the elastic scattering phase shift values obtained in [105] are used for the creation of intercluster potentials and the calculation of an astrophysical *S*-factor of the radiative $^{12}C(^{4}He,\gamma)^{16}O$ capture reaction [2,28, 106,122,123]. This process, alongside the threefold helium cycle, is present in a chain of thermonuclear reactions at a hot stage of the development of stars with the temperature reaching hundreds of millions of degrees Kelvin [107]. At such a high temperature, the interacting particles have sufficient energy for the essential increase in the probability of passing through a Coulomb barrier. In this case, they approach the area of strong interaction leading to an increase in the contribution of such a reaction, i.e. in terms of its energy efficiency in the total energy balance of stars.

2.3 Phase shift analysis of elastic $N^{12}C$, $p^{14}C$, and $N^{16}O$ scattering

Methods of phase shift analysis for particles with spins 0 + 1/2 and the results of phase shift analysis for the $p^{12}C$ system are considered. The latest experimental data obtained at low and astrophysical energies are given in the works of the Institute of Nuclear Physics (INP) of the Republic of Kazakhstan (RK); they will also be used further in our phase shift analysis.

2.3.1 Differential cross sections

Considering elastic scattering in the system of particles with spins 0 and 1/2, we will examine the spin-orbital splitting of the phase shifts, which occurs in the nuclear $N^{4}He$, $^{3}H^{4}He$, and $N^{12}C$ systems. In this case, the elastic scattering of nuclear particles can be completely described by two independent spin amplitudes (*A* and *B*) and the cross section is presented in the following form [6]

$$\frac{d\sigma(\theta)}{d\Omega} = \left|A(\theta)\right|^2 + \left|B(\theta)\right|^2, \tag{2.3.1}$$

where

$$A(\theta) = f_c(\theta) + \frac{1}{2ik}\sum_{L=0}^{\infty}\{(L+1)S_L^+ + LS_L^- - (2L+1)\}\exp(2i\sigma_L)P_L(\cos\theta) \ ,$$

$$B(\theta) = \frac{1}{2ik}\sum_{L=0}^{\infty}(S_L^+ - S_L^-)\exp(2i\sigma_L)P_L^1(\cos\theta) \ . \qquad (2.3.2)$$

Here, $S_L^{\pm} = \eta_L^{\pm}\exp(2i\delta_L^{\pm})$ is a scattering matrix; $\eta^{\pm}_L$ is the inelasticity parameters; and the sign "±" corresponds to the total moment of the system $J = L \pm 1/2$.

The Coulomb amplitude of f_c can be presented in the form

$$f_c(\theta) = -\left(\frac{\eta}{2k\sin^2(\theta/2)}\right)\exp\{i\eta\ln[\sin^{-2}(\theta/2)] + 2i\sigma_0\} \ , \qquad (2.3.3)$$

where $P_n^m(x)$ stands for the associated Legendre polynomials; ισ is the Coulomb parameter; μ is the reduced mass of particles; and k is the wave number of the relative movement of particles in the input channel.

The associated Legendre polynomials or function $P_n^m(x)$ are presented in the form

$$P_n^m(x) = (1 - x^2)^{m/2}\frac{d^m P_n(x)}{dx^m},$$

and for $m = 1$, they can be found by recurrent formulas of the form

$$P_{L+1}^1(x) = \frac{(2L+1)x}{L}P_L^1(x) - \frac{L+1}{L}P_{L-1}^1(x),$$

with the initial values

$$P_0^1(x) = 0 \ , \qquad P_1^1(x) = (1-x^2)^{1/2} \ , \qquad P_2^1(x) = 3xP_1^1(x) \ .$$

The values of $P_n^2(x)$, which we investigate further, are calculated by other recurrent formulas

$$P_{L+1}^2(x) = \frac{(2L+1)x}{L-1}P_L^2(x) - \frac{L+2}{L-1}P_{L-1}^2(x),$$

with the initial values

$$P_0^2(x) = P_1^2(x) = 0 \quad , \quad P_2^2 = 3(1-x^2) \quad , \quad P_3^2(x) = 5xP_2^2(x).$$

Through the reduced amplitudes A and B, it is possible to express the vector polarization in the elastic scattering of such particles [6]

$$P(\theta) = \frac{2\,\mathrm{Im}(AB^*)}{|A|^2 + |B|^2}.$$

Writing the expression for the amplitude $B(\Theta)$, we obtain

$$\mathrm{Re}\,B = \frac{1}{2k}\sum_{L=0}^{\infty}[a\cdot\sin(2\sigma_L) + b\cdot\cos(2\sigma_L)]P_L^1(x)\,,$$

$$\mathrm{Im}\,B = \frac{1}{2k}\sum_{L=0}^{\infty}[b\cdot\sin(2\sigma_L) - a\cdot\cos(2\sigma_L)]P_L^1(x)\,,$$

where

$$a = \eta_L^+\cos(2\delta_L^+) - \eta_L^-\cos(2\delta_L^-)\,,$$

$$b = \eta_L^+\sin(2\delta_L^+) - \eta_L^-\sin(2\delta_L^-)\,.$$

Using a similar method for the amplitude of $A(\Theta)$, it is possible to find the following recording format [108]

$$\mathrm{Re}\,A = \mathrm{Re}\,f_c + \frac{1}{2k}\sum_{L=0}^{\infty}[c\cdot\sin(2\sigma_L) + d\cdot\cos(2\sigma_L)]P_L(x)\,,$$

$$\mathrm{Im}\,A = \mathrm{Im}\,f_c + \frac{1}{2k}\sum_{L=0}^{\infty}[d\cdot\sin(2\sigma_L) - c\cdot\cos(2\sigma_L)]P_L(x)\,,$$

where

$$c = (L+1)\eta_L^+\cos(2\delta_L^+) + L\eta_L^-\cos(2\delta_L^-) - (2L+1)\,,$$

$$d = (L+1)\eta_L^+ \sin(2\delta_L^+) + L\eta_L^- \sin(2\delta_L^-) .$$

For the total cross section of the elastic scattering, it is possible to obtain [6]

$$\sigma_s = \frac{\pi}{k^2}\sum_L \left[(L+1)\left|1 - S_L^+\right|^2 + L\left|1 - S_L^-\right|^2 \right],$$

or

$$\sigma_s = \frac{4\pi}{k^2}\sum_L \left\{ (L+1)[\eta_L^+ \sin\delta_L^+]^2 + L[\eta_L^- \sin\delta_L^-]^2 \right\} .$$

All these expressions have been used to carry out the phase shift analysis of $N^{12}C$ and $N^{16}O$ elastic scattering at energies of 1.0–2.5 MeV [109].

2.3.2 Control of the computer program

The text of our computer program for calculating the total and differential cross sections of the elastic scattering of particles with half-integer spin, which was used to carry out the corresponding phase shift analysis, is fully described further on and was tested on elastic scattering in the p^4He system. Here, only one version of the control account for this program for p^4He scattering is given, in comparison to the data from [110], where the phase shift analysis for an energy of 9.89 MeV was made; positive *D* phase shifts and an average on all point value $\chi^2 = 0.60$ were obtained.

In the analysis in [110], 22 points of the cross section from [111] are used at an energy of 9.954 MeV (in [110] it is not specified which 22 points have been taken from the 24 points provided in [111]) along with several points of polarization from [110,112]. In the latter case, 10 points at 8 angles are used: 46.5°, 55.9°, 56.2°, 73.5°, 89.7°, 99.8°, 114.3°, and 128.3°; and three relate to the energies 9.89, 9.84, and 9.82 MeV.

The phase shifts from [110] are given in Table 2.3.1 along with average χ^2_σ for the differential cross sections according to our program, taking into account 24 points from [111] (the energy is, still, equal to 9.954 MeV), and these phase shifts turn out to be equal to 0.586. The results of these calculations are shown in Table 2.3.2. For the 10 experimental data points of the polarization in [110,112], at energies of 9.82–9.89 MeV and at 8

scattering angles with the phase shifts from [110], it is possible to obtain the value $\chi^2_p = 0.589$ (the energy is still equal to 9.954 MeV). The results are given in Table 2.3.3.

Table 2.3.1. The phase shifts of p^4He elastic scattering from [110].

E, MeV	S_0, deg.	$P_{3/2}$, deg.	$P_{1/2}$, deg.	$D_{5/2}$, deg.	$D_{3/2}$, deg.
9.954	119,3 $^{+2.0}_{-1.8}$	112,4 $^{+3.5}_{-5.2}$	65,7 $^{+2.7}_{-3.2}$	5,3 $^{+1.6}_{-5}$	3,7 $^{+1.6}_{-2.8}$

Table 2.3.2. The differential cross sections of p^4He elastic scattering. Here, θ° is the scattering angle in degrees; σ_e is the experimental cross sections; and σ_t is the calculation cross sections.

θ°	σ_e, mb/st	σ_t, mb/st	χ^2_i	θ°	σ_e, mb/st	σ_t, mb/st	χ^2_i
25.10	371.00	366.85	0.31	109.90	21.00	20.70	0.51
30.89	339.00	331.54	1.21	120.60	23.00	259	0.79
35.07	305.00	308.40	0.31	122.80	24.50	24.19	0.40
49.03	232.00	230.61	0.09	130.13	31.90	31.91	0.00
54.70	205.00	199.10	2.07	130.90	33.20	32.90	0.21
60.00	176.00	170.56	39	134.87	37.80	38.44	0.71
70.10	124.00	120.59	1.89	140.80	47.30	47.69	0.17
80.00	82.00	79.77	1.85	145.00	54.00	54.62	0.33
90.00	49.20	48.82	0.15	149.40	61.60	61.88	0.05
94.07	39.10	39.44	0.19	154.90	70.60	70.54	0.00
1017	26.20	26.39	0.13	160.00	78.40	77.71	0.19
106.90	22.00	215	0.12	164.40	83.00	82.94	0.00

If we average the value χ^2 by all known points (24 + 10 = 34), i.e. use a more general expression for χ^2, then

$$\chi^2 = \frac{1}{(N_\sigma + N_p)}\left\{\sum_{i=1}^{N}\left[\frac{\sigma_i^t - \sigma_i^e}{\Delta\sigma_i^e}\right] + \sum_{i=1}^{N}\left[\frac{P_i^t - P_i^e}{\Delta P_i^e}\right]\right\} = \frac{1}{(N_\sigma + N_p)}\left\{\chi_\sigma^2 + \chi_p^2\right\},$$

which gives the value $\chi^2 = 0.5875 \approx 0.59$; this is in a good agreement with the results of [110]. Here, N_σ and N_P are the number of data points on the

cross section (24 points) and polarization (10 points); σ^e, P^e, σ^t, and P^t are experimental and theoretical values of the cross sections and polarization; and $\Delta\sigma$ and ΔP are their errors.

Table 2.3.3. Polarization in p^4He elastic scattering.
Here, θ° is the scattering angle in degrees; P_e is the experimental polarization; ΔP_e is the experimental error for the polarization; and P_t is the calculation of polarization.

θ°	P_e, %	ΔP_e	P_t, %	χ^2_i
46.50	-330	10	-33.11	0.15
55.90	-41.30	20	-450	0.30
56.20	-44.40	0.90	-42.81	3.11
73.50	-62.60	3.00	-62.84	0.01
73.50	-64.80	1.90	-62.84	1.06
89.70	-76.10	3.60	-76.33	0.01
89.70	-75.50	40	-76.33	0.12
99.80	-59.30	50	-58.55	0.09
114.30	48.20	3.20	51.03	0.78
128.30	99.40	3.30	97.66	0.28

$S_0 = 119.01^o$, $P_{3/2} = 1125^o$, $P_{1/2} = 65.39^o$, $D_{5/2} = 5.24^o$, $D_{3/2} = 3.63^o$.

If we execute additional χ^2 minimization using this program, then for χ^2_σ, according to the cross section, we obtain 0.576; for the $\chi^2_p = 0.561$ polarization and average $\chi^2 = 0.572 \approx 0.57$ at the following phase shift values

$S_0 = 119.01^o$, $P_{3/2} = 1125^o$, $P_{1/2} = 65.39^o$, $D_{5/2} = 5.24^o$, $D_{3/2} = 3.63^o$,

which lie fully in the error band given in [110] and are shown in Table 2.3.1.

Thus, the program allows us to obtain further results, which coincide well with earlier analyses. Furthermore, this was tested according to the phase shift analysis, carried out in other works at low energies, and directly for the elastic scattering in the $p^{12}C$ system.

Previously, the phase shift analysis of excitation functions for $p^{12}C$ elastic scattering measured in [113], at energies in the range 400–1300 keV (l.s.) and angles 106–169°, was carried out in [114]. It was found that, for example, at $E_{lab} = 900$ keV the S phase shift has to lie in the area 153–154°. With the same experimental data, we obtained the value 152.7°. To obtain

this result, the scattering cross section from the excitation functions of [113] at energies of 866–900 keV were used. In Table 2.3.4, the results of our calculations of σ_t are compared to the experimental data for σ_e. In the last column of the table, the partial χ^2_i values on each point at a 10 % error are given for the experimental cross sections; for an average of all experimental points of χ^2, the value 0.11 was obtained.

Table 2.3.4. Comparison of the theoretical and experimental cross sections of $p^{12}C$ elastic scattering at an energy of 900 keV.

θ°	σ_e, mb/st	σ_t, mb/st	χ^2_i
106	341	341.5	1.90E-04
127	280	281	5.76E-03
148	241	251.2	1.80E-01
169	250	237.5	50E-01

At an energy of 751 keV (l.s.) for the *S* phase shifts, values in the range 155–157° were found in [114]. The results obtained by us for this energy are given in Table 2.3.5.

Table 2.3.5. Comparison of the theoretical and experimental cross sections of $p^{12}C$ elastic scattering at an energy of 750 keV.

θ°	σ_e, mb/st	σ_t, mb/st	χ^2_i
106	428	428.3	3.44E-05
127	334	342.8	6.91E-02
148	282	299.1	3.66E-01
169	307	279.9	7.82E-01

The data on the cross sections of the excitation functions in the energy range 749–754 keV were used; for the *S* phase shifts it was found to be 156.8° with an average $\chi^2 = 0.30$. Thus, using our program, at two energies of $p^{12}C$ elastic scattering, phase shifts coinciding with the results of the analysis made on the basis of excitation functions in [114] were obtained.

2.3.3 Phase shift analysis of $p^{12}C$ scattering

The control calculations given above are in good agreement with earlier results; therefore, using our program, the phase shift analysis [115] of new experimental data on differential cross sections of $p^{12}C$ scattering in

the energy range 230–1200 keV (l.s.) were made [116], measured in INP RK. The results of this analysis are given in Table 2.3.6 and presented as points in Fig. 2.3.1, allowing comparison with the data in [114], which are shown by the dashed line.

Table 2.3.6. The results of phase shift analysis of $p^{12}C$ elastic scattering at low energies taking into account only the *S* phase shift.

E_{cm}, keV	$S_{1/2}$, deg.	χ^2
213	2.0	1.35
317	5	0.31
371	7.2	0.51
409	36.2	0.98
422	58.2	3.69
434	107.8	0.78
478	153.3	56
689	156.3	2.79
900	153.6	55
1110	149.9	1.77

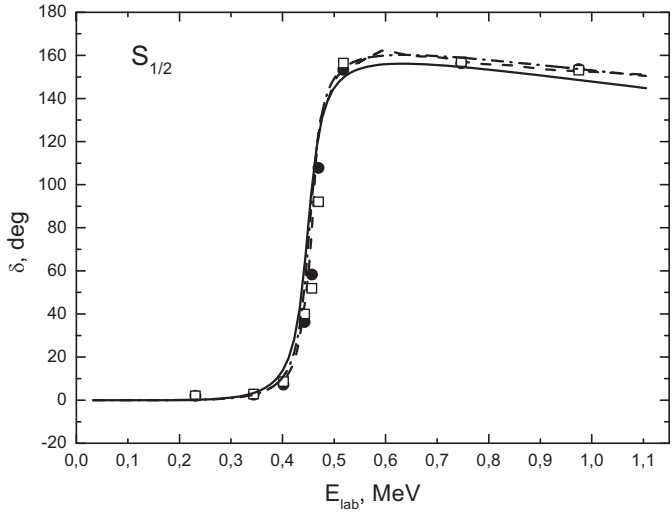

Fig. 2.3.1. The ^2S phase shift of $p^{12}C$ scattering at low energies. The points represent the results of phase shift analysis for the *S* phase shifts, taking into account the phase shift analysis of *S* waves; the open squares represent the results of the phase shift analysis for the *S* phase shifts taking into account the *S* and *P* waves; and the shaped curve represents the results found in [114].

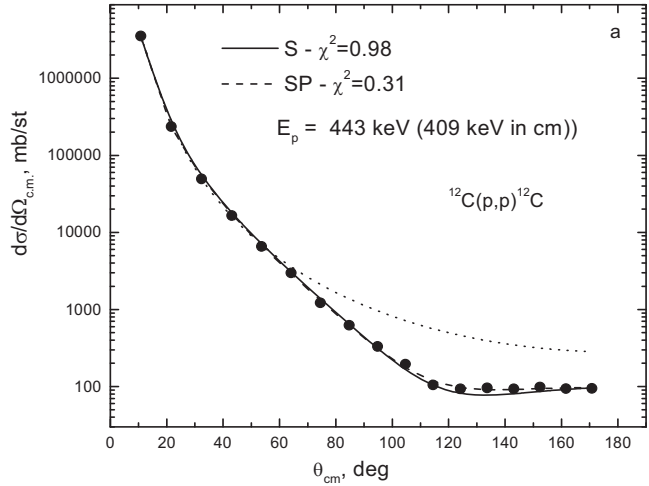

Fig. 2.3.2a. The differential cross sections of $p^{12}C$ elastic scattering. The solid curve was obtained on the basis of the phase shift analysis taking into account only the S wave; the dotted line represents Rutherford scattering; the dashed line represents the results of the phase shift analysis taking into account the *S* and *P* waves; and the points represent an experiment in [116].

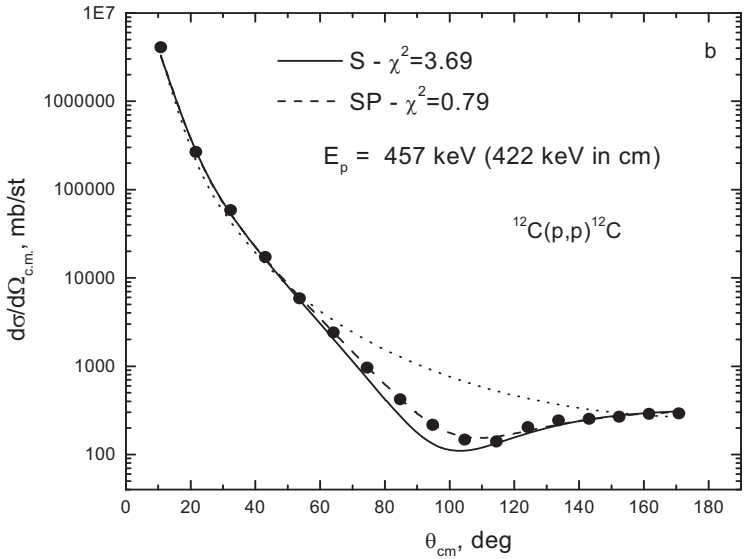

Fig. 2.3.2b. The differential cross sections of $p^{12}C$ scattering with the same signatures as Fig. 2.3.2a.

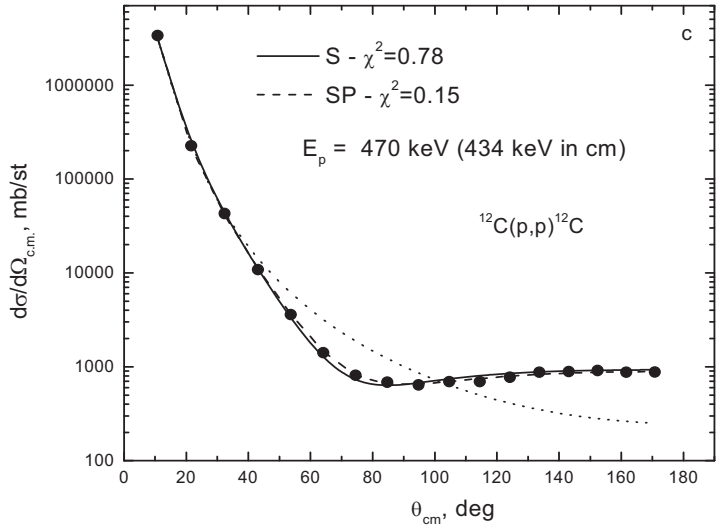

Fig. 2.3.2c. The differential cross sections of $p^{12}C$ scattering with the same signatures as Fig. 2.3.2a.

In figs. 2.3.2a, b, and c, the experimental differential cross sections in the resonance range at 457 keV (l.s.) are represented by points; the results of the calculation of these cross sections on the basis of Rutherford's formula are repesented by the dotted curve; the cross sections obtained from our phase shift analysis, which considers only the *S* phase shift, are represented by the solid line; and the analysis of the *S* and *P* scattering phase shifts is represented by the dotted curve. Looking at the figures, it is clear that in the resonance range it is not possible to describe well the cross section only on the basis of one *S* phase shift. The *P* wave presented in Fig. 2.3.3, the understanding of which considerably improves the description of the experimental data, begins to play a noticeable role. At a resonance energy of 457 keV (l.s.), for which the cross sections are shown in Fig. 2.3.2b, the account of the *P* waves reduces the value of χ^2 from 3.69 to 0.79.

In Fig. 2.3.3, it is clear that at low energies the $P_{1/2}$ phase shift goes higher than $P_{3/2}$, but at an energy of about 1.2 MeV they are crossed and $P_{3/2}$ goes higher in the negative range of the angles [117,118]. The value of the *S* phase shift taking into account the *P* wave practically does not change; its shape is presented in Fig. 2.3.1 by open squares. Accounting for the *D* wave in the phase shift analysis leads to its value being about one degree in the range of the *S* resonance and practically does not influence the behavior of the calculated differential cross sections.

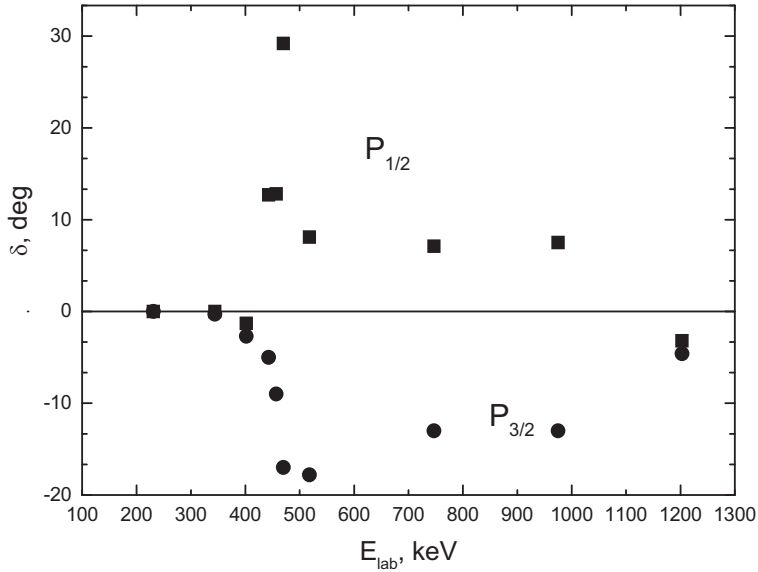

Fig. 2.3.3. The ^2P phase shifts of $p^{12}C$ scattering at low energies. The points represent $P_{3/2}$ and the squares represent the $P_{1/2}$ phase shifts, obtained as a result of phase shift analysis taking into account the S and P waves.

The total cross section of elastic scattering is represented by points in Fig. 2.3.4. These have been calculated on the basis of the experimental differential cross sections [116] of the S scattering phase shifts. The total cross sections obtained from the phase shift analysis of [114] are represented by circles. In Fig. 2.3.4, in the energy range 200–300 keV (l.s.), a plateau is observed. At the moment, it is not clear whether this was caused by experimental inaccuracy, unforeseen errors of the phase shift analysis, or that it really exists at these energies. For the clarification of this question, new measurements should be made of angular distributions of elastic $p^{12}C$ scattering in the energy range 100–150 to 300–400 keV, with an energy step of about 50 keV, or the excitation functions are required at different angles [109].

In the conclusion of this paragraph, we note that in this case another slightly different value than usual, $\hbar^2/m_0 = 41.80159$ MeV·fm^2, was used. This was obtained with slightly different values of the fundamental constants $\hbar^2$ and m_0 where the last value designates the atomic unit of mass. However, as will become clear, this distinction practically does not affect the results obtained for the scattering phase shifts.

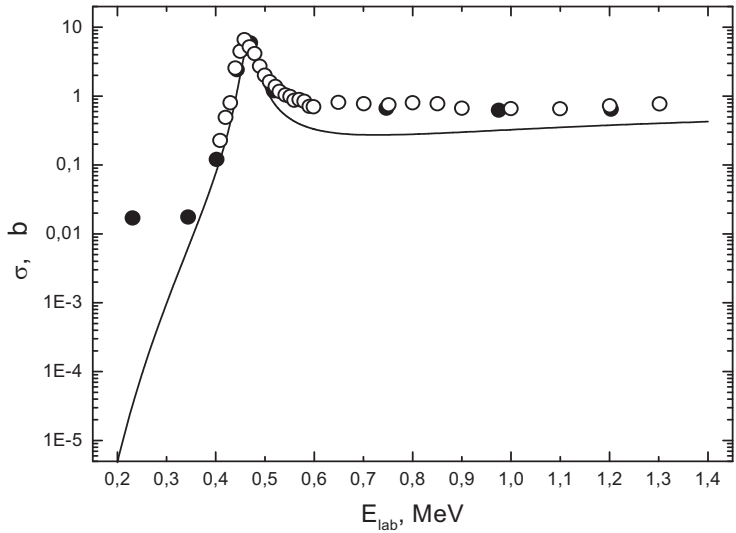

Fig. 2.3.4. The total cross sections for $p^{12}C$ elastic scattering. The points represent the total cross sections found from the scattering phase shift of [116] and the circles represent data from [113,114].

2.3.4 Phase shift analysis of $n^{12}C$ elastic scattering

In this paragraph, we continue our consideration of the phase shift analysis of elastic scattering for light nuclei. On the basis of the measurements in [119], we undertook a phase shift analysis of $n^{12}C$ scattering. We did not manage to find the results of an earlier phase shift analysis carried out for the $n^{12}C$ system, even at low energies, though they differ considerably from a similar analysis of $p^{12}C$ scattering found in [115]. The reason for these differences is the significant distinction between the spectral structure of ^{13}C and ^{13}N nuclei at energies of up to 1.5–2 MeV above the thresholds of $n^{12}C$ and $p^{12}C$ cluster channels [120].

In particular, in $p^{12}C$ elastic scattering there is a superthreshold resonance level of ^{13}N at an energy of 0.42 MeV with $J^{\pi} = 1/2^{+}$, which leads to the $^{2}S_{1/2}$ resonance of the phase shift; this has been shown in [115] in comparison to earlier results of phase shift analysis [113,114]. In the case of $n^{12}C$ scattering, there are no resonances in the spectra of ^{13}C up to an energy of 1.9 MeV. For this reason it remains interesting to determine the shape of the phase shifts of $n^{12}C$ elastic scattering taken from the experimental data at low and astrophysical energies.

This is particularly the case because the reaction of radiative capture in the $n^{12}C$ channel, at any energy, is included into the chain of thermonuclear reactions of preliminary nucleosynthesis [121]

… $^{7}Li(n,\gamma)^{8}Li(^{4}He,n)^{11}B(n,\gamma)^{12}B(\beta^{-})^{12}C(n,\gamma)^{13}C$ ... ,

which will lead us, finally, to an understanding of the initial formation of the Sun, the stars, and the whole of our universe [122,123].

Extracting the relevant information from the experimental differential cross sections of the elastic scattering phase shift allows us to construct the interaction potentials of two particles in the continuous spectrum and perform calculations on certain characteristics of their interaction in scattering processes and reactions. For example, the focus can be the astrophysical *S*-factors or the total cross sections of the reactions [124], including the neutron radiative capture of ^{12}C in the astrophysical energy range, which has been considered in our previous work [23,28,122].

Therefore, on the basis of the methods described above, phase shift analysis of the known experimental data on differential cross sections of $n^{12}C$ elastic scattering in the energy range 50-1040 keV (l.s.) was undertaken [119]. The results of our analysis for the *S* and *P* scattering phase shifts are presented in Fig. 2.3.5 and Table 2.3.7. To carry out the analysis, the χ^2 value was calculated for differential cross sections with an experimental error of 10 % [119]. The χ^2 value for each considered energy is given in the last column of Table 2.3.7.

Table 2.3.7. The results of the phase shift analysis of $n^{12}C$ elastic scattering at low energies for negative values of the ^{2}S phase shifts.

E_n, keV	$^{2}S_{1/2}$, deg	$^{2}P_{3/2}$, deg	$^{2}P_{1/2}$, deg	χ^2
50	-15.5	0.6	-0.3	0.023
100	-22	-2	3	0.016
157	-28.3	-1.0	-1.0	0.007
207	-32	-4	0.5	0.014
257	-35.6	-5	-0.4	0.009
307	-37.8	-4.6	3.3	0.033
357	-41.3	-2.7	-1.3	0.007
407	-43.7	-3.0	-1.8	0.027
457	-45.3	-5.1	5	0.029

507	-48.3	-3.9	-1.6	0.019
530	-49.1	-3.6	-3.4	0.020
630	-52.8	-5.4	-1.6	0.015
730	-56.0	-6.6	-0.6	0.031
830	-59.5	-6.2	-3.7	0.044
930	-61	-7.3	-3.7	0.042
1040	-65.4	-7.7	-4.6	0.096

In Fig. 2.3.5, it is clear that all ^2P phase shifts have values in the modulus of no more than 10°, but their influence reduces the χ^2 value by approximately an order of magnitude. The value of the ^2S phase shift gradually decreases and, as can be seen below, is well described by a Gaussian potential across the low energy range, included in the analysis.

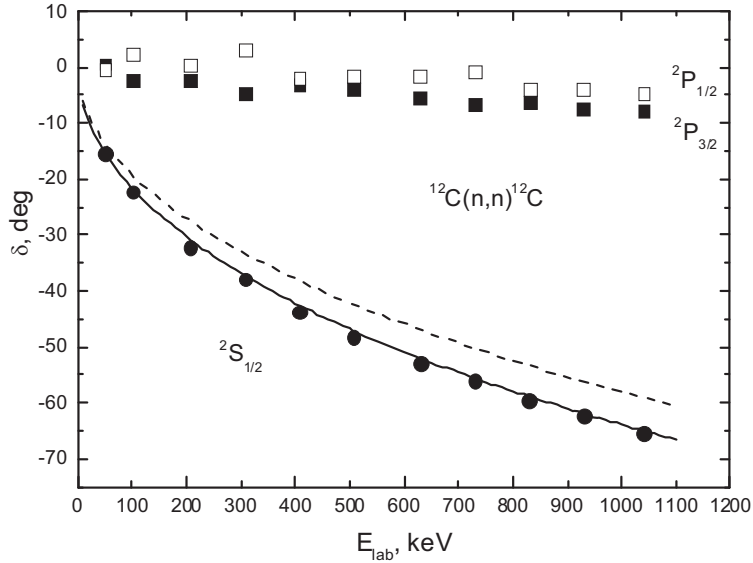

Fig. 2.3.5. Results of the phase shift analysis of $n^{12}C$ elastic scattering for the variant with negative values of the ^2S phase shifts. The points represent the results of phase shift analysis for the $^2S_{1/2}$ phase shift; the open squares represent the results of phase shift analysis for the $^2P_{1/2}$ phase shift; the black squares represent the results of phase shift analysis for the $^2P_{3/2}$ phase shift; and the curves represent the results of calculation with different potentials, as explained in the text.

In Fig. 2.3.6, the points represent the differential cross sections for some considered energies from [119] and the cross sections obtained from our phase shift analysis (the solid line), considering the *S* and *P* phase shifts given in Table 2.3.7. Accounting for the small values obtained for the ^2P phase shifts has allowed us to considerably improve the quality of the description of differential cross sections, even at the lowest energies in the range 50–100 keV.

Another variant for a set of phase shifts in which the ^2S phase shift has positive values, as well as the values of both ^2P phase shifts, is given in Fig. 2.3.7 and Table 2.3.8. The χ^2 values for this phase shift variant do not practically differ from the first set in Table 2.3.7, but the ^2S phase shift has a form close to resonance, although not observed in the spectra of ^{13}C resonances [120]. Therefore, the second set of phase shifts apparently does not correspond to the real situation and is given only as a demonstration of the ambiguity of phase shift sets.

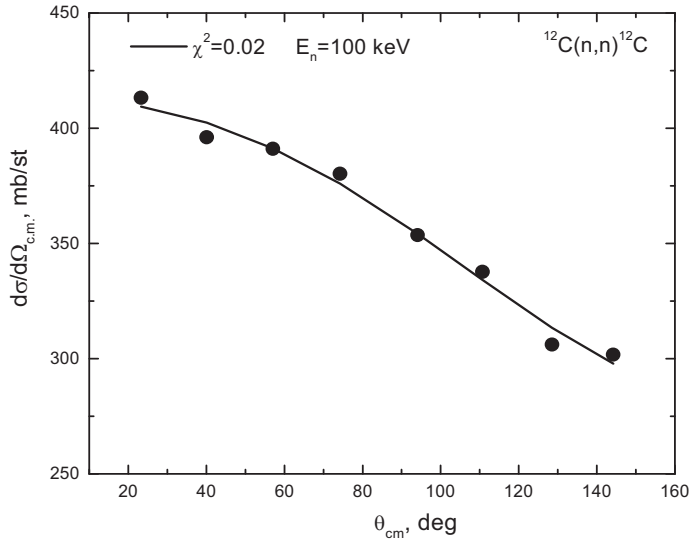

Fig. 2.3.6a. The differential cross sections of n^{12}C elastic scattering. The solid curve represents the results of the calculation of the cross sections with the found phase shifts, while the points represent the experimental differential cross sections of scattering [119].

To avoid this ambiguity, it is necessary to use certain physical principles, for example, information on the structure of the spectral levels of the nucleus, in this case ^{13}C [120].

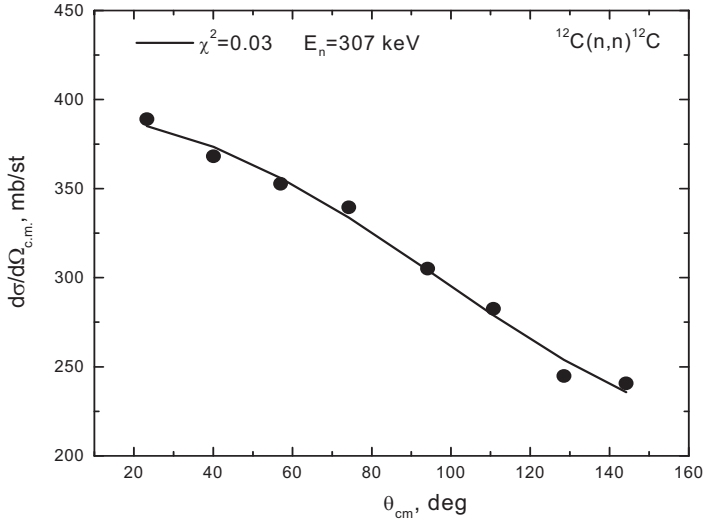

Fig. 2.3.6b. The same as in Fig. 2.3.6a.

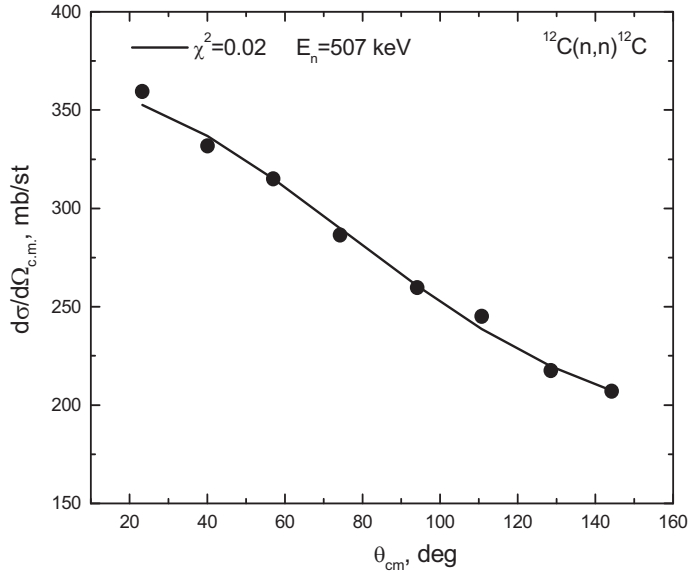

Fig. 2.3.6c. The same as in Fig. 2.3.6a.

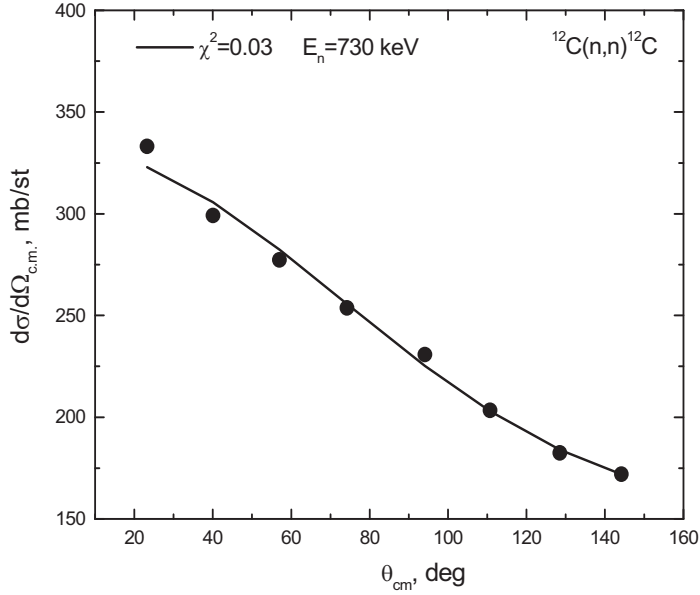

Fig. 2.3.6d. The same as in Fig. 2.3.6a.

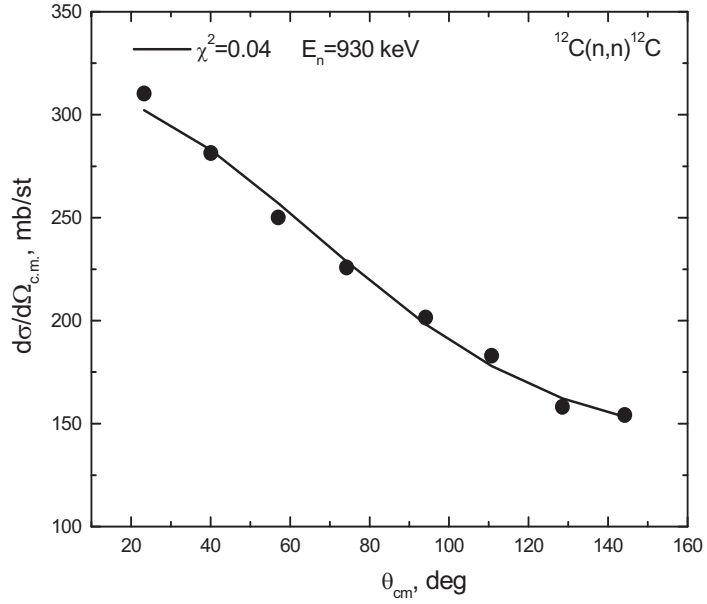

Fig. 2.3.6e. The same as in Fig. 2.3.6a.

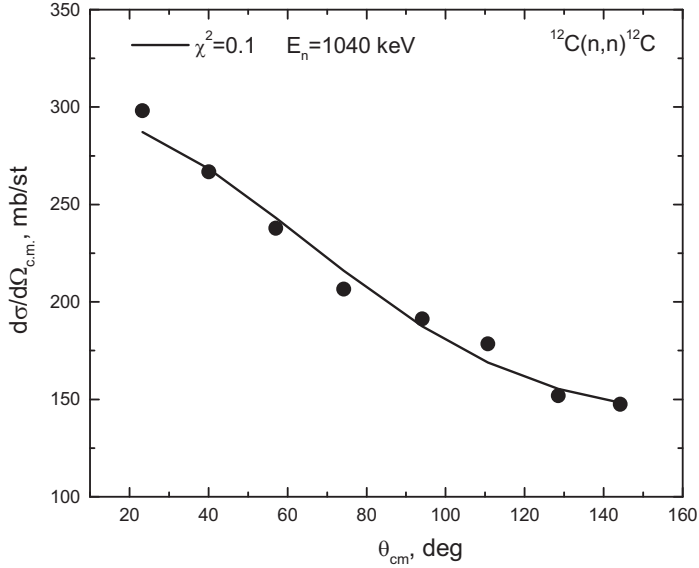

Fig. 2.3.6f. The same as in Fig. 2.3.6a.

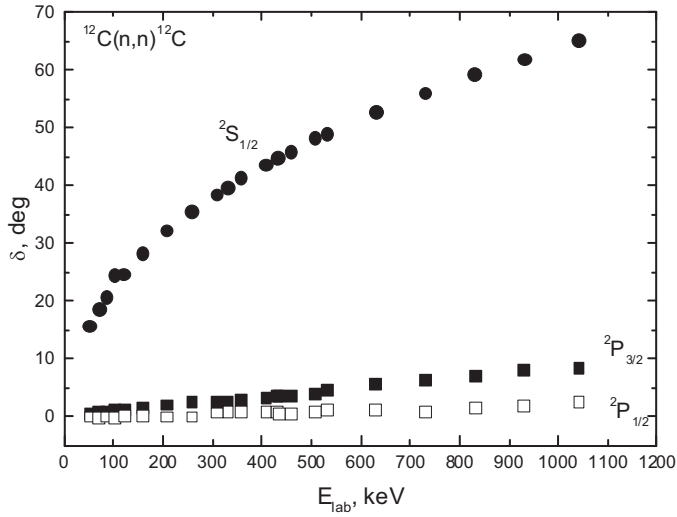

Fig. 2.3.7. Results of the phase shift analysis of $n^{12}C$ elastic scattering for variants with positive values of the ^2S phase shifts. The points represent the results of phase shift analysis for the $^2S_{1/2}$ phase shift; the open squares represent the results of phase shift analysis for the $^2P_{1/2}$ phase shift; and the black squares represent the results of phase shift analysis for the $^2P_{3/2}$ phase shift.

This information allows us to choose the real set of phase shifts of elastic scattering, the variants of which can be obtained through a similar analysis. In addition, it is possible to use the potential description of the process of scattering, which, as will be shown further, allows us to estimate the difference of scattering phase shifts for neutrons and protons on one nucleus in one potential, i.e. at a change in the Coulomb interaction.

Table 2.3.8. Results of the phase shift analysis of $n^{12}C$ elastic scattering at low energies for positive ^2S values.

E_{lab}, keV	$^2S_{1/2}$, deg	$^2P_{3/2}$, deg	$^2P_{1/2}$, deg	χ^2
50	15.7	0.6	0.06	0.036
100	24.5	1.1	0.0	0.029
157	28.3	1.5	0.1	0.007
207	33	1	0.0	0.014
257	35.6	2.7	0.0	0.009
307	38.4	2.7	0.1	0.05
357	41.3	2.9	1.0	0.007
407	43.6	3.4	1.0	0.028
457	45.8	3.8	0.7	0.037
507	48.3	4.2	1.0	0.019
530	50.0	4.7	1.2	0.021
630	52.8	5.6	1.1	0.015
730	56.1	6.5	0.8	0.031
830	59.3	7.1	1.6	0.045
930	61.9	8.1	1.9	0.044
1040	65.2	8.6	5	0.098

For example, in Fig. 2.3.5 the ^2S the phase shift of the potential with the point-like Coulomb term having a simple Gaussian form (1.6.2) is shown by the dashed curve and has the parameters

$$V_0 = -102.05 \text{ MeV}, \gamma = 0.195 \text{ fm}^{-2}. \quad (2.3.4)$$

This result was obtained previously for $p^{12}C$ scattering by the description of the astrophysical S-factor of proton radiative capture on ^{12}C in [125].

Such a potential describes the resonance form of the ^2S phase shift of $p^{12}C$ scattering correctly, as shown in Fig. 2.3.1, and acceptably coincides with the experimental data in the calculations of the astrophysical *S*-factor.

In Fig. 2.3.5, the calculations of the ^2S phase shifts were carried out for the $p^{12}C$ potential (2.3.4) specified above with the switched-off Coulomb interaction, i.e. for $n^{12}C$ scattering. From Fig. 2.3.5, it is clear that the ^2S phase shift of the $n^{12}C$ scattering process does not contain the resonance. It is, however, in complete agreement with the observed spectra of ^{13}C [120]. In addition, it is clear that the results of calculation of the ^2S phase shift are quite acceptable and we can transfer the results of the $n^{12}C$ phase shift analysis, especially at low energies.

For a more exact description of the data obtained by scattering phase shifts, it is necessary to change the potential depth at the same geometry to give -97.0 MeV, which differs by approximately 5 % from the initial parameters. The results of the calculation of the ^2S phase shift with such a potential are presented in Fig. 2.3.5 by the solid curve, precisely describing the position of points of the ^2S phase shift of $n^{12}C$ elastic scattering taken from the experiment.

Such a potential, like the previous one, still contains one bound forbidden state, the existence of which follows from the structural analysis of the forbidden and allowed bound states in the $N^{12}C$ system, as carried out in [2,28,122,125]. By averaging slightly the width of the capacity of γ, we obtain

$$V_0 = -99.0 \text{ MeV}, \quad \gamma = 0.2 \text{ fm}^{-2}, \tag{2.3.5}$$

and the phase shift of such variation of the potential does not differ from that provided in Fig. 2.3.5 described by the solid curve.

As a result of the phase shift analysis of experimental differential cross sections carried out, a set of phase shifts of $n^{12}C$ elastic scattering at energies of up to 1.0 MeV was obtained, which coordinated with the spectral levels of ^{13}C [120] and the potential calculations of the scattering phase shifts executed on the basis of the $p^{12}C$ interaction potential described earlier. The obtained set of scattering phase shifts allows us to describe the value and shape of the differential cross sections of angular distributions of $n^{12}C$ elastic scattering at low energies, which are of interest to a number of problems of nuclear astrophysics [28,122].

Once again, we emphasize that the results of the phase shift analysis, i.e. the elastic scattering phase shifts of the system of particles, which is $n^{12}C$ in this case, allow us to parametrize the intercluster partial interaction potentials of scattering processes in this system. Such potentials, in turn, can be used

further for the performance of certain calculations in various astrophysical applications, which are partially considered, for example, in [28,120].

For the calculation of characteristics of nuclei, the mass of ^{12}C was accepted as being equal to 12.0 amu, with the mass of the neutron $m_n = 1.00866491597$ amu [75]. We note that in carrying out the phase shift analysis, there is no basic value to use as an integer or exact mass of particles, because cross section errors are usually around 5–10 %.

2.3.5 Phase shift analysis of p^{14}C elastic scattering

Furthermore, we consider the possibility of carrying out phase shift analysis for elastic cross sections of p^{14}C scattering. The excitation functions of p^{14}C elastic scattering from [126], measured at 90°, 125°, 141°, and 165° in the energy range 0.6 to 3 MeV (l.s.) are shown by points in figs. 2.3.8a, b, c, and d.

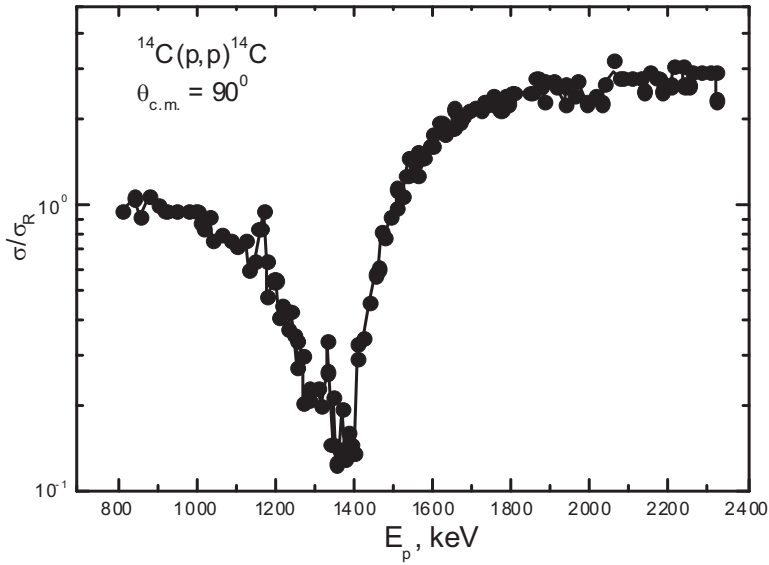

Fig. 2.3.8a. The excitation functions in p^{14}C elastic scattering in the range of the $^2S_{1/2}$ resonance [126]. The solid curve represents their approximation on the basis of the obtained phase shifts.

These data were used by us to carry out a phase shift analysis and extraction of the resonance shape of the $^2S_{1/2}$ scattering phase shift at 1.5 MeV. The methods of such an analysis have already been stated above, and

the results are presented in figs. 2.3.9a, b, c, and d by points. The solid curves in Fig. 2.3.8 show the cross sections calculated as a result of the analysis of scattering phase shifts.In our analysis, about 120 first points given in [126] in the energy range stated above were used.

In addition, the description of cross sections in the excitation functions was obtained, at least, at energies of up to 2–3 MeV; it is not necessary to consider the ^2P or ^2D scattering waves, i.e. their values can be accepted as being equal to zero. The χ^2 value at all energies and angles, as only one point in the cross sections of excitation functions for each energy and angle, has been considered, usually at the level of 10^{-2}–10^{-10}, and taking into account the partial scattering phase shift does not lead to its reduction.

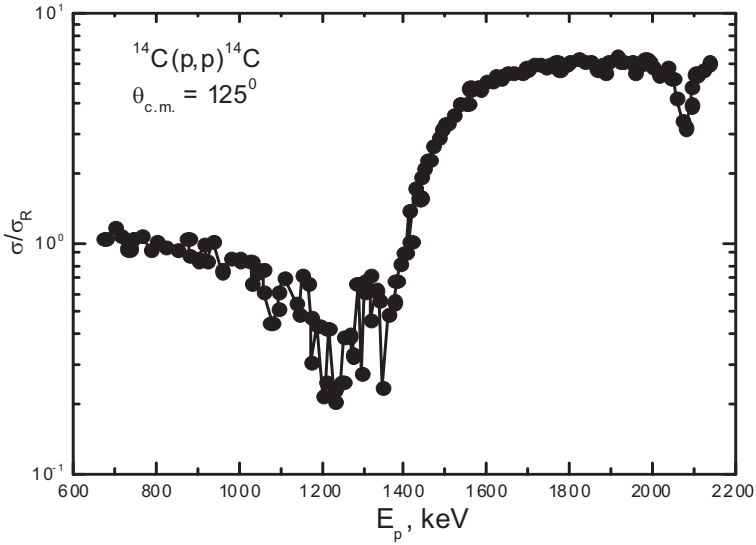

Fig. 2.3.8b. The excitation functions of $p^{14}C$ elastic scattering in the range of the $^2S_{1/2}$ resonance [126]. The solid curve represents their approximation on the basis of the obtained phase shifts.

The resonance energy, i.e. the energy at which the phase shift reaches 90°, as seen in Fig. 2.3.9, was obtained from the excitation function at a scattering angle of 90°. It falls in the interval 1535–1562 keV, for which the value of the phase shift concludes within the range 87–93° with the value of the phase shift of 90° for an energy of 1554 keV.

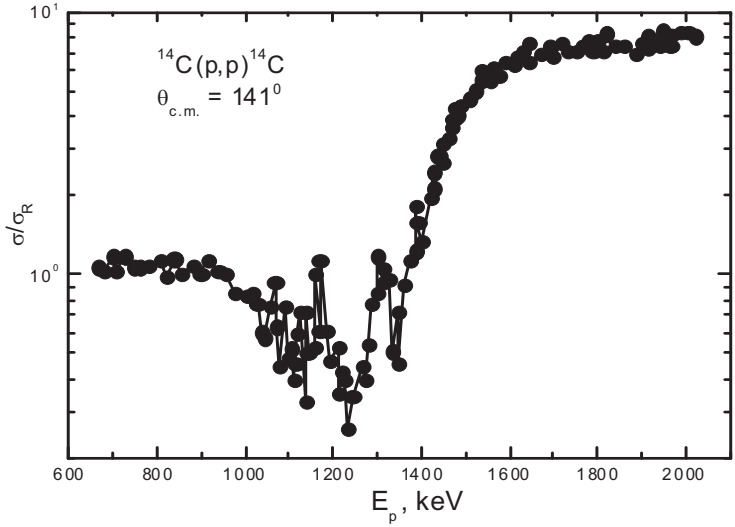

Fig. 2.3.8c. The excitation functions of $p^{14}C$ elastic scattering in the range of the $^2S_{1/2}$ resonance [126]. The solid curve represents their approximation on the basis of the obtained phase shifts.

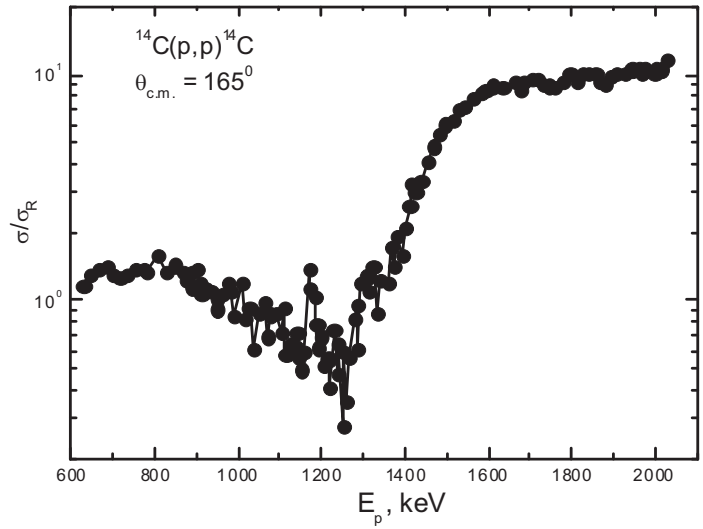

Fig. 2.3.8d. The excitation functions of $p^{14}C$ elastic scattering in the range of the $^2S_{1/2}$ resonance [126]. The solid curve represents their approximation on the basis of the obtained phase shifts.

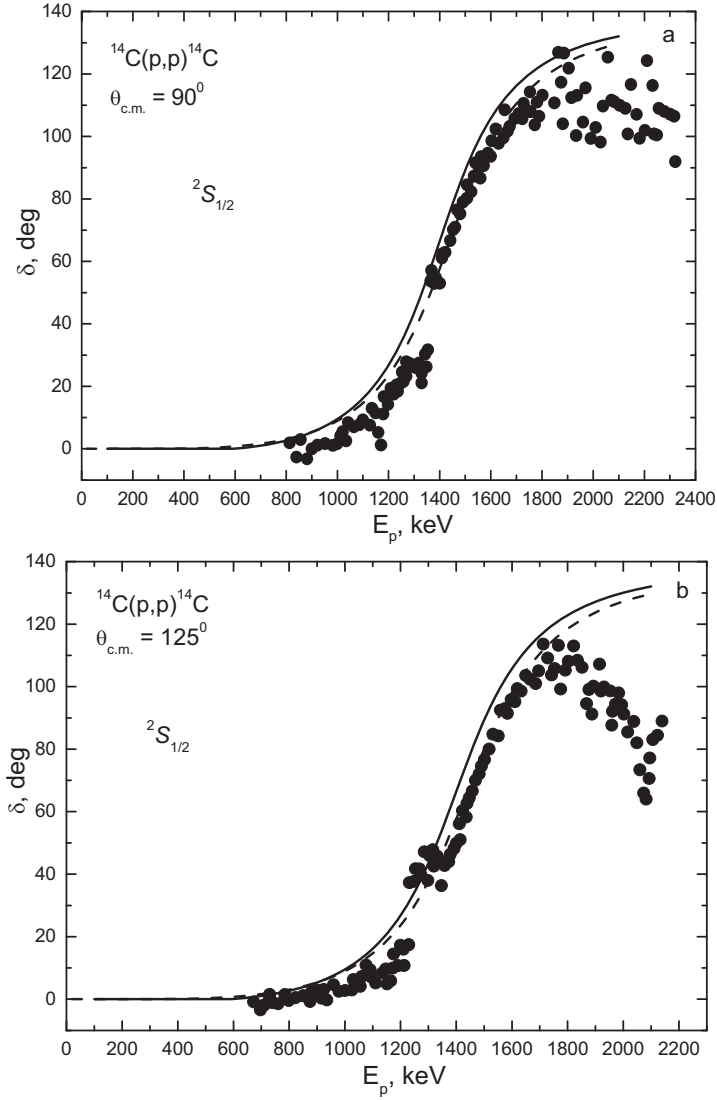

Fig. 2.3.9a, b. The $^2S_{1/2}$ phase shift of p^{14}C elastic scattering at low energies obtained on the basis of the excitation functions shown in Fig. 2.3.8. The points represent the results of our phase shift analysis made on the basis of data in [126] and the curves describe the calculation of the phase shift with the potentials given in the text.

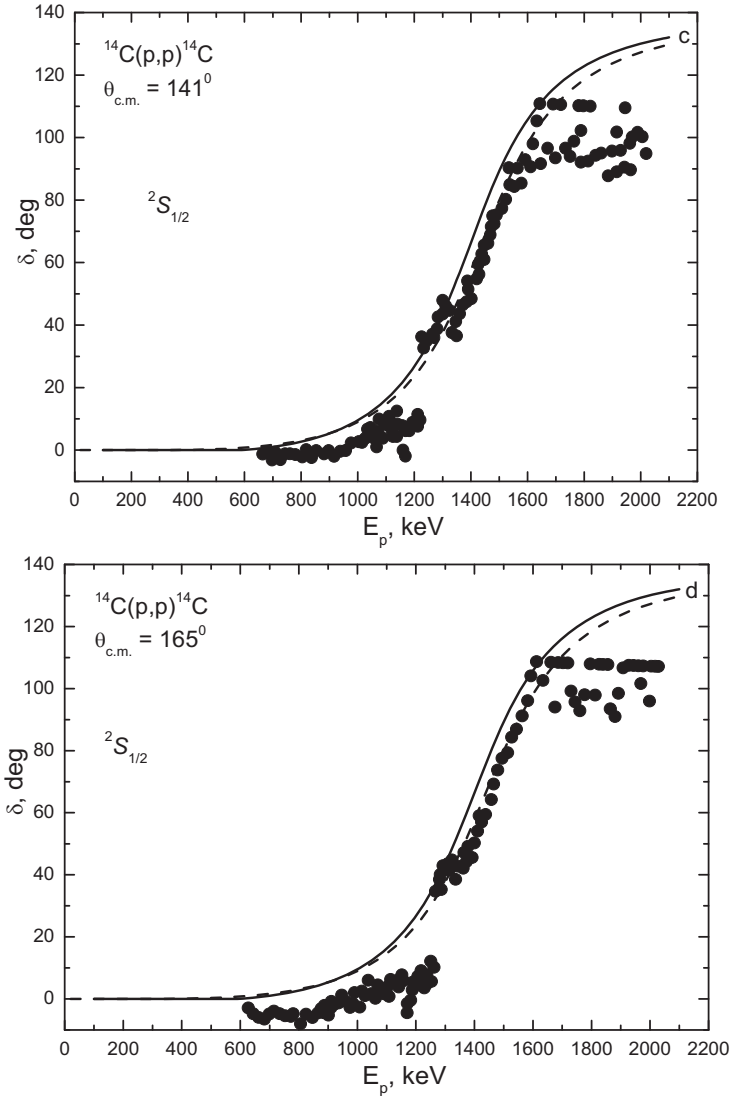

Fig. 2.3.9c, d. The $^2S_{1/2}$ phase shift of p^{14}C elastic scattering at low energies obtained on the basis of the excitation functions shown in Fig. 2.3.8. The points represent the results of our phase shift analysis made on the basis of the dat in [126] and the curves describe the calculation of the phase shift with the potentials specified in the text.

The resonance energy obtained from the excitation functions at 125° lies in the interval of 1551–1575 keV, for which the value of the phase shift concludes within the range 84–93°. The resonance energy obtained from the excitation function at 141° is in the interval 1534–1611 keV, for which the value of the phase shift concludes within the range 84–90° with the value of 90° at 1534, 1564, and 1611 keV.

The resonance energy obtained from the excitation function at 165° is in the interval 1544–1563 keV, for which the value of the phase shift concludes within the range 87–91°. At the marked scatter of values, it is possible to say only that the resonance value of the phase shift in 90° lies within the limits 1534–1611 keV, with an average energy value of 1572 keV in l.s.; this is generally in good agreement with the data in [120], where the value of the resonance energy 1509 keV is specified in l.s.

It is important to note that in [126] a detailed analysis of the resonances, including at 1.5 MeV, was not carried out, as it had previously been undertaken in [127] on the basis of the proton capture reaction on ^{14}C. Here, as is clear from the results of phase shift analysis, the resonance energy at 1.5 MeV is a little overestimated in relation to the results in [127]. However, as is clear in Fig. 2.3.8, errors in the experimental data by the scattering cross sections of excitation functions are too large to draw unambiguous conclusions about the energy of such resonance.

With additional, more modern, and more exact measurements of cross sections of p^{14}C elastic scattering, it becomes necessary to draw more certain conclusions about the resonance energy in the $^2S_{1/2}$ phase shift at 1.5 MeV on the basis of these data. The difference between the data obtained here and in [127] for the energies of this resonance at 63 keV, in general, does not play a basic role, but nevertheless it is clear where it is located.

Moving on to the construction of the potentials of p^{14}C elastic scattering, at the beginning we will consider the classification of the orbital states according to Young tableaux. We consider that the {4442} tableau corresponds to the ground bound state of ^{14}C [123,128,129]. The possible orbital Young tableaux for system $N = n_1 + n_2$ of particles can be defined as the direct external product of orbital tableaux of each subsystem, which, for the p^{14}C system within a 1*p*-shell, gives $\{1\} \times \{4442\} \rightarrow \{5442\} + \{4443\}$ [123,128]. The first of the obtained tableaux is compatible with the orbital moment $L = 0$ and is forbidden because, in an s-shell, there cannot be five nucleons and the second tableau is allowed and compatible with the orbital moment L, equal to one [123,128,129].

Thus, in the potential of the $^2S_{1/2}$ wave the forbidden bound state is contained and the ^2P waves only allow BS. The ground state of ^{15}N in the p^{14}C channel, which is at an energy of -10.2074 MeV [120], belongs to the

$^2P_{1/2}$ wave and does not contain the FS. (We note that the moment of ^{14}C is equal to $J^\pi = 0^+$ and the isospin T is equal to 1, as shown in [120].)

However, we do not have complete tables for the multiplication of Young tableaux for the system with more than eight particles [130], as used by us previously for similar calculations [123,128,129,131,132]. Therefore, the results obtained above should be considered only as the quality standard of the possible orbital symmetry for the BS, allowed or forbidden, in ^{15}N for the considered p^{14}C channel.

For the description of our analysis of the $^2S_{1/2}$ scattering phase shift, a simple Gaussian potential of the form (1.6.2) with the bound FS and the following parameters are used

$$V_0 = -5037.0 \text{ MeV}, \qquad \gamma = 12.0 \text{ fm}^{-2}, \qquad (2.3.6)$$

which gives us scattering phase shifts with resonance at 1500 keV in l.s. and a width of 530 keV in c.m.; these do not coordinate poorly with the available experimental data presented in Table 15.11 in [120]. In this work, the values 1509(4) keV are given in l.s. with a total width of 404.9±6.3 keV in c.m. and a proton width of 400.9±6.3 keV. The parameters of the potential (2.3.6) were selected so that, in general, it could correctly reproduce the resonance data in [120], obtained previously in [127].

The phase shift of such a potential is shown in figs. 2.3.9a, b, c, and d by the solid curves and at a resonance energy of 1500 keV reaches the value of 90(1)°. The energy behavior of the scattering phase shift, in general, correctly describes the scattering phase shifts obtained in the phase shift analysis considering the shift of resonance energy to approximately 70 keV, in relation to the results in [120,127]. The calculation curve of the phase shifts for this potential goes parallel to the points obtained in our phase shift analysis for all four scattering angles.

For a more exact description of the data obtained in the phase shift analysis, the potential required is

$$V_0 = -5035.5 \text{ MeV}, \qquad \gamma = 12.0 \text{ fm}^{-2}. \qquad (2.3.7)$$

This gives a resonance energy of 1550 keV, a width of 575 keV, and the calculation results of the $^2S_{1/2}$ phase shift are shown in Fig. 2.3.9 by a dashed curve. This curve clearly describes the results of the phase shift analysis.

All the potentials of the P scattering waves, as they do not contain the FS, can be set to equal zero. Such potentials lead to scattering phase shifts, which are also equal to zero. In the spectra of ^{15}N, there are two resonance levels, which can be carried to the P waves in the p^{14}C channel. One of these

lies at approximately 0.53 MeV and has the moment $J^{\pi} = 3/2^{-}$. However, their width in 0.2 keV and 8(3) keV is so small (see Table 15.11 in [120]) that it is not possible to construct the corresponding potentials according to these data [133].

It should also be noted that, at the known energy of the resonance level in the spectra of any nucleus [120] and its width, the potential of the $^2S_{1/2}$ waves is constructed completely unambiguously, if the number of BS, forbidden or allowed states in this partial wave is given, in this case being equal to one. In other words, it is impossible to find other combinations of the parameters V and γ that are capable of transferring the resonance energy of the level and its width correctly. The depth of such a potential of V unambiguously defines the location of the resonance, i.e. the resonance energy of the level and its width γ sets the certain width of this resonance state [28,122,123,125,128, 129,132,158] and has to correspond to the experimentally observed values [120]. In this case, for the correct reproduction of the resonance width in the case of 1509 keV, the potential width would have to be reduced, increasing the γ parameter. Only in this case would it be possible to obtain a more correct resonance width of about 400 keV.

2.3.6 Phase shifts and potentials of $n^{16}O$ scattering

To carry out calculations for radiative capture in the frame of the modified PCM [2], it is necessary to know the potentials of $n^{16}O$ elastic scattering in $^2S_{1/2}$, $^2P_{1/2}$, $^2P_{3/2}$, $^2D_{3/2}$, and $^2D_{5/2}$ waves, along with the interaction of the $^2D_{5/2}$ ground and first excited $^2S_{1/2}$ states of ^{17}O. For the transition to these BS, we can use the experimental data on total cross sections of radiative capture in [134].

For this system, as usual, the potentials of the scattering processes are constructed on the basis of elastic scattering phase shifts, at values higher than 1.1 MeV obtained in [135,136]. For the energy range 0.2–0.7 MeV, we have the results of the phase shift analysis in [137], based on measurements of the differential cross sections of $n^{16}O$ elastic scattering [138] in the resonance range of 0.433 MeV [103]. In [137], there are also some preliminary results of the phase shift analysis given in the range of the $^2D_{3/2}$ resonance at energies of 750–1200 keV.

New experimental data [139] on the excitation function at energies of 0.5 to 6.2 MeV are listed in the database in [140]; as far as we know, energies in the range of the $^2D_{3/2}$ resonance of 1.0 MeV [103] have not been considered in the phase shift analysis. The data in [139] have been used to carry out the phase shift analysis and the extraction of the shape of the phase shift in the $^2D_{3/2}$ wave of $n^{16}O$ scattering. The excitation functions used at

40° in l.s. or 42.3° in c.m. [139] are shown in Fig. 2.3.10 for the energy range 0.75 to 1.25 MeV (l.s.), represented by open circles. In our analysis, more than 500 points for the cross sections at different energies from the excitation functions obtained in [139] were used.

Let us note that the lower 0.7–0.8 MeV ambiguity of the data [139] sharply increases; however, for the extraction of the $^2D_{3/2}$ scattering phase shift it is sufficient to consider the energy range shown in Fig. 2.3.10, which has a rather small ambiguity. Such data can be useful for carrying out a phase shift analysis. Details of the method we used to find the phase shifts in the elastic scattering of particles with spin 1/2 + 0 are given above and in [141].

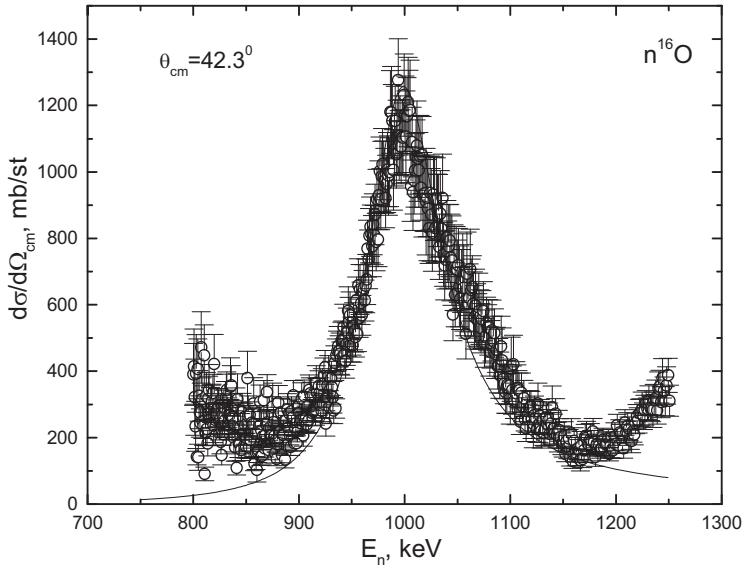

Fig. 2.3.10. Excitation functions of $n^{16}O$ elastic scattering in the range of the $^2D_{3/2}$ resonance at 1.0 MeV, shown by open circles [139]; the curve represents the calculation of the cross sections with the potential specified in the text.

The main expressions for the cross sections used in the phase shift analysis are given in Chapter 1, the beginning of this paragraph, and in [6,141]. The results of the present analysis of $n^{16}O$ elastic scattering in the energy range 0.75 to 1.25 MeV are shown in Fig. 2.3.11 by open circles. In Fig. 2.3.11, the black squares represent the results of the phase shift analysis in [135], while the values obtained above 1.1 MeV and the results of the analysis in [137] are given by triangles.

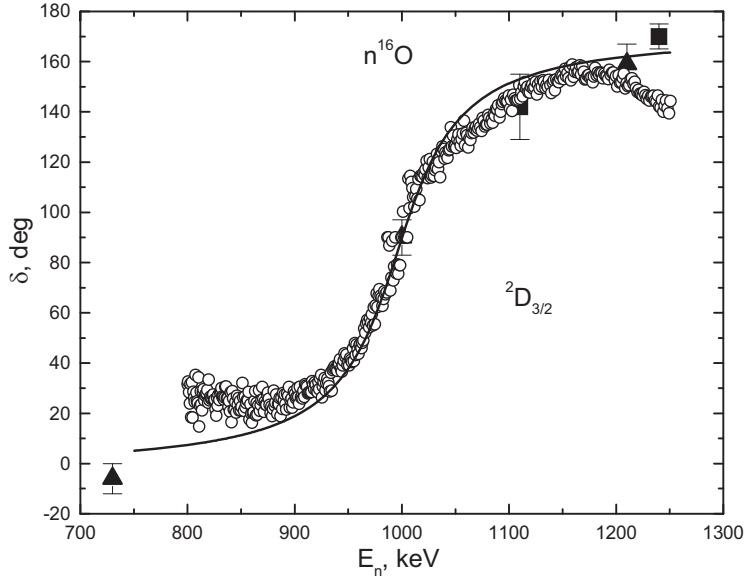

Fig. 2.3.11. $^2D_{3/2}$ phase shift of $n^{16}O$ elastic scattering at low energies. The open circles (○) describe the results of our phase shift analysis made on the basis of data presented in [139]; the black squares (■) describe the results of phase shift analysis in [135]; the triangles (▲) present the results of the analysis in [137]; and the solid curve represents the calculation of the phase shift with the potential specified in the text.

For the description of the cross sections in excitation functions [139], at least at energies of up to 1.2–1.25 MeV, it is not necessary to consider the $^2S_{1/2}$ scattering phase shift as its presence does not change the χ^2 value, i.e. its values can be accepted as being equal to zero. The χ^2 values, as only a single point in the cross sections for each energy level, have been considered; the average value is $4.7 \cdot 10^{-3}$ with a maximum partial value $\chi^2_i = 0.6$ at an energy of 999.5 keV.

To describe the $^2D_{3/2}$ scattering phase shift in Fig. 2.3.11 obtained through phase shift analysis, it is possible to use a simple Gaussian potential (1.6.2) with the parameters

$$V_{D3/2} = -95.797 \text{ MeV}, \qquad \gamma_{D3/2} = 0.17 \text{ fm}^{-2} \tag{2.3.8}$$

which does not have a bound FS and leads to the resonance energy of 1000 keV at the phase shift of 90.0(1)° with a width of 88 keV in l.s. or 83 keV in c.m. At

the same time, we have values in Table 17.17 [103] for the width value of 96 keV in c.m or 102 keV in l.s. at an energy of 1000±2 keV in l.s.

The energy dependence of the $^2D_{3/2}$ scattering phase shift of the potential (2.3.8) is shown in Fig. 2.3.11 by the solid curve. Such a potential describes the behavior of the phase shift obtained by us in the range of the resonance and agrees quite well with the previous extraction of the scattering phase shift carried out in [135,137]. The form of the cross sections of the excitation functions calculated with a $^2D_{3/2}$ phase shift of potential (2.3.8) at zero values of other phase shifts is shown in Fig. 2.3.10 by the solid curve. From these results, it is clear that the $^2D_{3/2}$ phase shift almost completely defines the behavior of such cross sections in the excitation function.

Furthermore, we consider the total cross sections for radiative capture, taking into account the $E1$ transitions from the $^2P_{3/2}$ resonance in $n^{16}O$ scattering at 433 keV to the $^2D_{5/2}$ ground and $^2S_{1/2}$ first excited state of ^{17}O. For the construction of the $^2P_{3/2}$ scattering potential, apart from the data on the location and width of such a level in [103] (see Table 17.17), we have used the results of the phase shift analysis [137] shown by triangles in Fig. 2.3.12.

As a result, we found that for the description of the resonance $^2P_{3/2}$ scattering phase shift at 433(2) keV (l.s.) with a width of 45 keV in c.m. or 48 keV in l.s. [103], the potential without the forbidden or allowed BS with the following parameters is required

$$V_{P3/2} = -1583.545 \text{ MeV}, \quad \gamma_{P3/2} = 6.0 \text{ fm}^{-2} \tag{2.3.9}$$

which leads to a width 44 keV in c.m. or 47 keV in l.s. at resonance of 433 keV (l.s.). The phase shift of such a potential at resonance energy is equal to 90.0(0.2)° and the complete dependence of the scattering phase shift from energy in the range of resonance is shown in Fig. 2.3.12 by the solid curves.

Here, again, it is necessary to note that the well-known resonance energy level in the spectrum of ^{17}O and its width, the construction of the potential is entirely clear. In other words, it is impossible to find other V_0 and γ parameters that would be capable of correctly describing the resonance energy of the level and its width, if the number of BS were given, which, in this case, would be equal to zero. The depth of such a potential unambiguously defines the provision of a resonance, i.e. the resonance energy of the level and its width sets a certain width of this resonance state.

In the spectra of ^{17}O below 1.0–1.3 MeV there are no resonance levels with $J^\pi = 1/2^-$ и $5/2^+$ moment [103], which can be compared to the $n^{16}O$ channel. Therefore, the $^2P_{1/2}$ and $^2D_{5/2}$ potentials of scattering waves have no bound FS or AS and can have zero depth, i.e. zero scattering phase shifts. Such an assumption has already been used by us and it use has been repaid

for some other systems of particles in the consideration of other processes of radiative capture [2].

Furthermore, to carry out calculations of radiative capture in the frame of the modified PCM, we need the interaction potentials of $n^{16}O$ clusters in the BS. We investigated the electromagnetic transitions to the ground bound state from $J^{\pi},T = 5/2^{+},1/2$ at an energy of -4.1436 MeV and first excited with $J^{\pi} = 1/2^{+}$ at -3.2729 MeV of ^{17}O in the $n^{16}O$ channel [103]. The width of such potentials was fixed on the basis of the correct description of the binding energy and the charge radius of ^{17}O being equal to 2.710(15) fm [103]; then, we compared the calculated asymptotic constants of the $n^{16}O$ channel with other independent data.

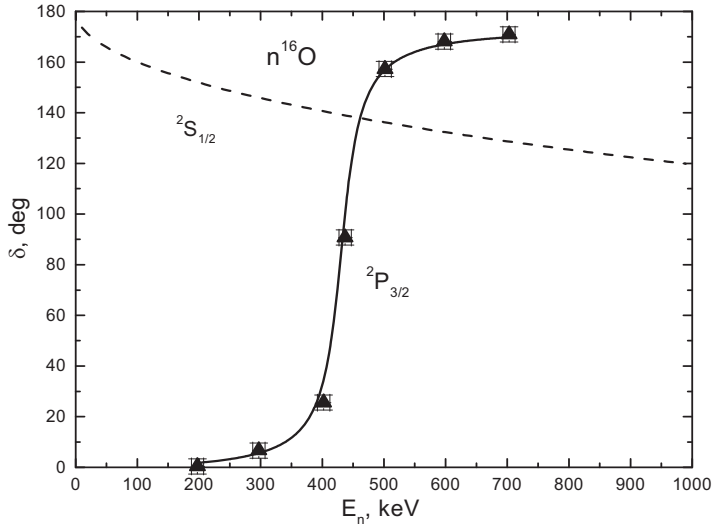

Fig. 2.3.12. $^{2}S_{1/2}$ and $^{2}P_{3/2}$ phase shifts of $n^{16}O$ elastic scattering at low energies. The triangles (▲) represent the results of the phase shift analysis in [137] and the solid curve describes the calculation of the phase shift with the potential specified in the text.

As a result, for the $^{2}D_{5/2}$ potential of the GS of ^{17}O in the $n^{16}O$ channel without the FS, the following parameters were found

$$V_{g.s} = -102.2656782 \text{ MeV}, \gamma_{g.s} = 0.15 \text{ fm}^{-2} \quad (2.3.10)$$

allowing us to obtain a binding energy of -4.1436000 MeV with an accuracy of 10^{-7} MeV [141], a charge radius of 2.71 fm, a mass radius of 2.73 fm, and

the dimensionless asymptotic constant (1.6.3) on an interval of distances of 6–16 fm equal to $C = 0.75(1)$. The phase shift of such a potential with one bound AS decreases smoothly and at an energy of 1.0 MeV accepts the value of 179.6º, i.e. it actually has a zero value.

As the charge radius of the neutron, as usual, the zero value was for the mass radius 0.8775(51) fm, equal to the charge radius of the proton specified in the base [75]. In [142], for the AC of the GS, the 0.9 $fm^{-1/2}$ was obtained, which, after recalculation with $\sqrt{2k_0} = 0.933$ to the dimensionless value, gives 0.96. In [65], for the GS the dimensionless value 0.77(8) is given, taking into account that the errors were completely coordinated with the value obtained above.

For the $^2S_{1/2}$ potential of the first excited state of ^{17}O in the $n^{16}O$ channel with one bound forbidden state [2], the following parameters were found

$$V_{S1} = -81.746753 \text{ MeV}, \quad \gamma_{S1} = 0.15 \text{ fm}^{-2}, \tag{2.3.11}$$

which gives a binding energy of -3.2729000 MeV relative to the threshold of the $n^{16}O$ channel, or 0.8707 MeV relative to the GS of ^{17}O with an accuracy of 10^{-7} MeV [141] and a charge radius of 2.71 fm, a mass radius of 2.80 fm, and AC on an interval of distances of 6–17 fm equal to C = 3.09(1). The phase shift of such a potential is shown in Fig. 2.3.12 by the shaped curves, smoothly falling down before reaching 119.6º at 1.0 MeV. For this $^2S_{1/2}$ level of [142] for the AC, the value of 3.01 $fm^{-1/2}$ was obtained, which, after recalculation with $\sqrt{2k_0} = 0.88$, gives 3.42. It appears in this case that, for the value of an asymptotic constant an acceptable agreement between the different results arises, with a difference between them of approximately 10 %.

For the additional control of the calculation of the energy of the bound state, the variation method [10,141], which, for the ground state, is already on a grid with dimension $N = 10$ with the independent variation of parameters for the potential (2.3.10), allowing us to obtain a value for the energy of -4.1435998 MeV, was used. The parameters of the variation wave function are specified in Table 2.3.9 and the value of the residuals does not exceed 10^{-8} [141]. The charge radius and asymptotic constant on the interval of 6–16 fm do not differ from the values obtained above in the FDM. As for the real binding energy in such a potential, it is possible to accept the average value of -4.1435999(1) MeV, the accuracy of the determination of the binding energy by two methods (FDM and VM) according to two computer programs was at the level of ±0.1 eV and thus in full compliance with the given error in the FDM program for the

binding energy of 10^{-7} MeV.

For the energy of the first excited, but bound state in the $n^{16}O$ channel, on a grid with dimensions $N = 10$ and the independent variation of parameters for the potential (2.3.11), the value for an energy of -3.2728998 MeV was obtained. The parameters of the variation wave function are specified in Table 2.3.10 and the value of the residuals does not exceed 10^{-10} [141].

Table 2.3.9. The variation parameters and coefficients of the decomposition of the radial WF in the $n^{16}O$ system for the ground potential of the $5/2^+$ state for potential (2.3.10). The WF normalization on an interval 0–30 fm is equal to N_0 = 9.999999999996603E-001.

i	α_i	C_i
1	2.970820484267648E-002	5.999898648526680E-002
2	1.355376641105716E-002	-5.268187781652860E-006
3	2.971441871730051E-002	-6.024647870785407E-002
4	6.553466412237838E-002	-3.087819670804185E-003
5	1.253831431831826E-001	-1.906462762571792E-002
6	2.156627509028788E-001	-6.585296562529887E-002
7	3.393826502547065E-001	-1.006636861923295E-001
8	5.166966410860497E-001	-4.627970949895152E-002
9	1.063579836670607	-1.116683372038532E-003
10	1.639614546923715	2.440471375269290E-004

Table 2.3.10. The variation parameters and coefficients of the decomposition of the radial WF in the $n^{16}O$ system for the potential first excited $1/2^+$ state for potential (2.3.11). The WF normalization on an interval of 0–30 fm is equal to N_0 = 9.999999975230215E-001.

i	α_i	C_i
1	1.268144327251019E-002	7.701423164869143E-003
2	4.193709029136675E-003	4.794229107401904E-005
3	2.881642596445175E-002	5.677769979981124E-002
4	6.245243687002310E-002	1.570309903921747E-001
5	1.259974114760052E-001	2.619817602771229E-001

6	2.163927688688810E-001	-4.833513946049395E-002
7	3.383830162751630E-001	-7.529455791580352E-001
8	5.187698913796229E-001	-4.062518687767323E-001
9	1.062316903143099	-5.106918680411997E-003
10	1.867671209905880	4.235490376362463E-004

The charge radius and asymptotic constant at an interval of 6–20 fm do not differ from the values obtained in the FDM calculations. For the real binding energy, we can accept the average value -3.2728999(1) MeV, i.e. the accuracy of determining the energy by two methods according to the two computer programs is also at the level of ±0.1 eV = ±100 meV. In all real calculations of the characteristics of ^{17}O for the value of ^{16}O mass, the value $m(^{16}\mathrm{O})$ = 15.994915 amu was used [143], with the mass of the neutron specified previously.

2.3.7 Phase shift analysis of p^{16}O scattering

It appears that one of the first measurements for the differential cross sections of p^{16}O elastic scattering with phase shift analysis undertaken at energies of 2.0–7.6 MeV were done in [144]. This analysis used the results of [145] and [146] and some unpublished results of [144] in two areas of energy: 2.0–4.26 MeV and 4.25–7.6 MeV. The resonance at 2.66 MeV in the laboratory system for the $^2P_{1/2}$ wave has been considered in detail.

Subsequently, the polarization of p^{16}O elastic scattering in the range 2.5–5.0 MeV was measured in [147] and a new phase shift analysis was made at these energies, which, however, obviously did not show resonance at 2.66 MeV [103]. Furthermore, in the figures in [148] and the table in [149] (with reference to [148]), the results of the detailed phase shift analysis of p^{16}O elastic scattering at energies of 1.5–3.0 and 2.5–3.0 MeV were given and in [148] the presence of a narrow resonance specified subsequently at an energy of 2.663(7) MeV with a width of 19(1) keV was confirmed. This corresponds to the first superthreshold state of ^{17}F at 3.104 MeV with $J^\pi = 1/2^-$ [103] and is compared to the $^2P_{1/2}$ wave in p^{16}O elastic scattering.

Processes of p^{16}O elastic scattering in the energy range 1.0–3.5 MeV have been considered in a number of works (see, for example, the review in [103] and [150,151]). In particular, in [152,153] the range 0.5–0.6 MeV to 2.0–2.5 MeV is considered. In [154], the measurements of the excitation functions at energies of 0.4 to 2.0 MeV were executed. However, in all these works [150-154], a phase shift analysis of the obtained experimental data was not made.

As a result, the phase shift analyses that are available today were mostly carried out in the 1960s and usually for 2.0–2.5 MeV and higher energies. There is only one point in the scattering phase shifts at 1.5 MeV obtained in [148] that has not subsequently been confirmed in other works. The study of an interval of energies from 2.0–2.5 MeV to 7–8 MeV and higher in the works given above is connected to the fact that the scattering phase shifts were constructed for further consideration of certain problems of nuclear physics and did not concern the area of astrophysical energies. Furthermore, we consider radiative capture in the field of astrophysical energy at approximately 2.0–2.5 MeV.

The results of the works listed above [150-154] and some other excitation functions and angular distributions are quite enough to carry out a phase shift analysis up to 2.0–2.5 MeV and further construction of the $p^{16}O$ interaction potentials on the found scattering phase shifts. Therefore, we carried out a phase shift analysis of the available experimental data from 0.4 to 2.5 MeV to obtain an understanding of the exact type of scattering phase shifts in this energy area. Additionally, we rechecked the results of some other phase shift analyses made in the 1960s.

2.3.7.1 Control of phase shift analyses

Firstly, we consider the results obtained through phase shift analysis, made on the basis of the angular distribution in [148] and with the energy range 1.5–3.0 MeV at four scattering energies in the range of angles 20–160°. In other words, we repeated the analysis found in [148], which was originally made in the 1960s. The results of the description of cross sections with the phase shifts taken in our analysis are represented by solid curves in figs. 2.3.13a, b, c, d, and e; the phase shifts are shown by open squares in Fig. 2.3.13e and can be compared to the data in [144,147,148,149]. The χ^2 value obtained with a 10 % experimental error is shown in figs. 2.3.13a, b, c, d, and e.

From the given results, it is clear that at an energy of 2.978 MeV the phase shift values in [148] and those obtained by us differ by 1.5–2°. For three other energies the coincidence is at a level of less than 1°, while for 2.48 MeV the results completely coincide. We further consider proton radiative capture on ^{16}O at an energy of around 2.5 MeV without taking into account the narrow resonance at 2.66 MeV [103]. The area of this resonance will not be considered in detail as the phase shift analysis has been studied previously in [144]. This is shown in Fig. 2.3.13e by open circles and also in the analysis of [148].

Let us give one more result for the angular distributions from [147] at an energy of 2.5 MeV. In Fig. 2.3.14, the differential cross sections measured in the angular distributions are shown by points; the results of our calculation of these cross sections with the found phase shifts are shown by the solid curve. The χ^2 value is equal to 0.67 with an experimental error of 10 %; this value was obtained during the analysis of the scattering phase shift shown in Fig. 2.3.14 and is equal to $S_{1/2} = 139.8°$; this phase shift is shown in Fig. 2.3.13e by the open triangle.

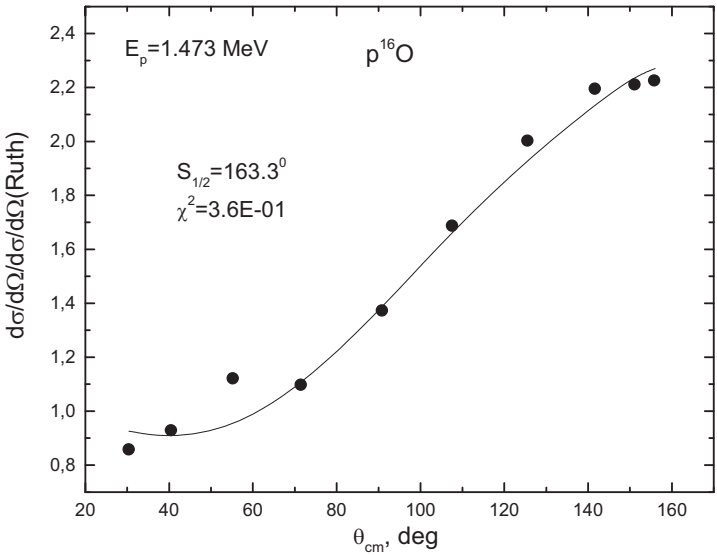

Fig. 2.3.13a. The angular distributions of $p^{16}O$ elastic scattering measured in [148] at a proton energy of 1.473 MeV. The solid curve represents the calculation of these cross sections with the obtained scattering phase shifts.

If we add the $P_{1/2}$ scattering phase shift to the analysis, then, for 10 iterations [10], we obtain $\chi^2 = 0.58$ along with the phase shifts $S_{1/2} = 140.3°$ and $P_{1/2} = 5.5°$. If we consider the $P_{3/2}$ phase shift, then after the same number of iterations, we find $\chi^2 = 0.57$ and the phase shifts $S_{1/2} = 139.7°$, $P_{1/2} = -4.5°$, and $P_{3/2} = 4.6°$. From this it is clear that taking into account the P phase shifts at an energy that adjacent to the narrow resonance region barely changes the value of the S phase shift and significantly improves the χ^2 value.

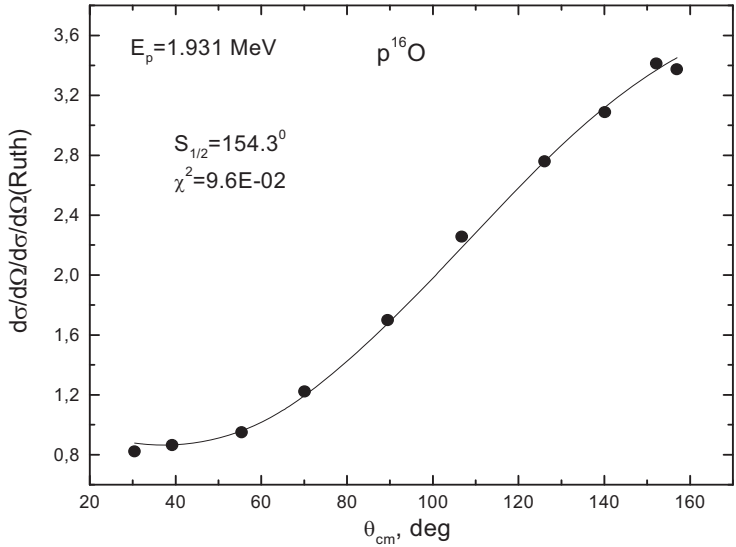

Fig. 2.3.13b. The same as in Fig. 2.3.13a, but at a proton energy of 1.931 MeV.

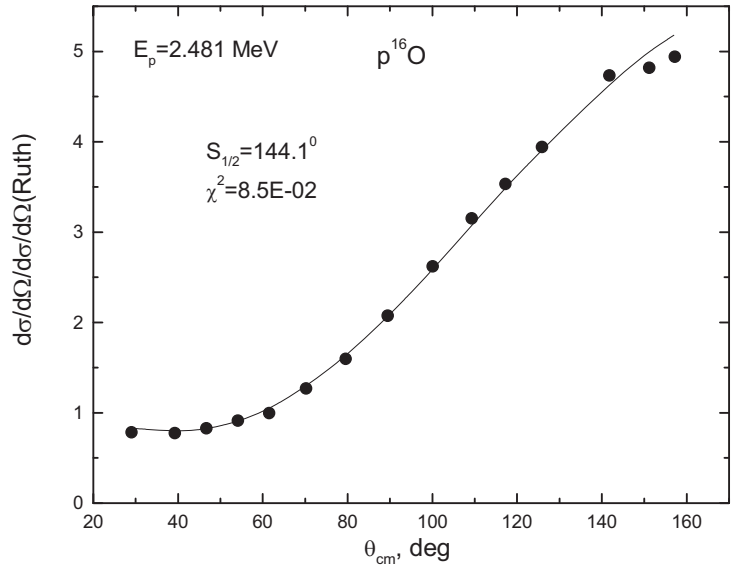

Fig. 2.3.13c. The same as in Fig. 2.3.13a, but at a proton energy of 2.481 MeV.

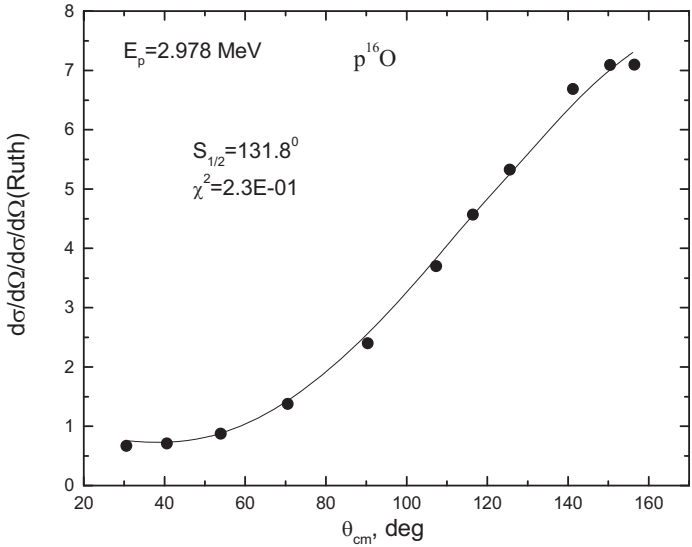

Fig. 2.3.13d. The same as in Fig. 2.3.13a, but at a proton energy of 2.978 MeV.

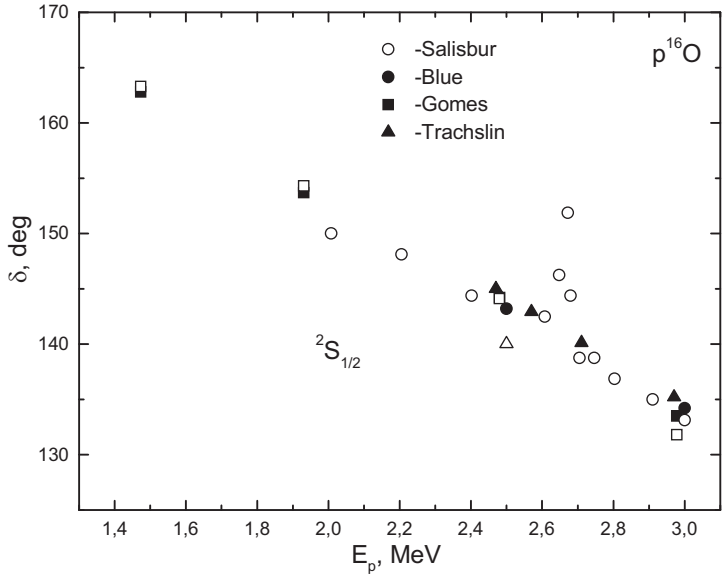

Fig. 2.3.13e. The phase shifts of p16O elastic scattering obtained from the angular distributions in [148] as open squares and from [147] by an open triangle. Other designations present the results from [144,147,148,149].

A phase shift analysis was also undertaken in [147]; for this energy, the following phase shifts were obtained: $S_{1/2} = 143.2°$, $P_{1/2} = 2.0°$, $P_{3/2} = 2.2°$, $D_{3/2} = 3.2°$, and $D_{5/2} = -1.6°$; the χ^2 value is not given in the article. With such phase shifts, the $\chi^2 = 0.62$ value with a 10 % experimental error was found in our calculations and the results for the cross sections of the elastic scattering are given in Fig. 2.3.14 by the dashed curve, which practically merges with the solid curve.

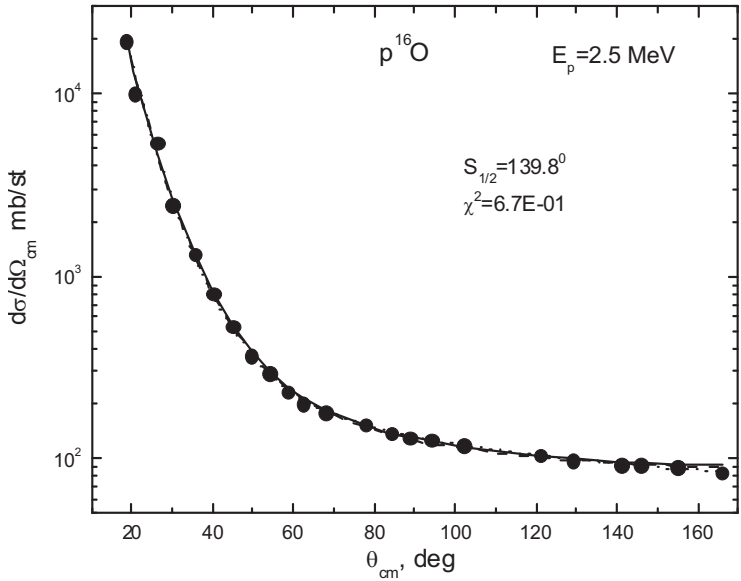

Fig. 2.3.14. The angular distributions of $p^{16}O$ elastic scattering measured in [147]. The curves describe the calculation of cross sections on the basis of various phase shift analyses.

If we execute a variation of the phase shifts given in [147], according to our program with 10 iterations, we obtain $\chi^2 = 0.57$ with phase shifts: $S_{1/2} = 140.8°$, $P_{1/2} = -2.8°$, $P_{3/2} = 4.6°$, $D_{3/2} = 3.1°$, and $D_{5/2} = -2.3°$. The scattering cross section with such phase shifts is shown in Fig. 2.3.14 by the dotted curves. From this figure it is clear that accounting for the D phase shifts does not change the χ^2 value.

2.3.7.2 New phase shift analysis

As already described in [154], the measurements of excitation functions of $p^{16}O$ elastic scattering at energies ranging from 0.4 to 2.0 MeV were carried out; however, a phase shift analysis for these data was not executed. The measurement results of the excitation functions performed in this work at a scattering angle of 171.5° in c.m. is shown in Fig. 2.3.15a by points. The results of our phase shift analysis, obtained on the basis of these data, are shown in Fig. 2.3.15b by circles and in Table 2.3.11. The phase shift is shown in Fig. 2.3.15b from 180° because, as described previously [2], in a *S* wave there has to be a forbidden bound state and at zero energy it is necessary to apply the generalized Levinson theorem for the determination of the phase shift [4].

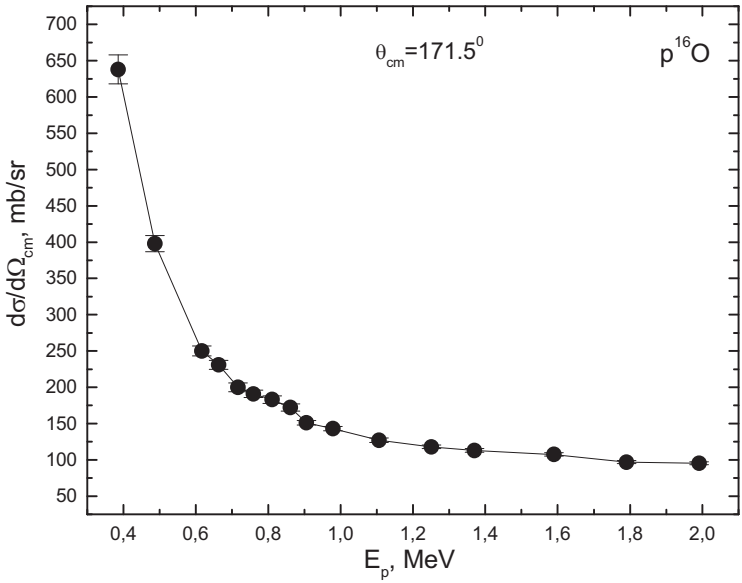

Fig. 2.3.15a. The excitation functions of $p^{16}O$ elastic scattering measured in [154]. The solid curve represents the calculation of the cross sections with the obtained scattering phase shifts.

The values of the cross sections calculated with the obtained phase shifts are shown in Fig. 2.3.15a by the solid curve. The χ^2 value provided in [154] with experimental error cross sections in the excitation functions is given in Fig. 2.3.15c by the solid curve. As can be seen from this figure, the χ^2 value

at different energies does not exceed 10^{-5}. As a result, one $S_{1/2}$ phase shift was found completely unambiguously. For all other results of the phase shift analyses made with excitation functions, the χ^2 value is approximately at the same level.

For comparison, in Fig. 2.3.15b the results of phase shift analyses from [144] are shown with a point at 2 MeV and [148] by squares at approximately 1.5 and 2 MeV. New results, represented by circles in Fig. 2.3.15b, show how the $^2S_{1/2}$ scattering phase shift forms at the lowest energies, playing a primary role in the consideration of thermonuclear processes of radiative capture at astrophysical energies.

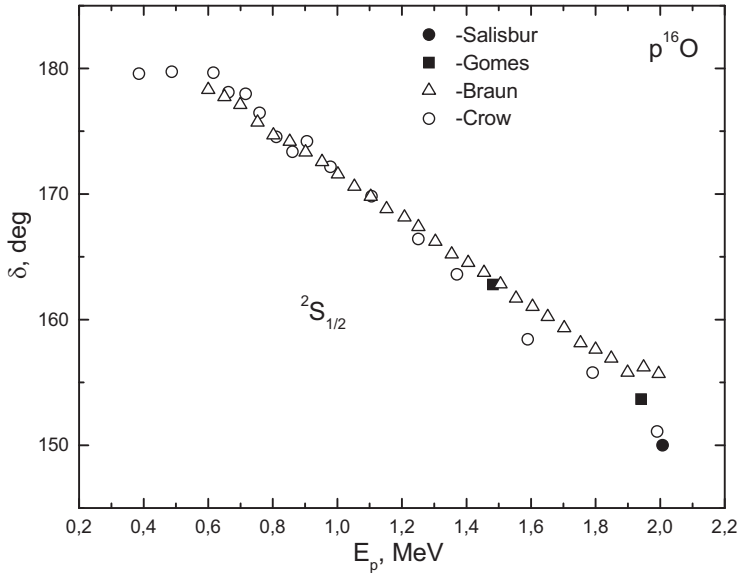

Fig. 2.3.15b. The phase shifts of $p^{16}O$ elastic scattering obtained by us from the excitation function of [154] shown by open circles and [152] by open triangles. A comparison with the results of the phase shift analyses is given in [144,148].

It is clear that at energies of 0.6 MeV and less this phase shift is almost equal to 180°. At energies higher than 1.5 MeV, there is good agreement with the previous results of phase shift analyses observed in [144,148]. The differences between the true and former results of scattering phase shifts obtained in the 1960s do not exceed 1–2°. Here, we note that the measurements of differential cross sections in [154] were performed in the mid-1970s and differ little from the data in [144,148]. However, in other

work the other value of constant $\hbar^2/m_0$ could be used to explain such a distinction in the phase shifts. We should note here that the value $\hbar^2/m_0$ = 41.4686 MeV fm^2 was usually used.

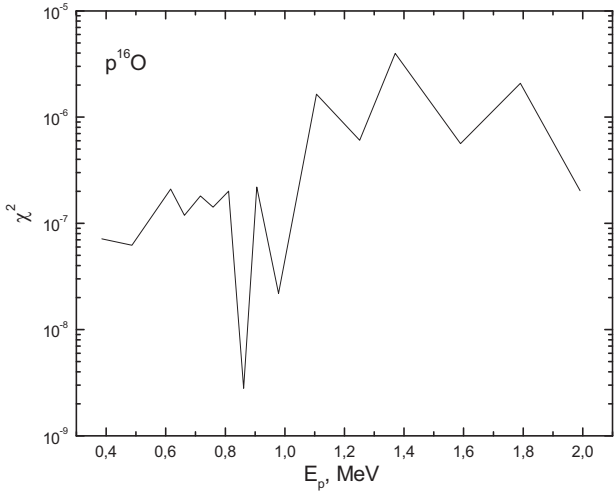

Fig. 2.3.15c. The χ^2 value obtained with the scattering phase shifts shown in Fig. 2.3.15b describing the experimental excitation functions [154].

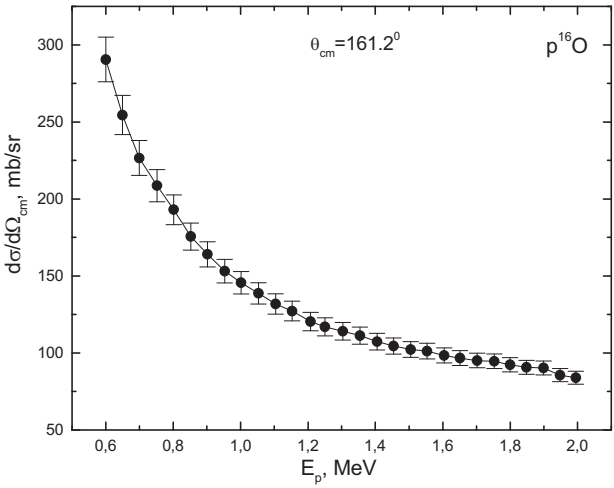

Fig. 2.3.15d. The excitation function of p^{16}O elastic scattering measured in [152]. The solid curve represents the calculation of the cross sections with the obtained scattering phase shifts.

Table 2.3.11. $^2S_{1/2}$ phase shift obtained by us from the data in [154].

E_p, MeV	Phase shift, deg.
0.3855	179.59
0.4871	179.74
0.6162	179.65
0.6631	178.11
0.7162	177.96
0.759	176.46
0.8108	174.55
0.8612	173.37
0.9058	174.19
0.979	172.17
1.1063	169.82
1.2508	166.43
1.3704	163.61
1.5898	158.42
1.7903	155.78
1.9909	151.09

We consider the data on excitation functions from [152] at energies of 0.6–2.0 MeV and a scattering angle of 160° in l.s. or 161.2° in c.m. The cross sections specified in [152] are given in l.s. and have been counted by us in c.m.—they are given by points in Fig. 2.3.15d with a 5 % error specified in [152]. For the recalculation of the cross sections, the following expression was used

$$\sigma_{cm} = \left| \frac{1+\gamma\cos(\theta_{cm})}{1+\gamma^2+2\gamma\cos(\theta_{cm})} \right|^{1.5} \sigma_{lab},$$

where $\gamma = m_1/m_2$ and m represent the masses of particles, meanwhile the m_1 particle is colliding. For the recalculation of cross sections, the integer values of mass were used.

As can be seen in Fig. 2.3.15b, the scattering phase shift obtained on the basis of data in [152] is shown by triangles; the results of our phase shift analysis present reasonably acceptable coordination with the previous extraction of phase shifts at energies of up to 2 MeV. An exception is provided by the two final points in the scattering phase shifts, which, as with the excitation functions [152] for these energies, differ a little from other

results. In Fig. 2.3.15d, the solid curve represents the results of the cross section calculation of $p^{16}O$ elastic scattering with the phase shifts found in our analysis, which were in good agreement with the measurements presented in [152].

Furthermore, [155] presents good results for the differential cross sections at energies of 0.8–2.5 MeV and an angle of 170° in l.s. or 170.6° in c.m. with a 4 % error. However, the phase shift analysis of these data, as far as we know, has not yet been carried out. The results for the excitation functions are presented in Fig. 2.3.16a by points and the scattering phase shifts corresponding to them, obtained in our analysis, are shown in Fig. 2.3.16b by triangles. In Fig. 2.3.16a, the differential cross sections calculated with these scattering phase shifts are shown by the solid curve.

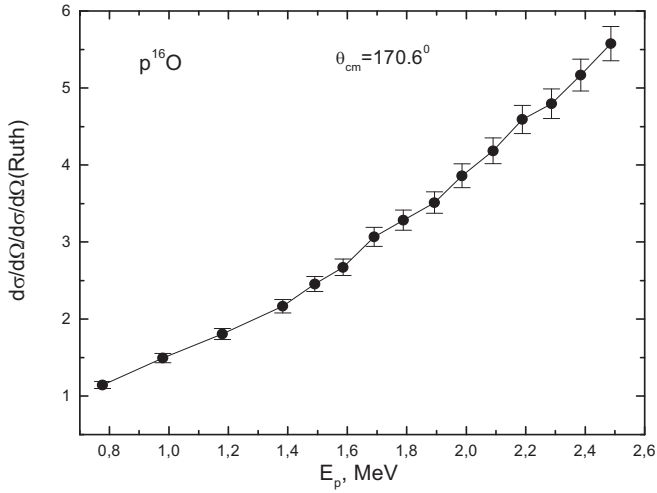

Fig. 2.3.16a. The excitation functions of $p^{16}O$ elastic scattering measured in [155]. The solid curve represents the cross sections calculated with the obtained scattering phase shifts.

In Fig. 2.3.16b, the coincidence of the results in [154] and [155] can be clearly seen, though the measurement of the excitation functions were executed at an interval of 10 years. The results of the phase shift analysis of the angular distributions taking into account only the $^2S_{1/2}$ phase shift given in [155] at energies of about 1.8 to 2.4 MeV are represented in Fig. 2.3.16b by squares. The results of the description of these angular distributions are presented in figs. 2.3.16b and c by solid curves and various points show the results of the experimental measurements with a 4 % error from [155].

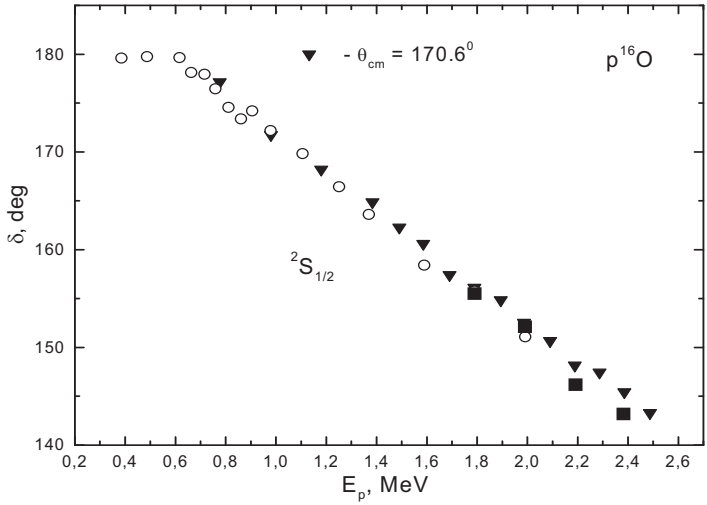

Fig. 2.3.16b. The triangle represents the phase shifts of $p^{16}O$ elastic scattering obtained from the excitation functions in [155]. The phase shifts in Fig. 2.3.15b, obtained on the basis of data in [154], are shown by circles. The squares present the results of the phase shift analysis of angular distributions from [155], shown in figs. 2.3.16c and d.

In [156], the excitation functions at angles of 90° and 120° in l.s. or 93.6° and 123.1° in c.m were measured in the energy range of protons from 0.5 to 3.5 MeV with a 5 % experimental error. The results for the second angle at energies of up to 2.5 MeV are represented by points in Fig. 2.3.17a and agreement between the experimental and calculated cross sections with the phase shifts, which are shown in Fig. 2.3.17b by black points, is represented by the solid curve.

A comparison of the scattering phase shifts obtained in this work (triangles) on the basis of the results [155] for the angle 170.6° in c.m. is given in Fig. 2.3.17b and shown in Fig. 2.3.16b by black triangles. The results in Fig. 2.3.17b were obtained on the basis of data in [154] at 171.5° in c.m., which, according to Fig. 2.3.15b, are acceptable and coordinate with the results of the phase shift analyses in [144,148], made earlier and shown by circles. The measurements in [156] were undertaken in the late 1990s, while the data in [144,148] were published in the 1960s. However, the results of the phase shift analysis obtained on their basis in the energy range 0.4–2.5 MeV are acceptable and coordinate well among themselves, as is clearly shown in figs. 2.3.15b, 2.3.16b, and 2.3.17b.

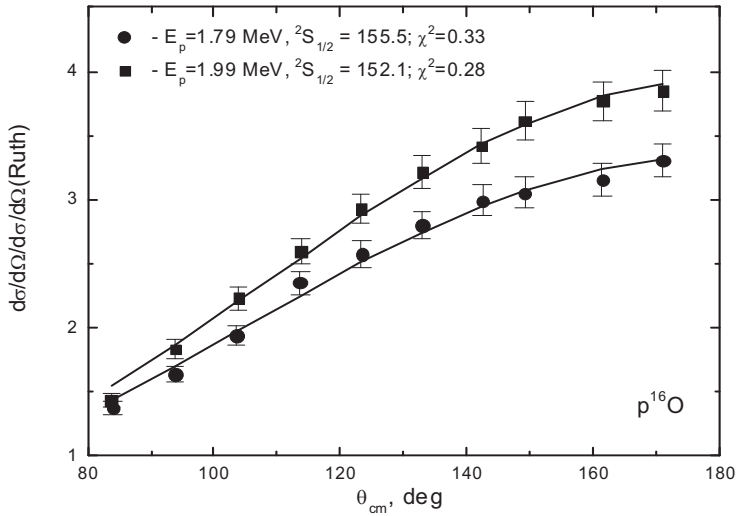

Fig. 2.3.16c. The angular distributions of $p^{16}O$ elastic scattering measured in [155]. The solid curves represent the cross sections calculated with the scattering phase shifts obtained in our phase shift analysis.

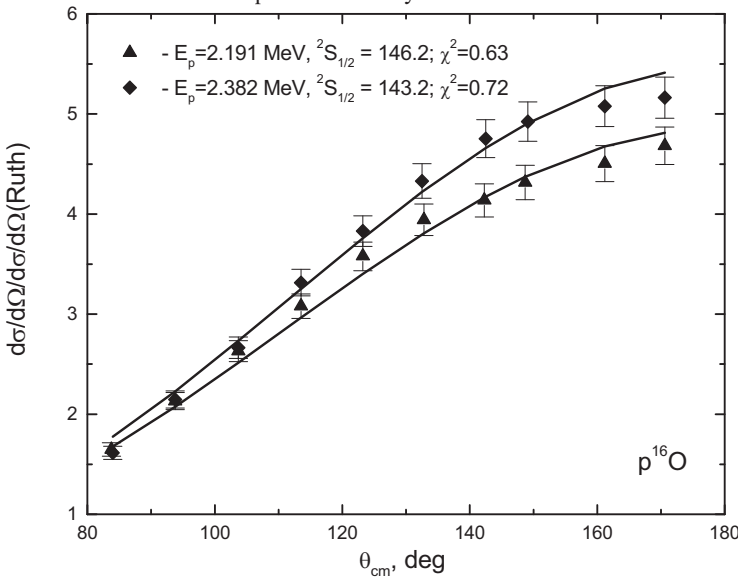

Fig. 2.3.16d. The angular distributions of $p^{16}O$ elastic scattering measured in [155]. The solid curves represent the cross sections calculated with the obtained scattering phase shifts.

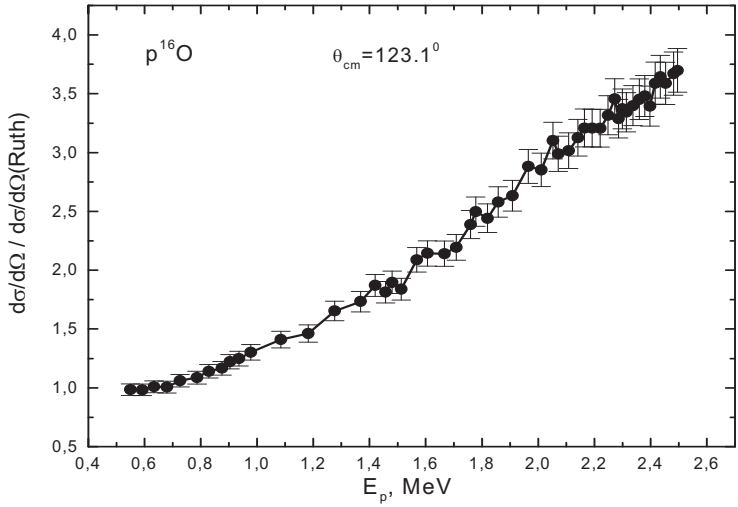

Fig. 2.3.17a. The excitation functions of $p^{16}O$ elastic scattering measured in [156]. The solid curve represents the cross sections calculated with the obtained phase shifts.

Let us consider newer experimental data on the excitation functions in [153] and undertake a phase shift analysis. In [153], measurements of the excitation functions at energies of 0.6 to 2.5 MeV and angles 140° and 178° in l.s. or 142.3° and 178.1° in c.m. are presented. In figs. 2.3.18a and 2.3.18c, the triangles and points show the results of these measurements; the results of our phase shift analysis obtained on the basis of such excitation functions are given in figs. 2.3.18b and 2.3.18d.

The values of the cross sections calculated with such phase shifts in figs. 2.3.18a and 2.3.18c are shown by solid curves. From the obtained results, the shape of the scattering $^2S_{1/2}$ phase shift at the lowest energies is visible—it exceeds 180° on 1–2° and is visible.

We should remember that, as the phase shift analysis is made on one point in the cross sections, i.e. at one value of the cross section at the given energy, the $S_{1/2}$ phase shift is completely unambiguous. Therefore, the excess 180° in scattering phase shifts may indicate the real error in determining the phase shifts of the experimental data. The phase shifts for both scattering angles in comparison to the results obtained by us for data from [154] are shown in Fig. 2.3.18d.

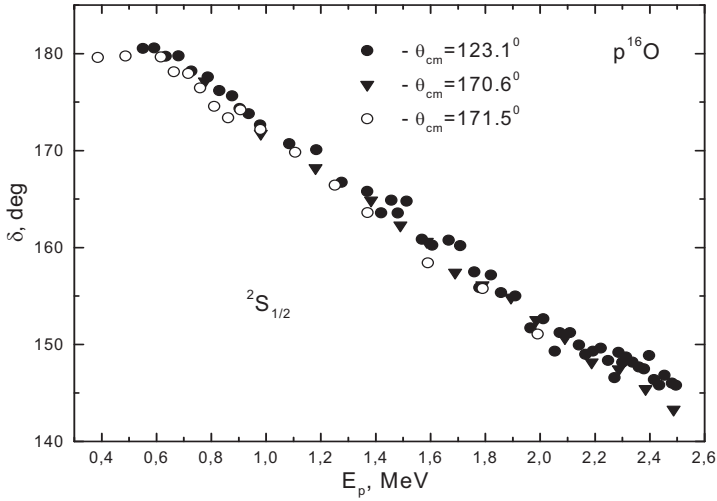

Fig. 2.3.17b. The phase shift of $p^{16}O$ elastic scattering obtained by us from the excitation functions of [156] is shown by black points. The phase shifts shown by circles in Fig. 2.3.15b were obtained on the basis of data in [154]. The results of the phase shift analysis of data in [155] shown in Fig. 2.3.16b are represented by triangles.

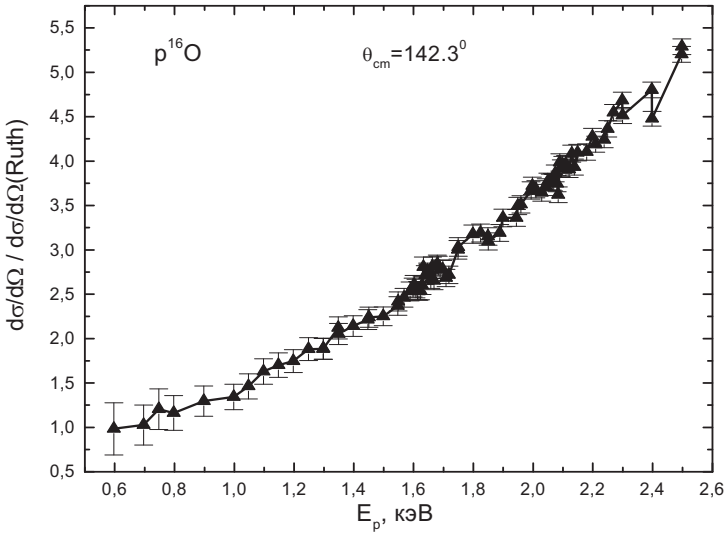

Fig. 2.3.18a. The excitation functions of $p^{16}O$ elastic scattering measured in [153]. The solid curve represents the cross sections calculated with the scattering phase shifts obtained in our phase shift analysis.

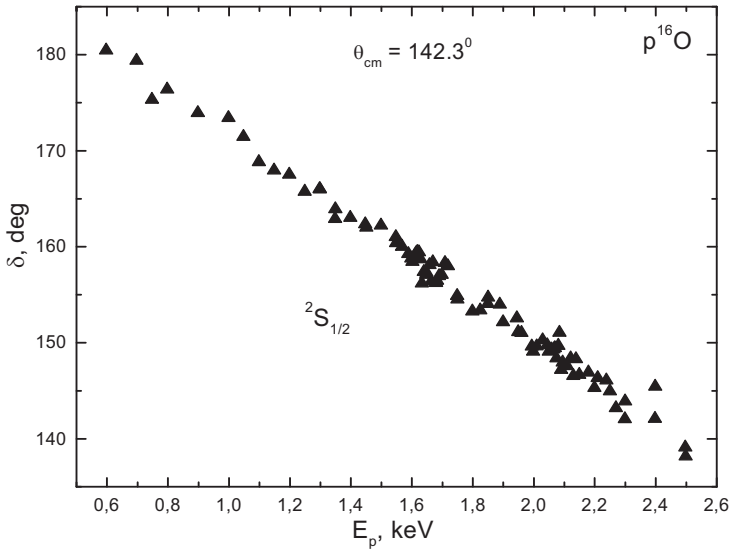

Fig. 2.3.18b. The phase shifts of $p^{16}O$ elastic scattering obtained by us from the excitation functions in [153].

From this figure, it is clear that there is good agreement in the scattering phase shifts between the results obtained in 1975 [154] and newer data published in 2002 [153]. For the previous results, obtained on the basis of data in [154], [155], and [156], a slightly larger divergence in the phase shifts is found. However, the results of our analysis of data at energies higher than 2.2 MeV [153] show a noticeable divergence in the scattering phase shifts obtained for these two angles, reaching 4–5° at an energy of 2.5 MeV.

In conclusion, we have considered the results of the phase shift analysis of measurements of the differential cross sections of the excitation functions and angular distribution of $p^{16}O$ elastic scattering given in [157]. In Fig. 2.3.19a, the points show the excitation functions and the solid curve shows the cross sections obtained by us with the found scattering phase shifts; the phase shifts are shown in Fig. 2.3.19b by black triangles. In the same figure, a comparison of the phase shifts we obtained on the basis of various experimental data are given by points, circles, and squares.

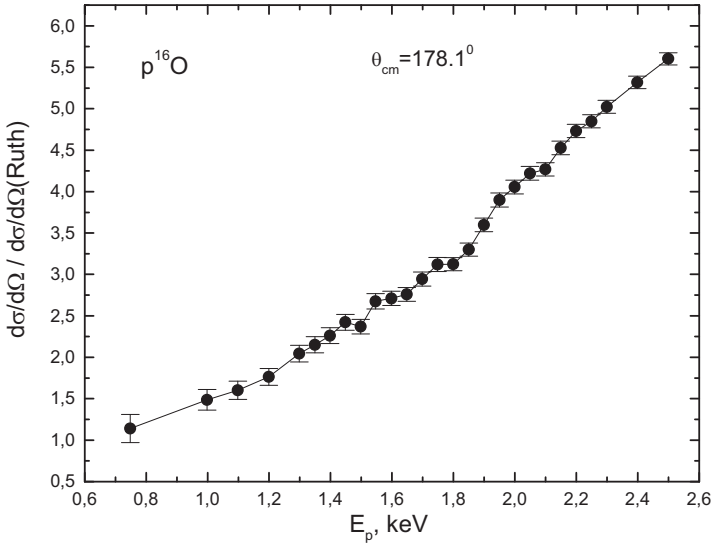

Fig. 2.3.18c. The excitation functions of $p^{16}O$ elastic scattering measured in [153]. The solid curve represents the cross sections calculated with the obtained scattering phase shifts.

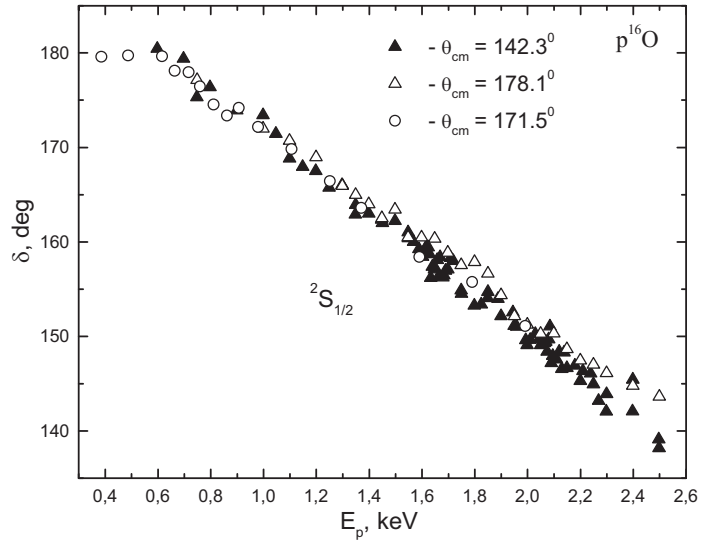

Fig. 2.3.18g. The phase shifts of $p^{16}O$ elastic scattering obtained by us from the excitation functions in [153]. A comparison with the results in [154] with open circles for angle 171.5° (see Fig. 2.3.15b).

It is clear that phase shifts below 0.8 MeV, obtained on the basis of data in [157], are located slightly below the results of our analysis of data in [154] shown by circles and with a difference of about 2–3°. Starting at 0.8 MeV and going up to 1.0 MeV, the results for our data coincide with the phase shifts in [154] at an accuracy of about 1°. Furthermore, the phase shifts obtained on the basis of the angular distributions measured in [157], represented in Fig. 2.3.19b by open triangles, along with a description of the cross sections and the χ^2 value at three energies are shown in Fig. 2.3.20. In Fig. 2.3.20b, it is clear that the greatest χ^2 value is almost equal to 1. Here, at a value higher than a ^2S wave, the components of the decomposition of the cross section in partial waves can make a contribution.

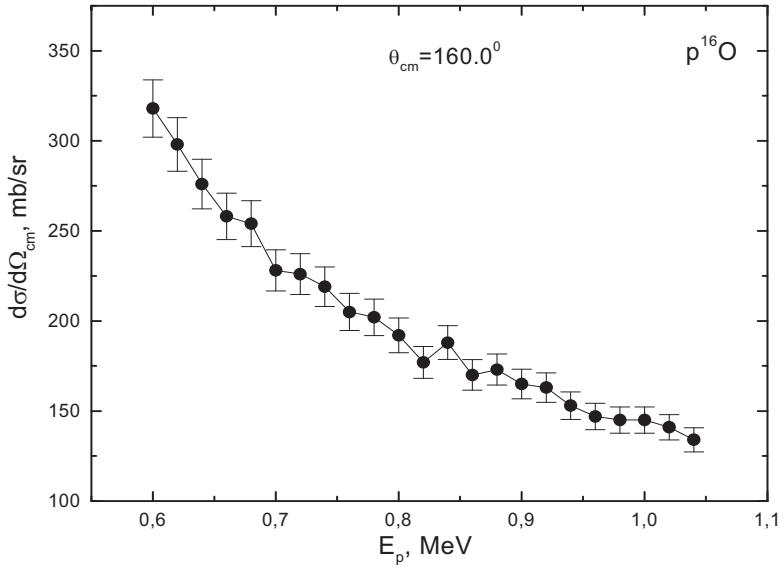

Fig. 2.3.19a. The excitation functions of $p^{16}O$ elastic scattering measured in [157]. The curve represents the calculation of these cross sections with the obtained scattering phase shifts.

Accounting for the contribution of the ^2P waves with 20 iterations gives the following values for the scattering phase shifts at $\chi^2 = 0.68$: $S = 172.4°$, $P_{1/2} = 2.4°$, and $P_{3/2} = 2.4°$. Accounting for the contribution of the P and D waves with the same number of iterations gives the following scattering phase shifts at $\chi^2 = 0.25$: $S = 177.0°$, $P_{1/2} = -8.8°$, $P_{3/2} = 10.9°$, $D_{3/2} = 1.7°$, and $D_{5/2} = 1.3°$. The results of calculation of the cross sections with these

phase shifts are shown in Fig. 2.3.20c by the dashed curve. Improvement of the description of cross sections only in the forward area of angles, i.e. approximately up to 70–80°, is observed. Such phase shifts, which agree reasonably well with those obtained above (Table 2.3.11) on the basis of the excitation functions, but at an energy of less than 0.8 MeV, are located below the results of the phase shift analysis obtained on the basis of the data in [154].

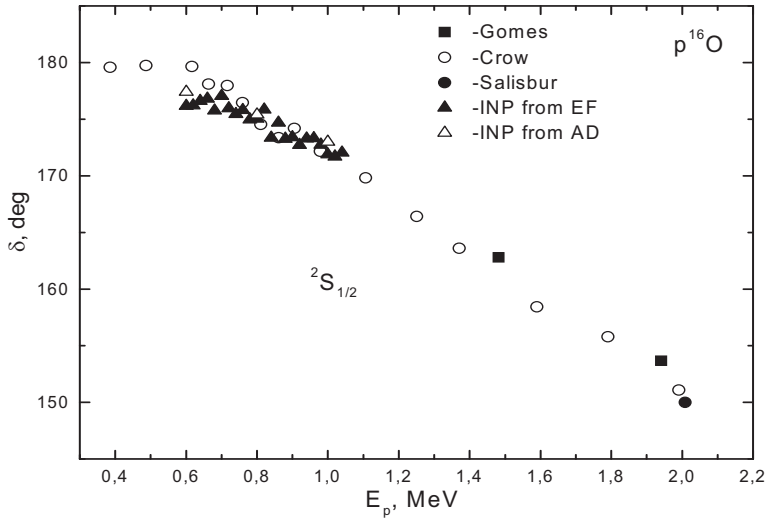

Fig. 2.3.19b. The phase shifts of $p^{16}O$ elastic scattering obtained by us from the differential cross sections in [157] shown by triangles. Other designations present the data in [144,148,154].

The accuracy of the phase shift analysis was estimated by us at the level of 2–3°, therefore the observed divergence in the results falls within the error limits. As such, new results for phase shifts of $p^{16}O$ elastic scattering, with a description of data on the excitation functions from several works for different scattering angles in the energy range 0.4–2.5 MeV were obtained. A summary of the results of our phase shift analysis is given in Fig. 2.3.21. Reasonably good agreement between all the results obtained and the earlier phase shift analysis is visible at an energy of approximately up to 2.0 MeV.

The results of the phase shift analysis, i.e. phase shifts of $p^{16}O$ elastic scattering, and the data of resonances of ^{17}F [103], allow us to parametrize the intercluster potentials of interaction of the scattering processes in the non-resonance $^2S_{1/2}$ wave.

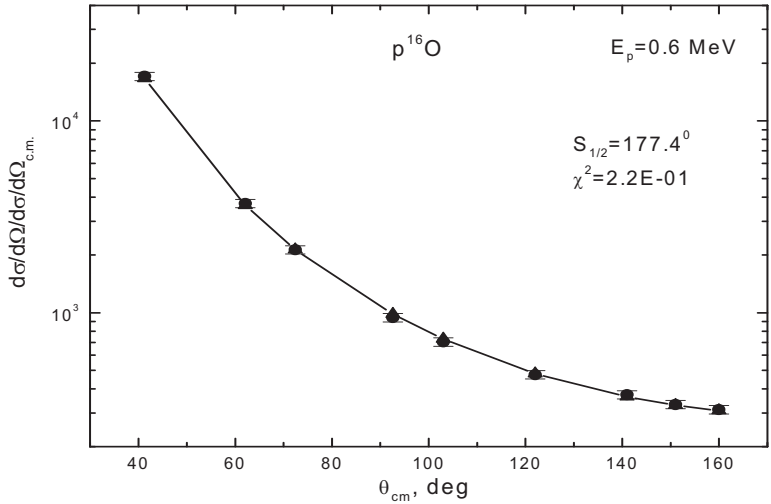

Fig. 2.3.20a. The angular distributions of $p^{16}O$ elastic scattering measured in [157] at a proton energy of 0.6 MeV. The solid curve represents the calculation of cross sections with the obtained scattering phase shifts.

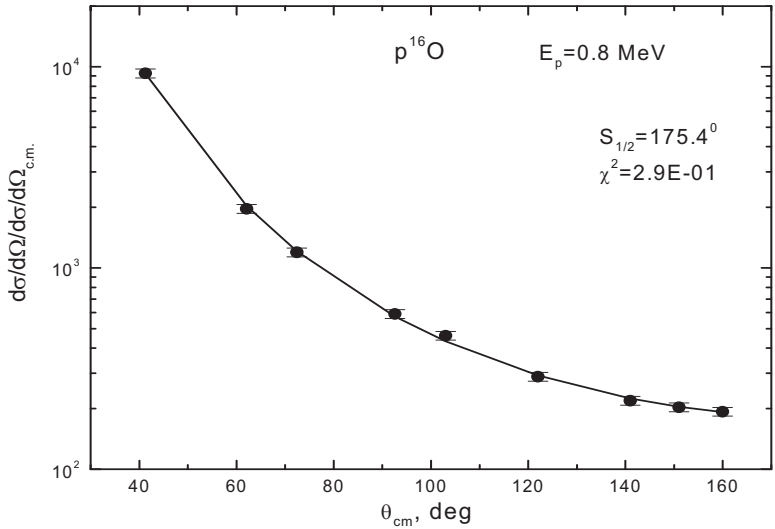

Fig. 2.3.20b. The same as in Fig. 2.3.20a, but at a proton energy of 0.8 MeV.

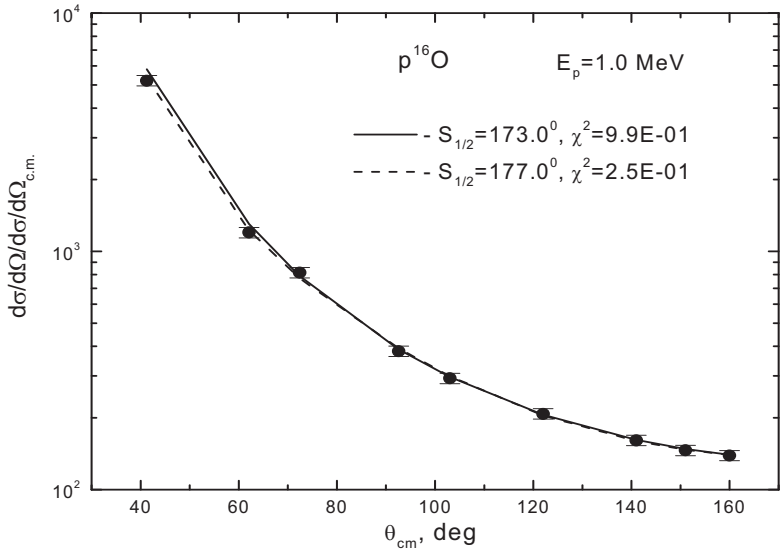

Fig. 2.3.20c. The same as in Fig. 2.3.20a, but at a proton energy of 1.0 MeV.

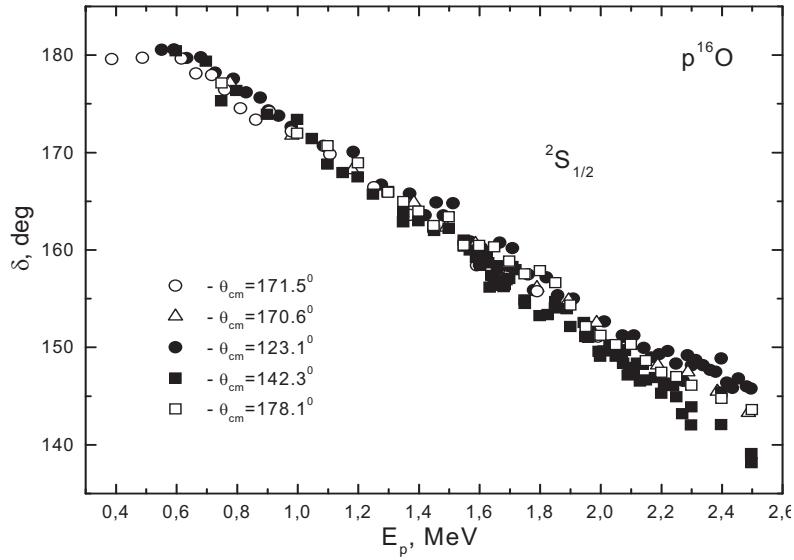

Fig. 2.3.21. All main phase shifts of $p^{16}O$ scattering obtained in this work from the excitation functions at angles higher than 120°.

Such potentials, in turn, can be used when performing calculations for various astrophysical problems, such as the radiative capture of particles on light nuclei, and, in this case, determination of the astrophysical *S*-factor of proton radiative capture on ^{16}O at ultra-low energies.

2.3.8 Program for $N^{12}C$, $p^{14}C$, and $N^{16}O$ phase shift analysis

Below, we provide the text of a computer program in Fortran-90 to carry out phase shift analysis of $p^{12}C$ elastic scattering. The program searches the elastic scattering phase shifts of two particles with experimental differential cross sections, using the methods previously described.

The description of the key parameters, variables, parameters of the interaction potentials, and the units of the program and subprograms are given in the list and do not practically differ from the designations used in the previous programs.

PROGRAM FAZ_ANAL_p12C

```
! * The program of the phase shift analysis of the p12C elastic scattering *
IMPLICIT REAL(8) (A-Z)
INTEGER I,L,LMA,NI,NV,LMI,LH,LMII,LMAA,LHH,NTTT,
NTT,NPP,NT,NTP
CHARACTER(34) AA
CHARACTER(33) BB
CHARACTER(25) AC
CHARACTER(24) BC
CHARACTER(3) NOM
CHARACTER(6) EX,EX1
COMMON /A1/
SE(0:50),DS(0:50),DE(0:50),NT,POLE(0:50),POLED(0:50),DS1(0:50),N
TP,XIS,XIP,XI1
COMMON /A2/ NTTT,GG,SS,LMII,LMAA,LHH,NP
COMMON /A3/ POL(0:50),TT(0:100),REZ(0:50)
COMMON /A4/ LH,LMI,NTT,NPP
COMMON/A5/ PI
DIMENSION ST(0:50),FP(0:50),FM(0:50),XP(0:50)
! ********** The initial values **********
PI=4.0D0*DATAN(1.0D0)
Z1=1.0D0! the P charge
Z2=6.0D0 ! the 12C charge
AM1=1.00727646577D0;! The mass of P
AM2=12.0D0; ! The mass of 12C
```

```
AM=AM1+AM2
A1=41.80159D0
PM=AM1*AM2/AM
B1=2.0D0*PM/A1
LMI=0; LH=1; LMA=0
! The minimum LMI and maximum LMA orbital! moment
EP=1.0D-05; LMII=LMI; LHH=LH; LMAA=LMA
! EP – accuracy of the search for a minimum of chi square
NV=1;! 1 – To carry out the minimization, 0 – without the minimization
FH=0.0123D0! The initial step
NI=10! The number of iterations
NP=2*LMA; NPP=NP
! ********** The set of the energy in c.m. **********
ECM=0.422D0 ! An energy in c.m.
NT=17; NTT=NT; NTTT=NT! The number of points in the angles
NOM='422'
EX='-1.TXT'; EX1='-R.DAT'
AC='G:\BASICA\FAZ-ANAL\p12C\c'
BC='G:\BASICA\FAZ-ANAL\p12C\'
AA=AC//NOM//EX
BB=BC//NOM//EX1
OPEN (1,FILE=AA)
DO L=1,NT
READ(1,*) TT(L),SE(L),DE(L)
SE(L)=SE(L)*1000.0D0
DE(L)=SE(L)*0.10D0
ENDDO
CLOSE(1)
OPEN (1,FILE="G:\BASICA\FAZ-ANAL\p12C\FAZ.DAT")
DO L=LMI,LMA,LH
READ(1,*) FP(L),FM(L)
ENDDO
CLOSE(1)
! ******* The transfer of the initial phase shifts to the radians *
DO L=LMI,LMA,LH
FM(L)=FM(L)*PI/180.0D0
FP(L)=FP(L)*PI/180.0D0
ENDDO
FH=FH*PI/180.0D0
DO I=LMI,LMA,LH
XP(I)=FP(I)
```

```
IF (I==LMA) GOTO 112
XP(I+LMA+LH)=FM(I+1)
112 ENDDO
! ********** Searching of the minimum of XI**2 **********
EL=ECM*AM1/PM
SK=ECM*B1
SS=DSQRT(SK)
GG=3.4495312D-002*Z1*Z2*PM/SS
CALL VAR(ST,FH,NI,XP,EP,XI,NV)
FM(0)=XP(0)
DO I=LMI,LMA,LH
FP(I)=XP(I)
IF (I==LMA) GOTO 111
FM(I+1)=XP(I+LMA+LH)
111 ENDDO
! ********** The printing of the results ***********************
PRINT *,"   EL, ECM, SK, SS=",EL,ECM,SK,SS
PRINT *
PRINT *,"          T                SE                ST                XI "
DO I=1,NT
PRINT *,TT(I),SE(I),ST(I),DS(I)
ENDDO
PRINT *
PRINT *,"   XI=(XIS+XIP),XIS,XIP=",XI,XIS,XIP
PRINT *
PRINT *,"          L            FP            FM"
DO L=LMI,LMA,LH
FM(L)=FM(L)*180.0D0/PI
FP(L)=FP(L)*180.0D0/PI
PRINT *,L,FP(L),FM(L)
ENDDO
OPEN (1,FILE=BB)
WRITE(1,*) " EL,ECM=",EL,ECM
WRITE(1,*) "XI=(XIS+XIP),XIS,XIP=",XI,XIS,XIP
WRITE(1,*) "          T                SE                ST                XI"
DO I=1,NT
WRITE(1,*) TT(I),SE(I),ST(I),DS(I)
ENDDO
WRITE(1,*) "
WRITE(1,*) "          L            FP            FM"
DO I=LMI,LMA,LH
```

```
WRITE(1,*) I,FP(I),FM(I)
ENDDO
OPEN (1,FILE="G:\BASICA\FAZ-ANAL\p12C\FAZ.DAT")
DO I=LMI,LMA,LH
WRITE(1,*) FP(I),FM(I)
ENDDO
CLOSE(1)
END

SUBROUTINE VAR(ST,PHN,NI,XP,EP,AMIN,NV)
!  The variation subprogramme for the minimization of a chi-square
IMPLICIT REAL(8) (A-Z)
INTEGER I,NI,NT,NV,NP,LMI,LH,NN,IN,NTT,NTP
COMMON                                                    /A1/
SE(0:50),DS(0:50),DE(0:50),NT,POLE(0:50),POLED(0:50),DS1(0:50),N
TP,XIS,XIP,XI1
COMMON /A3/ POL(0:50),TT(0:100),REZ(0:50)
COMMON /A4/ LH,LMI,NTT,NP
COMMON/A5/ PI
DIMENSION XPN(0:50),XP(0:50),ST(0:50)
DO I=LMI,NP,LH
XPN(I)=XP(I)
ENDDO
NN=LMI
PH=PHN
CALL DET(XPN,ST,ALA)
B=ALA
IF (NV==0) GOTO 3012
DO IIN=1,NI
NN=-LH
PRINT *,'FF=',ALA,IIN
1119  NN=NN+LH
IN=0
2229 A=B
XPN(NN)=XPN(NN)+PH*XP(NN)
IN=IN+1
CALL DET(XPN,ST,ALA)
B=ALA
IF (B<A) GOTO 2229
C=A
XPN(NN)=XPN(NN)-PH*XP(NN)
```

```
IF (IN>1) GOTO 3339
PH=-PH
GOTO 5559
3339 IF (ABS((C-B)/(B))<EP) GOTO 4449
PH=PH/2.0D0
5559 B=C
GOTO 2229
4449 PH=PHN
B=C
IF (NN<NP) GOTO 1119
AMIN=B
PH=PHN
ENDDO
3012 AMIN=B
DO I=LMI,NP,LH
XP(I)=XPN(I)
ENDDO
END

SUBROUTINE DET(XP,ST,XI)
! ******* The subroutine for chi-square calculation **********
IMPLICIT REAL(8) (A-Z)
INTEGER I,NT,NTP
COMMON /A1/ SE(0:50),DS(0:50),DE(0:50),NT,POLE(0:50),
POLED(0:50),DS1(0:50),NTP,XIS,XIP,XI1
COMMON /A3/ POL(0:50),TT(0:100),REZ(0:50)
DIMENSION XP(0:50),ST(0:50)
S=0.0D0
CALL SEC(XP,ST)
S1=0.0D0
DO I=1,NT
DS(I)=((ST(I)-SE(I))/DE(I))**2
S=S+DS(I)
ENDDO
XI=S/NT
END

SUBROUTINE SEC(XP,S)
! *** The subprogramme of the calculation of the scattering cross section *
IMPLICIT REAL(8) (A-Z)
INTEGER I,NT,LMI,LMA,LH,L
```

```
COMMON /A2/ NT,GG,SS,LMI,LMA,LH,NP
COMMON /A3/ POL(0:50),TT(0:100),REZ(0:50)
COMMON/A5/ PI
DIMENSION
S0(0:50),P(0:50),PP(0:50),FP(0:50),FM(0:50),XP(0:50),S(0:50)
DO I=LMI,LMA,LH
FP(I)=XP(I)
IF (I==LMA) GOTO 111
FM(I+1)=XP(I+LMA+LH)
111 ENDDO
FM(0)=FP(0)
CALL CULFAZ(GG,S0)
DO I=1,NT
T=TT(I)*PI/180.0D0
X=DCOS(T)
A=2.0D0/(1.0D0-X)
S00=2.0D0*S0(0)
BB=-GG*A
ALO=GG*DLOG(A)+S00
REC=BB*DCOS(ALO)
AMC=BB*DSIN(ALO)
REZ1=REC**2+AMC**2
REA=0.0D0
AMA=0.0D0
REB=0.0D0
AMB=0.0D0
DO L=LMI,LMA,LH
FPP=2.0D0*FP(L)
FMP=2.0D0*FM(L)
AA=DCOS(FPP)-DCOS(FMP)
BB=DSIN(FPP)-DSIN(FMP)
SL=2.0D0*S0(L)
CALL FUNLEG(X,L,PP)
REB=REB+(BB*DCOS(SL)+AA*DSIN(SL))*PP(L)
AMB=AMB+(BB*DSIN(SL)-AA*DCOS(SL))*PP(L)
LL=2*L+1
JJ=L+1
AA=JJ*DCOS(FPP)+L*DCOS(FMP)-LL
BB=JJ*DSIN(FPP)+L*DSIN(FMP)
CALL POLLEG(X,L,P)
REA=REA+(BB*DCOS(SL)+AA*DSIN(SL))*P(L)
```

```
AMA=AMA+(BB*DSIN(SL)-AA*DCOS(SL))*P(L)
ENDDO
REA=REC+REA
AMA=AMC+AMA
RE=REA**2+AMA**2
AM=REB**2+AMB**2
S(I)=10.0D0*(RE+AM)/4.0D0/SS**2
REZ(I)=REZ1*10.0D0/4.0D0/SS**2
POL(I)=2.0D0*(REB*AMA-REA*AMB)/(RE+AM)
ENDDO
END

SUBROUTINE POLLEG(X,L,P)
! ***** The subprogramme of calculation of the Legendre polinomials ***
IMPLICIT REAL(8) (A-Z)
INTEGER I,L
DIMENSION P(0:50)
P(0)=1.0D0; P(1)=X
DO I=2,L
P(I)=(2*I-1)*X/I*P(I-1)-(I-1)/I*P(I-2)
ENDDO
END

SUBROUTINE FUNLEG(X,L,P)
! *** The subprogramme of calculation of the Legendre functions *******
IMPLICIT REAL(8) (A-Z)
INTEGER I,L
DIMENSION P(0:50)
P(0)=0.0D0; P(1)=DSQRT(ABS(1.-X**2)); P(2)=3.0D0*X*P(1)
IF (L>=3) THEN
DO I=2,L
P(I+1)=(2*I+1)*X/I*P(I)-(I+1)/I*P(I-1)
ENDDO
ENDIF
END

SUBROUTINE CULFAZ(G,F)
! *** The subprogramme of calculation of the Coulomb phase shifts ***
IMPLICIT REAL(8) (A-Z)
INTEGER I,N
DIMENSION F(0:50)
```

```
C=0.5772156650D0; S=0.0D0; N=50
A1=1.202056903D0/3.0D0; A2=1.036927755D0/5.0D0
DO I=1,N
A=G/I-DATAN(G/I)-(G/I)**3/3.0D0+(G/I)**5/5.0D0
S=S+A
ENDDO
FAZ=-C*G+A1*G**3-A2*G**5+S
F(0)=FAZ
DO I=1,20
F(I)=F(I-1)+DATAN(G/I)
ENDDO
END
```

The following control was carried out at a resonance energy of 422 keV (c.m.) for $p^{12}C$ elastic scattering, taking into account the phase shift analysis in only one S wave.

EL, ECM, SK, SS = 4.574E-1 4.22E-1 1.87E-2 1.37E-1

θ	σ_e	σ_t	χ^2_i
10.83	409561	3256822.3428083	4.194371298676935
21.63	266969	227766.5412064077	2.156278956304461
32.39	58583.1	50674.784355610	1.8223143351212
43.07	17267.6	15925.09271621951	6.044624704055184E-1
53.66	5839.94	5640.62956376928	1.164778401875084E-1
64.14	2414.18	2060.5610732571380	2.145515754644307
74.5	965.24	740.3435278409627	5.428685268597148
84.71	422.29	265.4550687576415	13.793167214162040
94.79	217.01	120.1919175449456	19.9046247867550
104.7	147.11	103.6791667064438	8.715893867706498
114.5	140.23	133.5569838776437	2.264448667637590E-1
124.15	204.09	175.8612452117759	1.913110216888019
133.67	243.52	216.8648984979974	1.198095428652019
143.08	253.77	251.4932553653157	8.049114108914179E-3
152.39	267.64	278.2186995788807	1.562293138659170E-1
161.64	288.94	296.9745596276764	7.732302205565983E-2
170.84	292.72	308.0225110939944	2.732880319244108E-1

$$\chi^2 = 3.69$$

L	δ_p	δ_m
0	58.15	58.15

As a result, we obtained the phase shift *S* value of 58.15º at a rather large value of $\chi^2 = 3.69$. The value of the phase shifts and some other characteristics are shown rounded to the second sign after the comma. If we take into account the *P* wave in the analysis, then, for the scattering phase shifts we obtain the following control account:

EL, ECM, SK, SS = 4.57E-1 4.22E-1 1.87E-2 1.37E-1

θ	σ_e	σ_t	χ^2_i
10.83	4095610	3264781.541334357	4.115148756111661
21.63	266969	223190.0387772885	2.689114135211925
32.39	58583.1	49592.26685532391	2.355348513821907
43.07	17267.6	16111.41279780082	4.483243796400418E-1
53.66	5839.94	6059.579098437353	1.414498640631696E-1
64.14	2414.18	2415.589085838059	3.406713446204295E-5
74.5	965.24	982.7590318182862	3.294197102373393E-2
84.71	422.29	414.5062045985828	3.397513798561286E-2
94.79	217.01	205.28584114367	2.918797023030877E-1
104.71	147.11	149.1168415589131	1.860980323212324E-2
114.5	140.23	155.8558179281346	1.241662746301032
124.15	204.09	185.2840079884762	8.490808445689716E-1
133.67	243.52	219.3107960699812	9.883067178217969E-1
143.08	253.77	250.1596154521572	2.024073897229597E-2
152.39	267.64	274.7849530022851	7.126835104038670E-2
161.64	288.94	292.3439981186766	1.387916330759821E-2
170.84	292.72	302.7569167687375	1.175698198093965E-1

$\chi^2 = 7.90E-1$

L	δ_p	δ_m
0	52.13	52.13
1	-8.97	12.82

It is clear that, in assessing the phase shift analysis of the *S* and *P* scattering waves, the χ^2 value decreases from 3.69 till 0.79.

The following designations are used: EL is the energy of particles in the laboratory system; ECM is the energy of particles in the system of the center of mass; SK is the square of the wave number k^2; SS is the wave number k; L is the orbital moment; θ is the scattering angle; σ_e is the experimental cross sections; σ_t is the calculated cross sections; χ^2_i is partial χ^2 for angle i; δ_p is a phase shift with $J = L + 1/2$; δ_m is a phase shift at $J = L - 1/2$; and χ^2 is the average value on all points.

If we use the normal value of 41.4686 MeV·fm^2 for the $\hbar^2/m_0$ constant, then, as seen below, the χ^2 value changes by approximately 10 % and with some phase shifts on 0.5º, which do not practically affect the results even at the resonance energy:

$\chi^2 = 8.85E\text{-}1$

L	δ_p	δ_m
0	51.63	51.63
1	-9.40	12.87

From the given results, it is clear that at 422 keV (c.m.), the *S* phase shift almost reaches the resonance value of 90º. At energies in the range of the resonance with a width of less than 32 keV [120], a sharp increase in the phase shift is observed and the energy change is approximately 1 keV, which can lead to a change in the phase shift to 40–50º. Let us note that the accuracy of determining the considered experiment comes to about 1 keV, and the accuracy of the determination of the energy of the resonance level has a value of 0.6 keV [120].

The scattering phase shifts found from the phase shift analysis are used to construct the p^{12}C intercluster potentials, which, in turn, can be applied to the calculations of the astrophysical *S*-factors of proton radiative capture on ^{12}C [2,28,122,123,125]. This process is the first thermonuclear fusion reaction of the CNO (carbon-nitrogen-oxygen) cycle, which is present during later stages of the development of stable stars with partial hydrogen combustion. In this process, the core of the star begins to collapse considerably, resulting in an increase in pressure and temperature and, along with a proton-proton cycle, the following chain of thermonuclear processes called the CNO or carbon cycle [28,122] comes into play. The CNO cycle is a set of three interlinked processes, or, more precisely, partially blocked cycles. The first and the simplest of them is the CN cycle (the Bethe cycle or carbon cycle), which was described by Hans Bethe and, independently, by Carl Friedrich von Weizsäcker in 1939 [28,122,123].

2.4 Phase shift analysis of elastic p^{6}Li scattering

Let us consider the processes of p^{6}Li elastic scattering at astrophysical energies and the phase shift analysis of the available experimental data. The results of such phase shift analysis are needed for the creation of the intercluster interaction potentials in calculating the solutions of astrophysical problems [158].

2.4.1 The differential cross sections

Considering the scattering processes in the system of particles with spins 1/2 and 1 without spin-orbital splitting of phase shifts, the elastic scattering cross section is presented in its simplest form [6]

$$\frac{d\sigma(\theta)}{d\Omega} = \frac{2}{6}\frac{d\sigma_d(\theta)}{d\Omega} + \frac{4}{6}\frac{d\sigma_q(\theta)}{d\Omega}, \qquad (2.4.1)$$

where the indexes *d* and *q* belong to the doublet (with spin 1/2) and quartet (with spin 3/2) states of the p^{6}Li system and the cross sections themselves are expressed through the scattering amplitudes, which are registered like the expressions for the phase shift analysis in the ^{4}He^{4}He system

$$\frac{d\sigma_d(\theta)}{d\Omega} = \left|f_d(\theta)\right|^2, \qquad \frac{d\sigma_q(\theta)}{d\Omega} = \left|f_q(\theta)\right|^2,$$

where

$$f_{d,q}(\theta) = f_c(\theta) + f^N{}_{d,q}(\theta),$$

and

$$f_c(\theta) = -\left(\frac{\eta}{2k\sin^2(\theta/2)}\right)\exp\{i\eta\ln[\sin^{-2}(\theta/2)] + 2i\sigma_0\}\ , \qquad (2.4.2)$$

$$f_d^N(\theta) = \frac{1}{2ik}\sum_L (2L+1)\exp(2i\sigma_L)[S_L^d - 1]P_L(\cos\theta)\ ,$$

$$f_q^N(\theta) = \frac{1}{2ik}\sum_L (2L+1)\exp(2i\sigma_L)[S_L^q - 1]P_L(\cos\theta)\ ,$$

where $S_L^{d,q} = \eta_L^{d,q} \exp[2i\delta_L^{d,q}(k)]$ is a scattering matrix in a doublet (d) or quartet (k) spin state [6].

It is possible to use the simple expressions for the calculation of elastic scattering cross sections because, in the range of low energies of the spin-orbital, little splitting of the phase shifts arises and in the elastic scattering, there are no resonances with a certain total moment. This has been confirmed by the results of phase shift analysis made in [159], taken into account in the spin-orbit splitting of the phase shifts and which did not exceed a few degrees.

2.4.2 Phase shift analysis

The phase shift analysis of the differential cross sections and excitation functions for p^6Li elastic scattering, without a clear accounting of the doublet ^2P wave, was undertaken in [159]. Our phase shift analysis was carried out at lower energies, which are relevant to nuclear astrophysics, and take into account all of the lower partial waves, including the doublet ^2P wave, based on the differential cross sections specified in [160,161,162].

At an energy of 500 keV, on the basis of data in [162], we found the ^2S and ^4S scattering phase shifts, and these are given in Table 2.4.1 (No. 1). The results of calculation of the cross sections obtained agree quite well with the experimental data at an average on all points of $\chi^2 = 0.15$. The error of the differential cross sections of these data was accepted as being equal to 10 %. Analysis of the doublet ^2P and quartet ^4P phase shifts has shown that their numerical values are less than 0.1°.

The following five energies were found in new measurement results of the differential cross sections in [160,163]. The first of them, 593.0 keV, gives us the opportunity to find the $^{2,4}S$ phase shifts, which differ a little from the phase shifts for the previous energy and have the same χ^2; these are shown in Table 2.4.1 (No. 2). The phase shifts for the $^{2,4}P$ waves also tend towards zero.

Table 2.4.1. Results of phase shift analysis of p^6Li elastic scattering at low energies.

№	E_p, keV	^2S, deg.	^4S, deg.	^2P, deg.	^4P, deg.	χ^2
1	500	176.2	178.7	–	–	0.15
2	593.0	174.2	178.8	–	–	0.15
3-1	746.4	170.1	180.0	–	–	0.24

3-2	746.4	172.5	179.9	1.7	–	0.16
4-1	866.8	157.8	180.0	–	–	0.39
4-2	866.8	170.2	174.9	3.9	–	0.22
4-3	866.8	169.6	175.0	3.5	0.1	0.23
5-1	976.5	160.0	178.5	–	–	0.12
5-2	976.5	167.0	174.5	1.1	–	0.12
6-1	1136.3	144.9	180.0	–	–	0.58
6-2	1136.3	164.7	171.1	5.8	–	0.32
6-3	1136.3	166.4	169.9	5.5	0.1	0.32

The $^{2,4}S$ phase shifts were found at an energy of 746.7 keV (Table 2.4.1, No. 3-1), allowing us to describe the cross sections with an accuracy of $\chi^2 = 0.24$. Despite the smallness of the χ^2 value, an attempt to consider $^{2,4}P$ phase shifts was made. In the beginning, it was believed that the quartet ^4P phase shift was negligible following on from the results in [159], with an account only for 1.0–1.5 MeV. The results of our analysis, taking into account only the ^2P phase shifts, are presented in Fig. 2.4.1a and Table 2.4.1 (No. 3-2). It is clear that the value of the small doublet ^2P phase shift increases the ^2S wave value a little and reduces χ^2 to a value of 0.16. The account of the quartet ^4P phase shift has given a negligible value for its numerical value at less than 0.1°, which corresponds to the results in [159].

The result of the search of phase shifts for an energy of 866.8 keV taking into account only the $^{2,4}S$ waves is given in Table 2.4.1 (No. 4-1) and with $\chi^2 = 0.39$. The value of the ^2S phase shift appears to fall sharply in comparison to the previous energy. The account of the ^2P wave considerably increases its value (Fig. 2.4.1b and Table 2.4.1, No. 4-2) and reduces the χ^2 value by a factor of almost two. The attempt to consider the quartet ^4P phase shift gave results with a value of about 0.1° (Table 2.4.1, No. 4-3).

Any change of the ^4P wave on the large side, including at other values of other phase shifts, led to an increase in χ^2. At this energy, as well as at all other energies considered in [160,161], it is not possible to find any variant for a non-zero quartet phase shift at the χ^2 value tending towards the minimum. For the following energy, 976.5 keV, excluding the $^{2,4}P$ waves, the values of the ^2S and ^4S phase shifts have been found, as shown in Table 2.4.1 (No. 5-1). The subsequent account of the ^2P wave considerably increases the values of the ^2S phase shift, neglecting the ^4P wave, as is made clear in Fig. 2.4.1c and Table 2.4.1 (No. 5-2) at $\chi^2 = 0.12$.

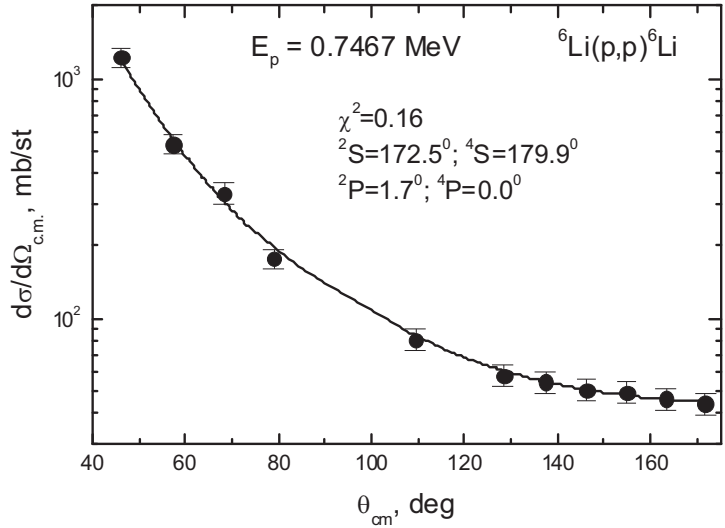

Fig. 2.4.1a. The cross sections of p^{6}Li elastic scattering at 746.7 keV. The solid curve represents the calculation of the cross sections with the found phase shifts.

If we include a quartet ^4P wave in the analysis, then it aspires to zero at the reduction of the χ^2 value. Energy of 1.1363 MeV considered in [160,161], even with an account of only the $^{2,4}S$ waves, leads to a rather small χ^2 equal to 0.58, as shown in Table 2.4.1 (No. 6-1). In this case, the account of the ^2P wave leads to a noticeable increase in the value of the ^2S phase shift and the corresponding results of the calculation of cross sections are shown in Fig. 2.4.1d and Table 2.4.1 (No. 6-2). The account of the quartet ^4P wave at this energy results in a value of about 0.1°, as shown in Table 2.4.1 (No. 6-3).

Thus, in the description of all experimental data from [160,161], accounting for the quartet ^4P waves in this energy range is not necessary, i.e. their values are equal to or less than 0.1°. This is in agreement with the results in [159]; however, the doublet ^2P phase shift reaches 5.5–6° and its value cannot be neglected. The general form of the ^2S and ^4S scattering phase shifts is shown further in Fig. 2.4.2a, while the doublet ^2P phase shifts are given in Fig. 2.4.2b. Despite the quite wide spacing of the results for the ^4S phase shifts, the doublet ^2S phase shift has a certain tendency to decrease, although here much more slowly than follows from the analysis in [159]. Not considering the doublet ^2P wave in our analysis, then for the ^2S phase shift the results are very close to the results of the phase shift analysis provided in [159].

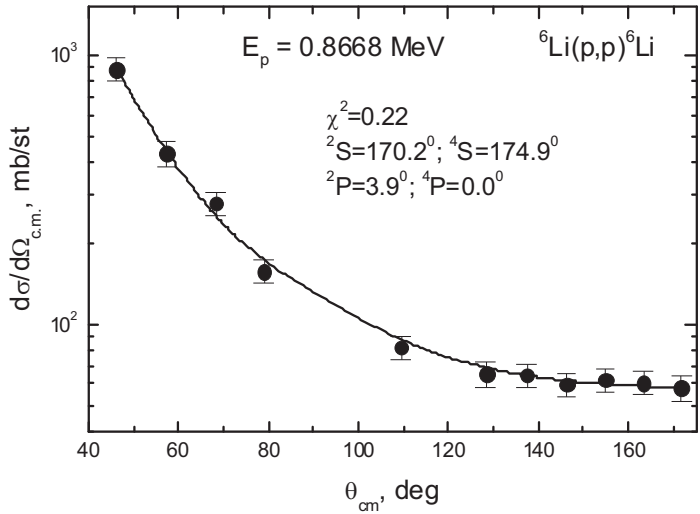

Fig. 2.4.1b. The cross sections of p^{6}Li elastic scattering at 866.8 keV. The solid curve represents the calculation of the cross sections with the found phase shifts.

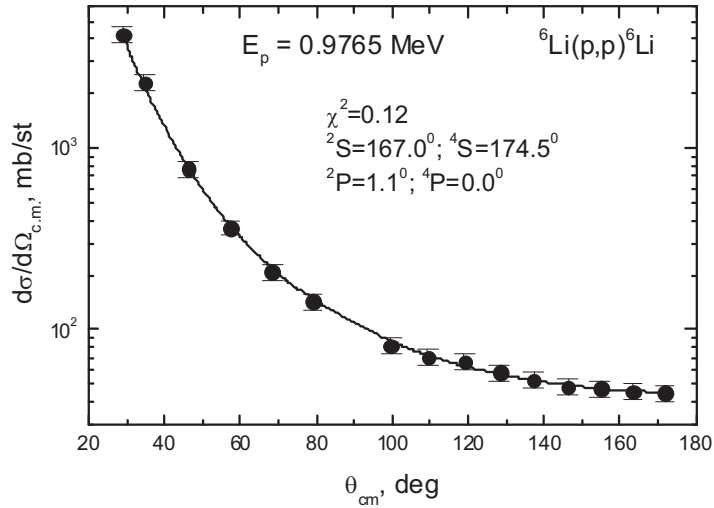

Fig. 2.4.1c. The cross sections of p^{6}Li elastic scattering at 976.5 keV. The solid curve represents the calculation of cross sections with the found phase shifts.

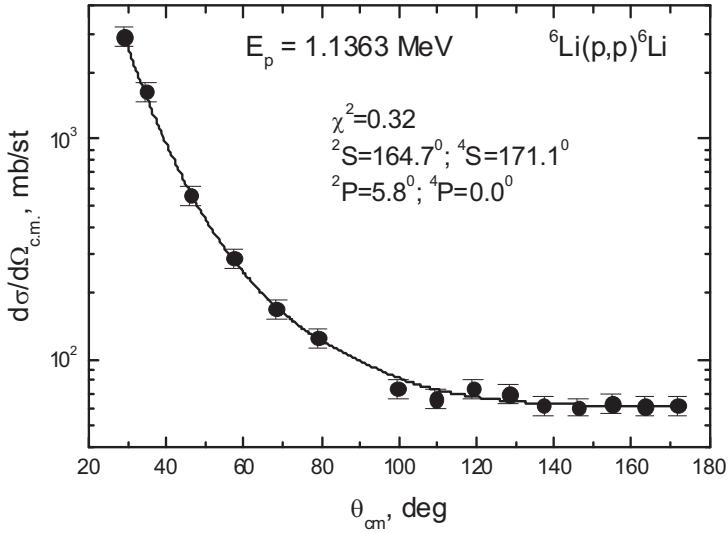

Fig. 2.4.1d. The cross sections of p^{6}Li elastic scattering at 1136.3 keV. The solid curve represents the calculation of cross sections with the found phase shifts.

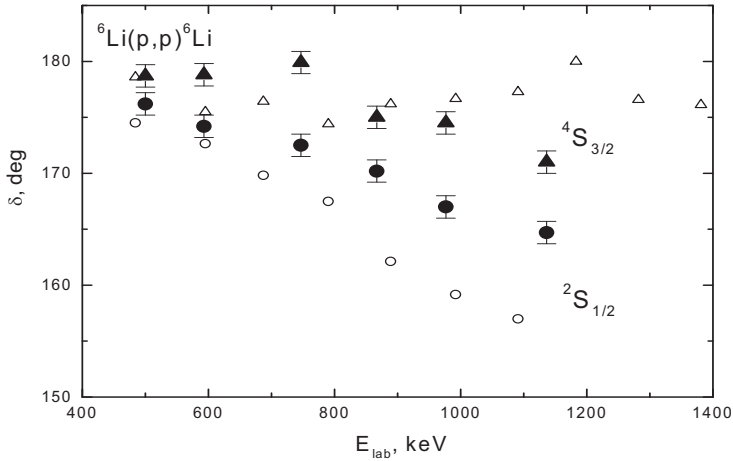

Fig. 2.4.2a. The doublet and quartet *S* phase shifts of p^{6}Li elastic scattering at low energies. The doublet and quartet *S* phase shifts in the presence of the ^2P wave, when the phase shift is accepted by ^4P is equal to zero, are given. The ^2S phase shift is shown by points and ^4S is shown by triangles [160,161,162]. For comparison of open triangles and circles, we have the results of the phase shift analysis given in [159].

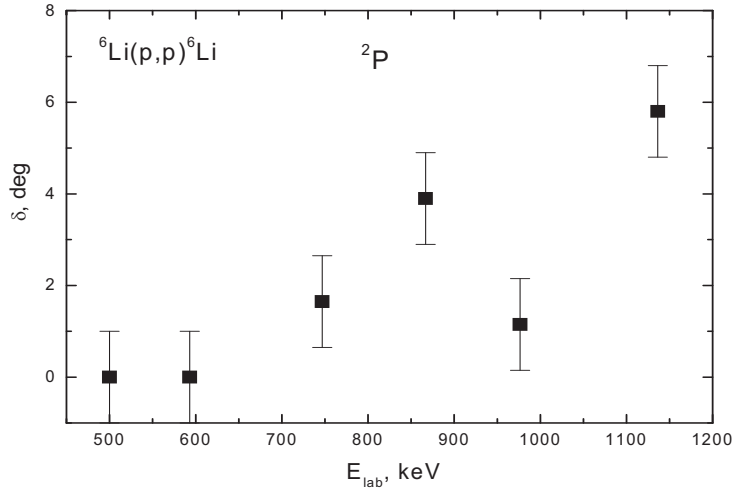

Fig.2.4.2b. The doublet ^2P phase shifts of p^{6}Li elastic scattering at low energies. The squares describe the results of our phase shift analysis for the ^2P phase shift at $^4P = 0$.

The errors of elastic scattering phase shifts given in Fig. 2.4.2 and defined by the ambiguity of the phase shift analysis. At almost the same χ^2 value, which can differ by 5–10 %, it is possible to obtain slightly different values for the scattering phase shifts. This ambiguity for the $^{2,4}S$ and ^2P phase shifts is estimated at the level of 1–1.5°.

2.4.3 Program for phase shift analysis

Below, we present the computer program in Fortran-90 to carry out the p^{6}Li phase shift analysis at low energies without spin-orbital splitting of the phase shifts, which was used for obtaining the results described above. The designations of key parameters of the program are the same as in the previous descriptions.

```
PROGRAM FAZ_ANAL_P6LI
! CALCULATE OF CROSS SECTION WITH COMPLEX
! PHASE SHIFTS FOR SYSTEM SPIN 1/2+1 WITHOUT LS
IMPLICIT REAL(8) (A-Z)
INTEGER
L,LL,TMA,T,LN,LV,NV,Z1,Z2,LN1,NT,NP,NPP,NI,NYS,NNN
REAL(8)
SECT(0:200),FK(0:200),FD(0:200),XP(0:200),FK1(0:200),FD1(0:200),S
```

```
0(0:200)
COMMON REAL(8) /A/
PI,ET(0:200),ES(0:200),ST(0:200),SSE(0:200),TE(0:200) /R/
LN1,NT,P1,NP,NPP,LV1,NNN,BB /T/
SECE(0:200),DS(0:200),DSEC(0:200),TMA /W/ GG,SS,LN,LV,NYS
CHARACTER(7) BB
CHARACTER(12) AA
CHARACTER(13) CC
!  *************** INPUT PARAMETERS ***************
!AA='SEC11363.DAT'
!AA='SEC9765.DAT'
!AA='SEC8668.DAT'
AA='SEC7467.DAT'
!AA='SEC495.DAT'
!AA='SEC989.DAT'
!AA='SEC640.DAT'
!AA='SEC1585.DAT'
BB='FAZ.DAT'
!CC='SECT11363.DAT'
!CC='SECT9765.DAT'
!CC='SECT8668.DAT'
CC='SECT7467.DAT'
!CC='SECT495.DAT'
!CC='SECT989.DAT'
!CC='SECT640.DAT'
!CC='SECT1585.DAT'
!EL=1.1363D0
!EL=0.9765D0
!EL=0.8668D0
!EL=0.7467D0
EL=0.7464D0
!EL=0.989D0
!EL=1.585D0
PI=4.0D0*DATAN(1.0D0)
P1=PI
NYS=0; ! =0 - P-6LI; =1 - 3HE-3HE
NNN=1;! THE NUMBER BY WHICH THE STEP AT EACH
ITERATION DECREASES
NV=1! =0 WITHOUT THE VARIATION = 1 WITH THE VARIATION
FH=0.0123D0;! THE INITIAL STEP
NI=10;! THE NUMBER OF ITERATIONS
```

```
EPP=1.0D-010;! THE ACCURACY
LN=0; LN1=LN
LV=0
LV1=LV; NPP=2*LV
TMA=11
NT=TMA
AM1=1.0D0; AM2=6.0D0; Z1=1; Z2=3
A1=41.4686D0
PM=AM1*AM2/(AM1+AM2)
B1=2.0D0*PM/A1
NP=NPP+2
! ************** PHASE SHIFTS FOR P- 6LI  ************
FD(0)=160.0D0
FD(1)=5.D0
FD(2)=1.D00
FK(0)=179.D0
FK(1)=3.0D0
FK(2)=1.1D0
OPEN (1,FILE=BB)
DO I=LN,LV
READ(1,*) FD(I),FK(I)
ENDDO
CLOSE(1)
OPEN (1,FILE=AA)
DO L=1,NT
READ(1,*) TE(L),SECE(L)
!,DSEC(L)
PRINT *, TE(L),SECE(L),DSEC(L)
ENDDO
CLOSE(1)
DO L=LN,LV
FD(L)=FD(L)*PI/180.0D0
FK(L)=FK(L)*PI/180.0D0
ET(L)=1.0D0
ES(L)=1.0D0
ENDDO
FH=FH*PI/180.0D0
!DO L=LN,LV
!XP(L)=FD(L)
!XP(L+LV+1)=FK(L)
!ENDDO
```

```
DO I=LN,LV
XP(2*I)=FD(I)
XP(2*I+1)=FK(I)
ENDDO
!   ********** TRANSFORM TO C.M. ******************
ECM=EL*PM/AM1
! ********  TOTAL CROSS SECTION  ******************
SK=ECM*B1
SS=DSQRT(SK)
GG=3.44476D-002*Z1*Z2*PM/SS
CALL CULFAZ(GG,S0)
DO I=1,NT
TT=TE(I)*PI/180.0D0
S00=2.0D0*S0(0)
X=DCOS(TT)
A=2.0D0/(1.0D0-X)
BBB=-GG*A
ALO=GG*DLOG(A)+S00
RECUL=BBB*DCOS(ALO)
AIMCUL=BBB*DSIN(ALO)
CUL=RECUL**2+AIMCUL**2
SCUL=CUL*10.0D0/4.0D0/SS**2
!SECE(I)=SECE(I)*SCUL
DSEC(I)=SECE(I)*0.1
!DSEC(I)=DSEC(I)*SCUL
ENDDO
SIGS=0.0D0; SIGT=0.0D0
DO LL=LN,LV
FK11=FK(LL)
FD11=FD(LL)
SIGS=SIGS+(2.0D0*LL+1.0D0)*DSIN(FK11)**2
SIGT=SIGT+(2.0D0*LL+1.0D0)*DSIN(FD11)**2
ENDDO
SIGS=10.0D0*4.0D0*PI*SIGS/SK
SIGT=10.0D0*4.0D0*PI*SIGT/SK
SIG=1.0D0/4.0D0*SIGS+3.0D0/4.0D0*SIGT
PRINT *,"                    SIGMS-TOT=",SIG
! **********  DIFFERENTIAL CROSS SECTION  **********
CALL VAR(SECT,FH,NI,XP,EPP,XI,NV)
PRINT *,'     T       SE        ST        XI'
DO T=1,TMA
```

```
WRITE(*,1) TE(T),SECE(T),SECT(T),DS(T)
ENDDO
1 FORMAT(1X,F8.3,3E15)
PRINT *,'   FD         FK'
DO L=LN,LV
!FD(L)=XP(L)*180.0D0/PI
!FK(L)=XP(L+LV+1)*180.0D0/PI
FD(L)=XP(2*L)*180.0D0/PI
FK(L)=XP(2*L+1)*180.0D0/PI
IF (FD(L)<+0.0D0) THEN
FD1(L)=FD(L)+180.0D0
ELSE
FD1(L)=FD(L)
ENDIF
IF (FK(L)<+0.0D0) THEN
FK1(L)=FK(L)+180.0D0
ELSE
FK1(L)=FK(L)
ENDIF
WRITE(*,3) FD1(L),FK1(L)
ENDDO
WRITE(*,5) XI
5 FORMAT(F15)
OPEN (1,FILE=CC)
WRITE(1,*)"       EL        ECM        XI"
WRITE(1,4) EL,ECM,XI
WRITE(1,*) "    T              SE              DS              ST              XI"
DO I=1,NT
WRITE(1,6)TE(I),SECE(I),DSEC(I),SECT(I),DS(I)
ENDDO
WRITE(1,*) "     FD           FK"
DO I=LN,LV
WRITE(1,3)FD1(I),FK1(I)
ENDDO
CLOSE(1)
OPEN (1,FILE=BB)
DO I=LN,LV
WRITE(1,3)FD(I),FK(I)
ENDDO
CLOSE(1)
6 FORMAT(1X,F8.3,4E15)
```

```
4 FORMAT(3F10.5)
2 FORMAT(4F10.5)
3 FORMAT(2F10.5)
END

SUBROUTINE VAR(ST,PHN,NI,XP,EP,AMIN,NV)
IMPLICIT REAL(8) (A-Z)
INTEGER I,LMI,NV,NI,NPP,NT,IIN,NN,NP,IN,KK,NNN
REAL(8) XPN(0:50),XP(0:50),ST(0:50),FD(0:50),FK(0:50)
COMMON REAL(8) /R/ LMI,NT,PI,NP,NPP,LV,NNN,BB
CHARACTER(7) BB
! ************************************************
!BB='FAZ.DAT'
DO I=LMI,NP
XPN(I)=XP(I)
ENDDO
CALL DET(XPN,ST,B)
IF (NV==0) GOTO 3013
! ---------------------------------------------------------------------
KK=1
DO IIN=1,NI
PH=PHN/KK
NN=-1
1119  NN=NN+1
IN=0
2229 A=B
XPN(NN)=XPN(NN)+PH*XPN(NN)
IF (XPN(NN)>PI)GOTO 1118
IF (NN>NPP+2) THEN
IF (XPN(NN)<0.0D0) GOTO 1118
ELSE
IN=IN+1
ENDIF
! ---------------------------------------------------------------------
CALL DET(XPN,ST,B)
IF (B<A) GOTO 2229
1118 XPN(NN)=XPN(NN)-PH*XPN(NN)
IF (XPN(NN)>PI .AND. NN/=0 .AND. NN/=1)THEN
XPN(NN)=XPN(NN)-PI
ENDIF
PRINT *,'1=',B,NN,XPN(NN)*180.0/PI
```

```
IF (IN>1) THEN
IF (ABS(B-A)<EP .OR. ABS(PH*XPN(NN))<EP) GOTO 4449
PH=PH/2.0D0
ELSE
PH=-PH/2.0D0
ENDIF
GOTO 2229
! ---------------------------------------------------------------------
4449 IF (NN+1<NP) THEN
PH=PHN
!/KK
GOTO 1119
ENDIF
PRINT *,'------------------------------------------------------------'
PRINT*, 'B=',B,IIN,PHN/KK/PI*180
PRINT *,'------------------------------------------------------------'
DO L=LMI,LV
FD(L)=XPN(2*L)*180.0D0/PI
FK(L)=XPN(2*L+1)*180.0D0/PI
ENDDO
OPEN (5,FILE=BB)
DO I=LMI,LV
WRITE(5,3)FD(I),FK(I)
ENDDO
CLOSE(5)
KK=NNN*KK
ENDDO
3013 AMIN=B
DO I=LMI,NP
XP(I)=XPN(I)
3 FORMAT(2F10.5)
ENDDO
END

SUBROUTINE DET(XP,ST,XI)
IMPLICIT REAL(8) (A-Z)
INTEGER I,NT
REAL(8) XP(0:50),ST(0:50)
COMMON REAL(8) /T/ SECE(0:200),DS(0:200),DSEC(0:200),NT
S=0.0D0
CALL SEC(XP,ST)
```

```
DO I=1,NT
DS(I)=((ST(I)-SECE(I))/DSEC(I))**2
S=S+DS(I)
ENDDO
XI=S/NT
END

SUBROUTINE SEC(XP,ST)
IMPLICIT REAL(8) (A-Z)
INTEGER TT,L,TMA,LMA,LMI,NYS
REAL(8) S0(0:20),P(0:20),ST(0:200),FK(0:200),FD(0:200),XP(0:200)
COMMON REAL(8) /A/
PI,ET(0:200),ES(0:200),SKS(0:200),SDS(0:200),TE(0:200) /T/
SE(0:200),DS(0:200),DE(0:200),TMA /W/ GG,SS,LMI,LMA,NYS
RECUL1=0.0D0; AIMCUL1=0.0D0
DO L=LMI,LMA
!FD(L)=XP(L)
!FK(L)=XP(L+LMA+1)
FD(L)=XP(2*L)
FK(L)=XP(2*L+1)
ENDDO
CALL CULFAZ(GG,S0)
DO TT=1,TMA
T=TE(TT)*PI/180.0D0
S00=2.0D0*S0(0)
X=DCOS(T)
A=2.0D0/(1.0D0-X)
BB=-GG*A
ALO=GG*DLOG(A)+S00
RECUL=BB*DCOS(ALO)
AIMCUL=BB*DSIN(ALO)
IF (NYS==0) GOTO 555
X1=DCOS(T)
A1=2.0D0/(1.0D0+X1)
BB1=-GG*A1
ALO1=GG*DLOG(A1)+S00
RECUL1=BB1*DCOS(ALO1)
AIMCUL1=BB1*DSIN(ALO1)
555 RET=0.0D0; AIT=0.0D0; RES=0.0D0; AIS=0.0D0
DO L=LMI,LMA
AL=ET(L)*DCOS(2.0D0*FK(L))-1.0D0
```

```
BE=ET(L)*DSIN(2.0D0*FK(L))
LL=2.0D0*L+1.0D0
SL=2.0D0*S0(L)
CALL POLLEG(X,L,P)
RET=RET+LL*(BE*DCOS(SL)+AL*DSIN(SL))*P(L)
AIT=AIT+LL*(BE*DSIN(SL)-AL*DCOS(SL))*P(L)
AL=ES(L)*DCOS(2.0D0*FD(L))-1.0D0
BE=ES(L)*DSIN(2.0D0*FD(L))
RES=RES+LL*(BE*DCOS(SL)+AL*DSIN(SL))*P(L)
AIS=AIS+LL*(BE*DSIN(SL)-AL*DCOS(SL))*P(L)
ENDDO
IF (NYS==0) GOTO 556
AIT=2.0D0*AIT
RET=2.0D0*RET
AIS=2.0D0*AIS
RES=2.0D0*RES
556 RETR=RECUL+RECUL1+RET
AITR=AIMCUL+AIMCUL1+AIT
RESI=RECUL+RECUL1+RES
AISI=AIMCUL+AIMCUL1+AIS
CUL=RECUL**2+AIMCUL**2
SCUL=CUL*10.0D0/4.0D0/SS**2
SKS(TT)=10.0D0*(RETR**2+AITR**2)/4.0D0/SS**2
SDS(TT)=10.0D0*(RESI**2+AISI**2)/4.0D0/SS**2
ST(TT)=(2.0D0/6.0D0*SDS(TT)+4.0D0/6.0D0*SKS(TT))
!/SCUL
ENDDO
END

SUBROUTINE POLLEG(X,L,P)
IMPLICIT REAL(8) (A-Z)
INTEGER L,I
REAL(8) P(0:20)
P(0)=1.0D0; P(1)=X
DO I=2,L
P(I)=(2*I-1)*X/I*P(I-1)-(I-1)/I*P(I-2)
!P(I)=(2.0D0*I-1.0D0)*X/(1.0D0*I)*P(I-1)-(1.0D0*I-
1.0D0)/(1.0D0*I)*P(I-2)
ENDDO
END
```

```
SUBROUTINE CULFAZ(G,F)
IMPLICIT REAL(8) (A-Z)
INTEGER I,N,J
REAL(8) F(0:20)
C=0.577215665D0; S=0.0D0; N=1000
A1=1.2020569030D0/3.0D0; A2=1.0369277550D0/5.0D0
DO I=1,N
A=G/(1.0D0*I)-DATAN(G/(1.0D0*I))-
(G/(1.0D0*I))**3/3.0D0+(G/(1.0D0*I))**5/5.0D0
S=S+A
ENDDO
FAZ=-C*G+A1*G**3-A2*G**5+S; F(0)=FAZ
DO J=1,10
F(J)=F(J-1)+DATAN(G/(J*1.0D0))
ENDDO
END
```

Below, we execute some control accounts in this program to search for the scattering phase shifts at an energy of 746.4 keV in c.m. (in Table 2.4.1, this is variant 3) taking into account *S* in the beginning and then *S* and *P* of the partial waves. The first of the control accounts, which was carried out only for a zero partial wave, gives the following results.

θ	σ_e	σ_t	χ^2_i
46.150	.12221E+04	.12206E+04	.14291E-03
57.340	.53259E+03	.56204E+03	.30591E+00
68.300	.33140E+03	.31229E+03	.33259E+00
79.020	.17700E+03	.19794E+03	.13992E+01
109.450	.81443E+02	.83291E+02	.51460E-01
128.310	.57902E+02	.60517E+02	.20406E+00
137.350	.54128E+02	.54215E+02	.25420E-03
146.160	.50402E+02	.49847E+02	.12139E-01
154.800	.49110E+02	.46852E+02	.21136E+00
163.290	.46213E+02	.44907E+02	.79861E-01
171.680	.43990E+02	.43811E+02	.16535E-02

δ_d	δ_k
170.08	179.99

$\chi^2 = 0.236$

In this control account, the phase shifts and χ^2 obtained coincide with the results given above in Table 2.4.1 (No. 3-1). The following designations are accepted: θ is the scattering angle; σ_e is the experimental cross section; σ_t is the calculated cross sections; χ^2_i is partial χ^2 for the *i* angle; δ_d is the doublet phase shift; δ_k is the quartet phase shift; and χ^2 is the average value on all experimental points.

For the account of two partial waves in the phase shift analysis, we have

θ	σ_e	σ_t	χ^2_i
46.150	.12221E+04	.11875E+04	.80049E-01
57.340	.53259E+03	.54118E+03	.26020E-01
68.300	.33140E+03	.29882E+03	.96658E+00
79.020	.17700E+03	.18906E+03	.46396E+00
109.450	.81443E+02	.80736E+02	.75339E-02
128.310	.57902E+02	.59753E+02	.10226E+00
137.350	.54128E+02	.54042E+02	.25495E-03
146.160	.50402E+02	.50126E+02	.29924E-02
154.800	.49110E+02	.47469E+02	.11164E+00
163.290	.46213E+02	.45758E+02	.97024E-02
171.680	.43990E+02	.44800E+02	.33889E-01

δ_d	δ_k
172.49	179.93
1.67	0.00

$\chi^2 = 0.164$

In this version of the account, the results coincide with the data given above in Table 2.4.1 (No. 3-2) [163]. The phase shifts of elastic scattering presented here were used for the creation of intercluster potentials [163] and calculation of the astrophysical *S*-factor of radiative proton capture on ^{6}Li [129,158,161].

2.5 Phase shift analysis and computer programs for scattering of non-identical particles with 1/2+1/2 spin

Let us consider some methods and computer programs in Fortran-90 for the phase shift analysis of processes of elastic scattering of non-identical particles with half-integer spin 1/2 + 1/2; for example, elastic scattering of N^3He, N^3H, or $p^{13}C$ etc.

2.5.1 System with spin-orbital interaction

The expressions used here for the differential cross sections, on the basis of which the program was written, are given in [10], together with similar programs in BASIC and for a triplet spin state considering only the spin-orbital splitting of the scattering phase shifts

$$\frac{d\sigma_t(\theta)}{d\Omega} = \frac{1}{3}\left[|A|^2 + 2\left(|B|^2 + |C|^2 + |D|^2 + |E|^2\right)\right], \tag{2.5.1}$$

where

$$A = f_c(\theta) + \frac{1}{2ik}\sum_{L=0}\{(L+1)\alpha_L^+ + L\alpha_L^-\}\exp(2i\sigma_L)P_L(\cos\theta)\,,$$

$$B = f_c(\theta) + \frac{1}{4ik}\sum_{L=0}\left\{(L+2)\alpha_L^+ + (2L+1)\alpha_L^0 + (L-1)\alpha_L^-\right\}\exp(2i\sigma_L)P_L(\cos\theta)\,,$$

$$C = \frac{1}{2ik\sqrt{2}}\sum_{L=1}\{\alpha_L^+ - \alpha_L^-\}\exp(2i\sigma_L)P_L^1(\cos\theta)\,, \tag{2.5.2}$$

$$D = \frac{1}{2ik\sqrt{2}}\sum_{L=1}\frac{1}{L(L+1)}\{L(L+2)\alpha_L^+ - (2L+1)\alpha_L^0 - (L-1)(L+1)\alpha_L^-\}\cdot$$

$$\cdot\exp(2i\sigma_L)P_L^1(\cos\theta)\,,$$

$$E = \frac{1}{4ik}\sum_{L=2}\frac{1}{L(L+1)}\{L\alpha_L^+ - (2L+1)\alpha_L^0 + (L+1)\alpha_L^-\}\cdot$$

$$\cdot\exp(2i\sigma_L)P_L^2(\cos\theta)$$

Here, the α value for each state with the total moment of $J = L \pm 1$ (α^+ and α^-) and $J = L$ (α^0) is determined.

For the scattering in the singlet spin state, we have the expression for the differential cross section

$$\frac{d\sigma_s(\theta)}{d\Omega} = \left|f_s(\theta)\right|^2,$$

where

$$f_s(\theta) = f_c(\theta) + f^N_s(\theta),$$

$$f_c(\theta) = -\left(\frac{\eta}{2k\sin^2(\theta/2)}\right)\exp\{i\eta\ln[\sin^{-2}(\theta/2)] + 2i\sigma_0\}\ , \qquad (2.5.3)$$

$$f_s^N(\theta) = \frac{1}{2ik}\sum_L (2L+1)\exp(2i\sigma_L)[S_L^s - 1]P_L(\cos\theta)\ .$$

Here, the designations of the variables are the same as for ^{4}He^{4}He scattering. The summarized cross section of the elastic scattering can now be defined in the form

$$\frac{d\sigma(\theta)}{d\Omega} = \frac{1}{4}\frac{d\sigma_s(\theta)}{d\Omega} + \frac{3}{4}\frac{d\sigma_t(\theta)}{d\Omega}.$$

Let us present the computer program for the investigation of scattering phase shifts in the system of non-identical particles with half-integer spin, namely, p^{3}He. This program considers the spin-orbital splitting of the scattering phase shifts, but does not take into account singlet-triplet mixing, which will be included in the next cross section.

PROGRAM FAZOVIY_ANALIZ_p3He_WITH_LS

```
IMPLICIT REAL(8) (A-Z)
INTEGER I,L,Z1,Z2,LMI,LH,LMA,LN,LV,NV,NI,NPP,NT,NTT,NP
DIMENSION ST(0:50),FT(0:50),XP(0:50)
COMMON /A/ LH,LMI,NT,PI,NP,NPP
COMMON /B/ SE(0:50),DS(0:50),DE(0:50),NTT
COMMON /C/ SS,GG,LN,LV,POL(0:50),TT(0:50)
COMMON /D/ FP(0:50),FPI(0:50),EP(0:50),F0(0:50),F0I(0:50),
E0(0:50),M(0:50),FMI(0:50),EM(0:50),FS(0:50),FSI(0:50), ES(0:50)
CHARACTER(9) BB
CHARACTER(7) AA
CHARACTER(15) CC
! ********* INPUT PARAMETERS **********
AA='SEC.DAT'
BB='FAZLS.DAT'
```

```
PI=4.0D0*DATAN(1.0D0)
P1=PI
Z1=1! The p charge
Z2=2! The 3He charge
AM1=1.0D0! The p weight
AM2=3.0D0! The 3He mass
AM=AM1+AM2
A1=41.46860D0
PM=AM1*AM2/(AM1+AM2)
B1=2.0D0*PM/A1
LMI=0! The initial orbital moment
LH=1! A step by the moment
LMA=2! The maximum moment
LN=LMI
LV=LMA
EPP=1.0D-005
NV=1! If 1 then to vary the phase shifts if 0 – without variation
FH=0.01D0
NI=5! The number of iterations
NPP=2*LMA
! ****** EXPERIMENTAL CROSS SECTION 11.48 *******
NT=17! The number of the experimental points
NTT=NT
! ************ FOR P-3HE ON E=11.48 ******************
OPEN (1,FILE=AA)
DO L=1,NT
READ(1,*) TT(L),SE(L)
ENDDO
CLOSE(1)
OPEN (1,FILE=BB)
DO I=LN,LV
READ(1,*) FP(I),F0(I),FM(I),FS(I)
ENDDO
CLOSE(1)
! ******* TRANSFORM TO RADIANS ******************
DO L=LN,LV,LH
FM(L)=FM(L)*PI/180.0D0
FP(L)=FP(L)*PI/180.0D0
F0(L)=F0(L)*PI/180.0D0
FMI(L)=FMI(L)*PI/180.0D0
FPI(L)=FPI(L)*PI/180.0D0
```

```
F0I(L)=F0I(L)*PI/180.0D0
FT(L)=FT(L)*PI/180.0D0
FS(L)=FS(L)*PI/180.0D0
FSI(L)=FSI(L)*PI/180.0D0
EP(L)=DEXP(-2.0D0*FPI(L))
EM(L)=DEXP(-2.0D0*FMI(L))
E0(L)=DEXP(-2.0D0*F0I(L))
ES(L)=DEXP(-2.0D0*FSI(L))
ENDDO
! ************************************************
FH=FH*PI/180.0D0
NP=2*NPP+1
DO I=LMI,LMA,LH
XP(I)=FP(I)
ENDDO
DO I=LMI,LMA-1,LH
XP(I+LMA+1)=F0(I+1)
ENDDO
DO I=LMI,LMA-1,LH
XP(I+2*LMA+1)=FM(I+1)
ENDDO
DO I=LMI,LMA,LH
XP(I+3*LMA+1)=FS(I)
ENDDO
DO I=LMI,LMA,LH
XP(I+4*LMA+2)=FPI(I)
ENDDO
DO I=LMI,LMA-1,LH
XP(I+5*LMA+3)=F0I(I+1)
ENDDO
DO I=LMI,LMA-1,LH
XP(I+6*LMA+3)=FMI(I+1)
ENDDO
DO I=LMI,LMA,LH
XP(I+7*LMA+3)=FSI(I)
ENDDO
!   ********** TRANSFORM TO C.M. ******************
EL=11.48D0
CC='SECTLS.DAT'
EC=EL*PM/AM1
SK=EC*B1
```

```
SS=DSQRT(SK)
GG=3.44476D-002*Z1*Z2*PM/SS
CALL VAR(ST,FH,NI,XP,EPP,XI,NV)
PRINT *,"                    XI-KV=",XI
! ********* TOTAL CROSS SECTION *****************
DO I=LMI,LMA,LH
FP(I)=XP(I)
ENDDO
DO I=LMI,LMA-1,LH
F0(I+1)=XP(I+LMA+1)
ENDDO
DO I=LMI,LMA-1,LH
FM(I+1)=XP(I+2*LMA+1)
ENDDO
DO I=LMI,LMA,LH
FS(I)=XP(I+3*LMA+1)
ENDDO
F0(0)=FP(0); FM(0)=FP(0)
DO I=LMI,LMA,LH
FPI(I)=XP(I+4*LMA+2)
ENDDO
DO I=LMI,LMA-1,LH
F0I(I+1)=XP(I+5*LMA+3)
ENDDO
DO I=LMI,LMA-1,LH
FMI(I+1)=XP(I+6*LMA+3)
ENDDO
DO I=LMI,LMA,LH
FSI(I)=XP(I+7*LMA+3)
ENDDO
F0I(0)=FPI(0); FMI(0)=FPI(0)
DO L=LN,LV,LH
EP(L)=DEXP(-2.0D0*FPI(L))
EM(L)=DEXP(-2.0D0*FMI(L))
E0(L)=DEXP(-2.0D0*F0I(L))
ES(L)=DEXP(-2.0D0*FSI(L))
ENDDO
SRT=0.0D0; SRS=0.0D0;   SST=0.0D0;  SSS=0.0D0
DO L=LN,LV,LH
AP=FP(L)
AM=FM(L)
```

```
A0=F0(L)
ASS=FS(L)
L1=2*L+3
L2=2*L+1
L3=2*L-1
SRT=SRT+L1*(1.0D0-EP(L)**2)+L2*(1.0D0-E0(L)**2)+L3*(1.0D0-
EM(L)**2)
SRS=SRS+L2*(1.0D0-ES(L)**2)
SST=SST+L1*EP(L)**2*DSIN(AP)**2+L2*E0(L)**2*DSIN(A0)**2+L
3*EM(L)**2*DSIN(AM)**2
SSS=SSS+L2*ES(L)**2*DSIN(ASS)**2
ENDDO
SRT=10.0D0*PI*SRT/SK/3.0D0
SRS=10.0D0*PI*SRS/SK
SIGR=1.0D0/4.0D0*SRS+3.0D0/4.0D0*SRT
SST=10.0D0*4.0D0*PI*SST/SK/3.0D0
SSS=10.0D0*4.0D0*PI*SSS/SK
SIGS=1.0D0/4.0D0*SSS+3.0D0/4.0D0*SST
!PRINT *,"                    SIGMS-TOT=",SIGS
PRINT *,"    T      SE         ST          XI"
DO I=1,NT
WRITE(*,2)TT(I),SE(I),ST(I),DS(I)
ENDDO
PRINT *,'   FP       F0       FM       FS'
DO L=LMI,LMA,LH
FM(L)=FM(L)*180.0D0/PI
FP(L)=FP(L)*180.0D0/PI
FMI(L)=FMI(L)*180.0D0/PI
FPI(L)=FPI(L)*180.0D0/PI
F0(L)=F0(L)*180.0D0/PI
F0I(L)=F0I(L)*180.0D0/PI
FS(L)=FS(L)*180.0D0/PI
FSI(L)=FSI(L)*180.0D0/PI
WRITE(*,2) FP(L),F0(L),FM(L),FS(L)
ENDDO
OPEN (1,FILE=CC)
WRITE(1,*)"      EL        ECM        XI"
WRITE(1,4) EL,EC,XI
WRITE(1,*) "    T             SE             ST             XI"
DO I=1,NT
WRITE(1,2) TT(I),SE(I),ST(I),DS(I)
```

```
ENDDO
WRITE(1,*) "    FP(L)    F0(L)    FM(L)    FS(L)"
DO L=LN,LV
WRITE(1,2) FP(L),F0(L),FM(L),FS(L)
ENDDO
CLOSE(1)
OPEN (1,FILE=BB)
DO L=LN,LV
WRITE(1,3) FP(L),F0(L),FM(L),FS(L)
ENDDO
CLOSE(1)
4 FORMAT(1x,3F10.3)
2 FORMAT(1x,4F10.3)
3 FORMAT(1x,4F14.7)
END

SUBROUTINE VAR(ST,PHN,NI,XP,EP,AMIN,NV)
IMPLICIT REAL(8) (A-Z)
INTEGER I,LMI,LH,NV,NI,NPP,NT,IIN,NN,NP
DIMENSION XPN(0:50),XP(0:50),ST(0:50)
COMMON /A/ LH,LMI,NT,PI,NP,NPP
! ********** THE SEARCH OF THE PHASE SHIFTS ********
DO I=LMI,NP,LH
XPN(I)=XP(I)
ENDDO
NN=LMI
PRINT *,NN,XPN(NN)*180.0D0/PI
PH=PHN
CALL DET(XPN,ST,ALA)
B=ALA
IF (NV==0) GOTO 3013
PRINT *,ALA
DO IIN=1,NI
NN=-LH
PRINT *,ALA,IIN
GOTO 1119
1159 XPN(NN)=XPN(NN)-PH*XP(NN)
1119  NN=NN+LH
IN=0
2229 A=B
XPN(NN)=XPN(NN)+PH*XP(NN)
```

```
IF (NP==2*NPP+1) GOTO 7777
IF (NN<(NP/2)) GOTO 7777
IF (XPN(NN)<0) GOTO 1159
7777 IN=IN+1
CALL DET(XPN,ST,ALA)
B=ALA
GOTO 5678
5678 CONTINUE
IF (B<A) GOTO 2229
C=A
XPN(NN)=XPN(NN)-PH*XP(NN)
IF (IN>1) GOTO 3339
PH=-PH
GOTO 5559
3339 IF (ABS((C-B)/(B))<EP) GOTO 4449
PH=PH/2
5559 B=C
GOTO 2229
4449 PH=PHN
B=C
IF (NN<NP) GOTO 1119
AMIN=B
PH=PHN
ENDDO
3013 AMIN=B
DO I=LMI,NP,LH
XP(I)=XPN(I)
ENDDO
END

SUBROUTINE DET(XP,ST,XI)
! ****************** THE DETERMINANT ***************
IMPLICIT REAL(8) (A-Z)
INTEGER I,NT
DIMENSION XP(0:50),ST(0:50)
COMMON /B/ SE(0:50),DS(0:50),DE(0:50),NT
S=0.0D0
CALL SEC(XP,ST)
DO I=1,NT
DS(I)=((ST(I)-SE(I)))**2/(0.025*SE(I))**2
S=S+DS(I)
```

```
ENDDO
XI=S/NT
END

SUBROUTINE SEC(XP,ST)
! ********** THE CROSS SECTION **********
IMPLICIT REAL(8) (A-Z)
INTEGER I,L,II,LH,LN,LV,NP,NPP,LMI,NT
COMMON                                                    /D/
FP(0:50),FPI(0:50),EP(0:50),F0(0:50),F0I(0:50),E0(0:50),FM(0:50),FMI(
0:50),EM(0:50),FS(0:50),FSI(0:50),ES(0:50)
COMMON /C/ SS,GG,LN,LV,POL(0:50),TT(0:50)
COMMON /A/ LH,LMI,NT,PI,NP,NPP
DIMENSION S0(0:50),P(0:50),P1(0:50),P2(0:50),ST(0:50),XP(0:50)
DO I=LN,LV,LH
FP(I)=XP(I)
ENDDO
DO I=LN,LV-1,LH
II=I+LV+1
F0(I+1)=XP(II)
ENDDO
DO I=LN,LV-1,LH
II=I+2*LV+1
FM(I+1)=XP(II)
ENDDO
DO I=LN,LV,LH
II=I+3*LV+1
FS(I)=XP(II)
ENDDO
F0(0)=FP(0); FM(0)=FP(0)
DO I=LN,LV,LH
II=I+4*LV+2
FPI(I)=XP(II)
ENDDO
DO I=LN,LV-1,LH
II=I+5*LV+3
F0I(I+1)=XP(II)
ENDDO
DO I=LN,LV-1,LH
II=I+6*LV+3
FMI(I+1)=XP(II)
```

```
ENDDO
DO I=LN,LV,LH
II=I+7*LV+3
FSI(I)=XP(II)
ENDDO
F0I(0)=FPI(0); FMI(0)=FPI(0)
DO L=LN,LV,LH
 EP(L)=DEXP(-2.0D0*FPI(L))
EM(L)=DEXP(-2.0D0*FMI(L))
E0(L)=DEXP(-2.0D0*F0I(L))
ES(L)=DEXP(-2.0D0*FSI(L))
ENDDO
CALL CULFAZ(GG,S0)
DO I=1,NT
T=TT(I)*PI/180.0D0
X=DCOS(T)
CALL CULAMP(X,GG,S0,RECUL,AMCUL)
CALL POLLEG(X,LV,P)
CALL FUNLEG1(X,LV,P1)
CALL FUNLEG2(X,LV,P2)
RES=0.0D0;    AMS=0.0D0;  REA=0.0D0;  AMA=0.0D0;  REB=0.0D0;
AMB=0.0D0
REC=0.0D0;  AMC=0.0D0;  RED=0.0D0;  AMD=0.0D0;  REE=0.0D0;
AME=0.0D0
DO L=LN,LV,LH
FP1=2.0D0*FP(L); FM1=2.0D0*FM(L); F01=2.0D0*F0(L)
SL=2.0D0*S0(L); C=DCOS(SL); S=DSIN(SL); FS1=2.0D0*FS(L)
AL1P=EP(L)*DCOS(FP1)-1.0D0
AL2P=EP(L)*DSIN(FP1)
AL1M=EM(L)*DCOS(FM1)-1.0D0
AL2M=EM(L)*DSIN(FM1)
AL10=E0(L)*DCOS(F01)-1.0D0
AL20=E0(L)*DSIN(F01)
A1=(L+1)*AL1P+L*AL1M
A2=(L+1)*AL2P+L*AL2M
REA=REA+(A2*C+A1*S)*P(L)
AMA=AMA+(A2*S-A1*C)*P(L)
B1=(L+2)*AL1P+(2*L+1)*AL10+(L-1)*AL1M
B2=(L+2)*AL2P+(2*L+1)*AL20+(L-1)*AL2M
REB=REB+(B2*C+B1*S)*P(L)/2.0D0
AMB=AMB+(B2*S-B1*C)*P(L)/2.0D0
```

```
IF (L<1) GOTO 2111
C1=AL1P-AL1M
C2=AL2P-AL2M
CC1=1.0D0/(DSQRT(2.0D0))
REC=REC+(C2*C+C1*S)*P1(L)*CC1
AMC=AMC+(C2*S-C1*C)*P1(L)*CC1
DD1=1.0D0/(DSQRT(2.0D0)*L*(L+1))
D1=L*(L+2)*AL1P-(2*L+1)*AL10-(L**2-1)*AL1M
D2=L*(L+2)*AL2P-(2*L+1)*AL20-(L**2-1)*AL2M
RED=RED+(D2*C+D1*S)*P1(L)*DD1
AMD=AMD+(D2*S-D1*C)*P1(L)*DD1
2111 IF (L<2) GOTO 2222
EE1=1.0D0/(2*L*(L+1))
E1=L*AL1P-(2*L+1)*AL10+(L+1)*AL1M
E2=L*AL2P-(2*L+1)*AL20+(L+1)*AL2M
REE=REE+(E2*C+E1*S)*P2(L)*EE1
AME=AME+(E2*S-E1*C)*P2(L)*EE1
2222 ENDDO
RES=0.0D0;  AMS=0.0D0
DO L=LN,LV,LH
SL=2.0D0*S0(L)
C=DCOS(SL)
S=DSIN(SL)
FS1=2.0D0*FS(L)
ALS=ES(L)*DCOS(FS1)-1.0D0
BS=ES(L)*DSIN(FS1)
RES=RES+(2*L+1)*(BS*C+ALS*S)*P(L)
AMS=AMS+(2*L+1)*(BS*S-ALS*C)*P(L)
ENDDO
9191 CONTINUE
RES=RECUL+RES
AMS=AMCUL+AMS
SES=10.0D0*(RES**2+AMS**2)/4.0D0/SS**2
REA=RECUL+REA
AMA=AMCUL+AMA
REB=RECUL+REB
AMB=AMCUL+AMB
AA=REA**2+AMA**2
BB=REB**2+AMB**2
CC=REC**2+AMC**2
DD=RED**2+AMD**2
```

```
EE=REE**2+AME**2
SET=10.0D0*(AA+2*(BB+CC+DD+EE))/4.0D0/SS**2/3.0D0
S=3.0D0/4.0D0*SET+1.0D0/4.0D0*SES
ST(I)=S
ENDDO
END

SUBROUTINE CULAMP(X,GG,S0,RECUL,AMCUL)
! ********* THE COULOMB AMPLITUDE **********
IMPLICIT REAL(8) (A-Z)
DIMENSION S0(0:20)
A=2.0D0/(1.0D0-X)
S00=2.0D0*S0(0)
BB=-GG*A
AL=GG*DLOG(A)+S00
RECUL=BB*DCOS(AL)
AMCUL=BB*DSIN(AL)
END

SUBROUTINE POLLEG(X,L,P)
! ****************** THE LEGENDRE POLYNOMIALS **********
IMPLICIT REAL(8) (A-Z)
INTEGER I,L
DIMENSION P(0:20)
P(0)=1.0D0
P(1)=X
DO I=2,L
P(I)=(2.0D0*I-1.0D0)*X/I*P(I-1)-(I-1.0D0)/I*P(I-2)
ENDDO
END

SUBROUTINE FUNLEG1(X,L,P)
! ****************** LEGENDRE POLYNOMIALS **********
IMPLICIT REAL(8) (A-Z)
INTEGER I,L
DIMENSION P(0:20)
P(0)=0.0D0
P(1)=DSQRT(ABS(1.0D0-X**2))
DO I=2,L
P(I)=(2.0D0*I-1.0D0)*X/(I-1.0D0)*P(I-1)-I/(I-1.0D0)*P(I-2)
ENDDO
```

```
END

SUBROUTINE FUNLEG2(X,L,P)
! ****************** THE LEGENDRE'S FUNCTION **********
IMPLICIT REAL(8) (A-Z)
INTEGER L
DIMENSION P(0:20)
P(0)=0.0D0
P(1)=0.0D0
P(2)=3.0D0*ABS(1.0D0-X**2)
DO I=3,L
P(I)=(2.0D0*I-1.0D0)*X/(I-2.0D0)*P(I-1)-(I+1.0D0)/(I-2.0D0)*P(I-2)
ENDDO
END

SUBROUTINE CULFAZ(G,F)
! ****************** THE COULOMB PHASE SHIFTS **********
IMPLICIT REAL(8) (A-Z)
INTEGER I,N
DIMENSION F(0:20)
C=0.577215665D0
S=0.D0
N=50
A1=1.202056903D0/3.D0
A2=1.036927755D0/5.D0
DO I=1,N
A=G/I-DATAN(G/I)-(G/I)**3/3.D0+(G/I)**5/5.D0
S=S+A
ENDDO
FAZ=-C*G+A1*G**3-A2*G**5+S
F(0)=FAZ
DO I=1,20
F(I)=F(I-1)+DATAN(G/I)
ENDDO
END
```

Here, we give the results of the control account using this program for the case of p^3He elastic scattering at an energy of 11.48 MeV, taking into account singlet-triplet mixing for χ^2 at a value of 0.45, which was obtained in [164,165]. The differential cross sections, their errors, and the scattering phase shifts obtained in the phase shift analysis, which we use for the control

calculations, i.e. we consider the cross sections and χ^2 obtained in [164,165] phase shifts, are expressed in tabular form in these works.

In listing these results, the following designations are used: θ is the scattering angle; σ_e is the experimental cross sections; σ_t is the calculated cross sections; χ^2_i is partial χ^2 for *i* angle ; χ^2 is the average χ^2 value; δ_m is the triplet phase shift with $J = L - 1$; δ_0 is the phase shift at $J = L$; δ_p is the phase shift at $J = L + 1$; and δ_s is the singlet scattering phase shift.

In the first line below, the phase shifts correspond to the orbital moment $L = 0$, in the second to $L = 1$, and in the third to $L = 2$.

$\chi^2 = 7.375E\text{-}001$

θ	σ_e	σ_t	χ^2_i
27.640	223.100	229.159	1.179
31.970	222.000	222.687	0.015
36.710	211.900	211.146	0 .020
82.530	54.270	53.522	0.302
90.000	36.760	36.249	0.309
96.030	25.700	25.467	0.133
103.800	16.780	16.162	2.165
110.550	13.210	12.598	3.444
116.570	13.210	13.120	0.075
125.270	20.260	19.962	0.341
133.480	32.210	32.333	0.023
140.790	45.950	46.975	0.794
147.210	58.820	61.388	3.052
153.900	75.460	76.517	0.313
162.140	92.720	93.062	0.022
165.670	97.700	98.823	0.212
166.590	101.100	100.157	0.139

δ_p	δ_0	δ_m	δ_s
-88.800	-88.800	-88.800	-84.600
66.700	49.400	44.300	21.400
2.500	2.500	2.500	-18.600

Because this program does not take into account singlet-triplet mixing, the results for χ^2 are slightly higher than in [164,165].

For the purposes of comparison, we give the results with the same phase shifts, using the the control calculation performed in BASIC in our previous work [10] where a value of $\chi^2 = 0.74$ was obtained.

θ	σ_e	σ_t
27.64	223.10	229.16
31.97	222.00	222.69
36.71	211.90	211.15
82.53	54.27	53.52
90.00	36.76	36.25
96.03	25.70	25.47
103.80	16.78	16.16
110.55	13.21	12.60
116.57	13.21	13.12
125.27	20.26	19.96
133.48	32.21	32.33
140.79	45.95	46.98
147.21	58.82	61.39
153.90	75.46	76.52
162.14	92.72	93.06
165.67	97.70	98.82
166.59	101.10	100.16

It is clear that these results coincide within the rounding errors, i.e. they do not depend on the language in which the program was written. However, the transition to Fortran-90 has allowed us to significantly increase the speed of operation of all the computer programs and to achieve higher precision in the search for the minimum χ^2 value.

If we execute a full variation of the phase shifts according to our new computer program in the search for the minimum χ^2 value, then, after about 3,000 iterations we obtain the following result for the differential scattering cross sections.

$\chi^2 = 2.27E\text{-}001$

θ	σ_e	σ_t	χ^2_i
27.640	223.100	224.854	0.099
31.970	222.000	221.150	0.023
36.710	211.900	211.107	0.022
82.530	54.270	53.832	0.104
90.000	36.760	36.715	0.002
96.030	25.700	26.026	0.257
103.800	16.780	16.737	0.011
110.550	13.210	13.072	0.175
116.570	13.210	13.423	0.415
125.270	20.260	19.928	0.430

133.480	32.210	31.955	0.100
140.790	45.950	46.330	0.109
147.210	58.820	60.563	1.405
153.900	75.460	75.569	0.003
162.140	92.720	92.038	0.087
165.670	97.700	97.785	0.001
166.590	101.100	99.116	0.616

δ_p	δ_0	δ_m	δ_s
-84.530	-84.530	-84.530	-93.630
56.144	46.185	42.904	44.694
3.404	3.584	4.982	-19.086

The new scattering phase shifts obtained differ only slightly from previous results, while the value of χ^2 has seen a more than threefold decrease.

2.5.2 System with spin-orbital and singlet-triplet mixing

Let us consider the scattering of non-identical particles with half-integer spin, taking into account spin-orbital interactions, the mixing of various orbital states at the expense of tensor forces, and the mixing of singlet and triplet states. The scattering differential cross section has a more complex form because the scattering phase shifts are included in the formulae for the cross sections and the coupling of parameters of states with different spin and orbital moments; the fullest expressions for such cross sections are given in [166]

$$\frac{d\sigma(\theta)}{d\Omega} = \frac{1}{2k^2}\{|A|^2 + |B|^2 + |C|^2 + |D|^2 + |E|^2 + |F|^2 + |G|^2 + |H|^2\}. \qquad (2.5.4)$$

The scattering amplitudes of A, B, C, etc. are registered in the following form

$$A = f_c^{'} + \frac{1}{4}\sum_{L=0}^{\infty} P_L(x)\left\{-\sqrt{L(L-1)}U^{L-1}_{L,1;L-2,1} + (L+2)U^{L+1}_{L,1;L,1} + (2L+1)U^{L}_{L,1;L,1} + \right.$$
$$\left. + (L-1)U^{L-1}_{L,1;L,1} - \sqrt{(L+1)(L+2)}\,U^{L+1}_{L,1;L+2,1}\right\},$$

$$B = f_c^{'} + \frac{1}{4}\sum_{L=0}^{\infty} P_L(x)\left\{\sqrt{L(L-1)}U_{L,1;L-2,1}^{L-1} + (L+1)U_{L,1;L,1}^{L+1} + (2L+1)U_{L,0;L,0}^{L} + \right.$$
$$\left. + LU_{L,1;L,1}^{L-1} + \sqrt{(L+1)(L+2)}\,U_{L,1;L+2,1}^{L+1}\right\},$$

$$C = \frac{1}{4}\sum_{L=0}^{\infty} P_L(x)\left\{\sqrt{L(L-1)}U_{L,1;L-2,1}^{L-1} + (L+1)U_{L,1;L,1}^{L+1} - (2L+1)U_{L,0;L,0}^{L} + \right.$$
$$\left. + LU_{L,1;L,1}^{L-1} + \sqrt{(L+1)(L+2)}\,U_{L,1;L+2,1}^{L+1}\right\}, \qquad (2.5.5)$$

$$D = -\frac{1}{4}i\sin\theta\sum_{L=1}^{\infty} P_L^{'}(x)/\sqrt{L(L+1)}\left\{-\sqrt{(L+1)(L-1)}U_{L,1;L-2,1}^{L-1} + \sqrt{L(L+1)}U_{L,1;L,1}^{L+1} - \right.$$
$$\left. - \sqrt{L(L+1)}U_{L,1;L,1}^{L-1} + \sqrt{L(L+2)}\,U_{L,1;L+2,1}^{L+1} - (2L+1)U_{L,1;L,0}^{L}\right\},$$

$$E = -\frac{1}{4}i\sin\theta\sum_{L=1}^{\infty} P_L^{'}(x)/\sqrt{L(L+1)}\left\{-\sqrt{(L+1)(L-1)}U_{L,1;L-2,1}^{L-1} + \sqrt{L(L+1)}U_{L,1;L,1}^{L+1} - \right.$$
$$\left. - \sqrt{L(L+1)}U_{L,1;L,1}^{L-1} + \sqrt{L(L+2)}U_{L,1;L+2,1}^{L+1} + (2L+1)U_{L,1;L,0}^{L}\right\},$$

$$F = -\frac{1}{4}i\sin^2\theta\sum_{L=2}^{\infty} P_L^{''}(x)/\sqrt{(L-1)L(L+1)(L+2)}\left\{-\sqrt{(L+1)(L+2)}U_{L,1;L-2,1}^{L-1} + \right.$$
$$+\sqrt{\frac{L(L-1)(L+2)}{L+1}}U_{L,1;L,1}^{L+1} - (2L+1)\sqrt{\frac{(L-1)(L+2)}{L(L+1)}}U_{L,1;L,1}^{L} +$$
$$\left. + \sqrt{\frac{(L-1)(L+1)(L+2)}{L}}U_{L,1;L,1}^{L-1} - \sqrt{L(L-1)}\,U_{L,1;L+2,1}^{L+1}\right\},$$

$$G = -\frac{1}{4}i\sin\theta\sum_{L=1}^{\infty} P_L^{'}(x)/\sqrt{L(L+1)}\left\{\sqrt{(L-1)(L+1)}U_{L,1;L-2,1}^{L-1} + (L+2)\sqrt{\frac{L}{L+1}}U_{L,1;L,1}^{L+1} - \right.$$
$$\left. - \frac{(2L+1)}{\sqrt{L(L+1)}}U_{L,1;L,1}^{L} - (L-1)\sqrt{\frac{(L+1)}{L}}U_{L,1;L,1}^{L-1} - \sqrt{L(L+2)}U_{L,1;L+2,1}^{L+1} - (2L+1)U_{L,0;L,1}^{L}\right\},$$

$$H = -\frac{1}{4}i\sin\theta\sum_{L=1}^{\infty} P_L^{'}(x)/\sqrt{L(L+1)}\left\{\sqrt{(L-1)(L+1)}U_{L,1;L-2,1}^{L-1} + (L+2)\sqrt{\frac{L}{L+1}}U_{L,1;L,1}^{L+1} - \right.$$
$$\left. - \frac{(2L+1)}{\sqrt{L(L+1)}}U_{L,1;L,1}^{L} - (L-1)\sqrt{\frac{(L+1)}{L}}U_{L,1;L,1}^{L-1} - \sqrt{L(L+2)}U_{L,1;L+2,1}^{L+1} + (2L+1)\,\mathrm{U}_{L,0;L,1}^{L}\right\}.$$

The scattering matrix is presented in the form

$$U^{J}_{L,S;L',S'} = U^{J}_{L',S';L,S} = \exp[i(\alpha_{L} + \alpha_{L'})](S^{J}_{L',S';L,S} - \delta_{L,L'}\delta_{S,S'}) ,$$

and, for example, at $L = 1$ and $J = 1$, taking into account the $\varepsilon^{1}_{1,0} = \varepsilon^{J}_{S,S'}$ coupling of the singlet and triplet states, we have

$$S^{1}_{1,0;1,0} = \cos^{2}\varepsilon^{1}_{1,0}\exp(2i\delta^{1}_{0,1}) + \sin^{2}\varepsilon_{1,1}\exp(2i\delta^{1}_{1,1}) ,$$

$$S^{1}_{1,1;1,1} = \sin^{2}\varepsilon^{1}_{1,0}\exp(2i\delta^{1}_{0,1}) + \cos^{2}\varepsilon_{1,1}\exp(2i\delta^{1}_{1,1}) ,$$

$$S^{1}_{1,0;1,1} = S^{1}_{1,1;1,0} = \frac{1}{2}\sin(2\varepsilon^{1}_{1,0})\left(\exp(2i\delta^{1}_{0,1}) - \exp(2i\delta^{1}_{1,1})\right),$$

where $\delta_{k,k'}$ is the Kronecker symbol; $x = \cos(\theta)$; the values without a stroke designate an initial state and those with a stroke designate the final at the same total J moment; the Coulomb α_{L} phase shifts are defined in paragraph 1, while the nuclear $\delta^{J}_{S,L}$ phase shifts are considered too complex to allow inelastic channels.

The $\varepsilon_{1} = \varepsilon^{J}_{S,S'}$ coupling of the triplet (S and S' spins, with the total moment being equal to 1) S and D states is defined by the following expressions for a scattering matrix

$$S^{1}_{0,0} = \cos^{2}\varepsilon_{1}\exp(2i\delta^{1}_{0}) + \sin^{2}\varepsilon_{1}\exp(2i\delta^{1}_{2}) ,$$

$$S^{1}_{2,2} = \sin^{2}\varepsilon_{1}\exp(2i\delta^{1}_{0}) + \cos^{2}\varepsilon_{1}\exp(2i\delta^{1}_{2}) ,$$

$$S^{1}_{0,2} = S^{1}_{2,0} = \frac{1}{2}\sin(2\varepsilon_{1})\left[\exp(2i\delta^{1}_{0}) - \exp(2i\delta^{1}_{2})\right].$$

The dashes in the Legendre polynomials designate the derivatives, while the Coulomb scattering amplitude is written in the form

$$f^{'}_{c}(\theta) = -\left(\frac{i\eta}{2\sin^{2}(\theta/2)}\right)\exp\left\{i\eta\ln[\sin^{-2}(\theta/2)]\right\} .$$

In the following, the derivatives of the polynomials are bound to the Legendre functions, as described earlier

$$P_n^m(x) = (1-x^2)^{m/2}\frac{d^m P_n(x)}{dx^m} = (1-x^2)^{m/2}\frac{d^{m+n}(x^2-1)^n}{dx^{m+n}} = \sin^m\theta\frac{d^m P_n(\cos\theta)}{(d\cos\theta)^m}.$$

If we neglect tensor interaction and singlet-triplet coupling in the expressions given above, then the scattering matrix will take the usual form of $\exp(2i\delta_{S,L})$ with a complex phase shift.

The following program written in Fortran-90 is based on all these expressions and includes a singlet-triplet coupling of EPS [166], considered for $L = 1$ only. In the program, the values of the experimental cross sections, their errors, and the scattering phase shifts are all clearly given. The designations of the variables, parameters, and units are the same as in the previous program.

With the operators

READ(1,*) TT(L),SE(L),DE(L)

and

READ(1,*) FP(I),F0(I),FM(I),FS(I),EPS(I)

at the beginning of the program, the following is read from the file

AA='SEC.DAT'

BB='FAZTENZ.DAT'

the same data are given in the program, i.e. the basic data can be used from the program or from these files.

PROGRAM FAZ_ANAL_P_3He_WIRH_LS_AND_TS
IMPLICIT REAL(8) (A-Z)
INTEGER
I,L,LH,LN,LV,LMA,LMI,NT,NP,NPP,Z1,Z2,LMI1,LH1,NT2,NT1,NI
DIMENSION ST(0:50),FP(0:50),F0(0:50),FM(0:50),FS(0:50),ES(0:50)
DIMENSION
XP(0:50),FPI(0:50),F0I(0:50),FMI(0:50),FSI(0:50),EPS(0:50),EP(0:50),E0(0:50),EM(0:50)

```
COMMON /B/ SE(0:50),DS(0:50),DE(0:50),NT
COMMON /C/ LH,LMI,NT1,PI,NP,NPP
COMMON /A/ SS,GG,P1,LMI1,LMA,LH1,NT2,POL(0:50), TT(0:50)
CHARACTER(11) BB
CHARACTER(7) AA
CHARACTER(12) CC
! *************** INPUT PARAMETERS ***************
AA='SEC.DAT'
BB='FAZTENZ.DAT'
CC='SECTTENZ.DAT'
PI=4.0D0*DATAN(1.0D0)
P1=PI
Z1=1
Z2=2
AM1=1.0D0
AM2=3.0D0
AM=AM1+AM2
A1=41.4686D0
PM=AM1*AM2/(AM1+AM2)
B1=2.0D0*PM/A1
LMI=0
LH=1
LMA=2
LN=LMI
LMI1=LMI
LV=LMA
LH1=LH
EPP=1.0D-05
NV=1
FH=0.01D0
NI=500
NPP=2*LMA
! **** EXPERIMENTAL CROSS SECTION 11.48 *********
SE(1)=223.1D0;    SE(2)=222.0D0;    SE(3)=211.9D0;    SE(4)=54.27D0;
SE(5)=36.76D0
SE(6)=25.7D0;     SE(7)=16.78D0;    SE(8)=13.21D0;    SE(9)=13.21D0;
SE(10)=20.26D0
SE(11)=321D0; SE(12)=45.95D0; SE(13)=58.82D0; SE(14)=75.46D0
SE(15)=92.72D0; SE(16)=97.7D0; SE(17)=101.1D0
DE(1)=5.58D0;      DE(2)=5.55D0;      DE(3)=5.3D0;      DE(4)=1.36D0;
DE(5)=0.92D0
```

```
DE(6)=0.64D0;      DE(7)=0.42D0;      DE(8)=0.33D0;      DE(9)=0.33D0;
DE(10)=0.51D0
DE(11)=0.81D0; DE(12)=1.15D0; DE(13)=1.47D0; DE(14)=1.89D0
DE(15)=32D0; DE(16)=44D0; DE(17)=53D0
TT(1)=27.64D0; TT(2)=31.97D0; TT(3)=36.71D0; TT(4)=853D0
TT(5)=90.0D0; TT(6)=96.03D0; TT(7)=103.8D0; TT(8)=110.55D0
TT(9)=116.57D0; TT(10)=125.27D0; TT(11)=133.48D0
TT(12)=140.79D0; TT(13)=147.21D0; TT(14)=153.9D0
TT(15)=1614D0; TT(16)=165.67D0; TT(17)=166.59D0
NT=17
NT1=NT
NT2=NT
! ********** DO P-3HE ON E=11.48 ******************
FP(0)=-88.8D0;    FPI(0)=0.D0
FP(1)=66.7D0;     FPI(1)=0.D0
FP(2)=5D0;       FPI(2)=0.D0
FP(3)=1.D0;        FPI(3)=0.D0
F0(0)=FP(0);             F0I(0)=0.D0
F0(1)=49.4D0;      F0I(1)=0.D0
F0(2)=5D0;        F0I(2)=0.D0
F0(3)=1.D0;         F0I(3)=0.D0
FM(0)=FP(0);           FMI(0)=0.D0
FM(1)=44.3D0;    FMI(1)=0.D0
FM(2)=5D0;      FMI(2)=0.D0
FM(3)=1.D0;        FMI(3)=0.D0
FS(0)=-84.6D0;    FSI(0)=0.D0
FS(1)=21.4D0;     FSI(1)=0.D0
FS(2)=-18.6D0;    FSI(2)=0.D0
FS(3)=1.D0;        FSI(3)=0.D0
EPS(1)=11.2D0
EPS(3)=0.D0
OPEN (1,FILE=AA)
DO L=1,NT
READ(1,*) TT(L),SE(L),DE(L)
ENDDO
CLOSE(1)
OPEN (1,FILE=BB)
DO I=LN,LV
READ(1,*) FP(I),F0(I),FM(I),FS(I),EPS(I)
ENDDO
CLOSE(1)
```

```
! ************ TRANSFORM TO RADIANS **************
DO L=LN,LV,LH
FM(L)=FM(L)*PI/180.0D0
FP(L)=FP(L)*PI/180.0D0
F0(L)=F0(L)*PI/180.0D0
EPS(L)=EPS(L)*PI/180.0D0
FMI(L)=FMI(L)*PI/180.0D0
FPI(L)=FPI(L)*PI/180.0D0
F0I(L)=F0I(L)*PI/180.0D0
FS(L)=FS(L)*PI/180.0D0
FSI(L)=FSI(L)*PI/180.0D0
EP(L)=EXP(-2.0D0*FPI(L))
EM(L)=EXP(-2.0D0*FMI(L))
E0(L)=EXP(-2.0D0*F0I(L))
ES(L)=EXP(-2.0D0*FSI(L))
ENDDO
! ************************************************
FH=FH*PI/180.0D0
NP=5*LMA+2
IF (NP>(5*LMA+2)) GOTO 9988
DO L=LN,LV,LH
FMI(L)=0
FPI(L)=0
F0I(L)=0
FSI(L)=0
ENDDO
9988 DO I=LMI,LMA,LH
XP(I)=FP(I)
ENDDO
DO I=LMI,LMA-1,LH
XP(I+LMA+1)=F0(I+1)
ENDDO
DO I=LMI,LMA-1,LH
XP(I+2*LMA+1)=FM(I+1)
ENDDO
DO I=LMI,LMA,LH
XP(I+3*LMA+1)=FS(I)
ENDDO
DO I=LMI,LMA,LH
XP(I+4*LMA+2)=EPS(I)
ENDDO
```

```
DO I=LMI,LMA,LH
XP(I+5*LMA+3)=FPI(I)
ENDDO
DO I=LMI,LMA-1,LH
XP(I+6*LMA+4)=F0I(I+1)
ENDDO
DO I=LMI,LMA-1,LH
XP(I+7*LMA+4)=FMI(I+1)
ENDDO
DO I=LMI,LMA,LH
XP(I+8*LMA+4)=FSI(I)
ENDDO
 ! ************ TRANSFOM TO C.M. ******************
EL=11.480D0
EC=EL*PM/AM1
SK=EC*B1
SS=DSQRT(SK)
GG=3.44476D-002*Z1*Z2*PM/SS
CALL VAR(ST,FH,LMA,NI,XP,EPP,XI,NV)
PRINT *,"                    XI-KV=",XI
 ! ************* TOTAL CROSS SECTION *************
DO I=LMI,LMA,LH
FP(I)=XP(I)
ENDDO
DO I=LMI,LMA-1,LH
F0(I+1)=XP(I+LMA+1)
ENDDO
DO I=LMI,LMA-1,LH
FM(I+1)=XP(I+2*LMA+1)
ENDDO
DO I=LMI,LMA,LH
FS(I)=XP(I+3*LMA+1)
ENDDO
DO I=LMI,LMA,LH
EPS(I)=XP(I+4*LMA+2)
ENDDO
F0(0)=FP(0); FM(0)=FP(0)
DO I=LMI,LMA,LH
FPI(I)=XP(I+5*LMA+3)
ENDDO
DO I=LMI,LMA-1,LH
```

```
F0I(I+1)=XP(I+6*LMA+4)
ENDDO
DO I=LMI,LMA-1,LH
FMI(I+1)=XP(I+7*LMA+4)
ENDDO
DO I=LMI,LMA,LH
FSI(I)=XP(I+8*LMA+4)
ENDDO
F0I(0)=FPI(0); FMI(0)=FPI(0)
DO L=LN,LV,LH
EP(L)=EXP(-2.0D0*FPI(L))
EM(L)=EXP(-2.0D0*FMI(L))
E0(L)=EXP(-2.0D0*F0I(L))
ES(L)=EXP(-2.0D0*FSI(L))
ENDDO
SRT=0.0D0; SRS=0.0D0;   SST=0.0D0;  SSS=0.0D0
DO L=LN,LV,LH
AP=FP(L)
AM=FM(L)
A0=F0(L)
ASS=FS(L)
L1=2*L+3
L2=2*L+1
L3=2*L-1
SRT=SRT+L1*(1.0D0-EP(L)**2)+L2*(1.0D0-E0(L)**2)+L3*(1.0D0-
EM(L)**2)
SRS=SRS+L2*(1.0D0-ES(L)**2)
SST=SST+L1*EP(L)**2*SIN(AP)**2+L2*E0(L)**2*SIN(A0)**2+L3*E
M(L)**2*SIN(AM)**2
SSS=SSS+L2*ES(L)**2*SIN(ASS)**2
ENDDO
SRT=10.0D0*PI*SRT/SK/3.0D0
SRS=10.0D0*PI*SRS/SK
SIGR=1.0D0/4.0D0*SRS+3.0D0/4.0D0*SRT
SST=10*4*PI*SST/SK/3
SSS=10.0D0*4*PI*SSS/SK
SIGS=1.0D0/4.0D0*SSS+3.0D0/4.0D0*SST
PRINT *,"                    SIGMS-TOT=",SIGS
PRINT *,"    T      SE       ST       XI"
DO I=1,NT
WRITE(*,2) TT(I),SE(I),ST(I),DS(I)
```

```
ENDDO
PRINT *,"    FP       F0       FM       FS       EPS"
DO L=LMI,LMA,LH
FM(L)=FM(L)*180.0D0/PI
FP(L)=FP(L)*180.0D0/PI
FMI(L)=FMI(L)*180.0D0/PI
FPI(L)=FPI(L)*180.0D0/PI
F0(L)=F0(L)*180.0D0/PI
F0I(L)=F0I(L)*180.0D0/PI
FS(L)=FS(L)*180.0D0/PI
FSI(L)=FSI(L)*180.0D0/PI
EPS(L)=EPS(L)*180.0D0/PI
WRITE(*,2) FP(L),F0(L),FM(L),FS(L),EPS(L)
ENDDO
!READ *, A
!IF (A==0) GOTO 1111
!PRINT
!PRINT *,"     T       POL "
!DO I=1,NT
!PRINT *,TT(I);POL(I)
!ENDDO
OPEN (1,FILE=CC)
WRITE(1,*)"      EL       ECM       XI"
WRITE(1,4) EL,EC,XI
WRITE(1,*) "   T            SE            DE            ST            XI"
DO I=1,NT
WRITE(1,3) TT(I),SE(I),DE(I),ST(I),DS(I)
ENDDO
WRITE(1,*) "    FP(L)   F0(L)   FM(L)   FS(L)"
DO L=LN,LV
WRITE(1,2) FP(L),F0(L),FM(L),FS(L),EPS(L)
ENDDO
CLOSE(1)
OPEN (1,FILE=BB)
DO L=LN,LV
WRITE(1,3) FP(L),F0(L),FM(L),FS(L),EPS(L)
ENDDO
CLOSE(1)
!OPEN (1,FILE=AA)
!DO L=1,NT
!WRITE(1,3) TT(L),SE(L),DE(L)
```

```
!ENDDO
!CLOSE(1)
4 FORMAT(3F10.5)
2 FORMAT(5F10.5)
3 FORMAT(4F14.7)
END

SUBROUTINE VAR(ST,PHN,LMA,NI,XP,EP,AMIN,NV)
! ******* THE SEARCH OF PHASE SHIFTS ******************
IMPLICIT REAL(8) (A-Z)
INTEGER I,LH,NT,NP,NPP,NN,NI,LMA,LMI
DIMENSION XPN(0:50),XP(0:50),ST(0:50)
COMMON /C/ LH,LMI,NT,PI,NP,NPP
DO I=LMI,NP,LH
XPN(I)=XP(I)
ENDDO
NN=LMI
PH=PHN
CALL DET(XPN,ST,ALA)
B=ALA
IF (NV==0) GOTO 3013
DO IIN=1,NI
NN=-LH
PRINT *,ALA,IIN
GOTO 1119
1159 XPN(NN)=XPN(NN)-PH*XP(NN)
1119  NN=NN+LH
IN=0
2229 A=B
XPN(NN)=XPN(NN)+PH*XP(NN)
IF (NN<(5*LMA+3)) GOTO 7777
IF (XPN(NN)<0) GOTO 1159
7777 IN=IN+1
CALL DET(XPN,ST,ALA)
B=ALA
IF (B<A) GOTO 2229
C=A
XPN(NN)=XPN(NN)-PH*XP(NN)
IF (IN>1) GOTO 3339
PH=-PH
GOTO 5559
```

```
3339 IF (ABS((C-B)/ABS(B))<EP) GOTO 4449
PH=PH/2
5559 B=C
GOTO 2229
4449 PH=PHN
B=C
IF (NN<NP) GOTO 1119
AMIN=B
PH=PHN
ENDDO
3013 AMIN=B
DO I=LMI,NP,LH
XP(I)=XPN(I)
ENDDO
END

SUBROUTINE DET(XP,ST,XI)
! ********** THE DETERMINANT **********
IMPLICIT REAL(8) (A-Z)
INTEGER I,NT
DIMENSION XP(0:50),ST(0:50)
COMMON /B/ SE(0:50),DS(0:50),DE(0:50),NT
S=0.0D0
CALL SEC(XP,ST)
DO I=1,NT
DS(I)=( (ST(I)-SE(I) )/DE(I) )**2
S=S+DS(I)
ENDDO
XI=S/NT
END

SUBROUTINE SEC(XP,ST)
! ********** THE CROSS SECTION **********
IMPLICIT REAL(8) (A-Z)
INTEGER I,II,L,LN,LV,LH,NT
COMMON /A/ SS,GG,PI,LN,LV,LH,NT,POL(0:50),TT(0:50)
DIMENSION
S0(0:50),P(0:50),P1(0:50),P2(0:50),XP(0:50),ST(0:50),F0(0:50),FP(0:50),
FM(0:50),FS(0:50),EPS(0:50)
DIMENSION
F0I(0:50),FPI(0:50),FMI(0:50),FSI(0:50),EP(0:50),EM(0:50),ES(0:50),E0
```

```
(0:50)
DO I=LN,LV,LH
FP(I)=XP(I)
ENDDO
DO I=LN,LV-1,LH
II=I+LV+1
F0(I+1)=XP(II)
ENDDO
DO I=LN,LV-1,LH
II=I+2*LV+1
FM(I+1)=XP(II)
ENDDO
DO I=LN,LV,LH
II=I+3*LV+1
FS(I)=XP(II)
ENDDO
DO I=LN,LV,LH
II=I+4*LV+2
EPS(I)=XP(II)
ENDDO
F0(0)=FP(0); FM(0)=FP(0)
DO I=LN,LV,LH
II=I+5*LV+3
FPI(I)=XP(II)
ENDDO
DO I=LN,LV-1,LH
II=I+6*LV+4
F0I(I+1)=XP(II)
ENDDO
DO I=LN,LV-1,LH
II=I+7*LV+4
FMI(I+1)=XP(II)
ENDDO
DO I=LN,LV,LH
II=I+8*LV+4
FSI(I)=XP(II)
ENDDO
F0I(0)=FPI(0); FMI(0)=FPI(0)
DO L=LN,LV,LH
EP(L)=DEXP(-2.0D0*FPI(L))
EM(L)=DEXP(-2.0D0*FMI(L))
```

```
E0(L)=DEXP(-2.0D0*F0I(L))
ES(L)=DEXP(-2.0D0*FSI(L))
ENDDO
CALL CULFAZ(GG,S0)
DO I=1,NT
T=TT(I)*PI/180.0D0
X=DCOS(T)
CALL CULAMP(X,GG,S0,RECUL,AMCUL)
CALL POLLEG(X,LV,P)
CALL FUNLEG1(X,LV,P1)
CALL FUNLEG2(X,LV,P2)
REA=0.0D0; AMA=0.0D0; REB=0.0D0; AMB=0.0D0; REC=0.0D0;
AMC=0.0D0; RED=0.0D0; AMD=0.0D0
REE=0.0D0; AME=0.0D0; RRG=0.0D0; AAG=0.0D0; REH=0.0D0;
AMH=0.0D0; REF=0.0D0; AMF=0.0D0
DO L=LN,LV,LH
FP1=2.0D0*FP(L)
FM1=2.0D0*FM(L)
F01=2.0D0*F0(L)
SL=2.0D0*S0(L)
C=DCOS(SL)
S=DSIN(SL)
FS1=2.0D0*FS(L)
SO=DSIN(EPS(L))**2
CO=DCOS(EPS(L))**2
AL1P=EP(L)*DCOS(FP1)-1.0D0
AL2P=EP(L)*DSIN(FP1)
AL1M=EM(L)*DCOS(FM1)-1.0D0
AL2M=EM(L)*DSIN(FM1)
AL10=SO*ES(L)*DCOS(FS1)+CO*E0(L)*DCOS(F01)-1.0D0
AL20=SO*ES(L)*DSIN(FS1)+CO*E0(L)*DSIN(F01)
A1=(L+2.0D0)*AL1P+(2.0D0*L+1.0D0)*AL10+(L-1.0D0)*AL1M
A2=(L+2.0D0)*AL2P+(2.0D0*L+1.0D0)*AL20+(L-1.0D0)*AL2M
REA=REA+(A1*C-A2*S)*P(L)/2.0D0
AMA=AMA+(A1*S+A2*C)*P(L)/2.0D0
ALS=CO*ES(L)*DCOS(FS1)+SO*E0(L)*DCOS(F01)-1.0D0
BS=CO*ES(L)*DSIN(FS1)+SO*E0(L)*DSIN(F01)
RES=(2.0D0*L+1.0D0)*(ALS*C-BS*S)
AMS=(2.0D0*L+1.0D0)*(ALS*S+BS*C)
B1=(L+1.0D0)*AL1P+L*AL1M
B2=(L+1.0D0)*AL2P+L*AL2M
```

```
REB=REB+(B1*C-B2*S+RES)*P(L)/2.0D0
AMB=AMB+(B1*S+B2*C+AMS)*P(L)/2.0D0
REC=REC+(B1*C-B2*S-RES)*P(L)/2.0D0
AMC=AMC+(B1*S+B2*C-AMS)*P(L)/2.0D0
IF (L<1) GOTO 1211
SI2=1.0D0/2.0D0*DSIN(2.0D0*EPS(L))
AL1=SI2*(ES(L)*DCOS(FS1)-E0(L)*DCOS(F01))
AL2=SI2*(ES(L)*DSIN(FS1)-E0(L)*DSIN(F01))
RE1=(2.0D0*L+1.0D0)*(AL2*C+AL1*S)/DSQRT(L*(L+1.0D0))
AM1=(2.0D0*L+1.0D0)*(AL2*S-AL1*C)/DSQRT(L*(L+1.0D0))
C1=AL1P-AL1M
C2=AL2P-AL2M
RED=RED+(C2*C+C1*S-RE1)*P1(L)/2.0D0
AMD=AMD+(C2*S-C1*C-AM1)*P1(L)/2.0D0
REE=REE+(C2*C+C1*S+RE1)*P1(L)/2.0D0
AME=AME+(C2*S-C1*C+AM1)*P1(L)/2.0D0
D1=(L+2.0D0)/(L+1.0D0)*AL1P-
(2.0D0*L+1.0D0)/(L*(L+1.0D0))*AL10-(L-1.0D0)/L*AL1M
D2=(L+2.0D0)/(L+1.0D0)*AL2P-
(2.0D0*L+1.0D0)/(L*(L+1.0D0))*AL20-(L-1.0D0)/L*AL2M
RRG=RRG+(D2*C+D1*S-RE1)*P1(L)/2.0D0
AAG=AAG+(D2*S-D1*C-AM1)*P1(L)/2.0D0
REH=REH+(D2*C+D1*S+RE1)*P1(L)/2.0D0
AMH=AMH+(D2*S-D1*C+AM1)*P1(L)/2.0D0
1211 IF (L<2) GOTO 2122
F1=1.0D0/(L+1.0D0)*AL1P-
(2.0D0*L+1.0D0)/(L*(L+1.0D0))*AL10+AL1M/L
F2=1.0D0/(L+1.0D0)*AL2P-
(2.0D0*L+1.0D0)/(L*(L+1.0D0))*AL20+AL2M/L
REF=REF+(F2*C+F1*S)*P2(L)/2.0D0
AMF=AMF+(F2*S-F1*C)*P2(L)/2.0D0
2122 ENDDO
RET=0.0D0; AMT=0.0D0; RES=0.0D0;  AMS=0.0D0
DO L=LN,LV,LH
SL=2.0D0*S0(L)
C=DCOS(SL)
S=DSIN(SL)
FS1=2.0D0*FS(L)
ALS=ES(L)*DCOS(FS1)-1.0D0
BS=ES(L)*DSIN(FS1)
RES=RES+(2.0D0*L+1.0D0)*(BS*C+ALS*S)*P(L)
```

```
AMS=AMS+(2.0D0*L+1.0D0)*(BS*S-ALS*C)*P(L)
ENDDO
RES=RECUL+RES
AMS=AMCUL+AMS
REA=RECUL+REA
AMA=AMCUL+AMA
REB=RECUL+REB
AMB=AMCUL+AMB
AA=REA**2+AMA**2
BB=REB**2+AMB**2
CC=REC**2+AMC**2
DD=RED**2+AMD**2
EE=REE**2+AME**2
FF=REF**2+AMF**2
HH=REH**2+AMH**2
GGG=RRG**2+AAG**2
SUM=AA+BB+CC+DD+EE+GGG+HH+FF
S=10.0D0*SUM/2.0D0/SS**2/4.0D0
ST(I)=S
! POL(I) = - 2*(REA*REE+AMA*AME+REB*REH
+AMB*AMH+REC*RRG+AMC*AAG+RED*REF+AMD*AMF)/SUM
ENDDO
END

SUBROUTINE CULAMP(X,GG,S0,RECUL,AMCUL)
! ********** THE COULOMB AMPLITUDE **********
IMPLICIT REAL(8) (A-Z)
DIMENSION S0(0:50)
A=2.0D0/(1.0D0-X)
S00=2.0D0*S0(0)
BB=-GG*A
AL=GG*DLOG(A)+S00
RECUL=-BB*DSIN(AL)
AMCUL=BB*DCOS(AL)
END

SUBROUTINE POLLEG(X,L,P)
! ********** THE LEGENDRE POLYNOMIALS **********
IMPLICIT REAL(8) (A-Z)
INTEGER I,L
DIMENSION P(0:50)
```

```
P(0)=1.0D0; P(1)=X
DO I=2,L
P(I)=(2.0D0*I-1.0D0)*X/I*P(I-1)-(I-1.0D0)/I*P(I-2)
ENDDO
END

SUBROUTINE FUNLEG1(X,L,P)
! ********** THE LEGENDRE FUNCTION **********
IMPLICIT REAL(8) (A-Z)
INTEGER I,L
DIMENSION P(0:50)
P(0)=0.0D0; P(1)=DSQRT(DABS(1.0D0-X**2))
DO I=2,L
P(I)=(2.0D0*I-1.0D0)*X/(I-1.0D0)*P(I-1)-I/(I-1.0D0)*P(I-2)
ENDDO
END

SUBROUTINE FUNLEG2(X,L,P)
! ********** THE LEGENDRE'S FUNCTION **********
IMPLICIT REAL(8) (A-Z)
INTEGER I,L
DIMENSION P(0:50)
P(0)=0.0D0; P(1)=0.0D0; P(2)=3.0D0*DABS(1.0D0-X**2)
DO I=3,L
P(I)=(2.0D0*I-1.0D0)*X/(I-2.0D0)*P(I-1)-(I+1.0D0)/(I-2.0D0)*P(I-2)
ENDDO
END

SUBROUTINE CULFAZ(G,F)
! ********** THE COULOMB PHASE SHIFTS **********
IMPLICIT REAL(8) (A-Z)
INTEGER I,N
DIMENSION F(0:50)
C=0.577215665D0; S=0.0D0; N=50
A1=1.202056903D0/3.0D0; A2=1.036927755D0/5.0D0
DO I=1,N
A=G/I-DATAN(G/I)-(G/I)**3/3.0D0+(G/I)**5/5.0D0
S=S+A
ENDDO
FAZ=-C*G+A1*G**3-A2*G**5+S
F(0)=FAZ
```

```
DO I=1,20
F(I)=F(I-1)+DATAN(G/(I))
ENDDO
END
```

With the same phase shifts as in the previous case [164,165], and without mixing, using this program we obtain the same result as given by the first as the control account for the previous program with $\chi^2 = 7.375E-001$

$\chi^2 = 7.375E-001$

θ	σ_e	σ_t	χ^2_i
27.64000	223.10000	229.15944	1.17923
31.97000	222.00000	222.68747	.01534
36.71000	211.90000	211.14558	.02026
82.53000	54.27000	53.52241	.30217
90.00000	36.76000	36.24893	.30859
96.03000	25.70000	25.46703	.13250
103.80000	16.78000	16.16202	2.16494
110.55000	13.21000	12.59755	3.44437
116.57000	13.21000	13.11973	.07482
125.27000	20.26000	19.96234	.34064
133.48000	32.21000	32.33282	.02299
140.79000	45.95000	46.97500	.79443
147.21000	58.82000	61.38791	3.05158
153.90000	75.46000	76.51701	.31277
162.14000	92.72000	93.06232	.02177
165.67000	97.70000	98.82336	.21196
166.59000	101.10000	100.15680	.13898

δ_p	δ_0	δ_m	δ_s	ε
-88.800	-88.800	-88.800	-84.600	0.000
66.700	49.400	44.300	21.400	0.000
2.500	2.500	2.500	-18.600	0.000

Initiation of mixing in the *P* wave, as shown in [164,165], allows us to better describe the cross sections of elastic scattering at the same phase shifts [164,165]

$$\chi^2 = 2.93E\text{-}001$$

θ	σ_e	σ_t	χ^2_i
27.640	223.100	228.038	0.783
31.970	222.000	221.732	0.002
36.710	211.900	210.383	0.082
82.530	54.270	54.215	0.002
90.000	36.760	36.966	0.050
96.030	25.700	26.151	0.497
103.800	16.780	16.739	0.010
110.550	13.210	13.031	0.295
116.570	13.210	13.394	0.310
125.270	20.260	19.972	0.400
133.480	32.210	32.075	0.028
140.790	45.950	46.482	0.214
147.210	58.820	60.704	1.642
153.900	75.460	75.656	0.011
162.140	92.720	92.029	0.089
165.670	97.700	97.733	0.000
166.590	101.100	99.054	0 .654

δ_p	δ_0	δ_m	δ_s	ε
-88.800	-88.800	-88.800	-84.600	0 .000
66.700	49.400	44.300	21.400	11.200
2.500	2.500	2.500	-18.600	0.000

The average χ^2 value is slightly less than 0.45, as given in [164,165]. The calculations in [164,165] were carried out at the beginning of the 1960s on rather simple computers and with rather low precision, leading to such a small distinction of the results for χ^2.

In the real calculations, a number of other values were used for the constants, for example, $\hbar^2/m_0$ and the mass of particles, and rounding of [164,165] phase shifts, as given in the mentioned articles, to the second sign after a comma can also exert an impact on the χ^2 value. As such, we may consider that the provided control accounts for an acceptable χ^2 value are in agreement with the results obtained in [164,165].

To make a comparison, we will give the results for the same scattering phase shifts and mixing parameters obtained previously in [10], using similar programs written in BASIC and with average $\chi^2 = 0.29$

θ	σ_e	σ_t	χ^2_i
27.64	223.10	228.04	0.78
31.97	222.00	221.73	0.00
36.71	211.90	210.38	0.08
82.53	54.27	54.22	0.00
90.00	36.76	36.97	0.05
96.03	25.70	26.15	0.49
103.80	16.78	16.74	0.01
110.55	13.21	13.03	0.29
116.57	13.21	13.39	0.31
125.27	20.26	19.97	0.32
133.48	32.21	32.07	0.03
140.79	45.95	46.48	0.21
147.21	58.82	60.70	1.64
153.90	75.46	75.66	0.01
162.14	92.72	92.03	0.09
165.67	97.70	97.73	0.00
166.59	101.10	99.05	0.66

Here, the results up to the rounding error coincide with each other and do not depend on the programming language.

If we execute a detailed variation of the scattering phase shifts and the mixing parameter ε, then we will obtain about 10,000 iterations. The best description of the available experimental data requires almost zero mixing

$\chi^2 = 2.25E\text{-}001$

θ	σ_e	σ_t	χ^2_i
27.640	223.100	224.736	0.086
31.970	222.000	221.181	0.022
36.710	211.900	211.217	0.017
82.530	54.270	53.839	0.100
90.000	36.760	36.717	0.002
96.030	25.700	26.025	0.259
103.800	16.780	16.736	0.011
110.550	13.210	13.072	0.175
116.570	13.210	13.423	0.415
125.270	20.260	19.927	0.427
133.480	32.210	31.953	0.101
140.790	45.950	46.328	0.108
147.210	58.820	60.562	1.405
153.900	75.460	75.570	0.003

162.140	92.720	92.043	0.085
165.670	97.700	97.791	0.001
166.590	101.100	99.123	0.611

δ_p	δ_0	δ_m	δ_s	ε
-83.342	-83.342	-83.342	-97.861	0 .000
52.520	50.021	50.444	44.905	-0.00017
3.222	0.122	2.667	-19.114	0.000

We can suggest that mixing is not required for the best description of the available experimental data, though the point at 147°, as well as in the case of the calculation in the previous program with χ^2 = 2.27E-001, is described rather poorly, even though the χ^2 averages practically coincide. Let us note that changing the mixing parameter ε to any direction leads to a noticeable increase in average χ^2, considerably worsening the description of the experimental data.

The results given in this paragraph have direct relevance to checking the operability of the computer programs written on the basis of known methods of calculating differential cross sections, but not to obtaining new results in the phase shift analysis of p^3He elastic scattering [10]. New results for the phase shift analysis in a system of particles with spin 1/2 + 1/2 are given as an example in the following paragraph for the $p^{13}C$ system.

2.5.3 Phase shift analysis of $p^{13}C$ elastic scattering taking into account the spin-orbit

Let us consider the $p^{13}C$ system of particles at low energies, to which the 1/2 + 1/2 spins correspond. At energies lower than 0.5–1 MeV, the deviation from the Rutherford value of the measured differential cross section can be characterized only by one point at a certain value of the scattering angle and the given energy. Such a deviation is fairly unambiguously described by one triplet *S* scattering phase shift, even in the resonance range of the $p^{13}C$ system.

On the basis of these representations, in [167,168] the measurement of the differential cross sections, namely, the excitation function for the $p^{13}C$ elastic scattering, was executed at energies between 0.25 and 0.75 MeV. Measurements of the cross sections at each energy level were taken only at one scattering angle and four values of the angles were used for the different energies. These data were used to carry out a phase shift analysis of $p^{13}C$ elastic scattering at low energies and for the definition of the resonance form of the triplet $^3S_1$ phase shift at an energy of 0.55 MeV.

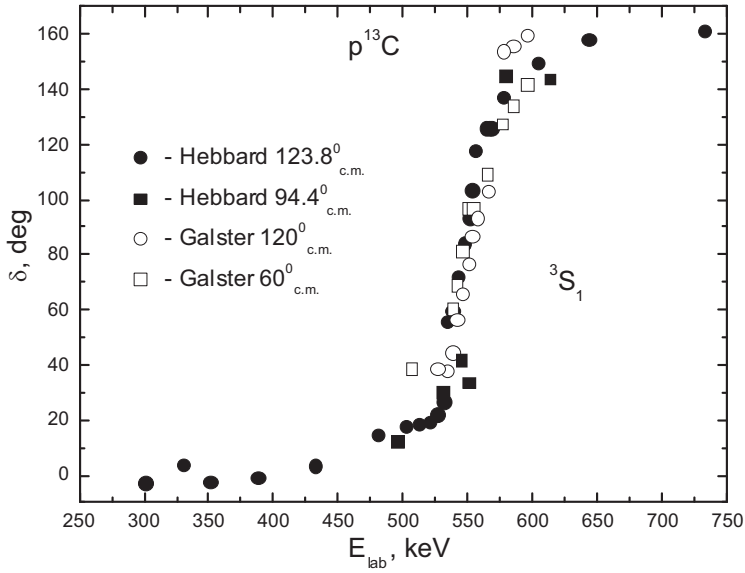

Fig. 2.5.1. The triplet $^3S_1$ phase shift of the $p^{13}C$ scattering at low energies. The points and squares give the results of our phase shift analysis data [167] at 94.4° and 123.8° in c.m., while the circles and open squares give the results of our phase shift analysis data [168] at 60° and 120° in c.m.

On the basis of the computer programs presented in the previous paragraph for spin-orbital mixing, a phase shift analysis of the experimental data on differential cross sections of the $p^{13}C$ elastic scattering (excitation functions in the energy range 300–750 keV l.s.) specified in [167,168] was undertaken. As a result of the phase shift analysis, it was shown that the singlet $^1S_0$ phase shift of the $p^{13}C$ elastic scattering in the considered energy range was close to zero with a value not exceeding 2–3 degrees. The form of the triplet $^3S_1$ phase shift is shown below in Fig. 2.5.1, while its values are given in tables 2.5.1 and 2.5.2. This phase shift has a clearly expressed resonance, which corresponds to the level of ^{14}N in the cluster $p^{13}C$ channel with $J^\pi,T = 1^-,1$ at an energy of 0.55 MeV (l.s.) [120].

Furthermore, the results of the phase shift analysis of the experimental data from [167] in the energy ranges 301–732 keV and 495–613 keV at two values of the angles, represented in Fig. 2.5.1 by black points and squares respectively, are given in Table 2.5.1. Table 2.5.2 contains the results of the phase shift analysis of experimental data from [168], represented in Fig. 2.5.1 by circles (at energies of 526–595 keV) and open squares (for energies

of 506–595 keV). According to [167], the extracted elastic scattering phase shift passes through 90° at an energy of 551 keV, while for the data in [168] this occurs at 557 keV.

Table 2.5.1. The results of the phase shift analysis of $p^{13}C$ elastic scattering at low energies for the experimental data in [167].
In the analysis, only one $^3S_1$ phase shift is considered, the others are considered equal or close to zero.

The $^3S_1$ phase shift was obtained from data in [167] at 123.8° (c.m.). Black points in Fig. 2.5.1.	
E_{lab}, keV	$^3S_1$, deg
301	-2.6
330	3.7
351	-2.1
388	-0.8
432	3.4
479.8	14.7
502	17.7
512	18.6
520.8	19.5
526	22.1
531.2	26.7
533.7	55.6
538	59.6
542.4	72.1
547.5	84.2
551.2	93.6
553.1	103.6
555.4	117.8
563.9	126.0
566	126.0
568.3	126.0
577.3	137.5

604	149.7
643.3	158.3
732.1	161.2
The $^3S_1$ phase shift was obtained from data in [167] at 94.4° (c.m.). Black squares in Fig. 2.5.1.	
E_{lab}, keV	$^3S_1$, deg
495	12.6
530	30.4
544.6	41.9
550	33.7
579	145.0
613	144.0

The width of the resonance is in the range 20–25 keV, which is in good agreement with the results of [120], where the value of 23(1) keV at a resonance energy of 551 keV is given. The resonance width taken from the experimental data for the triplet $^3S_1$ phase shifts has a smaller scattering and value than for $p^{12}C$ [115]; its description requires a very narrow potential leading us to the width order parameter of $\beta = 2–3$ fm^{-2} [169].

Table 2.5.2. The results of the phase shift analysis of $p^{13}C$ elastic scattering at low energies for the experimental data in [168]. In the analysis, only one $^3S_1$ phase shift is considered, the others being considered equal or close to zero.

The $^3S_1$ phase shift was obtained from data in [168] at 120° (c.m.). Circles in Fig. 2.5.1.	
E_{lab}, keV	$^3S_1$, deg
526	38.7
534	38.0
538	44.4
541	56.5
545	66.0
549.9	76.7
553	87.0

557	93.5
565.1	103.0
576.8	154.0
584.4	155.8
595.3	159.6
The $^3S_1$ phase shift was obtained from data in [168] at 60° (c.m.). Open squares in Fig. 2.5.1.	
E_{lab}, keV	$^3S_1$, deg
506.4	38.5
537.8	60.7
541.1	69.2
545.4	81.2
549.5	97.0
553.1	97.0
564.7	109.3
576.3	127.6
584.3	134.2
594.9	141.7

However, a rather exact extraction on the basis of the phase shift analysis of the triplet *S* phase shift from the experimental data gives us hope for the quite unambiguous creation of potential $p^{13}C$ interactions. The resonance form of the phase shift with such a small resonance width allows us to avoid, at the creation of potentials, continuous ambiguity peculiar to the optical model [6], because only a relatively certain width of the potential is capable of being used to describe its resonance form correctly.

Furthermore, the obtained scattering phase shifts are used for the creation of the intercluster interaction potentials [169] and the calculation of the astrophysical *S*-factor of proton radiative capture on ^{13}C [170] at astrophysical energies. This process is included in the CNO thermonuclear cycle as its second reaction. It makes an essential contribution to the energy exit of the thermonuclear reactions [124,170,171], which leads to the combustion of the Sun and other stars in our universe [28,122].

2.5.4. Phase shift analysis of n^{3}He elastic scattering

On the basis of the methods described above, the phase shift analysis of the known experimental data on differential cross sections of elastic n^{3}He scattering in the energy range 1–5 MeV (l.s.) was carried out [172,173,174]. The results of the first version of the phase shift analysis for the elastic scattering phase shifts are presented in Fig. 2.5.2. To carry out the analysis, the χ^2 value was calculated in [172-174] to address experimental errors for the differential cross sections.

In Fig. 2.5.2, it is clear that the *S* phase shifts of the n^{3}He scattering process do not contain resonances in full agreement with the observed spectra for ^{4}He [175]. The resonance with $J^{\pi},T = 0^-,0$ at 21.01 MeV in c.m. with a neutron width of $\Gamma_n = 0.2$ MeV, which for the $^3P_0$ phase shift is at 0.576 MeV in l.s., the higher threshold of the n^{3}He channel located at 20.578 MeV [175], lies below the available experimental data given in [172-174].

In Fig. 2.5.3, the differential cross sections are represented by points for the energies considered in [172-174] and solid curves show the cross sections obtained from our phase shift analysis, i.e. calculated with the n^{3}He scattering phase shifts, found here at energies of up to 5.0 MeV.

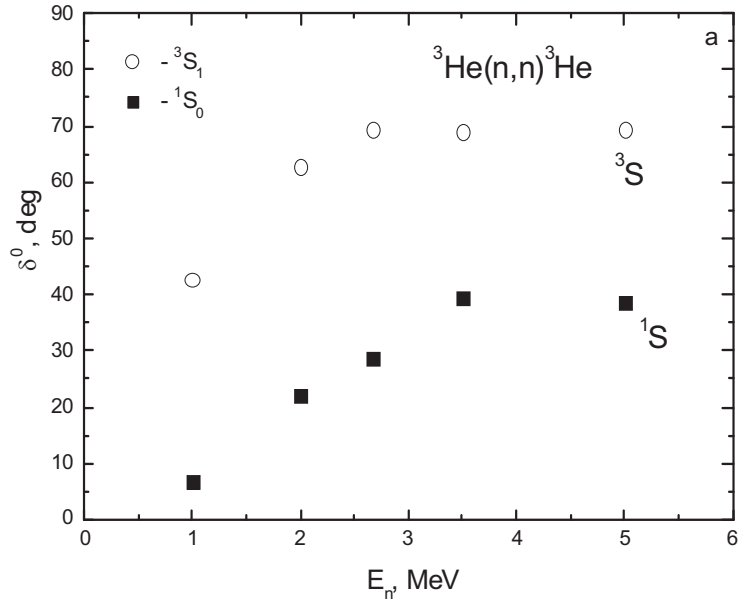

Fig. 2.5.2a. Phase shifts of n^{3}He elastic scattering at low energies.

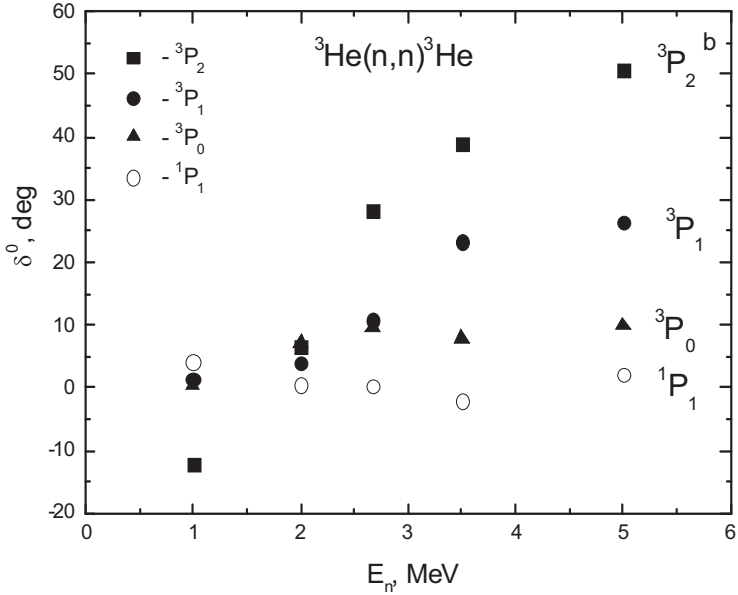

Fig. 2.5.2b. Phase shifts of n^{3}He elastic scattering at low energies.

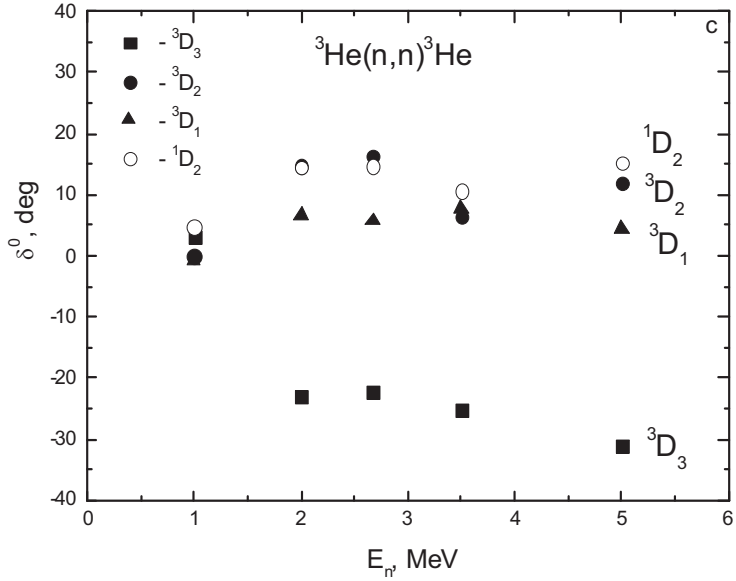

Fig. 2.5.2c. Phase shifts of n^{3}He elastic scattering at low energies.

The resonance with $J^{\pi},T = 2^{-},0$ at 21.84 MeV in c.m. with $\Gamma_n = 0.75$ MeV and $J^{\pi},T = 2^{-},1$ at 23:33 MeV in c.m. with $\Gamma_n = 2.37$ MeV, which lie in the scattering phase shifts at 1.68 MeV and 3.67 MeV in l.s., are not shown in the $^3P_2$ phase shifts. Finally, the two last resonances with $1^{-}1$, and $1^{-},0$ at 23.64 MeV with $\Gamma_n = 2.65$ MeV and 24.25 MeV in c.m. with $\Gamma_n = 2.87$ MeV [175] for the $^3P_1$ or $^1P_1$ scattering phase shifts, which have to be at energies of 4.08 MeV and 4.90 MeV in l.s., are also not shown in the phase shift analysis.

The lack of obvious resonances in the specified scattering phase shifts for these partial waves can be explained by the fact that their resonance energies lie a little away from the energies considered in this analysis—at these energies, the experimental data are just absent. In addition, some of these resonances have a width that is too large, being equal, in fact, to half the resonance energy, which also complicates the determination of their location in the available experimental data.

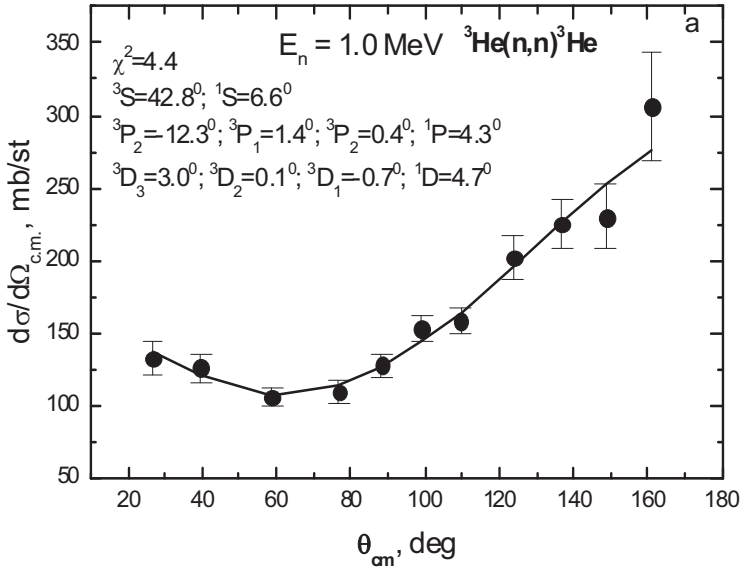

Fig. 2.5.3a. The differential cross sections of n^{3}He elastic scattering, with experimental data from [172].

In this version of the phase shift analysis, the singlet ^1S phase shift starts from zero, but, according to the Levinson theorem [4], in the presence of the bound states forbidden or allowed in this partial wave, the phase shift

has to begin with $N\pi$, where N is the number of such states. In this case, there are two bound states: the ground state and the first excited state at an energy of 20.21 MeV relative to the ground state. In ^{4}He, it lies below the threshold of the n^{3}He channel [175], i.e. in this channel, it is bound at an energy of -0.37 MeV.

Therefore, the $^1S_0$ phase shift has to begin at 360 degrees. We will call this the second version of the analysis and its results are presented in Fig. 2.5.4 (the $^1S_0$ phase shift is shown from 180° to place it with the $^3S_1$ phase shift in one figure) with the differential cross sections shown in Fig. 2.5.5. In Fig. 2.5.5, the points represent the experimental data for the differential cross sections [172-174] and the curves have been calculated using the found scattering phase shifts of the scattering cross sections.

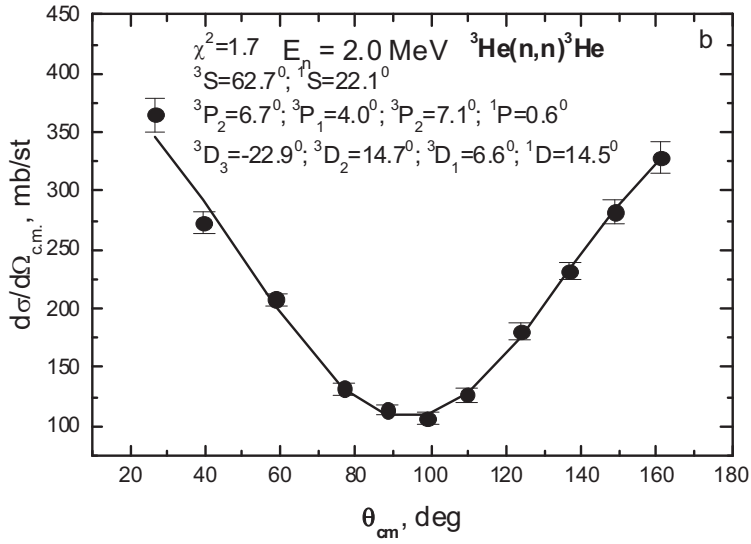

Fig. 2.5.3b. The differential cross sections of n^{3}He elastic scattering with experimental data from [172].

The variant phase shift analysis taking into account only S and P scattering waves, which appear sufficiently frequently for the description of the available differential cross sections at the considered energies, is discussed here. Comparing these results to the previous analysis, we can see that the D wave has a limited effect on the χ^2 value.

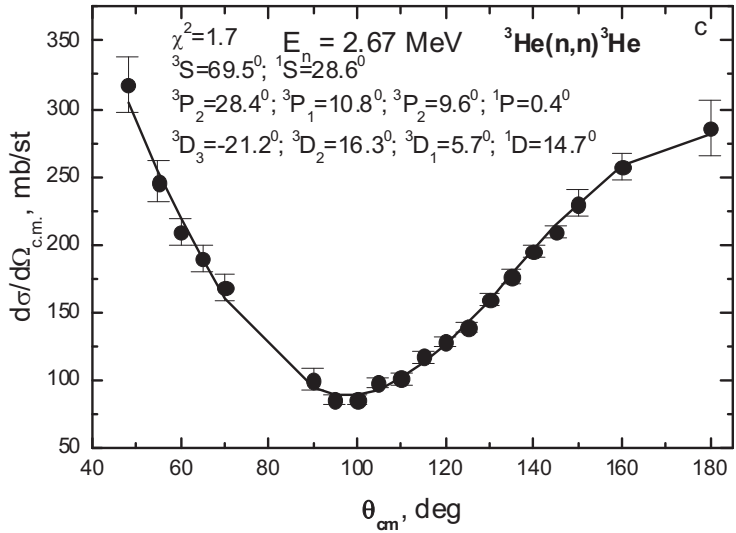

Fig. 2.5.3b. The differential cross sections of n^{3}He elastic scattering with experimental data from [173].

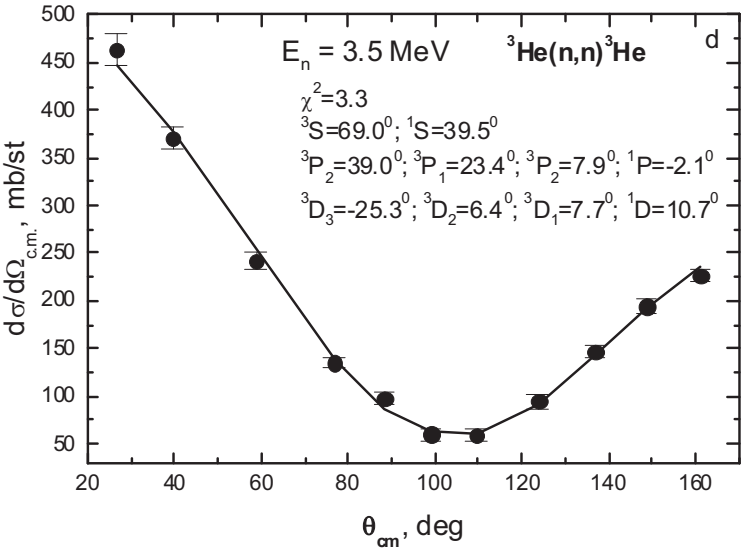

Fig. 2.5.3d. The differential cross sections of n^{3}He elastic scattering using experimental data from [172].

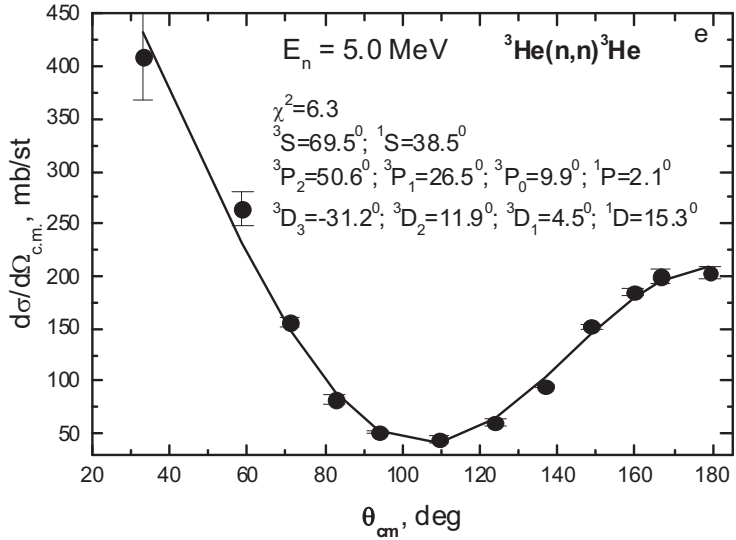

Fig. 2.5.3e. The differential cross sections of n^3He elastic scattering with experimental data from [174].

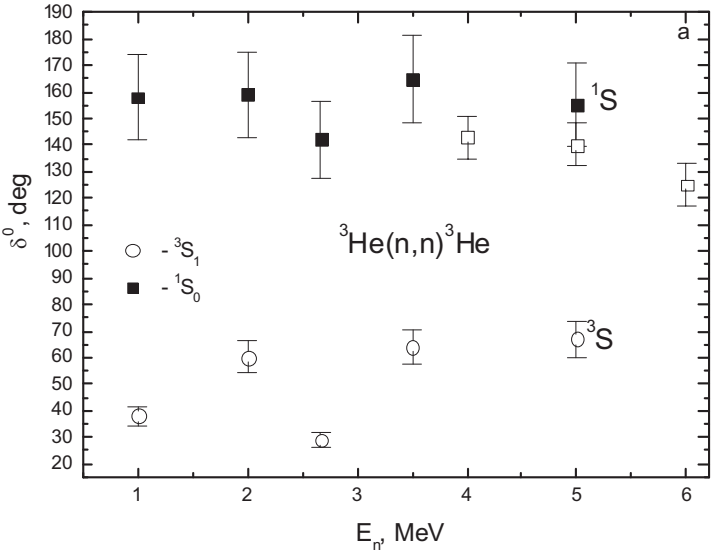

Fig. 2.5.4a. The phase shifts of n^3He elastic scattering at low energies. The points show the singlet phase shifts of p^3H elastic scattering in [176].

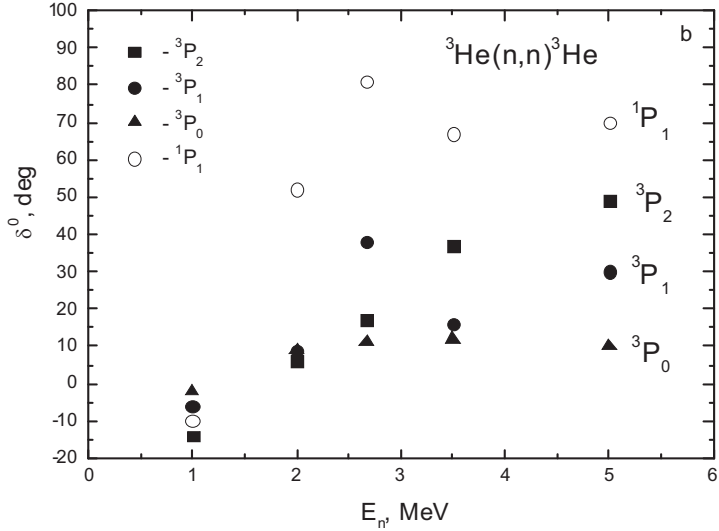

Fig. 2.5.4b. The phase shifts of n^{3}He elastic scattering at low energies. The singlet p^{3}H phase shifts of elastic scattering from [176] shown by points.

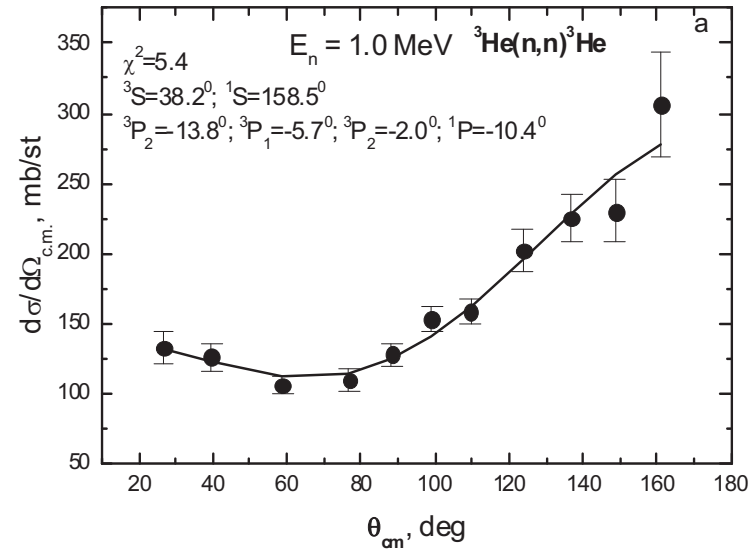

Fig. 2.5.5a. The differential cross sections of n^{3}He elastic scattering with experimental data from [172].

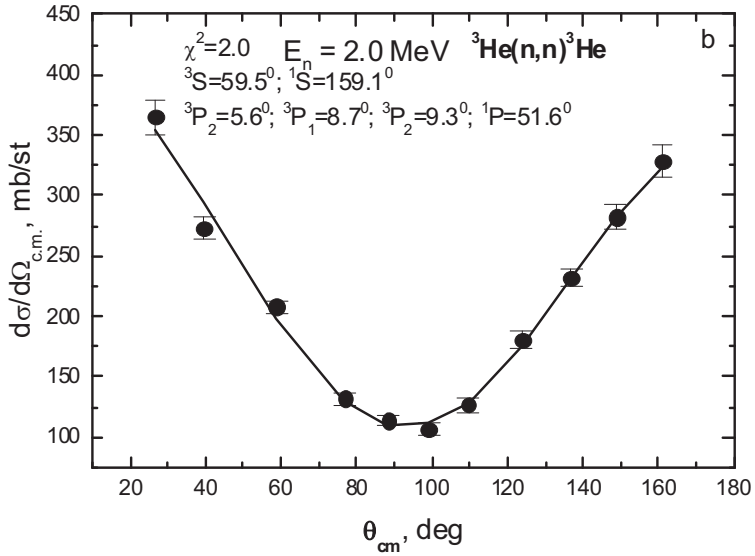

Fig. 2.5.5b. The differential cross sections of n^{3}He elastic scattering with experimental data from [172].

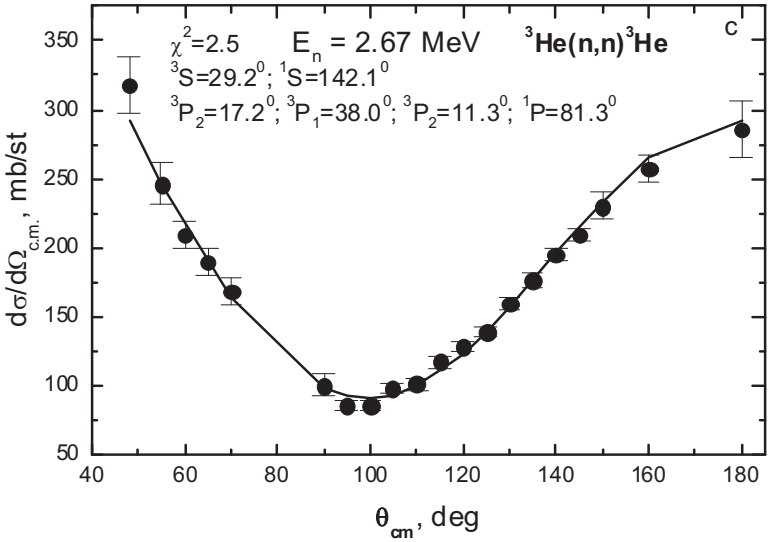

Fig. 2.5.5c. The differential cross sections of n^{3}He elastic scattering with experimental data from [173].

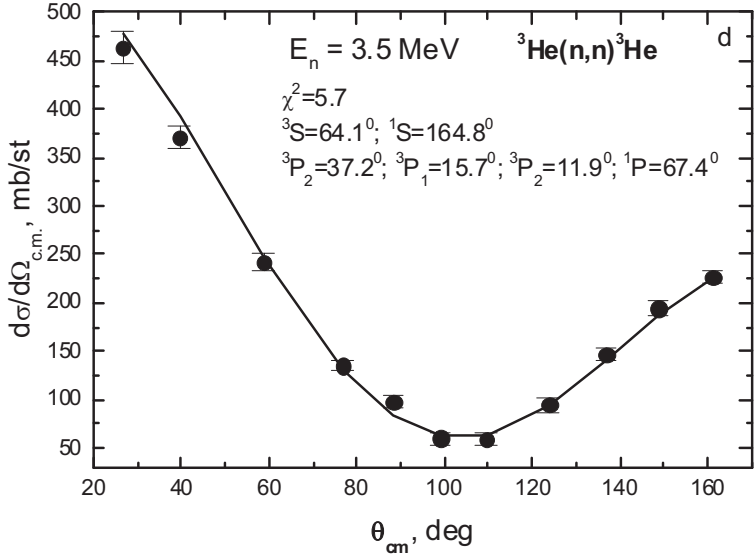

Fig. 2.5.5d. The differential cross sections of n^3He elastic scattering with experimental data from [172].

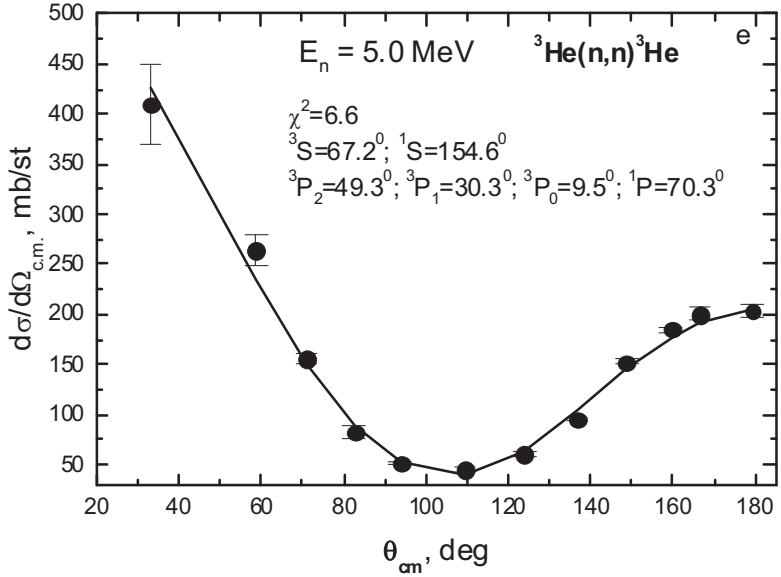

Fig. 2.5.5e. The differential cross sections of n^3He elastic scattering with experimental data from [174].

The error of the obtained scattering phase shifts is estimated at approximately 10 %, as shown in Fig. 2.5.4a for the singlet ^1S phase shifts, corresponding approximately to the error of the differential cross sections [172-174] used in the analysis. For the purposes of comparison, the open squares in Fig. 2.5.4a show the singlet p^3H phase shifts of the elastic scattering obtained previously in [176]. From these results it is clear that the singlet ^1S phase shift of the n^3He elastic scattering found in this analysis almost coincides with a similar phase shift for p^3H scattering [176,177].

Conclusion

As has been shown, the algorithm for the application of numerical methods to find the specific solutions of the general multiparameter variation problem for the functionality of χ^2, determining the accuracy of the description of the experimental data on the basis of the chosen theoretical representation, allows us to define quite unambiguously the scattering phase shifts of nuclear particles [10]. The methods and algorithms used have allowed us to obtain new results for the phase shift analysis of elastic n^3He, p^6Li, $p^{12}C$, $n^{12}C$, $p^{13}C$, $p^{14}C$, $n^{16}O$, $p^{16}O$, $^4He^4He$, and $^4He^{12}C$ scattering at low energies, including astrophysical ones.

The scattering phase shifts found in this way well describe the experimental cross sections of the elastic scattering, determining the location of some low-lying resonance levels of the atomic nuclei considered in these channels. The scattering phase shifts obtained here can be applied further for the creation of the intercluster potentials of interaction, which can be used for calculation of the total cross sections of photonuclear processes and the astrophysical *S*-factors at ultralow or thermal energies [122,178].

III

THE THREE-BODY MODEL

There is no exact theory that can explain all the properties of atomic nuclei. As a result, for the description of their structure, several models have been developed each of which is based on a specified set of experimental facts and allow one to explain certain properties of the nucleus [179]. In this chapter, we examine some of the results obtained for the three-body variational problem of the discrete spectrum with the decomposition of the wave on the basis of a non-orthogonal Gaussian function with independent variation of the decomposition parameters. The two-body potentials are based on the description of the elastic scattering phase shift of the corresponding particles, which have been partly described in the previous chapter. The methods of solving this problem are briefly described in the first chapter and used to consider some characteristics of the bound states of light atomic nuclei in three-body models.

Introduction

In the following works [69-71,180,181,182], the possibilities of the three-body model of ^{6}Li have been considered in detail. The ability of this model to describe almost all the observed characteristics of this nucleus have been shown, along with the significant degree of its clusterization in the ^{2}H^{4}He channel. Such a result may well explain some successes of the simple two-cluster model of light nuclei with forbidden states, in particular the ^{2}H^{4}He, ^{3}H^{4}He models of ^{6}Li and ^{7}Li nuclei [4,79,80,183], which give good descriptions of many experimental characteristics of the nucleic clusters.

The three-body model of the light atomic nuclei ^{7}Li, ^{9}Be, and ^{11}B, allows us to carry out an inspection and assessment of the pair intercluster potentials obtained from scattering phase shifts. This model has convinced us of the expediency of its further use for similar potentials in calculations connected to the consideration of some astrophysical characteristics of nuclear systems and processes at thermal, astrophysical, and low energies, such as those that take place in the Sun, the stars, and across our universe [4,28,80,122,132,184,185].

3.1 The three-body configurations of ^{7}Li and the three-body program

Let us consider the three-body single-channel cluster ^{4}He^{2}Hn model of ^{7}Li. In any single-channel model, three options of an arrangement of particles in a triangular configuration are possible, i.e. three possible channels. Moreover, one of these channels has the greatest probability of existence. As mentioned previously, some characteristics of the separate nuclei are caused primarily by one cluster configuration of the three-cluster system with smaller contributions from the other possible cluster channels. In this case, the single-channel three-cluster model allows us to identify the dominant cluster channel and mark out some of the main properties of the nuclear system caused by it.

Allocation of the prevailing cluster channel and testing of the intercluster potentials obtained on the basis of the elastic scattering phase shifts requires consideration of the single-channel variant of the three-body model. Furthermore, such potentials can be used for various astrophysical applications, including consideration of thermonuclear processes in the Sun and the universe more generally [28,122]. In addition, the single-channel model is much simpler in terms of numerical and program execution in comparison to the multichannel variant.

3.1.1 Potentials and phase shifts

In the variant layout of particles considered, we locate the ^{2}Hn clusters (particles 2 and 3) at the base of the triangle with the radius vector of relative distance $\boldsymbol{r} = \boldsymbol{r}_{23}$ and the orbital moment of relative movement of λ, which can accept 1/2 and 3/2 values. The ^{4}He (particle 1) is located at the top of the triangle with its location relative to the center of mass of the two-cluster system defined by the vector $\boldsymbol{R} = \boldsymbol{R}_{(23),1}$ and the moment l. Furthermore, we define $\boldsymbol{l} = \boldsymbol{l}_{12} + \boldsymbol{l}_{13}$, where $\boldsymbol{l}_{1i}$ stands for the orbital moments between particles 1 and i possess the values 2 and 3 (see Fig. 3.1.1).

The total spin of the $\boldsymbol{S} = \boldsymbol{S}_3 + \boldsymbol{S}_2$ system can have values of 1/2 and 3/2, i.e. the n^{2}H system can be in doublet and quartet spin states. The first of these corresponds to the ground state of the nucleus of tritium at $\lambda = 0$, which we will consider further in the single-channel variant of the three-body model of ^{7}Li used here. The total orbital angular momentum of the $\boldsymbol{L} = \boldsymbol{l} + \boldsymbol{\lambda}$ system, equal to 1, can be obtained, for example, from the combinations of 1 and $l = 1$ and $\lambda = 0$, considered as the n^{2}H system for the tritium nucleus [80]. The total angular momentum $J = S + L$ of the ground state of ^{7}Li, equal to 3/2, can be obtained from the combination of $L = 1$ and $S = 1/2$, which leads to $J = 1/2$

and 3/2 with negative parity. The moment $J = 3/2^-$ corresponds to the ground state of the nucleus and the moment $1/2^-$ corresponds to the first excited state at an energy of 0.478 MeV.

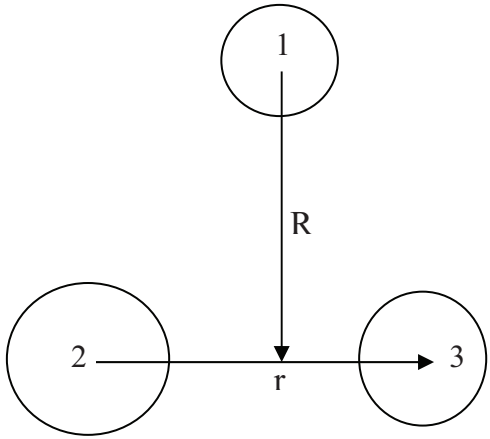

Fig. 3.1.1. Vector scheme of the three-cluster model.

As pair intercluster potentials, interactions of Gaussian form with a repulsion core (1.2.1) allowing them to correctly transfer the corresponding phase shifts of the elastic scattering were chosen. In the particle couple (13), according to the Young tableaux, the n^4He potential is used for the S wave ($l_{13} = 0$) with the parameters describing an experimental phase shift [186], as shown in Fig. 3.1.2.

In the particle couple (12), the triplet P_0 potential of the $^4He^2H$ interaction is used ($l_{12} = 1$), the parameters of which, in general, were specified by the three-body ^7Li binding energy, as the $^3P_0$ phase shifts shown in Fig. 3.1.3 and obtained in [187,188,189,190,191] display great ambiguity. The particle couple (23) is considered to display pure orbital symmetry, ^2Hn doublet S interaction ($l_{23} = \lambda = 0$) with repulsion, the parameters of which are fixed according to the bound state characteristics of the tritium nucleus. The phase shifts are shown in Fig. 3.1.4 by the solid line and the parameters of these potentials are specified in Table 3.1.1.

In each particle couple, only one state with a certain orbital moment and one potential for the given partial wave and spin state is used. This is justified if the states and potentials of other partial waves (in each particle couple) make a smaller contribution and lead only to small amendments to the calculation of the characteristics of the considered nucleus.

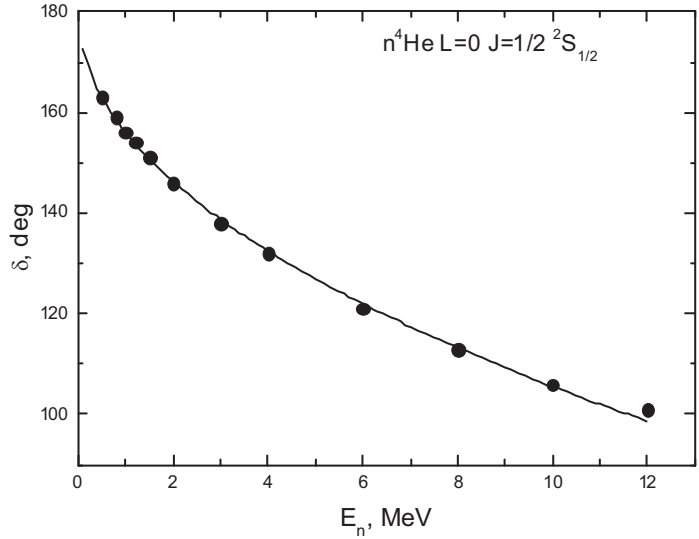

Fig. 3.1.2. The phase shifts of n^4He elastic scattering for $L = 0$ with experimental data from [186].

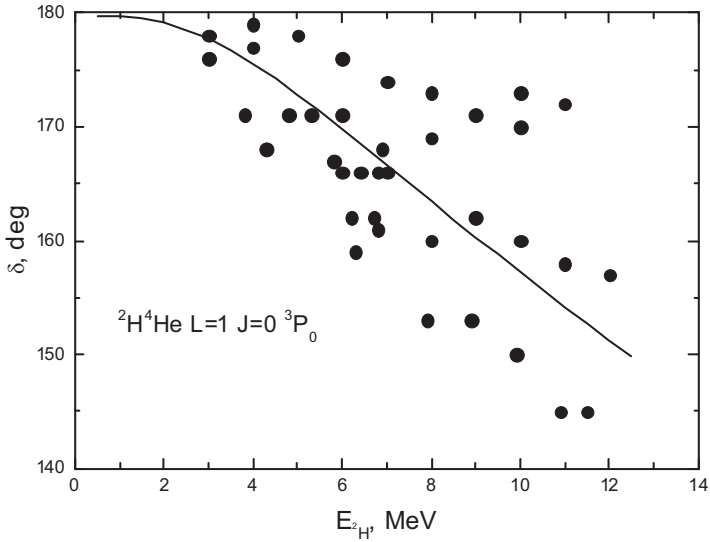

Fig. 3.1.3. The phase shifts of $^4He^2H$ elastic scattering for $L = 1$ and $J = 0$ with experimental data from [187-191].

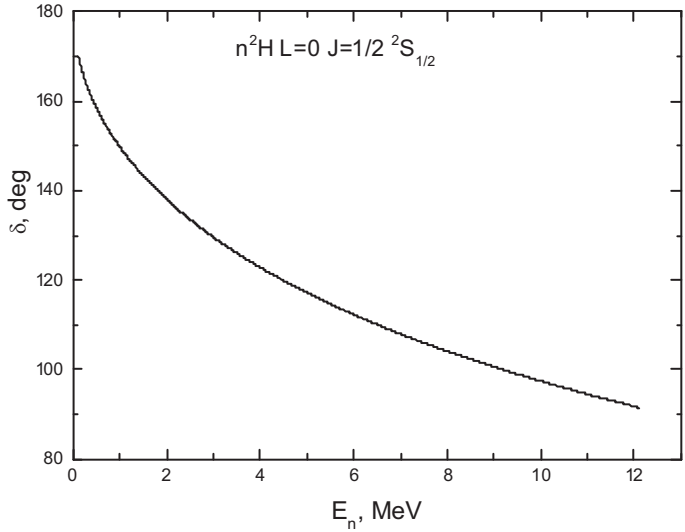

Fig. 3.1.4. The phase shifts of n^2H elastic scattering for $L = 0$.

Table 3.1.1. The parameters of the intercluster pair interaction potential.

Pair	System	$^{2S+1}L_J$	V_0, MeV	γ, fm^{-2}	V_1, MeV	δ, fm^{-2}
12	$^4He^2H$	$^3P_0$	-10.0	0.1	72.0	0.2
13	n^4He	$^2S_{1/2}$	-115.5	0.16	500	1.0
23	^2Hn	$^2S_{1/2}$	-78.78	0.3	200	2.0

Table 3.1.2. The characteristics of tritium in the n^2H model with potential from Table 3.1.1.

System	$^{2S+1}L_J$	E, MeV	R_z, fm	R_m, MeV	$C_w(R$, fm)
^2Hn	$^2S_{1/2}$	-6.257	2.17	2.13	2.01(1) (5–20)

It is possible to describe such a model as a single-channel model, as only one state with a certain orbital moment and spin and its interaction in each particle couple is considered. The characteristics of the bound state of the tritium nucleus with a potential, as shown in Table 3.1.1, are provided in Table 3.1.2. For the calculations of the characteristics of tritium in the ^2Hn channel and ^7Li in the three-body model, the proton radius equals 0.8768(69) fm [75], a neutron value that is equal to zero is used and the ^2H radius is accepted as being equal to 1.9660(68) fm [192]. For the ^4He radius, the value of 1.671(14) fm specified in [175] is used.

The value of the dimensionless asymptotic C_w constant for the ^{2}Hn system, the determination of which is given by expression (1.2.3), is also shown in Table 3.1.2. The specified C_w error is determined by averaging its value by the interval of distances given in brackets. The experimental value of the ^{3}H radius according to most modern data is equal to 1.7591(363) fm [143] and, in the considered channel, its binding energy is equal to -6.257 MeV [193].

3.1.2 Computer program

Below, we give the text of a computer program written in Fortran-90 for the calculation of the binding energy and WF of ^{7}Li in the ^{4}He^{2}Hn three-body channel. The program is based on the variation method with the decomposition of the WF on the basis of non-orthogonal variation and the independent variation of all parameters of decomposition, described in detail in the first chapter and [194], where a version of this program has been given in BASIC using the Borland Turbo Basic Compiler. All the parameters and variables are explained in the printout of the program or are similar to the parameters described earlier for other computer programs. For example, the value of Z with a number always designates a cluster charge, while its weight is designated in whole units, in this case, by the letter M with a number, and RK and RM with a digit representing the charge and mass radiuses of the clusters etc.

PROGRAM THREE_BODY_7LI

```
! The three-body program for 7Li
IMPLICIT REAL(8) (A-Z)
INTEGER I,J,K,NF, NV, NP,NITER,NP2,IJK,ITER,LA,IA
DIMENSION FF(0:500000),FU(0:500000),L(0:50,0:50),PH5(0:50)
COMMON /M/
T(0:50,0:50),L1(0:50,0:50),XP(0:50),VN12(0:50,0:50),VN13(0:50,0:50),
VN121(0:50,0:50),VN131(0:50,0:50),VN122(0:50,0:50),VN132(0:50,0:5
0),VN23(0:50,0:50),VN231(0:50,0:50),VN232(0:50,0:50),H(0:50,0:50),S
V(0:50),VK12(0:50,0:50),VK13(0:50,0:50),VK23(0:50,0:50),VCB(0:50,0
:50)
COMMON /A/
PM0,R122,PM23,A11,V122,M23,R121,V121,R132,M3,M2,M1
COMMON /B/ R131,V131,HC,R232,V232,R231,V231,PI,A23,A13,A12
COMMON /C/ PVC,EPP,ZYS,V132,PNC,NEV
CHARACTER(9) FILI,FILO
BBB(A,AA,K)=K**2/(2.*K+1.)+(2.*K+3.)*A/AA**2-K
```

```
Z1=2.0D0
Z2=1.0D0
Z3=0.0D0
M1=4.0D0
M2=2.0D0
M3=1.0D0
Z=Z1+Z2+Z3
M23=M3+M2
PM23=M3*M2/M23
AM0=M1+M2+M3
PM0=M1*M23/AM0
RK1=1.67D0
RK2=1.96D0
RK3=0.0D0
RM1=1.67D0
RM2=1.96D0
RM3=0.877D0
NF=6000
HF=0.005D0
BB=1.0D+030
LA=1
HC=0.010D0
PNC=-10.0D0
PVC=0.0D0
A11=41.46860D0
A12=1.4399750D0*Z1*Z2
A13=1.4399750D0*Z1*Z3
A23=1.4399750D0*Z3*Z2
P1=4.0D0*DATAN(1.0D0)
PI=DSQRT(P1)
! 1 - AL; 2 - D; 3 - N;    L  -  N-AL - 0, AL-D - 1, N-D - 0
! N-D
V231=-78.78D0; ! J= 1/2  ; LAM=0 E=6.257 RZ=2.17
! RM=2.13 Cw=2.01(1) 5-20 Fm
R231=0.3D0
V232=200.0D0
R232=2.0D0
! AL-D
V121=-10.0D0; ! J=0; L=1
R121=0.1D0
V122=72.0D0
```

```
R122=0.2D0
! AL-N
V131=-115.5D0; ! J=1/2; L=0
R131=0.16D0
V132=500.0D0
R132=1.0D0
! - - - - - - - - - - - - - - - - - - - - - - - - - - - - - - - - - - - -
NP=10
FILI='ALFAA.DAT'
FILO='ALFA2.DAT'
EP=3.0D-015;! THE ENERGY ACCURACY
EPP=2.0D-015;! THE DETERMINANT ACCURACY
NITER=30;! THE NUMBER OF ITERATIONS
NV=1;! IF =0 - THERE IS NO VARIATION, =1 - THE VARIATION OF
ALL PARAMETERS
PH=0.00001D0
IA=1
IF(IA==0) THEN
DO I=1,NP
XP(I)=I/10.0D0
XP(I+NP)=XP(I)*2.0D0
ENDDO
ELSE
OPEN (1,FILE=FILI)
READ(1,*)
DO I=1,NP
READ(1,*) J,XP(I),XP(I+NP)
ENDDO
CLOSE(1)
ENDIF
NP2=2*NP
AAA1: DO ITER=1,NITER
PH55=PH/ITER
50 FMIN=BB
DO IJK=1,NP2
60 PH5(IJK)=XP(IJK)*PH55
XP(IJK)=XP(IJK)+PH5(IJK)
IF (XP(IJK)<0.0D0) THEN
XP(IJK)=XP(IJK)-PH5(IJK)
GOTO 61
ENDIF
```

```
CALL MINIM(NP,F,LA,FILI)
CC=BB; BB=F
IF(NV==0) GOTO 7654
IF(F<CC)THEN
PRINT*, ITER,IJK,F,ABS(F-CC)
IF (ABS(F-CC)>=EP) GOTO 60
ELSE
XP(IJK)=XP(IJK)-PH5(IJK)
ENDIF
61 ENDDO
PH55=-PH55/2.0D0
IF (ABS(CC-F)>=EP/2.0D0) GOTO 50
ENDDO AAA1
7654 PRINT*,
"************************************************"
PRINT*, "E = ",F
PRINT*
PRINT*, "        N          ALFA                BET"
DO I=1,NP
PRINT*,I,XP(I),XP(I+NP)
ENDDO
PRINT*
899  CONTINUE
ZYS=1.0D0
ALA=F
CALL MINIM(NP,ALA,LA,FILI)
! - - - - - - - - - - - - - - - - - - THE NORMALIZATION - - - - - - - - - - - - - -
IF (LA==1) THEN
FA=3.; AF=2.
ENDIF
IF (LA==2) THEN
FA=15.; AF=6.
ENDIF
IF (LA<1 .OR. LA>2) STOP
CALL SVNOR(PI,LA,NP,XP,SV)
!----------------------CHECK OF THE NORMALIZATION-------------------
S=0.0D0
DO I=1,NP
DO J=1,NP
AL=XP(I)+XP(J)
BT=XP(I+NP)+XP(J+NP)
```

```
DO K=0,NF
R=HF*K
RR=(R**2)*AL
AB=(R**2)*DEXP(-RR)
FF(K)=AB
ENDDO
CALL SIMPS(NF,HF,FF,S1)
DO K=0,NF
R=HF*K
RR=(R**2)*BT
AC=R**(2*LA+2)*DEXP(-RR)
FU(K)=AC
ENDDO
CALL SIMPS(NF,HF,FU,S2)
S=S+SV(I)*SV(J)*S1*S2
ENDDO
ENDDO
SNOR=S
PRINT*
PRINT*, "   NORM =",SNOR,'       NEV-DET = ',NEV
PRINT*
PRINT*, '         N                SV'
DO I=1,NP
PRINT*,  I,SV(I)
ENDDO
6622 CONTINUE
! ******************* THE NORMALIZATION
******************
BN=LA+1.5
SS=0.
DO I=1,NP
DO J=1,NP
AL=XP(I)+XP(J)
BT=XP(I+NP)+XP(J+NP)
L(I,J)=1./AL**1.5/BT**BN
SS=SS+SV(I)*SV(J)*L(I,J)
ENDDO
ENDDO
SN=DSQRT(FA*P1/16./2.**LA*SS)
PRINT*
PRINT*, "  N= ", SN
```

```
! ******************  RM ***************************
S=0.
DO I=1,NP
DO J=1,NP
AL=XP(I)+XP(J)
BT=XP(I+NP)+XP(J+NP)
S=S+SV(I)*SV(J)/BT**BN/AL**1.5*(3.*PM23/AL+(2.*LA+3.)*PM0/B
T)
 ENDDO
 ENDDO
 RMM=P1*FA*S/2.**(LA+1)/16.
RRR=M1/AM0*RM1**2+M2/AM0*RM2**2+M3/AM0*RM3**2+RM
M/AM0
RM=DSQRT(RRR)
PRINT*, " RM = ", RM
! ******************  RZ ***************************
CCC=(Z1*M23**2+(Z2+Z3)*M1**2)/AM0**2
DDD=(Z2*M3**2+Z3*M2**2)/M23**2
EEE=-M1/AM0/M23*(Z2*M3-Z3*M2)
S=0.
SS=0.
SSS=0.
DO I=1,NP
DO J=1,NP
AL=XP(I)+XP(J)
BT=XP(I+NP)+XP(J+NP)
S=S+SV(I)*SV(J)*(2.*LA+3.)/BT**(LA+2.5)/AL**1.5
SS=SS+SV(I)*SV(J)*3./BT**(LA+1.5)/AL**2.5
SSS=SSS+SV(I)*SV(J)*AF/BT**(LA+2)/AL**2
ENDDO
ENDDO
RMM=FA/2**(LA+1)*P1/16.*(CCC*S+DDD*SS)+EEE*SSS
RRR=Z1/Z*RK1**2+Z2/Z*RK2**2+Z3/Z*RK3**2+RMM/Z
RZ=DSQRT(RRR)
PRINT*, " RZ = ",RZ
! ********************** Q ************************
QQ=-10.*2./5.*RMM+2.86
PRINT*, " Q = ",QQ
! ************** CONTROL ENERGY  *****************
SC=0.
SK=0.
```

```
SP=0.
SL=0.
S1=0.
S3=0.
S2=0.
SH=0.
DO I=1,NP
DO J=1,NP
S1=S1+SV(I)*SV(J)*VK12(I,J)
S2=S2+SV(I)*SV(J)*VK13(I,J)
S3=S3+SV(I)*SV(J)*VK23(I,J)
SC=SC+SV(I)*SV(J)*VCB(I,J)
SK=SK+SV(I)*SV(J)*T(I,J)
SP=SP+SV(I)*SV(J)*(VN12(I,J)+VN13(I,J)+VN23(I,J))
SL=SL+SV(I)*SV(J)*L1(I,J)
SH=SH+SV(I)*SV(J)*H(I,J)
ENDDO
ENDDO
SC1=S1*P1/16.0D0
SC2=S2*P1/16.0D0
SC3=S3*P1/16.0D0
SCU=SC1+SC2+SC3
SC=SC*P1/16.0D0
SK=SK*P1/16.0D0
SP=SP*P1/16.0D0
SL=SL*P1/16.0D0
SH=SH*P1/16.0D0
ST=SCU+SK+SP+SC
PRINT*
PRINT*, "COUL. ENERGY  VK = ",SCU," 12 = ",SC1," 13 = ",SC2," 23
= ",SC3
PRINT*, "CENTROB. ENERGY =  ",SC
PRINT*, "KINETICH. ENERGY =  ",SK
PRINT*, "M.E. OT L1 = ",SL
PRINT*, "POTENS. ENERGY =  ",SP
PRINT*, "POLNAY ENERGY ST =  ",ST
PRINT*, "POLNAY ENERGY SH =  ",SH
!-------------------------------------------------------------------------
PRINT*, "???"
READ*, AAA
IF(AAA==0) GOTO 2244
```

```
OPEN (1,FILE=FILO)
WRITE(1,*) '        N                ALFA                BETTA'
DO I=1,NP
WRITE(1,*) I,XP(I),XP(I+NP)
ENDDO
WRITE(1,*)
WRITE(1,*) 'E = ',F
WRITE(1,*)
WRITE(1,*)'SUM(H*SV-E*L*SV) FROM SV=',ALA
WRITE(1,*)
WRITE(1,*) '        N                SV'
DO I=1,NP
WRITE(1,*) I,SV(I)
ENDDO
WRITE(1,*)
WRITE(1,*) 'NOR= ',SNOR, SN
WRITE(1,*)
WRITE(1,*) 'NEV-DET=',NEV
WRITE(1,*)
WRITE(1,*) "RM=",RM," RZ=",RZ
WRITE(1,*)
WRITE(1,*) "Q=",QQ
CLOSE(1)
2244 CONTINUE
END

SUBROUTINE SIMPS(N,H,F,S)
IMPLICIT REAL(8) (A-Z)
INTEGER I,N
DIMENSION F(0:500000)
A=0.0D0;B=0.0D0
DO I=1,N-1,2
B=B+F(I)
ENDDO
DO I=2,N-2,2
A=A+F(I)
ENDDO
S=H*(F(0)+F(N)+2.0D0*A+4.0D0*B)/3.0D0
END
```

MINIM(NP,ALA,L,FILO)

```
IMPLICIT REAL(8) (A-Z)
INTEGER   NP,KK,JJ,L,K,I
COMMON /M/
T(0:50,0:50),L1(0:50,0:50),XP(0:50),VN12(0:50,0:50),VN13(0:50,0:50),
VN121(0:50,0:50),VN131(0:50,0:50),VN122(0:50,0:50),VN132(0:50,0:5
0),VN23(0:50,0:50),VN231(0:50,0:50),VN232(0:50,0:50),H(0:50,0:50),S
V(0:50),VK12(0:50,0:50),VK13(0:50,0:50),VK23(0:50,0:50),VCB(0:50,0
:50)
COMMON /A/
PM0,R122,PM23,A11,V122,M23,R121,V121,R132,M3,M2,M1
COMMON /B/ R131,V131,HC,R232,V232,R231,V231,PI,A23,A13,A12
COMMON /C/ PVC,EPP,ZYS,  V132,PNC,NEV
CHARACTER(9) FILO
BBB(A,AB,K)=(1.*K)**2/(2.*K+1.)+(2.*K+3.)*A/AB**2-(1.*K)
P1=4.0D0*DATAN(1.0D0)
PI=DSQRT(P1)
IF(L==1) THEN
FA=3.; FAA=1.;FFA=1.
ENDIF
IF(L==2) THEN
FA=15.; FAA=3.;FFA=2.
ENDIF
IF(L<1 .OR. L>2) THEN
PRINT*, "STOP"; STOP
ENDIF
A1: DO KK=1,NP
A5: DO JJ=1,NP
AL=XP(KK)+XP(JJ)
AL1=XP(KK)*XP(JJ)
BT=(XP(KK+NP)+XP(JJ+NP))
BT1=XP(KK+NP)*XP(JJ+NP)
H1=FA/2.**L*A11/PM23/BT*BBB(AL1,AL,0)/AL**0.5/BT**(L+0.5)
H2=FA/2.**L*A11/PM0/AL*BBB(BT1,BT,L)/AL**0.5/BT**(L+0.5)
T(KK,JJ)=H1+H2
L1(KK,JJ)=FA/2.**L/AL**1.5/BT**(L+1.5)
AA=AL*BT+R121*(AL+BT*(M3/M23)**2)
DD=(M3/M23)**2*R121+AL
VN121(KK,JJ)=FA/2.**L*V121*DD**L/AA**(L+1.5)
AA=AL*BT+R122*(AL+BT*(M3/M23)**2)
DD=(M3/M23)**2*R122+AL
```

```
VN122(KK,JJ)=FA/2.**L*V122*DD**L/AA**(L+1.5)
VN12(KK,JJ)=VN121(KK,JJ)+VN122(KK,JJ)
AA=AL*BT+R131*(AL+BT*(M2/M23)**2)
DD=(M2/M23)**2*R131+AL
VN131(KK,JJ)=FA/2.**L*V131*DD**L/AA**(L+1.5)
AA=AL*BT+R132*(AL+BT*(M2/M23)**2)
DD=(M2/M23)**2*R132+AL
VN132(KK,JJ)=FA/2.**L*V132*DD**L/AA**(L+1.5)
VN13(KK,JJ)=VN131(KK,JJ)+VN132(KK,JJ)
VN231(KK,JJ)=FA/2.**L*V231/BT**(L+1.5)/(AL+R231)**1.5
VN232(KK,JJ)=FA/2.**L*V232/BT**(L+1.5)/(AL+R232)**1.5
VN23(KK,JJ)=VN231(KK,JJ)+VN232(KK,JJ)
VK12(KK,JJ)=2.*FFA*A12/PI/AL**1.5/BT**(L+1)
VK13(KK,JJ)=2.*FFA*A13/PI/AL**1.5/BT**(L+1)
VK23(KK,JJ)=2./2.**L*FA*A23/PI/AL/BT**(L+1.5)
VCB(KK,JJ)=(1.*L)*(1.*L+1.)/2.**L*FAA*A11/AL**1.5/BT**(L+0.5)/
PM0
H(KK,JJ)=T(KK,JJ)+VN23(KK,JJ)+VN12(KK,JJ)+VN13(KK,JJ)+VCB(
KK,JJ)+VK12(KK,JJ)+VK13(KK,JJ)+VK23(KK,JJ)
ENDDO A5
ENDDO A1
CALL MINI(NP,ALA,DETER)
EE=ALA
OPEN (1,FILE=FILO)
WRITE(1,*) '        N                ALFA                    BETTA'
DO I=1,NP
WRITE(1,*) I,XP(I),XP(I+NP)
ENDDO
WRITE(1,*)
WRITE(1,*) 'E = ',EE
CLOSE(1)
IF (ZYS==1.0D0) THEN
CALL VEC(NP,ALA)
CALL SVNOR(PI,L,NP,XP,SV)
ENDIF
END

SUBROUTINE SVNOR(PI,L,NP,XP,SV)
IMPLICIT REAL(8) (A-Z)
INTEGER NP,L,I,J
DIMENSION SV(0:50),XP(0:50),A(0:50,0:50)
```

```
IF (L==1) THEN
FA=3.
ENDIF
IF (L==2) THEN
FA=15.
ENDIF
SS=0.
DO I=1,NP
DO J=1,NP
AL=XP(I)+XP(J)
BT=XP(I+NP)+XP(J+NP)
A(I,J)=1./AL**1.5/BT**(L+1.5)
SS=SS+SV(I)*SV(J)*A(I,J)
ENDDO
ENDDO
ANOR=DSQRT(16.*2.**L/FA/SS)/PI
DO I=1,NP
SV(I)=ANOR*SV(I)
ENDDO
END

SUBROUTINE MINI(NP,COR,D)
IMPLICIT REAL(8) (A-Z)
INTEGER C,  NP
COMMON /A/
PM0,R122,PM23,A11,V122,M23,R121,V121,R132,M3,M2,M1
COMMON /B/ R131,V131,HC,R232,V232,R231,V231,PI,A23,A13,A12
COMMON /C/ PVC,EPP,ZYS,  V132,PNC,NEV
PN=PNC; PV=PVC; H=HC; E=EPP
IF(PN>PV) THEN
PNN=PV; PV=PN; PN=PNN
ENDIF
A=PN
1 CALL DET(NP,A,D1); B=A+H
2 CALL DET(NP,B,D2)
IF (D1*D2>0.0D0) THEN
B=B+H; D1=D2
IF (B<=PV .AND. B>=PN) GOTO 2
C=0; RETURN; ELSE
A=B-H; H=H*1.0D-001
IF(ABS(D2)<E .OR. ABS(H)<E) GOTO 3
```

```
B=A+H; GOTO 1
ENDIF
3 C=1; COR=B; D=D2
END

SUBROUTINE DET(NP,LLA,S)
IMPLICIT REAL(8) (A-Z)
INTEGER I,J,K,NP
DIMENSION LLL(0:50,0:50),B(0:50,0:50),C(0:50,0:50),AAA(0:50,0:50)
COMMON /M/
T(0:50,0:50),L1(0:50,0:50),XP(0:50),VN12(0:50,0:50),VN13(0:50,0:50),
VN121(0:50,0:50),VN131(0:50,0:50),VN122(0:50,0:50),VN132(0:50,0:5
0),VN23(0:50,0:50),VN231(0:50,0:50),VN232(0:50,0:50),H(0:50,0:50),S
V(0:50),VK12(0:50,0:50),VK13(0:50,0:50),VK23(0:50,0:50),VCB(0:50,0
:50)
COMMON /A/
PM0,R122,PM23,A11,V122,M23,R121,V121,R132,M3,M2,M1
COMMON /B/ R131,V131,HC,R232,V232,R231,V231,PI,A23,A13,A12
COMMON /C/ PVC,EPP,ZYS,  V132,PNC,NEV
DO I=1,NP
DO J=1,NP
LLL(I,J)=(H(I,J)-LLA*L1(I,J))
B(I,J)=0.0D0
C(I,J)=0.0D0
ENDDO
ENDDO
GOTO 234
PRINT*, "                THE  LLL=H-E*L1" MATRIX
PRINT*
DO II=1,NP
DO KK=1,NP
PRINT*, LLL(II,KK)
ENDDO
PRINT*
ENDDO
234 CONTINUE
! - - - - LLLL - DECOMPOSITION ON THE TRIANGULAR - - - - - - -
DO I=1,NP
C(I,I)=1.0D0
B(I,1)=LLL(I,1)
C(1,I)=LLL(1,I)/B(1,1)
```

```
ENDDO
DO I=2,NP
DO J=2,NP
S=0.0D0
IF (J>I) GOTO 1
DO K=1,I-1
S=S+B(I,K)*C(K,J)
ENDDO
B(I,J)=LLL(I,J)-S
GOTO 2
1 S=0.0D0
DO K=1,I-1
S=S+B(I,K)*C(K,J)
ENDDO
C(I,J)=(LLL(I,J)-S)/B(I,I)
2 CONTINUE
ENDDO
ENDDO
! - - - - CHECK OF THE DECOMPOSITION OF THE LLL MATRIX - -
SS=0.0D0
DO I=1,NP
DO J=1,NP
S=0.0D0
DO K=1,NP
S=S+B(I,K)*C(K,J)
ENDDO
AAA(I,J)=S-LLL(I,J)
SS=SS+AAA(I,J)
ENDDO
ENDDO
NEV=SS
GOTO 678
PRINT*, "            FOR THE N=LLL-B*C =0" DETERMINANT
DO I=1,NP
PRINT*
DO J=1,NP
PRINT*,AAA(I,J)
ENDDO
ENDDO
PRINT*
678 CONTINUE
```

```
S=1.0D0
DO K=1,NP
S=S*B(K,K)
ENDDO
GOTO 991
PRINT 22, LLA,S,SS
PRINT*, "      DET=",S
PRINT*, "      NEV=",SS
991 CONTINUE
22 FORMAT(3E15.5)
END

SUBROUTINE VEC(NP,LLA)
IMPLICIT REAL(8) (A-Z)
INTEGER I,J,K,J1,I1,NP
DIMENSION
LLL(0:50,0:50),D(0:50),Y(0:50),B(0:50,0:50),AD(0:50,0:50),X(0:50),C(0
:50,0:50),E2(50)
COMMON /M/
T(0:50,0:50),L1(0:50,0:50),XP(0:50),VN12(0:50,0:50),VN13(0:50,0:50),
VN121(0:50,0:50),VN131(0:50,0:50),VN122(0:50,0:50),VN132(0:50,0:5
0),VN23(0:50,0:50),VN231(0:50,0:50),VN232(0:50,0:50),H(0:50,0:50),S
V(0:50),VK12(0:50,0:50),VK13(0:50,0:50),VK23(0:50,0:50),VCB(0:50,0
:50)
COMMON /A/
PM0,R122,PM23,A11,V122,M23,R121,V121,R132,M3,M2,M1
COMMON /B/ R131,V131,HC,R232,V232,R231,V231,PI,A23,A13,A12
COMMON /C/ PVC,EPP,ZYS,  V132,PNC,NEV
DO I=1,NP
DO J=1,NP
LLL(I,J)=(H(I,J)-LLA*L1(I,J))
B(I,J)=0.0D0
C(I,J)=0.0D0
ENDDO
ENDDO
DO I=1,NP-1
DO J=1,NP-1
AD(I,J)=LLL(I,J)
ENDDO
ENDDO
I1=1
```

```
I2=NP-1
J=NP
DO I=I1,I2
D(I)=-LLL(I,J)
ENDDO
NP=NP-1
CALL TRI(NP,AD,B,C,SOB)
! - - - - - - - - - - - - - - - - - - - - - - - - - - - - - - - - - - - - - - - - - - - - - - - -
Y(1)=D(1)/B(1,1)
DO I=2,NP
S=0.0D0
DO K=1,I-1
S=S+B(I,K)*Y(K)
ENDDO
Y(I)=(D(I)-S)/B(I,I)
ENDDO
X(NP)=Y(NP)
DO I=NP-1,1,-1
S=0.0D0
DO K=I+1,NP
S=S+C(I,K)*X(K)
ENDDO
X(I)=Y(I)-S
ENDDO
DO I=1,NP
SV(I)=X(I)
ENDDO
NP=NP+1
SV(NP)=1
S=0.0D0
DO I=1,NP
S=S+SV(I)**2
ENDDO
!PRINT*,'S=', S
SS=0.0D0
DO I=1,NP
SV(I)=SV(I)/DSQRT(ABS(S))
! SS=SS+SV(I)**2
ENDDO
!AN=1.0D0/DSQRT(ABS(SS))
!AN=1.0D0
```

```
!PRINT*, "                    H*SV-LA*L*SV=0"
SSS=0.0D0
DO I=1,NP
S=0.0D0
SS=0.0D0
DO J=1,NP
!SV(J)=SV(J)*AN
S=S+H(I,J)*SV(J)
SS=SS+LLA*L1(I,J)*SV(J)
ENDDO
E2(I)=S-SS
SSS=SSS+E2(I)
ENDDO
LLA=SSS
!DO I=1,NP
!PRINT*,"E2 = ",E2(I)
!ENDDO
PRINT*
PRINT*,'          SUM(H*SV-E*L*SV) FROM SV =',LLA
END

SUBROUTINE TRI(NP,AD,B,C,S)
IMPLICIT REAL(8) (A-Z)
INTEGER I,J,K,NP
DIMENSION AD(0:50,0:50),B(0:50,0:50),C(0:50,0:50),AAA(0:50,0:50)
DO I=1,NP
C(I,I)=1.0D0
B(I,1)=AD(I,1)
C(1,I)=AD(1,I)/B(1,1)
ENDDO
DO I=2,NP
DO J=2,NP
S=0.0D0
IF (J>I) GOTO 551
DO K=1,I-1
S=S+B(I,K)*C(K,J)
ENDDO
B(I,J)=AD(I,J)-S
GOTO 552
551 S=0.0D0
DO K=1,I-1
```

```
S=S+B(I,K)*C(K,J)
ENDDO
C(I,J)=(AD(I,J)-S)/B(I,I)
552 CONTINUE
ENDDO
ENDDO
! - - - - - - - - - - - - - - - - - - - - - - - - - - - - - - - - - - - - - - - - - - - - - - - -
SS=0.0D0
DO I=1,NP
DO J=1,NP
S=0.0D0
DO K=1,NP
S=S+B(I,K)*C(K,J)
ENDDO
AAA(I,J)=S-AD(I,J)
SS=SS+AAA(I,J)
ENDDO
ENDDO
GOTO 578
PRINT*, "                    NEV = AD - B*C =0"
DO I=1,NP
DO J=1,NP
PRINT*,AAA(I,J)
ENDDO
ENDDO
578 S=1.0D0
DO K=1,NP
S=S*B(K,K)
ENDDO
! GOTO 9753
! PRINT*, "          DET=",S
!PRINT*,S
PRINT*, "          NEV-TRI=",SS
!PRINT*,SS
9753 PRINT*
END

SUBROUTINE WW(SK,L,GK,R,N,H,WH)
IMPLICIT REAL(8) (A-Z)
INTEGER I,L,N,NN
DIMENSION V(50000)
```

```
H=H
N=N
SS=DSQRT(ABS(SK))
AA=GK/SS
BB=L
NN=500
HH=.02D0
ZZ=1+AA+BB
AAA=1.0D0/ZZ
NNN=2000
DO I2=1,NNN
AAA=AAA*I2/(ZZ+I2)
ENDDO
GAM=AAA*NNN**ZZ
RR=R
CC=RR*SS*2
DO I=0,NN
TT=HH*I
V(I)=TT**(AA+BB)*(1+TT/CC)**(BB-AA)*DEXP(-TT)
ENDDO
CALL SIMPS(NN,HH,V,S)
WH=S*DEXP(-CC/2.0D0)/(CC**AA*GAM)
END
```

3.1.3 The three-body results

Below, we present the results of analysis using this program for ^{7}Li with the variant of three-body configuration considered above for nine members of the decomposition of the three-body wave function (1.5.4) by the Gaussian functions:

E = -8.7165 04042795002

N	ALPHA (α)	BETA (β)
1	2.695013648564534E-001	5.552519454982658E-002
2	6.073846174799727E-002	5.582211053901705E-002
3	1.481076486508074E-001	1.500571262902319E-001
4	1.219211094860576E-001	2.100593191345530E-001
5	1.583008396850423E-001	6.443497149569889E-001
6	1.572092636709496E-001	6.485407339616155E-001

7	2.048327219956353E-001	5.160938755052593E-001
8	2.920843757329559E-001	3.970902201955188E-001
9	1.185843962546213	7.762432248877493E-002

SUM(H*SV-E*L*SV) FROM SV = -3.048700181196296E-011
NORM = 9.999999999986114E-001
NEV-DET = -9.947598300641403E-014

N	SV
1	-2.006282287524374E-002
2	-1.041690910372422E-002
3	-1.956124177741528E-001
4	1.721055580493311E-001
5	-33.347719101844450
6	31.786460544316070
7	2.111064771161292
8	-5.187214457242435E-001
9	4.082610488279214E-002

RM = 2.771546765454730

For ten members of the decomposition of the WF by the Gaussian functions, we obtain the following results:

E = -8.7176 07265169926

N	ALPHA (α)	BETA (β)
1	2.667953617399743E-001	5.601125106169563E-002
2	5.941262333765297E-002	5.493848544738812E-002
3	1.393163512886810E-001	1.556109489548065E-001
4	1.235101199700397E-001	1.918288577203961E-001
5	1.584363057560162E-001	6.454611171440240E-001
6	1.578191661203245E-001	6.479935485451310E-001
7	2.037134087039333E-001	5.101654896420405E-001
8	2.707874198704808E-001	4.030486689121375E-001
9	1.211284751587861	7.694488373218295E-002
10	4.678503078478220	7.811004516393501E-002

NEV-TRI = 3.979039320256561E-013

SUM(H*SV-E*L*SV) FROM SV = -3.541195364720196E-009

NORM = 9.999999999949636E-001
NEV-DET = 3.836930773104541E-013

N	SV
1	2.090487646994713E-002
2	9.678149889880678E-003
3	2.816715670580448E-001
4	-2.562071190446284E-001
5	65.304218586437270
6	-63.510565912605150
7	-2.554362633383337
8	7.253463724545455E-001
9	-4.040198847629709E-002
10	8.813225618937962E-004

NN = 9.999999999997704E-001
RM = 2.792145900219183
RZ = 2.517493303959341
Q = -35.515670530665620

COUL. ENERGY VK = 7.722608537158121E-001
CENTROB. ENERGY = 1.906186930356347
KINETICH. ENERGY = 15.485397205276890
POTENS. ENERGY = -26.881452254540800

POLNAY ENERGY ST = -8.717607265191750
POLNAY ENERGY SH = -8.717607265145604

The results for different N practically coincide and their difference with a value of about 1 keV shows the saturation of the process of the convergence calculation for the three-body energy. For the purposes of comparison, we give the experimental value of the three-body binding energy of -8.724 MeV of ^{7}Li [195]. This differs from the energy obtained above by only 6–7 keV.

For the mass and charge radii, values of 2.79 fm and 2.52 fm, respectively, were obtained. The last of these appears significantly greater than the values of the experimental data: 2.39(3) fm and 2.35(10) fm [195]. However, here, as shown in [80], using the ^{2}Hn potential leads to an overestimation of the tritium radius (see Table 3.1.2), which also has an influence on the radius of ^{7}Li. As such, the deuteron cluster needs to be deformed, both in the tritium kernel and in ^{7}Li, because, in its free state,

deuteron presents a very friable system. To obtain the correct charge radius of ^{7}Li, equal to 2.39(3) fm, it is necessary to reduce the radius of the deuteron cluster by approximately 30 % from the original, as has been described previously for a tritium nucleus [80], and to accept it as being approximately equal to 1.4 fm.

The value of -35.5 mb was obtained in the calculations given above for the quadrupole moment of ^{7}Li, which is not much less than the values in the known data: -40.7(8) mb [195] and -36.6(3) mb [196]. The normalizations NORM and NN of the wave function, obtained in two different ways and equal in both cases to a unit with fine precision, are given in the results of the calculation. The accuracy to which the eigenvectors are determined is not less than 10^{-8} and the residuals of triangularization NEV-TRI and calculation of the NEV-DET determinant are at the level of 10^{-12}–10^{-13}.

In the considered configuration of the cluster layout, there is the possibility of variation in the parameters of the P_0 potential in the ^{4}He^{2}H channel, because of large errors in the elastic scattering phase shifts. This allowed us to compensate while not accounting for other orbital configurations, i.e. a single-channel model, and to obtain the correct binding energy of the nucleus. At the same time, this configuration clearly allocates the ^{4}He^{3}H structure of ^{7}Li, which has the highest probability of existence [80,197]. Therefore, the additional variation of the P_0 parameters of the potential allows us to specify the binding energy of ^{7}Li having been brought into good agreement with the experimental value.

In the conclusion of this paragraph, we will pay attention to the subsequent lines of the list given above as

E = -8.7176 0726 51 69926

and

POLNAY ENERGY ST = -8.7176 0726 51 91750
POLNAY ENERGY SH = -8.7176 0726 51 45604

showing the three-body binding energy of ^{7}Li in the calculations given above. The difference in the numerical values of this energy shows the accuracy to which it is decided by different methods, with an order of $\varepsilon \sim 10^{-10}$ MeV.

Let us note that the modern value of the deuteron radius is equal to 2.1402(28) fm [75], while for ^{4}He it is equal to 1.6753(28) fm [143], which is slightly more than the values 1.97 fm and 1.67 fm [76-78,192] used here. The most modern value for the charge radius of ^{7}Li is equal to 2.4017(281) fm [143] or 2.4173(280) fm, as given in [198]. However, these results for

the three-body model were obtained by us in the late 1990s [199] and therefore slightly older values of all cluster radiuses were used here.

3.2 Three-body model of ^{9}Be

Let us move on to considering ^{9}Be in the model of the three-body cluster ^{4}He^{3}H^{2}H. Let us assume that there are ^{3}H^{2}H clusters at the base of a triangle of three particles (particles 23), with the orbital moment of relative movement $\lambda = 0$ and spin 1/2, i.e. only the doublet status of these clusters is considered. ^{4}He (particle 1) is located at the top of the triangle and its location is relative to the center of mass of the two-cluster system defined by the orbital moment l.

The total spin of the system of three particles of the orbital moment $\boldsymbol{L} = \boldsymbol{l} + \boldsymbol{\lambda}$ is equal to 1 and is considered equal to 1/2, and can be obtained, for example, from the combination $l = 1$ and $\lambda = 0$ ($l = l_{\alpha t} + l_{\alpha d}$) at $l_{\alpha t} = 1$ и $l_{\alpha d} = 0$. Here, it is supposed that this orbital configuration dominates in the considered ^{4}He^{3}H^{2}H model, i.e. the single-channel three-body model of this nucleus is also considered. In the case of such a configuration of clusters, the total moment of the $\boldsymbol{J} = \boldsymbol{L} + \boldsymbol{S}$ system is equal to $3/2^{-}$ and $1/2^{-}$, the first of which corresponds to the GS of ^{9}Be.

3.2.1 Potentials and scattering phase shifts

In the calculations, the binary intercluster potentials for the ^{4}He^{3}H and ^{4}He^{2}H systems with a repulsion core and forbidden state in the ^{3}H^{2}H channel of usual form are used (1.2.1). The parameters of the pair intercluster potentials are given in the first six columns of Table 3.2.1. In the seventh column, the channel systems of the ^{4}He^{3}H binding energy are given for ^{7}Li and the ^{4}He^{2}H channel for ^{6}Li; in the eighth column, the mean square charge radii of the bound states of these particle couples are given; and in the ninth column, the dimensionless asymptotic constants of the bound states in two-body channels with the Whittaker function are found (1.2.3).

The parameters of the potentials are used to precisely reproduce the corresponding experimental elastic scattering phase shifts, as shown further in figs. 3.2.1, 3.2.2, and 3.2.3.

In the capacity of the potential ^{3}H^{2}H cluster system, pure interactions according to Young tableaux [183] are used; the results of the calculation of phase shifts with such potentials are represented in Fig. 3.2.1 by a solid line. The error band of the determination of pure ^{3}H^{2}H phase shifts [183], which comes out from the experimental data described in [200], is shown by the dashed line in Fig. 3.2.1. The points and squares show the scattering

phase shifts taken from the experimental data and mixed according to Young tableaux, which are also given in [200]. The circles and open squares describe the RGM (resonating group method) of calculation of the mixed scattering phase shifts [201].

Table 3.2.1. The parameters of the potentials in binary cluster systems and the main characteristics of the bound states.

System	$^{2S+1}L_J$	V_0, MeV	γ, fm^{-2}	V_1, MeV	δ, fm^{-2}	E, MeV	R_z, fm	C_W
^{4}He^{3}H	$^2P_{1/2}$	-85.82	0.13	90.0	0.2	-1.989	2.6	3.86(1)
^{3}H^{2}H	$^2S_{1/2}$	-44.5887	0.15	4.5	0.015	–	–	–
^{4}He^{2}H	$^3S_1$	-71.91	0.15	70.0	0.2	-1.474	2.66	3.27(1)

The ^{3}H^{2}H potential used for analysis of the peripheral repulsion contains the bound forbidden state at an energy of -11.49 MeV. We did not manage to find other parameters of the potential, i.e. we were unable to find the bound forbidden level using which it would be possible to describe the pure doublet $^2S_{1/2}$ phase shift of ^{3}H^{2}H elastic scattering. This form of interaction, with a very small improvement in the depth of the ^{3}H^{2}H potential by 0.0887 MeV, previously fixed on the scattering phase shifts [80], allows us to obtain the correct value of the three-body binding energy of ^{9}Be. Thus, the depth of this potential was changed to give the best description of the binding energy of ^{9}Be in the three-body channel; this change resulted in a value of 0.0877 MeV.

For the ^{4}He^{3}H systems, the potential of the first excited $^2P_{1/2}$ state without the forbidden bound level is used, the phase shift of which is shown by the solid line in Fig. 3.2.2. This successfully describes the scattering phase shift [202,203] and gives what appears to be the best description of the characteristics of ^{9}Be in the three-body model, in comparison to the $^2P_{3/2}$ potential, the phase shift of which is shown in Fig. 3.22 by the dashed curve. Thus, on the basis of these results, it is necessary to consider that the cluster ^{4}He^{3}H system is in ^{9}Be in a virtual excited $^2P_{1/2}$ state, but not on the basic $^2P_{3/2}$ level. Perhaps, in the future, this result can be checked by other independent methods or approaches.

The potential in the ^{4}He^{2}H system, which offers the best way to describe the characteristics of the bound state of ^{6}Li in the ^{4}He^{2}H model, is specified in Table 3.2.1 and has no FS. The description of the $^3S_1$ scattering phase shift [187–191] is shown in Fig. 3.2.3 by the solid line, together with

extraction from the experimental data of the scattering phase shifts presented by the points.

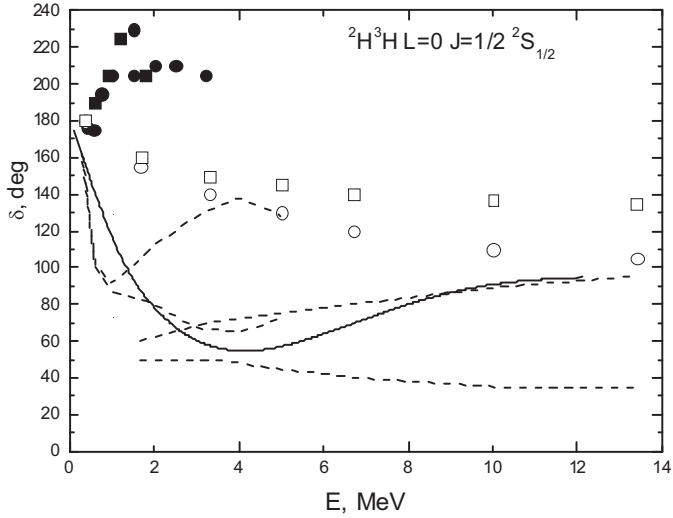

Fig. 3.2.1. The pure phase shifts of $^3H^2H$ elastic scattering for the *S* wave. The solid line describes the results of calculation of the phase shift with a potential from Table 3.2.1 and the dashed line gives the error band in determining pure phase shifts [183], resulting [200] from the experimental data. The points and squares represent the scattering phase shifts taken from the experimental data in [200]. The circles and open squares give the RGM calculations of the scattering phase shifts [201].

3.2.2 The three-body results and photo cross sections

Below, we provide a section of the computer program, described in the previous paragraph of this chapter, that sets out the characteristics of clusters and pair potentials.

```
! - - - - - - - - - - - - - - - - - - - - - - - - - - - - - - - - - - - - - -
Z1=2.0D0
Z2=1.0D0
Z3=1.0D0
M1=4.0D0
M2=3.0D0
M3=2.0D0
```

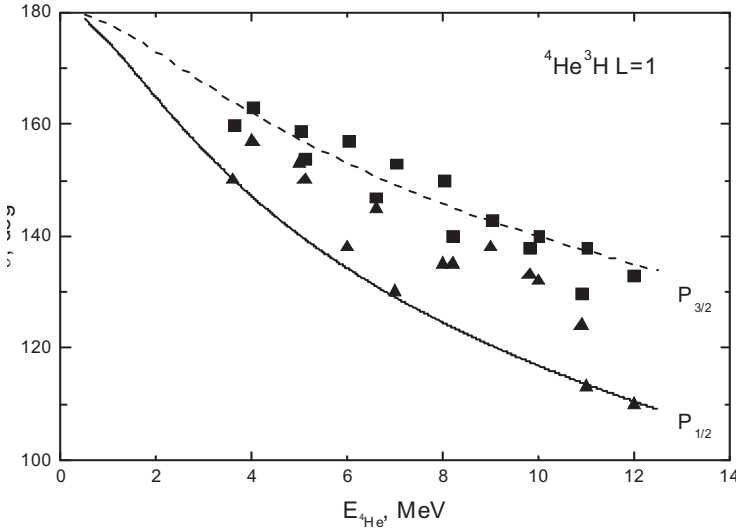

Fig. 3.2.2. The phase shifts of ^{4}He^{3}H elastic scattering for the P wave. The triangles represnts $P_{1/2}$ and the squares represent $P_{3/2}$ scattering phase shifts taken from the experimental data [202,203].

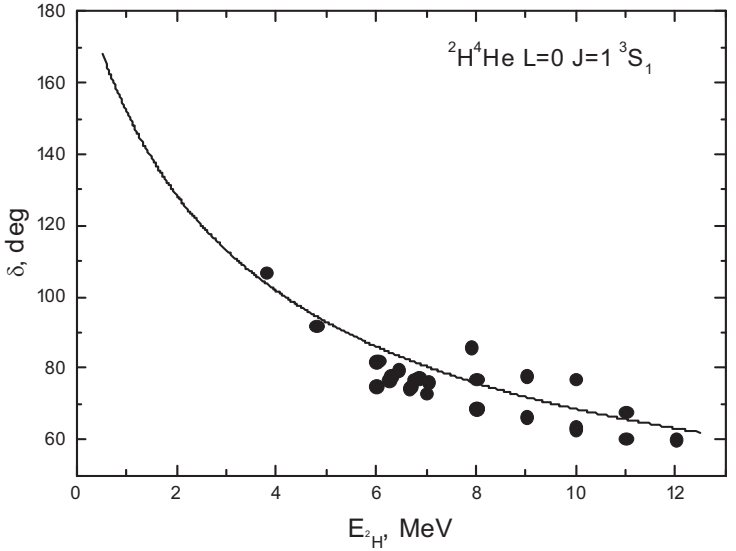

Fig. 3.2.3. The phase shifts of ^{4}He^{2}H elastic scattering at $L = 0$. The points describe the experimental data in [187-191].

```
RK1=1.670D0
RK2=1.70D0
RK3=1.960D0
RM1=1.670D0
RM2=1.70D0
RM3=1.960D0

! 1 - AL; 2 - T; 3 - D;    L  -  AL-T - 1, AL-D -0, D-T - 0
! D-T
V231=-44.5887D0      ; ! J= 1  ; L=0
R231=0.150D0
V232=4.50D0
R232=0.0150D0

! AL-D
V131=-71.90D0    ; ! J=1/2 ; L=0
R131=.150D0
V132=70.0D0
R132=0.20D0

! AL-T
V121=-85.820D0    ; ! J=1/2 ; L=1
R121=.130D0
V122=90.0D0
R122=0.20D0
! - - - - - - - - - - - - - - - - - - - - - - - - - - - - - - - - - - - - -
```

Using the pair intercluster potentials described above, we find the three-body wave function and the parameters and coefficients of decomposition at $N = 10$, which are given in tables 3.2.2 and 3.2.3. The binding energy of ^{9}Be along with the normalization of the WF Nor and its charge radius of R_z are given in Table 3.2.4. As can be seen in the these tables, the characteristics of ^{9}Be obtained are in good agreement with the available experimental data and the normalization of the three-body WF is almost equal to the unit.

Table 3.2.2. The α_i and β_i parameters of the decomposition of the three-body wave function (1.5.4) of ^{9}Be in the three-body model.

i	α_i	β_i
1	3.273095667111755E-001	8.983828859473847E-002
2	3.172872902170442	1.207723068311927E-001
3	1.844963898289113E-001	5.507018219497912E-002
4	9.153345511558431E-002	1.025123206313353E-001
5	2.213721392830491E-001	3.620573882275837E-001
6	2.269904002428514E-001	4.017242168731691E-001
7	1.985961231123472E-001	1.634388187790707E-001
8	5.073985961415315E-001	4.769549654021469E-001
9	5.124708157837092E-001	4.828596792375761E-001
10	3.843254062764651E-001	2.094550079909185E-001

Table 3.2.3. The C_i coefficients of decomposition of the three-body wave function (1.5.4) of ^{9}Be in the three-body model.

i	C_i
1	2.564677848067949E-002
2	-2.825587985872606E-003
3	3.379570860934880E-003
4	1.204452338550613E-002
5	-6.029327933110736E-001
6	4.606318693160417E-001
7	1.677085370227155E-001
8	-3.310475484431805
9	3.189208283959322
10	1.415768198190696E-001

Table 3.2.4. Some characteristics of ^{9}Be in the three-body cluster model.

Characteristics	Calculation	Experiment
E , MeV	-19.1632	-19.1633 [204]
R_z , fm	2.56	2.519(12) [204]
Nor.	9.999999999999867E-001	

The experiment described in [204] achieves good agreement with the calculation of the three-body energy of ^{9}Be; because there are big errors and uncertainties in the ^{3}H^{2}H scattering phase shifts and the creation of pure phase shifts leads to ambiguities, the depth of this potential varied a little. The initial depth of the attracting part with which the phase shift given in Fig. 3.2.1 is equal to V_0 = -44.5 MeV, while in discovering the three-body binding energy, a slightly bigger value V_0 = -44.5887 MeV was used. Such changes in the depth of the potential do not practically exert an impact on the elastic scattering phase shifts.

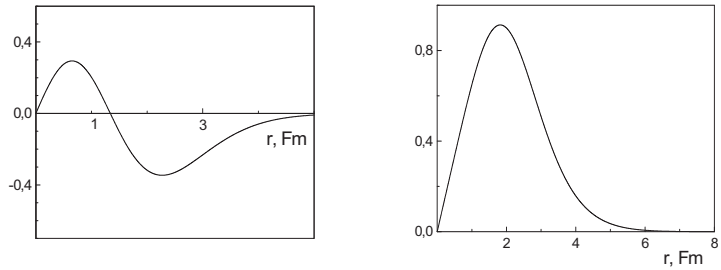

a b

Fig. 3.2.4. The radial functions of the relative movement of clusters in the ^{6}Li+^{3}H channel of ^{9}Be: *a* shows the ^{4}He^{4}Hen model and *b* gives the ^{4}He^{3}H^{2}H model.

Figs. 3.2.4a and b present a comparison of the radial ^{3}H+^{6}Li functions of the relative movement constructed for the ^{4}He^{4}Hen and ^{4}He^{3}H^{2}H models. In using the potentials in the single-channel model for ^{4}He^{3}H^{2}H, the ^{9}Be brings us to the node-free 1P WF of the relative movement. At the same time, the ^{4}He^{4}Hen model, constructed with the pair potentials of deep attraction containing the FS, gives the nodal 3P wave function. The solid curve in Fig. 3.2.4a corresponds to the resulting wave function. The two-body wave functions ^{3}H+^{6}Li of the channel are further used in the calculation of the cross sections of the photodisintegration of ^{9}Be (^{9}Be(γ,^{3}H)^{6}Li)

[205], presented in figs. 3.2.5a and b, together with the experimental data in [206].

It should be noted that the shapes of the photodisintegration cross section calculated in these two models do not practically differ, although there are some quantitative divergences. This is fully explained by the similarity of the "tail" of the two different wave functions at large distances, in turn, leading to similar results at the relatively low energies for the photodisintegration of ^{9}Be in the two-body ^{3}H^{6}Li channel considered.

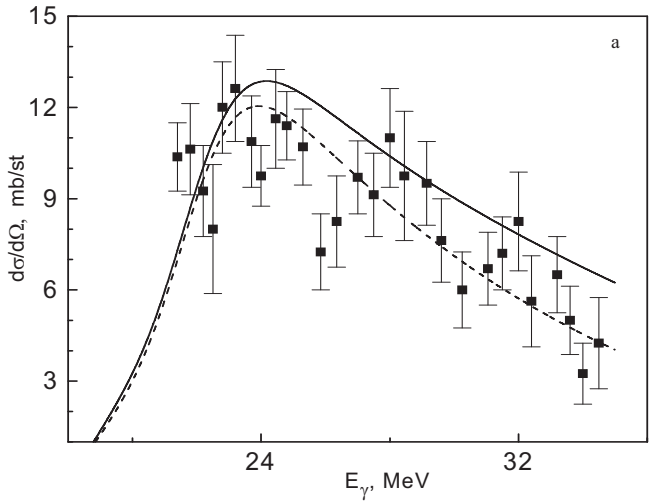

Fig. 3.2.5a. The differential cross sections of the ^{9}Be(γ,^{3}H)^{6}Li process. The squares represent the experiment in [206]. In the theoretical calculation for the n^{4}He^{4}He model, the dashed line shows the dipole *E1* transition and the solid curve describes the total cross section.

Thus, within the considered variation methods, new results for the three-body ^{4}He^{3}H^{2}H cluster model of ^{9}Be are obtained [205]. In these calculations, a non-orthogonal variation basis, with the independent variation of all parameters of the decomposition of the WF by the Gaussian functions and the intercluster potentials, which are pure in certain cases according to analysis with Young tableaux and agree with the elastic scattering phase shifts in two-body systems, is used.

It appears that the variants of the interaction potentials between the clusters lead to the correct binding energy of ^{9}Be, to the description of some other characteristics in the three-body cluster channel, and to a reasonable explanation of the experimental differential cross sections of the considered

response of the photodisintegration of ^{9}Be in the two-body ^{3}H^{6}Li channel.

Further development of the theoretical approaches in this direction requires the solution of the three-body problem with the coupling of the channels, i.e. taking into account the various partial waves in each two-body shoulder of the three-body system [205]. However, the single-channel approach considered here allows us to obtain the correct cross section of the process of photodisintegration in the low energy range. Therefore, it is quite natural to execute the calculations further at energies of the γ-quantum tending to zero. Thus, we consider the region of astrophysical energies as these are of most interest to problems of nuclear astrophysics and thermonuclear processes in the universe.

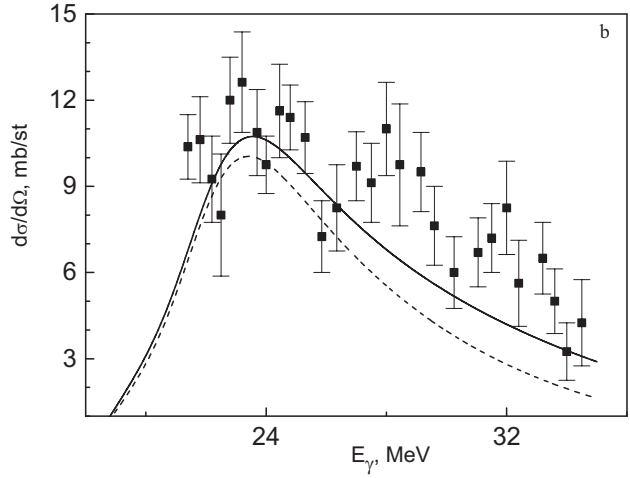

Fig. 3.2.5b. For the differential cross sections of the ^{9}Be(γ,^{3}H)^{6}Li process, the squares describe the experiment [206]. In the theoretical calculation for the ^{4}He^{3}H^{2}H model, the dashed line represents the dipole *E1* transition and the solid curve shows the total cross section.

3.3 The three-cluster structure of ^{11}B

Let us consider the possibility of using the three-body model for the following odd light atomic ^{11}B nucleus, which can be presented as a three-body ^{4}He^{4}He^{3}H structure. The moment of the ground state of ^{11}B is equal to $3/2^{-}$ and can be formed at $\lambda = 0$ and $l = 1$ as the ^{4}He moment is equal to zero, and ^{3}H has half-integer spin of 1/2. In the model, the triangle basis still consists of particles 2 and 3, with two α particles and zero relative moment

λ . The orbital moment l is equal to 1 and can be obtained from the $l_{12} = 1$ and $l_{13} = 1$ combination. We should remember that here $l = l_{12} + l_{13}$ and the moments of l_{12} and l_{13} are the orbital moments between particles 1 and 2, and 1 and 3, and particle 1, and lying at the top of the triangle is the nucleus ^{3}H.

In the capacity of intercluster potentials, the ^{4}He^{3}H interactions in the ground $^2P_{3/2}$ state of ^{7}Li are used. We suppose that this orbital configuration dominates in the considered single-channel ^{4}He^{4}He^{3}H model. Of course, in the multichannel variant of the three-body model, the contribution, for example, of the $l_{12} = 1$ and $l_{13} = 0$ or $l_{12} = 0$ and $l_{13} = 1$ configurations, which also lead to $l = 1$, is possible.

Let us remember that (item 1.6), in the calculations, at each value of the variation α_i and β_i parameters, which vary independently from each other, we find some energy of the system E, giving the zero determinant. Changing these parameters, we carry out the search for the minimum three-body energy of E, which is the eigen energy of the variation problem. Then, we increase the dimension of the basis N and we repeat all calculations until the size of the eigenvalue, i.e. the E_N binding energy, at the next dimension of basis N does not begin to differ from the previous E_{N-1} value at size ε, which is usually set at the level of 1.0–2.0 keV. This minimum energy will also be the real binding energy of the three-particle system, i.e. the binding energy of a nucleus in such a model, and the dimension of the non-orthogonal Gaussian basis usually does not exceed 10–12 [207].

3.3.1 Potentials and phase shifts

In the present calculations for the ^{4}He^{3}H and ^{4}He^{4}He systems, the binary intercluster potentials with the repulsion core (1.2.1), the parameters of which are specified in Table 3.3.1, are used. The scattering phase shifts corresponding to such potentials are shown in figs. 3.2.2 and 3.3.1 by the dashed lines. The experimental data for the ^{4}He^{4}He elastic scattering are taken from [84,86,208,209].

Table 3.3.1. Parameters of pair intercluster potentials.

System	$^{2S+1}L_J$	V_0, MeV	γ, fm^{-2}	V_1, MeV	δ, fm^{-2}
^{4}He^{4}He	$^1S_0$	-204.0	0.2025	500.0	0.36
^{4}He^{3}H	$^2P_{3/2}$	-102.317	0.15	90.0	0.2

The ^{7}Li binding energy in the ^{4}He^{3}H channel of -2.467 MeV, with the potential from Table 3.3.1 and integer mass values of particles, accurately

coincides with the experimental value [195]. The charge radius is equal to 2.40 fm and the asymptotic constant at an interval of 7–16 fm is equal to $C_w = 3.57(1)$ [65,80].

Table 3.3.2. The convergence of the three-body *E* binding energy of ^{11}B depends on the number of *N* Gaussian functions in the decomposition of the WF. The experimental value of ^{11}B binding energy in this channel is equal to -11.131 MeV [210].

N	4	6	8	10	12
E, MeV	-10.832	-10.985	-11.070	-11.072	-11.079

As the charge and mass radius of a triton the value 1.70 fm and for ^{4}He the value 1.67 fm [76-78] were accepted. Let us remember that a modern value of the charge radius of ^{7}Li is equal to 2.4017(281) fm [143]:

$$\chi_L(r) = C_w W_{-\eta L+1/2}(2k_0 r). \qquad (3.3.1)$$

In Fig. 3.3.1, the $^1S_0$ phase shift of ^{4}He^{4}He elastic scattering with the Ali-Bodmer potential is shown by solid lines, giving a slight underestimation of the three-body binding energy of the ^{4}He^{4}He^{3}H system in ^{11}B.

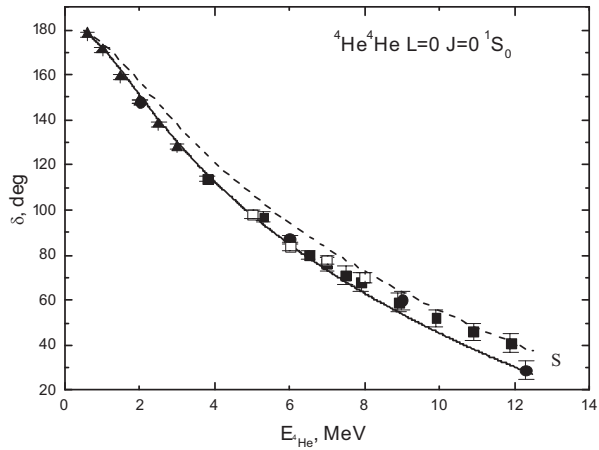

Fig. 3.3.1. ^{4}He^{4}He elastic scattering phase shifts at $L = 0$. The solid line gives the result for the Ali-Bodmer [208] potential and the dashed line gives its modified variant from Table 3.3.1. The experimental data in the figure are taken from: [208] – ●, [84] – ▲, [209] – □, [86] – ■.

It takes a little, approximately 7 %, to increase the depth of its attractive part (see Table 3.3.1) and to obtain an almost correct value of the binding energy, the convergence of which is shown in Table 3.3.2 based on the number of the members of the decomposition of the wave function. The phase shift of such a potential is presented in Fig. 3.3.1 by the dashed curve and is slightly above the phase shifts taken from the experiment on ^{4}He^{4}He elastic scattering. The necessity of changing the depth of the ^{4}He^{4}He potential is likely connected to the single-channel of the model used here, in which only one admissible orbital configuration with an intercluster $^2P_{3/2}$ potential of the bound ^{4}He^{3}H state is considered at $l = 1$ for l_{12} and $l_{13} = 1$, the parameters of which are specified in Table 3.3.1. Accounting for other ^{4}He^{3}H configurations, also with $l = 1$, but at $l_{12} = 1$ and $l_{13} = 0$ or $l_{12} = 0$ and $l_{13} = 1$, we can increase the three-body binding energy; it is not necessary to change the depth of the ^{4}He^{4}He potential.

3.3.2 Three-body results

3.3.2.1 First variant of the intercluster potentials

Below we give a section of the program, fully printed out in subitem 3.1.2. The characteristics of clusters and potentials and their interaction are written as follows.

```
! - - - - - - - - - - - - - - - - - - - - - - - - - - - - - - - - - - -
Z1=1.0D0
Z2=2.0D0
Z3=2.0D0
M1=3.0D0
M2=4.0D0
M3=4.0D0
…
RK1=1.7D0
RK2=1.67D0
RK3=1.670D0
RM1=1.7D0
RM2=1.67D0
RM3=1.670D0
…
! 1 - T; 2 - AL; 3 - AL;   L  -  AL1-AL2 - 0, AL1-T - 1, AL2-T - 1
! AL-AL
V231=-204.0D0      ; ! J= 0  ; LAM=0
```

```
R231=0.2025D0
V232=500.0D0
R232=0.36D0
…
! AL-T
V131=-102.317D0 ;    ! J=3/2; L=1
R131=0.15D0
V132=90.0D0
R132=0.2D0
…
! AL-T
V121=V131    ;  ! J=3/2; L=1
R121=R131
V122=V132
R122=R132
! - - - - - - - - - - - - - - - - - - - - - - - - - - - - - - - - - - - -
```

The parameters and coefficients of the decomposition of the wave function of the system $^{4}He^{4}He^{3}H$ for $N = 10$ in ^{11}B are specified below and the results for the energy are shown above in Table 3.3.2.

E = -11.072136455745790 (N = 10)

N	ALPHA (α)	BETA (β)
1	7.731577265613154E-002	1.240840193536184E-001
2	1.641040105068961E-001	2.285876535575549E-001
3	4.870741010024022E-001	1.536884862684963E-001
4	2.513045621382256E-001	3.041700707766410E-001
5	2.033807929862554E-001	3.450251748941237E-001
6	6.368494296100554E-001	1.898054241645994E-001
7	3.430614492885307E-001	1.441809735418989E-001
8	3.520135247366762E-001	2.289195177072528E-001
9	2.131971494536152E-001	3.314403264542553E-001
10	4.968108631879107E-001	2.048954900045679E-001

SUM(H*SV-E*L*SV) FROM SV = -1.776356839400251E-013
NORM = 9.999999999998579E-001
NEV-DET = 1.364242052659392E-012

N	SV
1	7.141139314701980E-002
2	6.873184414416353E-001
3	7.416580078033560E-001
4	4.203984406616693
5	3.779698938600395
6	-1.470993620114665
7	-6.275457436460156E-001
8	-3.525509423084515
9	-7.047436459053254
10	3.191334856523210

N = 9.999999999999705E-001
RM = 2.633871831198857
RZ = 2.630340587104462

COUL. ENERGY VK = 4.106613183539739
12 = 1.219823574100133
13= 1.219823574100133
23= 1.666966035339474
CENTROB. ENERGY = 4.025371560588050
KINETICH. ENERGY = 8.030009418604076
POTENS. ENERGY = -27.234130618489780
POLNAY ENERGY ST = -11.072136455757920
POLNAY ENERGY SH = -11.072136455745180

Similar results are achieved for the energy and WF at the dimension $N = 12$.

E = -11.079033093916390 (N = 12)

N	ALPHA (α)	BETA (β)
1	6.409144140489247E-002	1.019587659674352E-001
2	1.258066165364320E-001	1.811335435670906E-001
3	5.502163968570325E-001	1.563736148998969E-001
4	1.093264054668316E-001	2.915855267598159E-001
5	1.333280173011495E-001	4.867098271947788E-001
6	8.577841282629973E-001	1.559124765668210E-001
7	2.427745646298275E-001	9.280370272042079E-002
8	4.374090344872209E-001	1.607892257131171E-001
9	2.506356884255520E-001	3.365880418027703E-001
10	5.992286208956132E-001	1.732142250126302E-001

11 2.513360250891818E-001 3.505196617789699E-001
12 9.123756893621239E-001 1.549639056362407E-001
SUM(H*SV-E*L*SV) FROM SV = 4.089173444299377E-012
NORM = 1.000000000000028
NEV-DET = 1.818989403545857E-012

N	SV
1	2.405128330550160E-002
2	2.838460999953977E-001
3	3.355552135939775
4	6.347242717086900E-002
5	-7.943048747668001E-002
6	-5.622161796232756
7	-1.975249769693670E-002
8	-2.913336286105724
9	-1.743989588892319
10	9.471131965767997E-001
11	1.677487262418139
12	4.030809374250345

N = 1.000000000000014
RM = 2.635529943243490
RZ = 2.631840422205140

COUL. ENERGY VK = 4.103278121515663
12 = 1.218338113251590
13 = 1.218338113251590
23 = 1.666601895012484
CENTROB. ENERGY = 4.011294763849525
KINETICH. ENERGY = 8.028619034600876
POTENS. ENERGY = -27.222225013883560
POLNAY ENERGY ST = -11.079033093917500
POLNAY ENERGY SH = -11.079033093917130

From this, it is clear that the errors in the search for the determinant NEV-DET are of the order of 10^{-12}, the total error of the search for the energy and eigenvectors determined by the expression *(H-EL)C* appears less than $4.1 \cdot 10^{-12}$, and the normalization of the obtained wave function differs from the unit only by the 12–14 sign after a comma.

3.3.2.2 Second variant of the intercluster potentials

It should be noted that calculation of the mean square radius results in a value that is slightly greater than the experimental value for the charge ^{11}B radius equal to 2.406(29) fm [143], in spite of the fact that the ^{7}Li radius in the ^{4}He^{3}H channel has the correct value. We need to pay attention to that fact that the radii of ^{7}Li (2.4017(281) fm) [143] and ^{11}B (2.406(29) fm) [143] practically coincide. It appears that, in the ^{4}He^{3}H configuration if ^{7}Li is in the ^{11}B three-body ^{4}He^{4}He^{3}H model, then it has to be slightly compressed, as earlier for the deuteron in ^{7}Li.

Therefore, we take the ^{4}He^{3}H potential with the parameters of the attractive part V_0 = -121.405 MeV and γ = 0.18 fm^{-2}, with no change in its repulsion (see tables 3.3.1 and 3.3.3). This leads to a ^{7}Li binding energy of -2.467 MeV with integer values of the mass of particles that completely coincide with the experimental value [195]. The charge radius is equal to 2.24 fm and the asymptotic constant at an interval of 5–15 fm has the value C_w = 2.58(1) [65,80]. In this potential, ^{7}Li is slightly deformed, i.e. it is compressed in comparison to its free state.

Table 3.3.3. New variant of the parameters of the pair potentials.

System	$^{2S+1}L_J$	V_0, MeV	γ, fm^{-2}	V_1, MeV	δ, fm^{-2}
^{4}He^{4}He	$^{1}S_0$	-193.0	0.2025	500.0	0.36
^{4}He^{3}H	$^{2}P_{3/2}$	-121.405	0.18	90.0	0.2

Furthermore, to obtain the correct value of the three-body energy, as described below, it is necessary to deform the ^{4}He^{4}He potential much less, i.e. to accept its depth of -193.0 MeV without changing its other parameters, as shown in Table 3.3.3. The phase shift of elastic scattering is described in Fig. 3.3.2 by the dashed curves and does not practically differ from the results for the standard of the Ali-Bodmer potential, shown by the solid line.

Further use of the phase shift of the ^{4}He^{3}H interaction potential is shown in Fig. 3.3.3, which, in comparison to the results presented in Fig. 3.2.2, passes slightly above and, in fact, on the upper bound of the phase shifts of ^{4}He^{3}H elastic scattering taken from the experimental data [202,203].

Let us present a section of the program in which the interaction potentials of the clusters are written as follows:

```
! - - - - - - - - - - - - - - - - - - - - - - - - - - - - - - - - - - - -
! 1 - T; 2 - AL; 3 - AL;   L  -  AL1-AL2 - 0, AL1-T - 1, AL2-T - 1
```

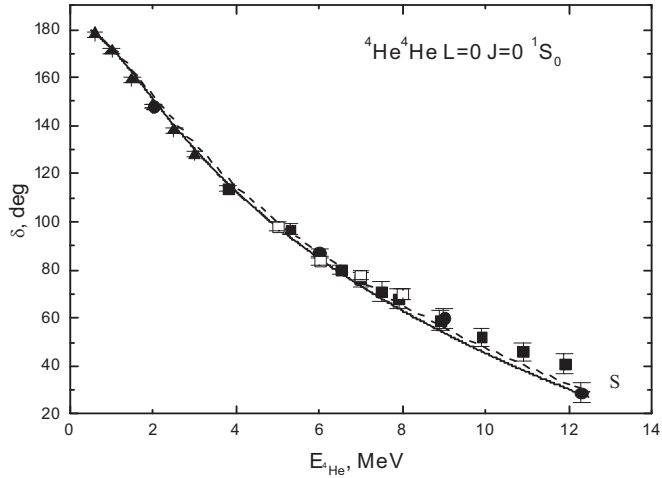

Fig. 3.3.2. The phase shifts of ^{4}He^{4}He elastic scattering at $L = 0$, with the solid line giving the results for the Ali-Bodmer [208] potential and the dashed line describing its modified variant in Table 3.3.3. The experimental data are taken from: [208] – •, [84] – ▲, [209] – □, [86] – ■.

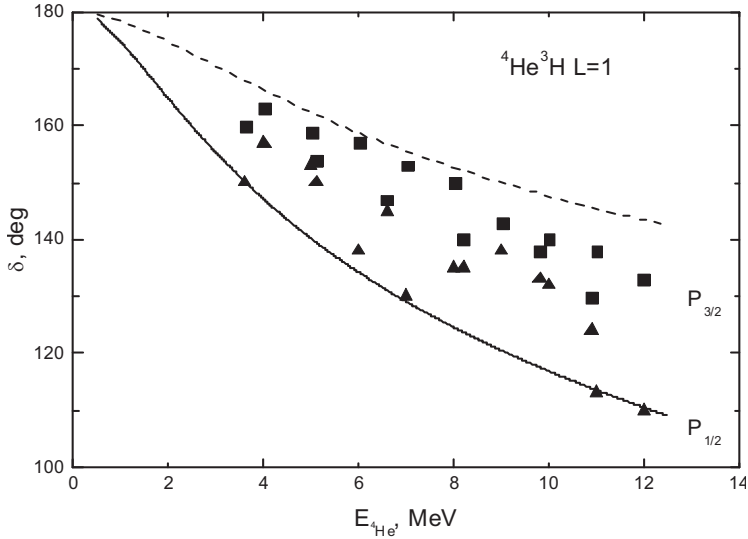

Fig. 3.3.3. The phase shifts of ^{4}He^{3}H elastic scattering for the *P* wave. The triangles and squares present the elastic scattering phase shifts taken from the experimental data [202,203]. The curves describe the calculations with different potentials, the parameters of which are shown in the figure and in Table 3.3.3.

```
! AL-AL
V231=-193.0D0      ; ! J= 0  ; LAM=0
R231=0.2025D0
V232=500.0D0
R232=0.36D0

! AL-T
V131=-121.405D0 ;    ! J=3/2; L=1
R131=0.18D0
V132=90.0D0
R132=0.2D0
…
! AL-T
V121=V131    ;  ! J=3/2; L=1
R121=R131
V122=V132
R122=R132
! - - - - - - - - - - - - - - - - - - - - - - - - - - - - - - - - - - - -
```

Below, we give the results of the calculation of the three-body binding energy of ^{11}B in the ^{4}He^{4}He^{3}H channel with the potentials described above for the 10 members of decomposition of the WF by the Gaussian functions.

E = -11.031463381093430

N	ALPHA (α)	BETA (β)
1	6.860823790482709E-002	1.372018518013886E-001
2	1.979200374955967E-001	1.975207162666516E-001
3	4.887720500875407E-001	1.729550202313665E-001
4	1.536806478562412E-001	3.328419037585270E-001
5	9.581401187947329E-002	4.647401165174852E-001
6	7.235261491934235E-001	2.130457228008369E-001
7	2.517628737184591E-001	1.646905851358956E-001
8	3.718525859440748E-001	2.263181658977888E-001
9	2.301200947513070E-001	3.053675821366754E-001
10	5.342732966940103E-001	2.386280212884875E-001

SUM(H*SV-E*L*SV) FROM SV = 1.456612608308205E-012
NORM = 9.999999999999014E-001
NEV-DET = 0.000000000000000E0

N	SV
1	5.144041160323528E-002
2	6.941910561622631E-001
3	5.424054031163350E-001
4	1.121880192698402
5	-1.131115274640460E-001
6	-8.746059242237850E-001
7	-5.773075026219299E-001
8	-1.357323308702923
9	-1.431015963101069
10	1.939168998797320

N = 9.999999999999950E-001
RM = 2.545788338764759
RZ = 2.554149440825896

COUL. ENERGY VK = 4.549379683245643
12 = 1.434603714056763
13 = 1.434603714056763
23 = 1.680172255132118
CENTROB. ENERGY = 5.629493999635255
KINETICH. ENERGY = 9.387040848724377
POTENS. ENERGY = -30.597377914995690
POLNAY ENERGY ST = -11.031463383390410
POLNAY ENERGY SH = -11.031463383390960

The results of calculation for $N = 12$ give the following:

E = -11.032671516388140

N	ALPHA (α)	BETA (β)
1	6.866999434690753E-002	1.308910045752647E-001
2	1.149793056566817E-001	1.884387791693870E-001
3	5.539896465720190E-001	1.648434683949910E-001
4	1.528193850522205E-001	3.151598143556194E-001
5	1.052759959020325E-001	3.918444921609474E-001
6	8.827637468448799E-001	1.561502493903658E-001
7	2.403581793183441E-001	1.111462488829206E-001
8	5.436244156008828E-001	1.700073788396006E-001
9	2.569650583366106E-001	3.146550134272712E-001

10	5.752686749704641E-001	1.756637188474036E-001
11	2.882071283272155E-001	3.321865686346414E-001
12	9.046635125615116E-001	1.547378005133593E-001

SUM(H*SV-E*L*SV) FROM SV = -4.312994406063808E-012
NORM = 1.000000000006423
NEV-DET = 9.094947017729282E-013

N	SV
1	4.219506029644921E-002
2	6.537938394165033E-002
3	10.984160595778020
4	1.332911137207201
5	-1.904812220035353E-001
6	-16.076855570816770
7	-3.480370810845272E-002
8	-19.639156270511190
9	-3.254715851761231
10	11.029434819668920
11	1.864459157683097
12	13.879575716434890

N = 9.999999999999663E-001
RM = 2.545605920214188
RZ = 2.553862814168674
COUL. ENERGY VK = 4.545338040958250
12 = 1.432617674939411
13 = 1.432617674939411
23 = 1.680102691079429
CENTROB. ENERGY = 5.611694081091503
KINETICH. ENERGY = 9.392846392977125
POTENS. ENERGY = -30.582550036090190
POLNAY ENERGY ST = -11.032671521063310
POLNAY ENERGY SH = -11.032671521338680

From this, it is clear that even in this case the ^{11}B radii are approximately equal to 2.55 fm and appear much greater than the experimental values of 2.406(29) fm [143]. However, to obtain the correct binding ^{11}B energy, it is not practically required to deform the ^{4}He^{4}He potential and the pair ^{4}He^{3}H interaction can be coordinated with the scattering phase shifts, as shown in Fig. 3.3.3.

Of course, it is still possible to change the $^4He^3H$ potential; making it narrower will lead to a reduction in the ^7Li radius and, as a result, we can possibly obtain the correct ^{11}B radius. However, as is apparent in Fig. 3.3.3, at such a change in the potential it is not possible to correctly describe the phase shift of $^4He^3H$ elastic scattering from the experiment, which tends to see an increase in values with the increase in the depth of the potential, as shown in tables 3.3.1 and 3.3.3. This tendency is also clear when we compare figs. 3.2.2 and 3.3.3. In this sense, the second variant of the potentials considered here is optimal from the point of view of the minimum change in the parameters, which is well defined on the basis of the experimental scattering $^4He^4He$ phase shifts of the potential.

Meanwhile, such a variant of the potential allows us to maintain a reasonable form of the calculation of $^4He^3H$ scattering phase shifts, as shown in Fig. 3.3.3. On the other hand, it is always possible to consider that, because of the large three-body binding energy of ^{11}B, which is greater than the binding energy of a triton cluster in the $3N$ channel, its deformation is quite possible, i.e. there is a small compression with a decrease in the radius. Indeed, in a free state, the radius of tritium (^3H) appears greater than the radius of ^4He and if the tritium is strongly linked to the nucleus, its radius can decrease a little, having reduced thereby the ^{11}B radius.

It is clear from the results given above that the three-body model in this case allows us to obtain a reasonable description of some of the main characteristics of an odd ^{11}B nucleus. Though the available errors of the phase shift analysis result in uncertainty in the parameters of intercluster potentials, in their limits it is practically possible to construct the potentials giving quite acceptable results for the description of the main characteristics of ^{11}B.

In addition, the single-channel model also gives some uncertainty as to the reduction of the interaction potentials, which, as has already been described, allows only the consideration of two and three-channel configurations (based on the orbital moment) for some particle couples.

Conclusion

The alternative method for finding the eigenvalues of the generalized matrix problem, considered on the basis of variation methods of the solution of the Schrödinger equation using a non-orthogonal variation basis, avoids possible instabilities that arise during the application of the usual methods of solving the mathematical model, i.e. Schmidt orthogonalization [194].

Using the variation methods, new results for the three-body models of ^7Li, ^9Be, and ^{11}B nuclei have been obtained. A non-orthogonal variation

basis, independent variation of the parameters, intercluster potentials, pure Young tableaux, and coordinated elastic scattering phase shifts in two-body channels have all been used for this end. All these results allow us to correctly reproduce some of the experimental characteristics of the bound states of these nuclei and cross sections of some photonuclear processes.

Once again, our focus is on the three-body model, which allows us to carry out, in particular, an investigation of the pair intercluster potentials constructed on the basis of scattering phase shifts. The results obtained on this basis convince us of the expediency of further use of similar interactions for calculations relevant to the consideration of astrophysical characteristics of nuclear systems and thermonuclear reactions. For example, astrophysical *S*-factors or total cross sections of the processes of radiative capture of nucleons by light atomic nuclei at low and ultralow energies proceed in the universe at different stages of its evolution, formation, and development [4,79,80,184].

AUTHOR INFORMATION

Dubovichenko Sergey Borisovich - Laureate of the al-Farabi State Prize of the Republic of Kazakhstan (RK) in the field of science and technology; doctor of physical and mathematical sciences in the RK and the Russian Federation (RF), professor; vice-president and academician of the European Academy of Natural Sciences (EU); academician of the Peter's Academy of Sciences and Arts (RF); academician of the Russian Academy of Natural History (RF); academician of the International Academy of Informatization (RK); academician of the New York Academy of Sciences (US); member of the International Astronomical Union (IAU); member of the American Physical Society; member of the European Physical Society; laureate of the European Gold Medal, Gauss Medal, and Honorary Cross "Merit"; laureate of the State Scientific Stipend of RK; laureate of the International Soros Grant; laureate of the Komsomol Prize of Kaz.SSR 1984 (in the former USSR); chief of Kazakhstan department (www.eans.kz) of European Academy of Natural Sciences (www.eanw.org) in the field of physics and astrophysics; head of the nuclear astrophysics laboratory at Fesenkov Astrophysical Institute of the National Center of Space Research and Technologies of Aerospace Agency of Ministry Digital Development, Innovation and Aerospace Industry of RK.

E-mail: dubovichenko@mail.ru
Web-site: www.dubovichenko.ru

Fesenkov Astrophysical Institute - Observatory 23, Kamenskoe plato, 050020, Almaty, Republic of Kazakhstan, www.aphi.kz.

REFERENCES

1. Nichitiu F. Phase shift shifts analysis in physics. Romania: Acad. Publ. 1980. 416p.
2. Dubovichenko S.B. Primordial nucleosynthesis of the Universe. Third edition of the book “Selected method for nuclear astrophysics”, corrected and added. Germany, Saarbrucken: Lambert Academy Publ. GmbH&Co. KG. 2014. 668p.
3. Nichitiu F. Methods for determining resonances in phase shift shift analysis // Phys. Part. Nucl. 1981. V.12. №4. P.805-847.
4. Nemets O.F., Neudatchin V.G., Rudchik A.T., Smirnov Y.F., Tchuvil'sky Yu.M. Nucleon association in atomic nuclei and the nuclear reactions of the many nucleons transfers. Kiev: Naukova dumka 1988. 488p. (in Russian).
5. Dubovichenko S.B. Partial-wave analysis of elastic ^{4}He^{4}He scattering in the energy range 40-50 MeV // Phys. Atom. Nucl. 2008. V.71. P.65-74.
6. Hodgson, P.E. The Optical model of elastic scattering. Oxford: Clarendon Press 1963. 211p.
7. Marchuk G.I., Kolesov V.E. Application of numerical methods for the calculation of neutron cross-cross sections. M.:Atromizdat 1970. 304p.
8. Structure of atomic nuclei, Ed. Flugge S., Springer – Verlag, Berlin - Gottingen – Heidelberg, 1957.
9. Mott N., Massy H. The theory of atomic collisions, Oxford, Claren Press, 1965.
10. Dubovichenko S.B. Calculation method of the nuclear characteristics. Almaty: Complex 2006. 311p.; arXiv:1006.4947 [nucl-th]. (in Russian).
11. Brown G.E., Jackson A.D. The nucleon - nucleon interaction, North - Holland Pablishing Company, Amsterdam, 1976.
12. Bateman H., Erdeyn A. Math. library. Higher transcendental functions. V.2. M.: Nauka. 1968. 295p. (in Russian).
13. Lebedev N.N. Special functions and their applications. M.: Fiz.-Math. Lit. 1963. 358p. (in Russian).
14. Dubovichenko S.B. The program of calculation of actual nuclear scattering phase shift shifts // Bull. Kaz.GASA. Almaty. 2003. №9/10. P.220-227.

15. Dubovichenko S.B. The program of calculation of complex nuclear scattering phase shift shifts // Abstracts. Computational and Informational Technologies in Science. Engineering and Education. Kaz.NU Almaty. Kazakhstan. 6 - 10 October. 2004; http://www.ict.nsc.ru/ws/show_abstract.dhtml?ru+110+7834+S.
16. Popov B.A., Tesler G. S. Computer calculation of functions. Kiev: Naukova dumka. 1984. 598p. (in Russian).
17. http://physics.ucsc.edu/~peter/242/numerov.pdf .
18. Dubovichenko S.B. Numerical methods for the solution of the Schrödinger equation // Bull. AGU Fiz.-math. Ser. Almaty. 2004. №9. P.82-87.
19. Filchakov P.F. Numerical and graphical methods of Applied Mathematics. Live: 1870. 792p.
20. Dymarskiy Ya.S. et al. Programmer handbook. L.: 1963. 628p.
21. Polozhiy G.N. Math workshop. M.: Fiz. – math. Literature. 1960. 512p.
22. Danilina N.I. Numerical methods. M.: High School. 1976. 368p.
23. Dubovichenko S.B. Properties of the light nuclei in potential cluster model. Almaty: KazSU. 332p. KazINTI. 1998. №8172 Ka98. (in Russian).
24. Zaguskii V.L. Guide on numerical methods of solution of equations. M.: Fiz.-Mat. Lit. 1960. 215p. (in Russian).
25. Melent'ev P.V. Approximate calculus. M.: Fiz.-Mat. Lit. 1962. 387p. (in Russian).
26. Demidovich B.P., Maron I.F. Foundation of calculus mathematics. M.: Nauka. 1966. 664p. (in Russian).
27. Korn G., Korn T. Mathematical Handbook. New-York: McGraw Hill Book Co. 1968. 832p.
28. Dubovichenko S.B. Thermonuclear processes of the Universe. Second edition, revised and updated. Series "Kazakhstan space research" V.7. Almaty: A-tri 2011. 402p.; arXiv:1012.0877 [nucl-th]. (in Russian).
29. Kukulin V.I., Neudachin V.G., Smirnov Yu.F., El Khovari R. The role of the Pauli principle in the formation of optical potentials // Bull. Acad. Sci. USSR Ser. Fiz. 1974. V.38. P.2123-2128.
30. Voevodin V.V., Kuznetsov Y.A. Reference mathematical library. Matrix and calculations. M .: Fiz.-Math. Lit. 1984. 318p. (in Russian).
31. Dubovichenko S.B., Chechin L.M. Variational methods for solution of the Schrödinger equation // Bull. ASU Fiz.-Math. Ser. 2003. №.2 (8). P.50-58.
32. Brown G.E., Jackson A.D. The nucleon-nucleon interaction. Amsterdam: North-Holland Publ. Co. New York: American Elsevier Publ.

Co. 1976. 242p.
33. Dubovichenko S.B., Chechin L.M. Methods for solving of the generalized eigenvalue problem// Bull. Kaz.NPU. ser. phys.-math. Almaty. Kazakhstan. 2003. №1(7). P.110-115.
34. Dubovichenko S.B., Takibaev N.Zh., Chechin L.M Physical Processes in the Far and Near Space. Almaty: Daik-Press 2008. 228p.; arXiv:1012.1705 [nucl-th]. (in Russian).
35. Skornyakov L.A. Reference mathematical library. General algebra. Moscow: Nauka 1990. 591p. (in Russian).
36. Popov B.A., Tesler G. S. Computer calculation of functions. Kiev: Naukova Dumka 1984. 598p. (in Russian).
37. Demidovich B.P., Maron I.F. Foundation of calculus mathematics. Moscow: Nauka 1966. 664p. (in Russian).
38. Dubovichenko S.B., Chechin L.M. Modern methods of programming the actual physical problems // Book: Current problems and challenges of informatization in Kazakhstan. Almaty. Kazakhstan. 2004. P.358-390.
39. Janke - Emde - Losch. Tafeln hoherer funktionen, Stuttgard, 1960.
40. Luke Yu.L. Mathematical functions and their approximations. New York: Academic Press. 1975. 568p.
41. Melkanoff M. A fortran program for elastic scattering analysis with nuclear optical model // Univ. California Pres., Berkley, Los Angeles, 1961, 116p.
42. Lutz H.F., Karvelis M.D. Numerical calculation of coulomb wave functions for repulsive coulomb fields // Nucl. Phys., 1963, V.43, P.31-44.
43. Melkanoff M. Nuclear optical model calculations. // Meth. in Comput. Phys., Acad. press, N-Y, 1966, V.6, P.1-80.
44. Gody W.J., Hillstrom K.E. Chebyshev approximations for the coulomb phase shift shifts // Meth. Comput., 1970, V.111, P.671-677.
45. Smith W.R. Nuclear penetrability and phase shift shift subroutine // Usics Communs., 1969, V.1, P.106-112.
46. Froberg C.E. Numerical treatment of Coulomb wave functions // Rev. Mod. Phys., 1955, V.27, P.399-411.
47. Abramowitz M. Tables of Coulomb wave function, v.1, Washington, N.B.S., 1952, 141p.
48. Barnet A., et al. Coulomb wave function for all real η and ρ // Comput. Phys. Comm., 1974, V.8, P.377-395.
49. Danilov V. L. et al. Reference mathematical library. Mathematical analysis. Functions, limits and continued fractions. M.: Fiz.-Mat. Lit. 1961. 439p. (in Russian).

50. Kuznetsov D. S. Special functions. M.: Graduate School. 1965. 272p. (in Russian).
51. Dubovichenko S.B., Chechin L.M. Calculating methods of the Coulomb functions and scattering phase shift shifts // Bull. KazNPU. ser. phys.-math. Almaty. 2003. №1(7). P.115-122.
52. Handbook of mathematical functions. Edit. M. Abramowitz and I. Stegun. NBS., 1964.
53. Dubovichenko S.B., Zhusupov M.A. On calculation of the Coulomb wave functions // Interaction of radiative with matter. Alma-Ata. KazSU. 1980. P.99-104.
54. Dubovichenko S.B., Zhusupov M.A. The computation of Coulomb scattering phase shift shifts // Bull. Acad. Sci. KazSSR ser. phys.-math. 1981. № 6. P.24-26.
55. Reid R.V. Local phenomenological nucleon - nucleon potentials // Ann. Phys. 1968. V.50. P.411-448.
56. Dubovichenko S.B., Mazhitov M. Variation calculations of the ^{6,7}Li nuclei in cluster models with forbidden states // Bull. Acad. Sci. KazSSR ser. phys.-math. 1987. №4. P.55-64.
57. Neudatchin V.G., Kukulin V.I., Boyarkina A.N., Korennoy V.P. A microscopic substantiated optical potential for αt system including nucleon exchange // Lett. Nuovo Cim., 1972, V.5, P.834-838.
58. Neudatchin V.G., Kukulin V.I., Korotkikh V.L., Korennoy V.P. A microscopically substantiated local optical potential for $\alpha\alpha$ scattering // Phys. Lett., 1971, V.34B, P.581-583.
59. Kurdyumov I.V., Neudatchin V.G., Smirnov Y.F., Korennoy V.P. The high energy limit for the αd form factors in the ^{6}Li nuclei // Phys. Lett., 1972, V.40B, P.607-610.
60. Neudachin V.G., Smirnov Yu.F. Forbidden states in systems of two and three composite particles // Modern problems of optics and atomic physics. Kiev: Kiev State University. 1974. P.225-241.
61. Dubovichenko S.B., Dzhazairov-Kakhramanov A.V. Calculation of coulomb form factors of lithium nuclei in a cluster model based on potentials with forbidden states // Phys. Atom. Nucl. 1994. V.57. P.733-740.
62. Van Niftrik G., Brokman K., Van Oers W. Elastic scattering of 51 MeV alpha particles from helium // Congr. Int. Phys. Nucl. Patis. 1964, V.2, P.858-860.
63. Mukhamedzhanov A.M., Tribble R. E. Connection between asymptotic normalization coefficients, sub threshold bound states, and resonances // Phys. Rev. 1999. V.C59. P.3418-3424.

64. Angulo C. et al. A compilation of charged-particle induced thermonuclear reaction rates // Nucl. Phys. 1999. V.A656. P.3-183.
65. Plattner G.R., Viollier R.D. Coupling constants of commonly used nuclear probes // Nucl. Phys. 1981. V.A365. P.8-12.
66. Blokhintsev L.D., Borbey I., Dolinsky E.I. Nuclear vertex constants // Phys. Part. Nucl. 1977. V.8. P.1189-1245.
67. Kukulin V.I., Vorontchev V.T., Pomerantsev V.N Three body calculation of A=9 nuclei with super-symmetric αα potential // Few Body Syst. 1995. V.1. P.191-202.
68. Voronchev V.T. et al. The study of the structure and properties of nuclei with A = 9 in the framework of multi-cluster dynamic model 2α + N // Phys. Atom. Nucl. 1994. V.57. P.1964-1980.
69. Kukulin V.I. et al. Detailed study of the cluster structure of light nuclei in a three body model. I. Ground state of ^{6}Li // Nucl. Phys. 1984. V.A417. P.128-156.
70. Kukulin V.I. et al. Detailed study of the cluster structure of light nuclei in a three body model. II. The spectrum of low lying of nuclei with A=6 // Nucl. Phys. 1986. V.A453. P.365-388.
71. Kukulin V.I. et al. Detailed study of the cluster structure of light nuclei in a three body model. III. Electromagnetic structure of ^{6}Li // Nucl. Phys. 1990. V.A517. P.221-263.
72. Varshalovich D.A., Moskaliev A.N., Khersonsky V.K. Quantum theory of angular momentum. L.: Nauka 1973. 436p.
73. Dubovichenko S.B. Variational methods in the three-body model // Bull. Kaz.GASA. Almaty. Kazakhstan. 2003. №9(10). P.227-232.
74. Dubovichenko S.B. A computer program for calculating the characteristics of the nucleus ^{7}Li // Bull. Kaz.NTU. Almaty. Kazakhstan. 2004. №5. P.174-182.
75. http://physics.nist.gov/cgi-bin/cuu/Value?mud|search_for =atomnuc!
76. Juster F.P. et al. Tritium electromagnetic form factors // Phys. Rev. Lett. 1985. V.55. P.2261-2264.
77. Beck D.H. et al. Tritium form factors at low q // Phys. Rev. 1984. V.C30. P.1403-1408.
78. Sick I. Precise nuclear radii from electron scattering // Phys. Lett. 1982. V.B116. P.212-214.
79. Dubovichenko S.B., Uzikov Yu.N. Astrophysical *S*-factors of reactions with light nuclei // Phys. Part. Nucl. 2011. V.42. P.251-301.
80. Dubovichenko S.B. Light nuclei and nuclear astrophysics. Second Edition, corrected and enlarged. Saarbrucken: Lambert Academy Publ. GmbH&Co. KG. 2013. 316p.
81. Afnan I.R., Tang Y.C. Investigation of nuclear three-and four-body

systems with soft-core nucleon-nucleon potentials // Phys. Rev. 1968. V.175. P.1337-1345.
82. Krasnopolsky V.M., Kukulin V.I. A new many particle variational method // Czech. J. Phys. 1977. V.B27. P.290-304; Krasnopolsky V.M., Kukulin V.I. A stochastic variational method for few body systems // J. Phys. 1977. V.G3. P.795-811.
83. Dubovichenko S.B. Phase shift analysis of ^{4}He-^{4}He scattering at energies of 40–50 MeV // Rus. Phys. J. 2007. V.50. P.605-611.
84. Heydenberg N.P., Temmer G.M. Alpha-Alpha scattering at low energies // Phys. Rev. 1956. V.104. P.123-134.
85. Russel J.L. et al. Scattering of alpha particles from Helium // Phys. Rev. 1956. V.104. P.135-142.
86. Tombrello T.A., Senhouse L.S. Elastic scattering of Alpha particles from Helium // Phys. Rev. 1963. V.129. P.2252-2258.
87. Nilson R. et al. Alpha-Alpha particle scattering in the energy range 13 to 22.9 MeV // Phys. Rev. 1956. V.104. P.1673-1680.
88. Nilson R. et al. Investigation of excited states in ^{8}Be by α-particle scattering from Helium // Phys. Rev. 1958. V.109. P.850-860.
89. Steigert F.E., Samson M.B. Alpha-Alpha scattering from 12.88 to 21.62 MeV // Phys. Rev. 1953. V.92. P.660-664.
90. Chien W.S., Brown R.E. Study of the $\alpha\alpha$ system below 15 MeV // Phys. Rev. 1970. V.C10. P.1767-1784.
91. Bredin D.J. et al. The scattering of alpha particles by helium // Proc. Roy. Soc. 1959. V.A251. P.143-155.
92. Darriulat P., Igo G., Pugh H.G. Elastic scattering of alpha particles by helium between 53 and 120 MeV // Phys. Rev. 1965. V.137. P.B315-B323.
93. Conzett H.E. et al. Alpha-alpha scattering in the 36.8 to 47.3 MeV // Phys. Rev. 1960. V.117. P.1075-1079.
94. Igo G. Optical model analysis of the scattering of alpha particles from helium // Phys. Rev. 1960. V.117. P.1079-1085.
95. Burcham W.E. et al. Alpha-alpha scattering at 38/5 MeV // Nucl. Phys. 1957. V.3. P.217-220.
96. Burtebaev N. et al. Reprint № 88-01 INP. Alma-Ata. Kazakhstan. 1988. (in Russian)
97. Van Niftrik G. J.C. et al. Elastic scattering of 51 MeV alpha particles from helium // In “Compt. Congr. Int. Phys. Nucl.” Paris. 1964. V.2. P.858-860.
98. Dubovichenko S.B. A computer program for the phase shift analysis of the elastic scattering ^{4}He^{4}He // Book: Current problems and challenges of informatization in Kazakhstan. Almaty. Kazakhstan. 2004.

P.327-351.
99. Dubovichenko S.B., Burtebayev N., Dzhazairov-Kakhramanov A.V., Zazulin D.M. Phase shift shift analysis and potential description of the elastic $^{4}He^{12}C$ scattering at low energies // Uz. J. Phys. 2009. V.11. № 2. P.87-94.
100. Jones C.M. et al. The scattering of alpha particles from ^{12}C // Nucl. Phys. 1962. V.37. P.1-9.
101. Dubovichenko S.B. Photonuclear processes in the $^{4}He^{12}C$ channel of the ^{16}O nucleus in potential cluster models // Phys. Atom. Nucl. 1996. V.59. P.421-427.
102. Plaga R. et al. The scattering of alpha particles from ^{12}C and the $^{12}C(\alpha,\gamma)^{16}O$ stellar reaction rate // Nucl. Phys. 1987. V.A465. P.291-316.
103. Tilley D. R., Weller H. R., Cheves C. M. Energy levels of light nuclei A=16,17 // Nucl. Phys. 1993. V.A564. P.1-183.
104. Dubovichenko S.B. et al. Phase shift shifts analysis of elastic $^{4}He^{12}C$ scattering at energies 1.5-6.5 MeV // Dokl. Nat. Acad. Sci. Rep. Kazakhstan. 2008. №6. P.24-32.
105. Dubovichenko S.B. et al. Phase shift shifts analysis and potential description of elastic $^{4}He^{12}C$ scattering at low energies // Rus. Phys. J. 2009. V.52. P.715-724.
106. Dubovichenko S.B., Dzhazairov-Kakhramanov A.V. Astrophysical *S*-factor of the radiative $^{4}He^{12}C$ capture reaction at low energies // Bull. Russian Academy of Sciences: Physics. 2011. V.75. P.1517-1522; Dubovichenko S.B., Dzhazairov-Kakhramanov A.V. Astrophysical *S*-factor of the $^{4}He^{12}C$ radiative captures at low energies // Uz. J. Phys. 2009. V.11. №4. P.239-246; Dubovichenko S.B., Dzhazairov-Kakhramanov A.V. Astrophysical *S*-factor $^{4}He^{12}C$ radiative capture at low energies // Dokl. Nat. Acad. Sci. Rep. Kazakhstan. 2009. №2. P.9-15.
107. Salpeter E.E. Nuclear reactions in stars // Phys. Rev. 1957. V.107. P.516-525; Salpeter E.E. Nuclear Reactions in stars without hydrogen // Astrophys. Jour. 1952. V.115. P.326; Rolfs C. Nuclear reactions in stars far below the Coulomb barrier // Prog. Part. Nucl. Phys. 2007. V.59. P.43-50.
108. Dubovichenko S.B. Program for seek of phase shift shifts elastic scattering for particles with spin 1/2 // Bull. Kaz.NTU. Almaty. Kazakhstan. 204. №3. P.137-144.
109. Dubovichenko S.B. Phase shift shifts analysis of the differential cross cross section for elastic $p^{12}C$ scattering at astrophysical energies // Bull. Nat. Acad. Sci. Rep. Kazakhstan. ser. phys.-math. 2007. №6. P.58-67.

110. Jahns M.F., Bernstein E.M. Polarization in pα scattering // Phys. Rev. 1967. V.162. P.871-877.
111. Barnard A., Jones C., Well J. Elastic scattering of 2-11 MeV proton by ^{4}He // Nucl. Phys. 1964. V.50. P.604-620.
112. Brown R.I., Haeberli W., Saladin J.X. Polarization in the scattering of protons by α particles // Nucl. Phys. 1963. V.47. P.212-213.
113. Jackson H.L. et al. The ^{12}C(p,p)^{12}C differential cross cross section // Phys. Rev. 1953. V.89. P.365-269.
114. Jackson H.L. et al. The excited states of the ^{13}N nucleus // Phys. Rev. 1953. V.89. P.370-374.
115. Dubovichenko S.B. Phase shift anlysis of elastic p^{12}C scattering for astrophysical energies // Rus. Phys. J. 2008. V.51. P.1136-1143.
116. Zazulin D.M. et al. Scattering of protons from ^{12}C // The 6th Int. Conf. "Modern Problems of Nuclear Physics" Tashkent. Uzbekistan. 2006. P.127; Baktybaev M.K. et al. Elastic scattering of protons from ^{12}C, ^{16}O and ^{27}Al // The 4th Eurasia Conf. "Nucl. Sci. and its Appl." Baku. Azerbaijan. 2006. P.56.
117. Moss S.J., Haeberli W. The polarization of protons scattered by Carbon // Nucl. Phys. 1965. V.72. P.417-435.
118. Barnard A.C.L. et al. Cross cross section as a function of angle and complex phase shift shifts for the scattering of protons from ^{12}C // Nucl. Phys. 1966. V.86. P.130-144.
119. Lane R.O. et al. The Angular Distributions of Neutrons Scattered from Various Nuclei // Ann. Phys. 1961. V.12. P.135.
120. Ajzenberg-Selove F. Energy level of light nuclei A=13,14,15 // Nucl. Phys. 1991. V.A523. P.1-196.
121. Heil M. et al. The (n,γ) cross cross section of ^{7}Li // Astrophys. Jour. 1998. V.507. P.997-1002; Guimaraes V. and Bertulani C.A. Light radioactive nuclei capture reactions with phenomenological potential models // arXiv:0912.0221v1 [nucl-th] 1 Dec 2009; Masayuki Igashira, Toshiro Ohsaki Neutron capture nucleosynthesis in the Universe // Sci. Tech. Adv. Materials 2004. V.5. P.567-573; Nagai Y. et al. Fast neutron capture reactions in nuclear astrophysics // Hyperfine Interactions 1996. V.103. P.43-48; Liu Z.H. et al. Asymptotic normalization coefficients and neutron halo of the excited states in ^{12}B and ^{13}C // Phys. Rev. 2001. V.C64. P.034312(1- 5); Horvath A. et al. Cross cross section for the astrophysical ^{14}C(n,γ)^{15}C reaction via the inverse reaction // Astrophys. Jour. 2002. V.570. P.926-933.
122. Dubovichenko S.B. Thermonuclear processes of the Universe. Almaty: APHI 2010. 339p.;
http://nuclphys.sinp.msu.ru/thpu/index.html. (in Russian).

123. Dubovichenko S.B. Thermonuclear Processes of the Universe. First English edition. New-York: NOVA Sci. Publ. 2012. 194p.; https://www.novapublishers.com/catalog/product_info.php?products_id=31125.
124. Adelberger E.G. et al. Solar fusion cross cross sections. II. The pp chain and CNO cycles // Rev. Mod. Phys. 2011. V.83. P.195-245.
125. Dubovichenko S.B., Dzhazairov-Kakhramanov A.V. Astrophysical *S*-factor for $p^{12}C \rightarrow {}^{13}N\gamma$ radiative capture // Rus. Phys. J. 2009. V.52. P.833-840.
126. Henderson J.D. et al. Capture and elastic scattering of proton be ^{14}C // Phys. Rev. 1968. V.172. P.1058-1062.
127. Bartholomew G.A. et al. Capture radiative and neutrons from the bombardment of ^{14}C with protons // Can. Jour. Phys. 1955. V. 33(8). P.441-456; Bartholomew G.A. et al. Note on the T = 3/2 State in ^{15}N // Can. Jour. Phys. 1956. V. 34. P.147.
128. Dubovichenko S.B. Neutron Capture by Light Nuclei at Astrophysical Energies // Phys. Part. Nucl. 2013. V.44. P.803-847; Dubovichenko S.B., Dzhazairov-Kakhramanov A.V., Burkova N.A. Neutron radiative capture by ^{2}H, ^{6}Li, ^{7}Li, ^{12}C and ^{13}C at astrophysical energies // Int. J. Mod. Phys. 2013. V.E22. P.1350028(1-52); Dubovichenko S.B., Dzhazairov-Kakhramanov A.V., Afanasyeva N.V. Neutron radiative capture by ^{9}Be, ^{14}C, ^{14}N, ^{15}N and ^{16}O at astrophysical energies // Int. J. Mod. Phys. 2013. V.E22. P.1350075(1-53); Dubovichenko S.B., Dzhazairov-Kakhramanov A.V. Neutron radiative capture by ^{2}H, ^{6}Li, ^{7}Li, ^{12}C, ^{13}C, ^{14}C and ^{14}N at astrophysical energies // Book: The Universe Evolution. Astrophysical and Nuclear Aspects. New-York, NOVA Sci. Publ. 2013. P.49-108.
129. Dubovichenko S.B., Dzhazairov-Kakhramanov A.V. Astrophysical *S*-factors of radiative capture of protons on ^{2}H, ^{3}H, ^{6}Li and ^{12}C nuclei // Int. J. Mod. Phys. 2012. V.E21. P.1250039(1-44).
130. Itzykson C., Nauenberg M. Unitary groups: Representations and decompositions // Rev. Mod. Phys. 1966. V. 38. P. 95-101.
131. Dubovichenko S.B. Light nuclei and nuclear astrophysics. Second Edition, corrected and enlarged. Germany, Saarbrucken: Lambert Academy Publ. GmbH&Co. KG. 2013. 320p.
132. Dubovichenko S.B. Dzhazairov-Kakhramanov A.V. Astrophysical *S*-factor of the radiative $p^{2}H$ capture // Euro. Phys. J. 2009. V.A39. P.139-143; Dubovichenko S.B., Dzhazairov-Kakhramanov A.V. The $^{7}Li(n,\gamma)^{8}Li$ radiative capture at astrophysical energies // Ann. der Phys. 2012. V.524. P.850-861.

133. Dubovichenko S.B., Dzhazairov-Kakhramanov A.V. Phase shift shifts analysis of $p^{14}C$ scattering at energy $^2S_{1/2}$ resonance // Rus. Phys. J. 2015. V.58. №9. P.1258-1264
134. Igashira M. et al. Measurement of the $^{16}O(n,\gamma)^{17}O$ reaction cross cross section at stellar energies and critical role of nonresonance P-wave neutron capture // Astrophys. Jour. 1995. V.441. P.L89-L92; Igashira M., Kitazawa H. and Takaura K. Valence-neutron capture in the 434 keV $P_{3/2}$-wave resonance of ^{16}O // Nucl. Phys. 1992. V.A536. P.285-296.
135. Hickey G. T. et al. R-matrix and Phase shift-Shift analyses of neutron polarization measurements from $n^{16}O$ scattering // Nucl. Phys. 1974. V.A225. P.470-480.
136. Johnson C. H., Fowler J. L. Scattering of neutrons from ^{16}O in the 2.2- to 4.2-MeV energy range // Phys. Rev. 1967. V.162. P.890-899.
137. Fowler J.L., Cohn H.O. Oxygen differential neutron scattering and phenomenological nuclear potentials // Phys. Rev. 1958. V.109. P.89-93.
138. Okazaki A. Scattering of polarized neutrons by heavy nuclei // Phys. Rev. 1955. V.99. P.55-58.
139. Schouky I. Untersuchung der niveaustruktur von ^{17}O und ^{29}Si im bereich zwischen neutronenbindungsenergie und 12 MeV anregungs-energie // KFK-2503. 7708.
140. http://www-nds.iaea.org/exfor/exfor.htm .
141. Dubovichenko S.B. Calculation method of the nuclear characteristics. Nuclear and thermonuclear processes. Second edition, revised and updated. Germany, Saarbrucken: Lambert Acad. Publ. GmbH&Co. KG. 2012. 425p.;
https://www.lap-publishing.com/catalog/details //store/ru/book/978-3-659-21137-9/metody-rascheta-yadernyh-kharacteristic.
(in Russian).
142. Huang J.T., Bertulani C.A., Guimaraes V. Radiative capture of protons and neutrons at astrophysical energies and potential models // Atom. Data and Nucl. Data Tabl. 2010. V.96. P.824-847.
143. http://cdfe.sinp.msu.ru/cgi-bin/muh/rad-chartnucl.cgi?zmin=0&zmax=14&tdata=123456 .
144. Salisbury S.R. and Richards H.T. ^{17}F Level Parameters // Phys. Rev. 1962. V.126. P.2147-2158.
145. Henry R.R., Philips G.C., Reich C.W., and Russell J.L. Elastic scattering of proton by Oxygen in the energy region of 2.5 to 5/6 MeV // Bull. Amer. Phys. Soc. 1956. V.1. P.96.
146. Salisbury S., Hardie G., Oppliger L., and Bangle R. Proton-Oxygen

Differential Scattering Cross Cross sections // Phys. Rev. 1962. V.126. P.2143-2146.
147. Blue R.A. and Haeberli W. Polarization of Protons Elastically Scattered by Oxygen // Phys. Rev. 1965. V.137. №2B. P.B284-B293.
148. Gomes V., Douglas R.A., Polga T. and Sala O. The E_p = 2.66 MeV resonance in $^{16}O(p,p)^{16}O$ // Nucl. Phys. 1965. V.A68.P.417-425.
149. Trachslin W. and Brown L. Polarization and phase shift shifts in $^{12}C(p,p)^{12}C$ and $^{16}O(p,p)^{16}O$ from 1.5 and 3 MeV // Nucl. Phys. 1967. V.A101. P.273-287.
150. Amirikas R., Jamieson D.N. and Dooley S.P. Measurement of (p,p) elastic cross cross sections for C, O and Si in the energy range 1.0-3.5 MeV // Nucl. Instr. Meth. in Phys. Res. 1993. V.B77. P.110-116.
151. Gurbich A.F. Evaluation of non-Rutherford proton elastic scattering for oxygen // Nucl. Instr. Meth. in Phys. Res. 1997. V.B129. P.311-316.
152. Braun M., Fried T. Elastic backscattering cross cross section of proton on Oxygen // Z. Phys. 1983. V.A311. P.173-175.
153. Ramos A.R. et al. Measurement of (p,p) elastic differential cross-cross sections for carbon, nitrogen, oxygen, aluminium and silicon in the 500–2500 keV range at 140_ and 178_ laboratory scattering angles // Nucl. Instr. Meth. in Phys. Res. 2002. V.B190. P.95-99.
154. Chow H.C., Griffithsa G.M., Hall T.H. The $^{16}O(p,\gamma)^{17}F$ Direct Capture Cross Cross section with an Extrapolation to Astrophysical Energies // Can. Jour. Phys. 1975. V.53. P.1672-1687.
155. Luomajarvi M., Rauhala E. and Hautala M. Oxygen detection by non - Rutherford proton backscattering below 2.5 MeV // MIN 1985. V.B9. P.255-258.
156. Morlock R. et al. Halo Properties of the First $1/2^+$ State in ^{17}F from the $^{16}O(p, \gamma)^{17}F$ Reaction // Phys. Rev.Lett. 1997. V.79. P.3837-3840.
157. Burtebayev N.T., Dubovichenko S.B., Zazulin D.M., Dzhazairov-Kakhramanov A.V., Kerimkulov Zh.K., Nassurlla M., Mukhamejanov Y.S., Omarov Ch.T., Tkackenko A.S., Shmygaleva T.A. New measuremrnts and phase shift analysis of elastic $p^{16}O$-scattering at astrophysical energies // In press.
158. Dubovichenko S.B. et al. Astrophysical *S*-factor of radiative p^6Li capture at low energies // Rus. Phys. J. 2010. V.53. P.743-749; Dubovichenko S.B. Astrophysical *S*-factor radiative p^6Li capture // Dokl. Nat. Acad. Sci. Rep. Kazakhstan. 2009. №6. P.41-45.
159. Petitjean C., Brown L., Seyler R. Polarization and phase shift shifts in $^6Li(p,p)^6Li$ from 0.5 to 5.6 MeV // Nucl. Phys. 1969. V.A129. P.209-219.

160. Baktybaev M.K. et al. The scattering of protons from ^{6}Li and ^{7}Li nuclei // The 4th Eurasia Conf. "Nucl. Sci. and its Appl." Baku. Azerbaijan. 2006. P.62; Burtebaev N. et al. The new experimental data on the elastic scattering of protons from ^{6}Li, ^{7}Li, ^{16}O and ^{27}Al nuclei // The 5th Eurasian Conf. "Nucl. Sci. and its Appl.". Ankara. Turkey. 2008. P.40.
161. Dubovichenko S.B. et al. Astrophysical S factor for the radiative-capture reaction p^{6}Li $\rightarrow$ ^{7}Beγ // Phys. Atom. Nucl. 2011. V.74. P.984-1000.
162. Skill M. et al. Differential cross cross section and analyzing power for elastic scattering of protons on ^{6}Li below 2 MeV // Nucl. Phys. 1995. V.A581. P.93-106.
163. Dubovichenko S.B., Dzhazairov-Kakhramanov A.V. Phase shift analysis of elastic p^{6}Li scattering at astrophysical energies // Rus. Phys. J. 2010. V.53. P.458-464.
164. Tombrello T.A. Phase shift shift analysis for ^{3}He(p,p)^{3}He // Phys. Rev. 1965. V.138. P.B40-B47.
165. Clegg T. et al. The elastic scattering of protons from ^{3}He from 4.5 to 11.5 MeV // Nucl. Phys. 1964. V.50. P.621-628.
166. Tombrello T.A. et al. The scattering of protons from ^{3}He // Nucl. Phys. 1962. V.39. P.541-550.
167. Hebbard D.F., Vogl J.L. Elastic scattering and radiative capture of protons by ^{13}C // Nucl. Phys. 1960. V.21. P.652-675.
168. Galster W. et al. Target and detection techniques for the ^{13}N(p,γ)^{14}O reaction using radioactive ion beams: ^{13}C(p,γ)^{14}N reaction as a test case // Phys. Rev. 1991. V.C44. P.2776-2787.
169. Dubovichenko S.B. Phase shift shifts analysis of the elastic p^{13}C scattering // Phys. Atom. Nucl. 2012. V.75. P.285-290.
170. Dubovichenko S.B. Astrophysical *S*-factor radiative p^{13}C capture // Phys. Atom. Nucl. 2012. V.75. P.173-181.
171. Fowler W.A. Experimental and Theoretical Nuclear Astrophysics: the Quest for the Original of the Elements. Nobel Lecture. Stockholm. 8 Dec. 1983.
172. Seagrave J.D., Cranberg L., Simmons J.E. Elastic Scattering of Fast Neutrons by Tritium and ^{3}He // Phys. Rev. 1960. V.119. P.1981-1991.
173. Sayres A.R., Jones K.W., Wu C.S. Interaction of Neutrons with ^{3}He // Phys. Rev. 1961. V.122. P.1853-1863.
174. Haesner B. et al. Measurements of the ^{3}He and the ^{4}He total neutron cross cross sections up to 40 MeV // Phys. Rev. 1983. V.C28. P.995-999.
175. Tilley D.R., Weller H.R., Hale G.M. Energy levels of light nuclei A=4 // Nucl. Phys. 1992. V.A541. P.1-157.

176. Kankowsky R. et al. Elastic scattering of polarized protons on tritons between 4 and 12 MeV // Nucl. Phys. 1976. V.A263. P.29-46.
177. Dubovichenko S.B., Omarov Ch.T. Phase shift shifts analysis of n^3He elastic scattering // Rus. Phys. J. 2016. V.59. P.884-891.
178. Dubovichenko S.B. Astrophysical S factors of radiative $^3He^4He$, $^3H^4He$, and $^2H^4He$ capture // Phys. Atom. Nucl. 2010. V.73. P.1517-1522; Dubovichenko S.B. Astrophysical *S*-factor of the $p^7Li \rightarrow {}^8Be\gamma$ capture at low energies // Rus. Phys. J. 2010. V.53. P.1254-1263; Dubovichenko S.B. Astrophysical *S*-factor of the $p^9Be \rightarrow {}^{10}B\gamma$ radiative capture // Rus. Phys. J. 2011. V.54. P.814-821.
179. Kapitonov I.M., Ishkhanov B.S., Orlin V.N. Models of atomic nuclei. Moscow: Moscow state university 2009. http://nuclphys.sinp.msu.ru/nucmod/nucmod1.htm (in Russian).
180. Lehman D.R., Parke W.C. Shell structure of the A=6 ground states from three body dynamics // Phys. Rev. 1983. V.C28. P.364-382.
181. Lehman D.R., Parke W.C. A=6 structure from three body dinamics // Phys. Rev. Lett. 1983. V.50. P.98-101.
182. Lehman D.R. Excluded bound state in the $S_{1/2}$ N^4He interaction and the three body bilding energies of ^6He and ^6Li // Phys. Rev. 1982. V.C25. P.3146-3154.
183. Dubovichenko S.B., Dzhazairov-Kakhramanov A.V. Electromagnetic effects in light nuclei and the cluster potential model // Phys. Part. Nucl. 1997. V.28. №6. P.615-641.
184. Neudatchin V.G., Sakharuk A.A., Smirnov Yu.F. Generalized potential description of interaction of the lightest cluster scattering and photonuclear reactions // Sov. J. Part. Nucl. 1992. V.23. P.210-271; Neudatchin V.G., Struzhko B.G., Lebedev V.M. Supermultiplet potential model of the interaction of light clusters and unified description of various nuclear reactions // Phys. Part. Nucl. 2005. V.36. P.468-519.
185. Dubovichenko S.B. Contribution of the M1 process to the astrophysical *S*-factor of the p^2H radiative capture // Rus. Phys. J. 2011. V.54. P.157-164; Dubovichenko S.B. Astrophysical S factors for radiative proton capture by ^3H and ^7Li nuclei // Phys. Atom. Nucl. 2011. V.74. P.358-370.
186. Ali S., Ahmad A.A.Z., Ferdous N. A suvey of N^4He interaction // Prepr. Int. Center for Theor. Phys. 1984. 1C/84/195. 108p.
187. Schmelzbach P. et al. Phase shift shift analysis of $^2H^4He$ elastic scattering // Nucl. Phys. 1972. V.A184. P.193-213.
188. McIntair L., Haeberli W. Phase shift shift analysis of $^2H^4He$ scattering // Nucl. Phys. 1967. V.A91. P.382-398.

189. Bruno M., Cannata F., D'Agostino M., Maroni C., Massa I. Experimental study on low energy $^{2}H(^{4}He,^{4}He)^{2}H$ elastic scattering // INFN Italy. Bologna. 1981. AE-81/9. 15P.
190. Jenny B. et al. Phase shift shift analysis of dα elastic scattering between 3 and 43 MeV // Nucl. Phys. 1983. V.A397. P.61-101.
191. Keller L., Haeberli W. Vector polarization measurements and phase shift shift analysis for $^{2}H^{4}He$ scattering between 3 and 11 MeV // Nucl. Phys. 1970. V.A156. P.465-476.
192. Simon G., Schmitt Ch., Walther V.H. Elastic electron and magnetic $e^{2}H$ scattering at low momentum transferred // Nucl. Phys. 1981. V.A364. P.285-296.
193. Purcell J.E. et al. Energy levels of light nuclei A=3 // Nucl. Phys. 2010. V.A848. P.1-74.
194. Dubovichenko S.B. Calculation method of the nuclear characteristics. Third edition, corrected and added. Germany, Saarbrucken: Lambert Academy Publ. 2013. 480p. (in Russian).
195. Tilley D.R. et al. Energy level of light nuclei A=5,6,7 // Nucl. Phys. 2002. V.A708. P.3-163.
196. Ajzenberg-Selove F. Energy levels of light nuclei A=5-10 // Nucl. Phys. 1979. V.A320. P.1-224.
197. Neudatchin V.G. et al. Generalized potential model description of mutual scattering of the lightest $p^{2}H$, $^{2}H^{3}He$ nuclei and the corresponding photonuclear reactions // Phys. Rev. 1992. V.C45. P.1512-1527.
198. Mueller P. et al. Nuclear charge radius of ^{8}He // Phys. Rev. Lett. 2007. V.99. P. 2501-2505.
199. Dubovichenko S.B. Three bode model of the ^{7}Li // Bull. Russ. Academy of Sci. Ser. Fiz. 2000. V.64. P.2289-2292.
200. Jenny B. et al. Phase shift shift analysis of $^{3}He(^{2}H,^{2}H)^{3}He$ scattering // Nucl. Phys. 1980. V.A337. P.77-85.
201. Kanada H. et al. Characteristic features of specific distortion in light nuclear systems // Nucl. Phys. 1986. V.A457. P.93-97; Kanada H., Kaneko T., Tang Y.C. Multiconfiguration resonating group study of the five-nucleon system // Nucl. Phys. 1989. V.A504. P.529-532; Chwieroth F.S., Tang Y.C., Tompson D.R. Microscopic coupled channel study of the five-nucleon system with RGM // Phys. Rev. 1974. V.C9. P.56-65; Chwieroth F.S. et al. Study of $^{2}H^{3}H$ and $^{2}H^{3}He$ systems with RGM // Phys. Rev. 1973. V.C8. P.938-942; Shen P.N. et al. Specific distortion effect in the five-nucleon system // Phys. Rev. 1975. V.C31. P.2001-2008.
202. Spiger R., Tombrello T.A. Scattering of He^{3} by He^{4} and of He^{4} by Tritium // Phys. Rev. 1967. V.163. P.964-984.

203. Ivanovich M., Young P.G., Ohlsen G.G. Elastic scattering of several hydrogen and helium isotopes from tritium // Nucl. Phys. 1968. V.A110. P.441-462.
204. Tilley D.R. et al. Energy level of light nuclei. A=8,9,10 // Nucl. Phys. 2004. V.A745. P.155-363.
205. Burkova N.A., Dubovichenko S.B. $^{4}He^{3}H^{2}H$ three-body model of the ^{9}Be nucleus // Rus. Phys. J. 2008. V.51. P.99-104.
206. Shoda K., Tanaka T. Clusters in the photodisintegration of ^{9}Be // Phys. Rev. 1999. V.C59. P.239-252.
207. Dubovichenko S.B. A three body model of the ^{11}B nucleus // Jour. Exper. Theor. Phys. 2011. V.113. P.221–226.
208. Ali S. and Bodmer A.R. Phenomenological $\alpha\alpha$ potential // Nucl. Phys. 1966. V.80. P.99-112.
209. Jones C.M. et al. Alpha-alpha scattering in the energies range 5 to 9 MeV // Phys. Rev. 1969. V.117. P.525-530.
210. Ajzenberg-Selove F. Energy level of light nuclei A=11,12 // Nucl. Phys. 1990. V.A506. P.1-158.